Head Office: Università degli Studi di Padova

Department of Physics and Astronomy "Galileo Galilei"

Philosophiae Doctoral Course in PHYSICS

Interactions of Gravitational Waves with Large-Scale-Structures

Thesis written with the financial contribution of Università degli Studi di Padova

Coordinator: Prof. Giulio Monaco

Supervisor: Prof. Sabino Matarrese

Co-Supervisor: Prof. Nicola Bartolo

Ph.D. Student: Pritha Bari

Anno Accademico 2022/2023

To myself

Acknowledgements

I am deeply grateful to my supervisor, Prof. Sabino Matarrese, for his exceptional support, mentorship, and invaluable guidance throughout the entirety of this thesis. His unwavering commitment, insightful feedback, and encouragement have been instrumental in shaping the direction and accomplishments of this research. Being a part of his esteemed research group at the University of Padova has been an extraordinary privilege and a source of immense personal and academic growth.

I am also grateful to my co-supervisor, Prof. Nicola Bartolo, for his valuable input and feedback. His expertise and constructive criticism have greatly contributed to the overall quality of this thesis. I extend my heartfelt appreciation to Dr. Daniele Bertacca for his collaboration and assistance. His contributions have greatly enriched the depth and breadth of this study, and I am truly grateful for the valuable lessons I have learned from him on how to approach and tackle complex problems. His expertise and guidance have been instrumental in shaping my research methodology and analytical skills. I express my deepest gratitude to Angelo for his invaluable guidance in both research and life. I am particularly grateful for his patience and unwavering support in academic discussions during the challenging times of the pandemic. His mentorship and understanding have been indispensable to my growth and development as a researcher. I would like to express my sincere appreciation to Guillem for the engaging academic discussions we have had, not only related to our own project but also encompassing broader perspectives. I am grateful for his willingness to share knowledge and engage in meaningful discussions. I would like to extend my gratitude to Serena for our valuable academic discussions during the early stages of my PhD journey.

In addition to the exceptional individuals I have had the privilege of working with, I am deeply honored to be a member of the cosmology group at the University of Padova. The dynamic and vibrant atmosphere fostered specially by the young students in the group has been incredibly inspiring and uplifting. I would like to express my sincere gratitude to Sarah and Giovanni for their warm welcome and invaluable assistance when I first arrived. I am hopeful that I will again have the opportunity to collaborate with the remarkable individuals I have worked with in the future, and I eagerly look forward to potential collaborations with other members of the group. I gratefully acknowledge the funding from the Italian

Ministry of Education, University, and Research (MIUR) through the 'Dipartimenti di eccellenza' project Science of the Universe.

A good working environment plays a pivotal role in producing good work, and I am incredibly grateful to have had the support and camaraderie of my friend and office neighbour, Matteo. While we may hold differing philosophical views on life, we both share a deep appreciation for the importance of a peaceful and quiet workplace, infused with laughter and humor. I would also like to extend my heartfelt thanks to Yousry for his delightful Egyptian sweets. Lastly, I am indebted to Sukannyadi for making my time in Padova even more enjoyable through her continuous supply of delicious food and hosting joyful gatherings.

I would like to take a moment to express my heartfelt appreciation for the unwavering support and assistance of Saikatda, Sanchari, and Shamikda during the challenging times I faced. Their constant presence and encouragement have been a source of strength and hope, uplifting me against all odds.

It is difficult to put into words the depth of my gratitude for the incredible individuals I had the privilege of meeting during my master's studies. Dibyashree, Indranee, Shefali, Sanjukta, Ruma, Sheuly, and Pritam have all played an undeniable role in my personal and academic growth. I genuinely treasure the memories we created together and will forever hold a special place in my heart for each of them. I would be remiss not to mention two remarkable teachers from my time in the master's programme, Prof. Subhaditya Bhattacharya and Prof. Debaprasad Maity. They encouraged and helped me going beyond their academic responsibilities. I am forever grateful for their mentorship and will always hold them in the highest regard.

I am immensely grateful to Prof. Arup Roy, my college professor, for not only teaching me the wonders of physics but also instilling in me the values of compassion and ethics. I am grateful to Anindita and Paulamidi for being wonderful roommates and creating countless mischievous memories during my college life. I thank Puja for providing me with a sense of comfort and familiarity during my transition from a small town to the bustling city of joy.

I would like to express my sincere appreciation to Suchetana and Momi, my dearest friends from school, for their incredible friendship and the positive impact they have brought into my life. I would like to sincerely thank my esteemed teachers, Shankar Sir, Kishori Babu, Shambhu Babu, Naba Babu, and Jagannath Sir, for their remarkable guidance during my school years, which continues to inspire and guide me in my endeavours.

I would like to express my deepest gratitude to my father for introducing me to my lifelong companion and source of solace - books. To my mother, the strongest person I have ever known, I offer my heartfelt appreciation for being the rock upon which I lean during challenging times and the voice of encouragement

that pushes me to reach for my dreams.

Lastly, I would like to express my heartfelt appreciation to myself, as this thesis is dedicated to the inner strength and resilience that has carried me through this journey. May our collaboration continue to lead to joyous and fulfilling experiences in the future.

In conclusion, I would like to express my profound gratitude to all the individuals, including myself, who have contributed to my journey and supported me along the way.

Contents

ABSTRACT

This thesis focuses on the investigation of two intriguing phenomena related to gravitational waves (GWs). The first aspect of our research centers around the novel effect of producing matter density perturbations from the GWs energy density fluctuations and the consequent effect on the matter power-spectrum. By examining the correction it adds to power-spectrum of the underlying matter of large-scale-structures in the universe, we propose a unique avenue for indirectly detecting and constraining GWs. We begin by demonstrating this effect in the matter-dominated era, and then extend our analysis to encompass all epochs of cosmic evolution, utilizing standard perturbation theory to study the intricate interplay between GWs and matter perturbations. In addition, we delve into the fascinating realm of GWs modulation induced by scalar inhomogeneities. As GWs traverse the inhomogeneous regions of the universe, they undergo modulation due to the presence of scalar perturbations. This modulation effect, as we show, provides a unique signature for primordial chiral GWs, that can differentiate it from scalar-induced GWs. By studying the characteristics of modulated GWs, we gain valuable insights into the intricate dynamics of the early universe and the interaction between GWs and scalar perturbations.

Introduction

In 1964, Arno Penzias and Robert Wilson discovered the Cosmic Background Radiation (CMB) while trying to detect radio waves bounced off Echo balloon satellites. The temperature of the radiation was estimated to be 3.5 K, and this discovery began the era of precision cosmology. In the early Universe, free electrons and protons combined to form neutral hydrogen when the temperature of the radiation was of order 10^4 K. This caused the mean free path of the photons to lengthen, and they decoupled from the plasma at redshift $z \sim 1100$ and travelled freely through space. Today, the CMB can be used to probe the very early epochs of the Universe by studying the relationship between temperature fluctuations and the underlying density perturbations that created them.

The standard Hot Big Bang paradigm for the universe has been replaced by inflation [1–3] due to some basic shortcomings of the former, the most prominent ones being the horizon problem and the flatness problem. To solve these, the Universe had to undergo a phase of accelerated expansion, namely inflation, which is by far the most trusted theory as it also explains the cosmological observables [4]. Inflation has three strong predictions: (a) a flat Universe (b) almost scale-invariant spectrum of nearly-Gaussian curvature perturbations, and (c) almost scale-invariant spectrum of gravitational waves (GWs). The first two has already been confirmed and tightly constrained by the latest observations [5] ($\Omega_K = 0.0007 \pm 0.0019$, 68%, TT, TE, EE+lowE +lensing+BAO, and $n_s = 0.9649 \pm 0.0042$, 68%, TT, TE, EE+lowE +lensing). The third one, i.e. the GWs are a potentially observable smoking gun of inflation, yet to be detected, and hence one of the major goals of present-day cosmology.

The recent groundbreaking detection of GWs gave a boost to the observational search for the same, followed by an inevitable push on the theoretical side of research directions related to the study of GWs. On September 14, 2015, the Laser Interferometer Gravitational-Wave Observatory (LIGO) detected a transient gravitational-wave signal from a binary black hole merger [6]. The sources of astrophysical GWs include binary systems of compact objects e.g. black holes or neutron stars or isolated compact objects e.g. pulsars [7]. Apart from these resolved sources, a stochastic background may be formed via the coherent superposition of GWs which fall under the sensitivity radar of the interferometers, hence remaining undetected till date [8–12]. Rendering more difficulty to the situation, another stochastic

background of cosmological GWs is expected, produced via some early Universe phenomena, such as e.g. inflation [13], phase transitions [14] etc. This work focuses on the GWs produced via inflation only.

One of the targets of present [15–17] and future [18–22] GWs interferometers is the detection and characterization of the stochastic GWs background from the cosmological sources. Besides having a feeble interaction with all matter components, cosmological GWs have an additional difficulty of being overshadowed by the astrophysical background. Although the background generated by the amplification of quantum vacuum fluctuations is expected to be too low, there are many well-established mechanisms which can produce large-amplitude GWs which can be 'seen' in future observations. The lack of interaction also keeps the information carried by the GWs uncorrupted, bringing to us the pristine snapshot of the early Universe at a temperature below the Planck scale $\sim 10^{19}$ eV, when the GWs decoupled from the primordial plasma. This information is otherwise unobtainable, as it predates the time of CMB decoupling.

Marking the second major breakthrough in modern cosmology following the first detection of GWs in 2015, Pulsar timing array (PTA) collaborations, NANOGrav, EPTA/InPTA, PPTA, and CPTA, have presented evidence [23–26] for an isotropic stochastic gravitational wave background. This event represents a pivotal milestone in the field of physics, possibly heralding the advent of gravitational wave astronomy in the early Universe. Before this discovery, the main channel to detect this cosmological background has been looking for the B-mode polarisation of CMB, as only GWs (and not scalar modes at linear order) contribute to the parity-odd B-mode component, and there are many CMB surveys targeted specifically at detecting it. Till now there is no detection of it, which has put a tight constraint on the tensor-to-scalar ratio r (< 0.032) has been put on their amplitude on CMB scales through the joint observation of Planck, BICEP2/Keck, and WMAP. Adding LIGO-Virgo-KAGRA data to those obtained from CMB scales, a tighter constraint ($r < 0.028$) has been obtained recently. The next-generation ground-based CMB experiment CMB-S4 aims to optimize the constraint on $r\,(< 0.001)$ at 95% Confidence Level (CL). Before CMB-S4, LiteBIRD and Simons Observatory plan to set an upper limit $r < 0.002$ and $r < 0.01$ respectively.

Apart from CMB and interferometer experiments, recently primordial GWs have also been sought in theoretical studies through their imprint on large-scale-structures (LSS). The main avenues through which we can expect to detect GWs are: local quadrupolar anisotropy in the mass distribution or the galaxies, the modification of angular positions and redshifts of the galaxies, and their shear. This thesis will introduce a new effect that can contribute to these indirect methods of detecting or constraining primordial GWs by detecting their signature on LSS.

Next, we investigate the modulation of GWs by scalar perturbations. Unlike perturbations generated from scratch, this phenomenon occurs when GWs propagate through the inhomogeneities of the universe

and experience second-order modulation. We highlight a crucial characteristic that could potentially serve as a distinguishing factor between these modulated GWs and the conventional scalar-induced GWs.

The thesis is structured as follows. In the upcoming chapter, we revisit perturbation theory to establish a solid foundation. Chapter 2 focuses on gravitational waves (GWs) and their detection through their impact on large-scale structure (LSS). In Chapter 3, we provide a concise overview of scalar-induced GWs, which is closely related to our research. Next, in Chapter 4, we introduce our novel effect, which involves the generation of matter density perturbations from the energy density of GWs. We demonstrate its impact on the matter power-spectrum during the matter-dominated era. Moving forward, we expand our study to cover all evolutionary epochs of the Universe in Chapter 5. In Chapter 6, we investigate scalar-modulated tensors and their unique signature. Finally, we conclude and offer an outlook on our work. Additional information and detailed calculations can be found in the appendices.

Chapter 1

Cosmological Perturbations

1.1 Dynamics of the homogeneous Universe

Viewed on a sufficiently large scale, the properties of the Universe are the same for all observers.

The above quoted *Cosmological Principle* basically states that the spatial distribution of matter in the Universe is homogeneous and isotropic when viewed by a co-moving observer, on a large enough scale ($\sim 100\,\mathrm{Mpc}$). The geometric properties of the Universe are described thanks to the so called flat Friedmann-Lemaître-Robertson-Walker (FLRW) metric that can be expressed as

$$ds^2 = a^2(\eta)\left[-d\eta^2 + d\boldsymbol{x}^2\right], \tag{1.1.1}$$

where η is the conformal time of the observer, related to the cosmic/coordinate time t as $d\eta = dt/a(t)$, t being the proper time of the same, and $a(t)$ is the scale factor, measuring the expansion rate of the Universe. The dynamics of this expansion is encapsulated in the time dependence of $a(t)$. Another important relevant quantity is the Hubble parameter, which is given by $H = \dot{a}/a$[1]. To get the time evolution of the scale factor, one needs to solve the Einstein's equations

$$R_{\mu\nu} - \frac{1}{2}g_{\mu\nu}R = 8\pi G\, T_{\mu\nu} + \Lambda g_{\mu\nu}, \tag{1.1.2}$$

which relates the space-time geometry with the stress-energy tensor $T_{\mu\nu}$ of the energy component of the Universe. In the above equation, $R_{\mu\nu}$, $g_{\mu\nu}$, and R represents, respectively, the Ricci tensor, metric, and the Ricci scalar. Λ is the cosmological constant.

The simplest picture of the Universe assumes that it is filled with a perfect fluid, i.e. having zero viscosity. In this excellent approximate scenario, one can write its stress-energy tensor as

$$T_{\mu\nu} = \big(\rho + P\big)u_\mu u_\nu + P g_{\mu\nu}, \tag{1.1.3}$$

[1] A dot signifies a derivative w.r.t. time t.

where ρ, p are the matter energy density and the isotropic pressure respectively. The velocity four-vector $u^\mu \equiv dx^\mu/d\tau$ is normalised as $u_\mu u^\mu = -1$, τ being the proper time of the observer. To solve the Einstein's equations, one needs a constraint, which comes in the form of the equation of state of the matter. Assuming a barotropic fluid, i.e. one whose pressure depends only on its density, we can write $P = \omega\rho$. For radiation and cold dark matter, this equation of state parameter ω takes the value $1/3$ and 0 respectively. For a cosmological constant, $\omega = -1$.

Plugging Eq. (1.1.3) into Eq. (1.1.2) produces two coupled, non-linear ordinary differential equations, namely, the Friedmann Equations

$$H^2 = \frac{8\pi G}{3}\rho + \frac{\Lambda}{3}, \tag{1.1.4}$$

$$\dot{H} + H^2 = -\frac{1}{6}(\rho + 3\,P). \tag{1.1.5}$$

These are the basic equations to know the dynamics of a homogeneous, isotropic Universe, being supplemented by the energy-momentum conservation equation

$$D^\mu T_{\mu\nu} = 0, \tag{1.1.6}$$

D_μ being the covariant derivative. The above equation gives us the continuity equation and Euler equation for $\mu = 0, i$ respectively. The continuity equation

$$\dot{\rho} + 3H(\rho + P) = 0, \tag{1.1.7}$$

gives us the scale-factor dependence of the matter energy density

$$\rho \propto a^{-3(1+\omega)}, \tag{1.1.8}$$

which for radiation, cold dark matter, and Λ, becomes $\rho \propto a^{-4}, a^{-3}$, and *constant* respectively. When applied with the Friedmann equations Eqs. (1.1.4), we have the time evolution of the scale factor

$$a(t) \propto \begin{cases} t^{2/3(1+\omega)} & \omega \neq -1 \\ e^{Ht} & \omega = -1. \end{cases} \tag{1.1.9}$$

Defining the density parameter Ω for a species as the ratio between the energy density ρ and the critical energy density $\rho_c = 3H^2/8\pi G$, $\Omega = \rho/\rho_c$, the first Friedmann equation can be written as ($H_0 = 67.66\,\mathrm{km\,s^{-1}Mpc^{-1}}$ is the present-day Hubble constant [5].)

$$\left(\frac{H}{H_0}\right)^2 = \sum_i \Omega_i a^{-3(1+\omega_i)}, \tag{1.1.10}$$

where i covers all species; $\sum_i \Omega_i = 1$.

After the end of inflation, the scalar field driving inflation goes on to oscillate, and its energy density is converted into conventional matter through reheating. In the simplest standard scenario, we have a Universe where the radiation component dominates the energy budget of the Universe just after inflation.

This does not last forever, as radiation decays faster than matter, and at a redshift $z_{eq} \sim 3400$, matter overcomes the former to dominate the energy content. From the observation of the brightness of type Ia Supernovae, it was deduced that we are now going through an accelerated expansion phase of the Universe, despite the gravitational attraction of the matter in the universe [27]. This can be accounted for by a positive value of the cosmological constant Λ, equivalent to the presence of a positive vacuum energy, dubbed "dark energy". This ΛCDM model has become a cornerstone of modern cosmology, and has gained strong support from the latest *Planck* observations. *Planck* has set the values for the energy density of the components of present-day Universe as $\Omega_\Lambda = 0.6847, \Omega_m = 0.3166$ [5].

1.2 Linear perturbation theory

Although a perfectly homogeneous and isotropic Universe is a very good approximation on the large scales, and also is strongly supported by the observations (the temperature anisotropy of CMB is only 1 part in 10^5, making it mostly smooth), there are still some deviation from this perfection. It is necessary to explain these observed temperature and polarisation anisotropies of CMB and the structures of the universe, and to clarify the generation and the evolutionary behaviour of them. It is commonly accepted that the seeds were generated during inflation and stretched over astronomical scales because of the rapid expansion of the Universe during the (quasi) de Sitter epoch. These seeds were small primordial perturbations which slowly increased in amplitude due to gravitational instability to form the structures we observe at the present time on the scales of galaxies and galaxy clusters.

Put simply, the theory of spacetime perturbations aims to find approximate solutions to field equations by considering them as small deviations from a known exact background solution. However, in spacetime theories like general relativity, we must also account for perturbations in the geometry of spacetime itself, not just in the fields within that geometry. The problem of describing the growth of small perturbations in the context of general relativity reduces to solving the Einstein's equations linearised about a homogeneous and isotropic background. Therefore, one can split any quantity $\mathcal{Q}(t, \boldsymbol{x})$ into an ideal homogeneous time-dependent background $\overline{\mathcal{Q}}(t)$ and a small, spatially dependent, and random perturbation on top of that, describing how the real space-time deviates from this background.

$$\delta\mathcal{Q}(\boldsymbol{x}, t) \equiv \mathcal{Q}(\boldsymbol{x}, t) - \overline{\mathcal{Q}}(t)\,. \tag{1.2.1}$$

In linear perturbation theory, $\delta\mathcal{Q}/\mathcal{Q} \ll 1$ is always maintained. The quantity $\mathcal{Q}$ can be the components of the metric $g_{\mu\nu}$ and the stress-energy tensor $T_{\mu\nu}$

$$\begin{aligned} g_{\mu\nu} &= g^{(0)}_{\mu\nu}(t) + \delta g_{\mu\nu}(\boldsymbol{x}, t)\,, \\ T_{\mu\nu} &= T^{(0)}_{\mu\nu}(t) + \delta T_{\mu\nu}(\boldsymbol{x}, t)\,. \end{aligned} \tag{1.2.2}$$

Any perturbation can be categorised based on the type of the field(s) from which they were constructed, i.e. how those fields transform under three-space coordinate transformations on the constant-time hypersurface. The three distinct types are scalar, vector and tensor perturbations. This SVT decomposition ensures that the different Fourier modes of the perturbations do not interact with each other, and hence can be studied independently (in the linear order). This helps in simplifying the differential equations for evolution of the perturbations. Let us first talk about metric perturbations. The components of a perturbed spatially flat FLRW metric can be written as

$$\begin{aligned} g_{00} &= -a^2(\eta)\left(1+2\sum_{r=1}^{\infty}\frac{\psi^{(r)}}{r!}\right), \\ g_{0i} &= a^2(\eta)\sum_{r=1}^{\infty}\frac{\omega_i^{(r)}}{r!}, \\ g_{ij} &= a^2(\eta)\left\{\left(1-2\sum_{r=1}^{\infty}\frac{\phi^{(r)}}{r!}\right)\delta_{ij}+\sum_{r=1}^{\infty}\frac{\chi_{ij}^{(r)}}{r!}\right\}. \end{aligned} \tag{1.2.3}$$

Here r is the order of the perturbation, for linear order, it is 1. Comparing with Eq. (1.1.1), we can understand that the functions $\psi, \omega_i, \phi, \chi_{ij}$ are the said perturbations. In our case, the shift $\omega_i^{(r)}$ can be decomposed as

$$\omega_i^{(r)} = \partial_i\omega^{(r)} + \omega_i^{(r)\perp}, \tag{1.2.4}$$

where $\omega_i^{(r)\perp}$ is a solenoidal vector, i.e., $\partial^i\omega_i^{(r)\perp} = 0$. Similarly, the traceless part of the spatial metric can be decomposed at any order as

$$\chi_{ij}^{(r)} = D_{ij}\chi^{(r)||} + \partial_i\chi_j^{(r)\perp} + \partial_j\chi_i^{(r)\perp} + \chi_{ij}^{(r)T}, \tag{1.2.5}$$

where $\chi_i^{(r)\perp}$ is again a solenoidal vector field, and $\chi_{ij}^{(r)T}$ is transverse and trace-less, i.e. $\partial^i\chi_{ij}^{(r)T} = \chi^{(r)T}{}_i^i = 0$. The operator D_{ij} is defined as

$$D_{ij} = \partial_i\partial_j - \frac{1}{3}\nabla^2\delta_{ij}. \tag{1.2.6}$$

Counting the number of independent functions we used to form $\delta g_{\mu\nu}$, we have 4 functions for scalar and vector perturbations each, and 2 functions for tensor perturbations (a symmetric three-tensor has 6 independent components and there are 4 constraints). Thus we have 10 functions all together, which is just the number of degrees of freedom of $\delta g_{\mu\nu}$.

Next we have the perturbations of the stress-energy tensor $T_{\mu\nu}$ from Eq. (1.1.3)

$$\begin{aligned} \rho &= \rho^{(0)} + \sum_{r=1}^{\infty}\frac{\delta^{(r)}\rho}{r!}, \\ u^\mu &= a^{-1}\left(\delta_0^\mu + \sum_{r=1}^{\infty}\frac{v^{\mu(r)}}{r!}\right), \end{aligned} \tag{1.2.7}$$

where the velocity perturbation $v^{i(r)}$ can also be split into a scalar and vector (solenoidal) part

$$v_i^{(r)} = \partial_i v^{(r)} + v_i^{(r)\perp}. \tag{1.2.8}$$

The metric perturbations are coupled to the same in the stress-energy tensor through the perturbed Einstein's equations

$$\delta G^{(r)}_{\mu\nu} = 8\pi G \delta T^{(r)}_{\mu\nu} \,. \tag{1.2.9}$$

Solving these equations along with the $\nu = 0$-th and $\nu = i$-th component of Eq. (1.1.6) will give us the evolution of the perturbations at each order. The study of perturbations is done more easily in Fourier space

$$X(\boldsymbol{x}, t) = \frac{1}{(2\pi)^3} \int d^3k \, e^{i\boldsymbol{k}.\boldsymbol{x}} X_{\boldsymbol{k}}(t) \,. \tag{1.2.10}$$

A perturbation is said to have helicity m if its amplitude is multiplied by $e^{im\psi}$ under rotation of the coordinate system around $\boldsymbol{k}$ by an angle ψ

$$X_{\boldsymbol{k}} \to e^{im\psi} X_{\boldsymbol{k}} \,. \tag{1.2.11}$$

Scalar, vector and tensor perturbations have helicity 0, ± 1 and ± 2, respectively.

1.3 Gauge issue

In the realm of differential geometry, it is fundamental to compare tensor quantities at the same point to make their comparison meaningful. However, given that $\mathcal{Q}(\boldsymbol{x}, t)$ and $\overline{\mathcal{Q}}(t)$ are defined in different space-times, a prescription for identifying points in these space-times must first be established to make any comparison possible. This is where gauge choices come in - they provide a one-to-one correspondence or map between the physical and background space-times. Any change in this map is considered a gauge transformation, and the freedom to choose this map leads to an inherent arbitrariness in the value of the perturbation of $\mathcal{Q}$ at any given space-time point, unless it is gauge invariant. This is the famous 'gauge problem', which is largely discussed over the years [28–32]. Let us begin by defining gauge transformations in the context of small perturbations of a homogeneous and isotropic background space-time. We start by considering a physical space-time manifold $\mathcal{M}$ and selecting a coordinate system x^α on it. The background functions, denoted as ${}^{(0)}\mathcal{Q}(x^\alpha)$, are fixed with respect to the coordinates. Hence, in a second coordinate system $\tilde{x}^\alpha$, the background functions will retain the same functional dependence on x^α. As mentioned before, the perturbation $\delta\mathcal{Q}$ at point p is defined as

$$\delta\mathcal{Q} \equiv \mathcal{Q}(x^\alpha(p)) - {}^{(0)}\,\mathcal{Q}(x^\alpha(p)) \tag{1.3.1}$$

in the first system of coordinates. In the second, we have

$$\widetilde{\delta\mathcal{Q}} \equiv \widetilde{\mathcal{Q}}(\tilde{x}^\alpha(p)) - {}^{(0)}\,\mathcal{Q}(\tilde{x}^\alpha(p)) \,. \tag{1.3.2}$$

The transformation $\delta\mathcal{Q} \to \widetilde{\delta\mathcal{Q}}$ is referred to as the gauge transformation corresponding to the change of variables $x^\alpha \to \tilde{x}^\alpha$ on the manifold $\mathcal{M}$. One may write infinitesimal coordinate transformation as

$$x^\alpha \to \tilde{x}^\alpha = x^\alpha + \xi^\alpha \,, \tag{1.3.3}$$

where ξ^α are infinitesimally small functions of space and time. As a result of this transformation, the following change occurs:

$$\Delta\mathcal{Q} = \widetilde{\delta\mathcal{Q}} - \delta\mathcal{Q} = \mathcal{L}_\xi \mathcal{Q}\,, \tag{1.3.4}$$

where $\mathcal{L}_\xi$ is the Lie derivative in the direction of ξ^α. The transformation (1.3.3) changes the perturbations of the metric as

$$\delta g_{\mu\nu} \to \delta\tilde{g}_{\mu\nu} = \delta g_{\mu\nu} + \Delta g_{\mu\nu}\,. \tag{1.3.5}$$

It is evident that the metric perturbation is not invariant when there is a change of coordinates. This leads to two possible options for handling the equations: First, select a specific space-time slicing and maintain it consistently. Second, choose a collection of variables that are entirely gauge-invariant to describe the system.

1.3.1 Choosing a gauge

By separating the temporal and spatial components, the gauge transformation tensors can be expressed as

$$\begin{aligned}\xi^{(0)}_{(r)} &= \alpha_{(r)}\,,\\ \xi^{(i)}_{(r)} &= \partial^i\beta_{(r)} + d^i_{(r)}\,,\end{aligned} \tag{1.3.6}$$

with $\partial_i d^i_{(r)} = 0$. It is possible to confirm that the new functions in the new coordinate system are related to the old ones via the relations

$$\begin{aligned}\tilde{\psi} &= \psi - \mathcal{H}\,\alpha - \alpha'\,,\\ \tilde{\phi} &= \phi + \mathcal{H}\,\alpha\,,\\ \tilde{\omega} &= \omega + \alpha - \beta'\,,\\ \tilde{\chi}^{||} &= \chi^{||} - \beta\,.\end{aligned} \tag{1.3.7}$$

As there exist two functions, α and β, which can be appropriately selected to choose the gauge, the freedom of gauge choice allows for the imposition of two conditions on the four functions ψ, ϕ, ω, and $\chi^{||}$. Here, we mention some gauges that we will utilize throughout our work [31, 32].

- **Synchronous gauge** Assuming $\psi = 0$, it can be inferred that the proper-time separation between two neighboring hyper-surfaces along the normal vector corresponds to the coordinate-time separation that defines these hyper-surfaces. Out of the various gauge conditions associated with proper-time slicing, the synchronous gauge is the most frequently employed [33, 34]. It is defined by further imposing the condition $\omega = 0$. Upon observation, it can be noted that the conditions

stated above does not entirely remove the gauge freedom of the spatial coordinates. Instead, it leaves a certain degree of freedom as described by

$$\eta \to \tilde{\eta} + \frac{1}{a} C_1(\boldsymbol{x}) \,,$$
$$x^i \to \tilde{x}^i + C_1{}^{,i}(\boldsymbol{x}) \int \frac{d\eta}{a} + C_2{}^{,i}(\boldsymbol{x}) \,, \tag{1.3.8}$$

where $C_{1,2}(\boldsymbol{x})$ are arbitrary functions of $\boldsymbol{x}$. The remaining coordinate freedom in the synchronous gauge results in the manifestation of unphysical gauge modes. This makes it challenging to interpret synchronous gauge calculations, particularly for scales exceeding the Hubble radius. The metric in this gauge looks like

$$ds^2 = a^2(\eta) \left[-d\eta^2 + \gamma_{ij}(\mathbf{x}, \eta) dx^i dx^j \right] \,, \tag{1.3.9}$$

where

$$\gamma_{ij} = \left\{ \left(1 - 2 \sum_{r=1}^{\infty} \frac{\phi^{(r)}}{r!} \right) \delta_{ij} + \sum_{r=1}^{\infty} \frac{\chi_{ij}^{(r)}}{r!} \right\} . \tag{1.3.10}$$

- **Co-moving time-orthogonal gauge** This gauge is fixed by the requirement $v = \omega = 0$, i.e. the fluid four-velocity can be made orthogonal to the constant time spatial hyper-surfaces. The metric looks like

$$ds^2 = a^2(\eta) \left[- \left(1 + 2 \sum_{r=1}^{\infty} \frac{\psi^{(r)}}{r!} \right) d\eta^2 + \gamma_{ij}(\mathbf{x}, \eta) dx^i dx^j \right] \,, \tag{1.3.11}$$

  where γ_{ij} is given by Eq. (1.3.10).

- **Poisson gauge** As discussed in [35, 36], the Poisson gauge is given by $\omega_i{}^{,i} = \chi_{ij}{}^{,j} = 0$. These can be further simplified to $\omega = \chi^{||} = \chi_i{}^{\perp} = 0$. This gauge serves as an extension to the longitudinal gauge ($\omega_i = \chi_{ij} = 0$) to also accommodate vector and tensor perturbations. The longitudinal gauge is not suitable for studying perturbations beyond the linear regime because the scalar, vector, and tensor modes are coupled dynamically. While one can start with purely scalar linear perturbations as initial conditions for the second-order theory, the non-linear effects can generate vector and tensor modes, which makes it necessary to consider all modes when analyzing the system. Therefore, in order to study the full non-linear dynamics of the system, it is essential to include all the modes and use a gauge that can accommodate them, such as the Poisson gauge.

  In this gauge, the gauge-invariant variables Φ and Ψ coincide with ψ and ϕ respectively. Exploiting this fact, one can derive the equations of motion for Φ and Ψ in a simple and elegant manner by first transitioning to the Poisson gauge. These derived equations of motion can then be generalized to obtain the gauge-invariant equations of motion. The metric takes the form

$$ds^2 = a^2(\eta) \left[- \left(1 + 2 \sum_{r=1}^{\infty} \frac{\Phi^{(r)}}{r!} \right) d\eta^2 + \sum_{r=1}^{\infty} \frac{\omega_i^{(r)\perp}}{r!} d\eta \, dx^i \right.$$
$$\left. + \left\{ \left(1 - 2 \sum_{r=1}^{\infty} \frac{\Psi^{(r)}}{r!} \right) \delta_{ij} + \sum_{r=1}^{\infty} \frac{\chi_{ij}^{(r)T}}{r!} \right\} dx^i dx^j \right] .$$

1.3.2 Gauge-invariant variables

Through a combination of the variables in Eq. (1.3.7), it is feasible to form gauge-invariant variables, with the simplest combination yielding the Bardeen potentials [29]

$$\begin{aligned}\Phi &= \psi + (1/a)\left[(\omega - \chi^{||\prime})a\right]^{\prime}\,,\\ \Psi &= \phi - \mathcal{H}\left[(\omega - \chi^{||\prime})\right]\,.\end{aligned} \tag{1.3.12}$$

Certainly, there exists an infinite variety of gauge-invariant variables since any combination of gauge-invariant variables retains the property of gauge-invariance. Another important gauge-invariant scalar quantity is the curvature perturbation on uniform-density hyper-surfaces ζ. The intrinsic spatial curvature on hyper-surfaces on constant conformal time η and for a flat universe is given by

$${}^{(3)}R = \frac{4}{a^2}\nabla^2\phi\,, \tag{1.3.13}$$

the quantity ϕ is usually referred to as the curvature perturbation, which is not gauge-invariant. The gauge-invariant quantity, which is the curvature perturbation on uniform-density hyper-surfaces, is defined by

$$-\zeta = \phi + \frac{H}{\dot{\bar{\rho}}}\delta\rho\,. \tag{1.3.14}$$

One significant characteristic of the variable ζ is that it stays constant beyond the horizon for adiabatic perturbations in matter. Another important gauge-invariant scalar is the co-moving curvature perturbation

$$\mathcal{R} = \phi - \frac{H}{\rho^{(0)} + P^{(0)}}v\,, \tag{1.3.15}$$

where δq is given by: $T^0_i = \partial_i v$.

1.4 Linear matter density perturbations

The expansion of the universe, which pulls particles of all kinds apart, tends to counteract the gravitational attraction. The faster the universe expands, the slower the formation of structure proceeds. In a non-expanding space, a small overdensity will grow exponentially under the influence of gravity (assuming no pressure perturbations exist). However, in an expanding universe, this exponential growth is slowed down to a power-law or logarithmic rate over time. It is worth noting that during radiation domination, the growth of structure is slower than during later stages of matter domination.

With the help of Euler, continuity, and Poisson equation ($\nabla^2\Phi = 4\pi G a^2\delta\rho$), we have, in a matter-dominated Universe

$$\delta'' + \mathcal{H}\delta' - 4\pi G\bar{\rho}a^2\delta = 0\,, \tag{1.4.1}$$

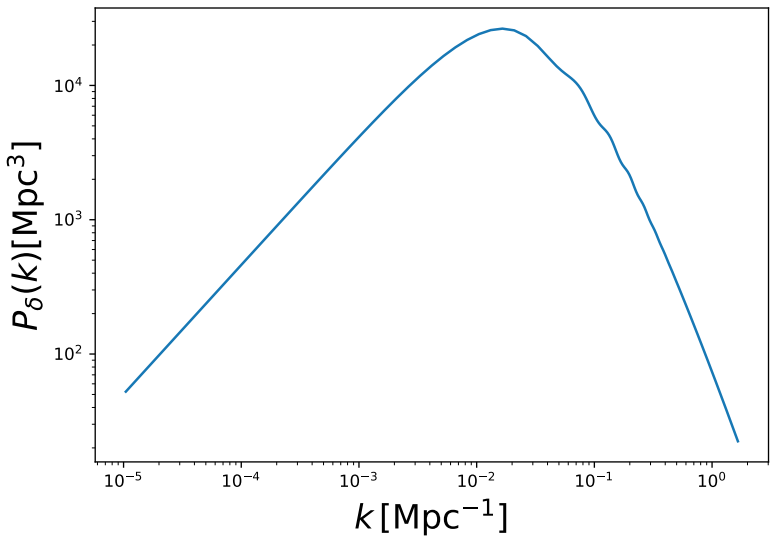

Figure 1.1: The dimensional matter power-spectrum at redshift $z = 0$ according to linear perturbation theory. On large scales, it grows as k. The power-spectrum turns over around $k_{eq} = 0.01\mathrm{Mpc}^{-1}$ corresponding to the horizon size at matter-radiation equality. Beyond the peak, the power falls as k^{-3}. This plot was produced by using CLASS [37].

where $\delta = (\rho(\boldsymbol{x}, t) - \overline{\rho}(t))/\overline{\rho}(t) = \delta\rho/\rho$ is the linear density contrast, $\overline{\rho} = \rho^{(0)}$ being the background energy density. This results in the following growth of matter-density contrast

$$\delta = c_1(\boldsymbol{x})\eta^2 + c_2(\boldsymbol{x})\eta^{-3}\,. \tag{1.4.2}$$

The growing mode gives the rate of growth of density perturbations. In a Universe where the expansion is driven by a combination of radiation and matter, the Hubble parameter is given by

$$\mathcal{H}^2\frac{y}{y+1} = \frac{8\pi G}{3}a^2\overline{\rho}_{\mathrm{m}}\,; \quad y = \frac{a}{a_{eq}}; \quad \Omega_{\mathrm{m}} = \frac{y}{y+1}\,, \tag{1.4.3}$$

where $\overline{\rho}_{\mathrm{m}}$ is the background density of dark matter, and the equation is expressed in terms of the new variable y instead of the usual conformal time, for the ease of calculation [38]. The perturbation in matter sector then satisfies the following evolution equation

$$\frac{d^2\delta}{dy^2} + \frac{2+3y}{2y(y+1)}\frac{d\delta}{dy} - \frac{3}{2y(y+1)}\delta = 0\,, \tag{1.4.4}$$

which is the famous Meszaros' equation (more on this in Chapter 5). In a purely radiation-dominated Universe, $\delta \propto \ln a$, which is comprehensibly much slower than the growth rate $\delta \propto a$ in a matter-dominated phase.

The power-spectrum (defined in the next section) of matter perturbations is given in Fig. 1.1. There is a turnover in the power-spectrum at a scale k_{eq} corresponding to the one which enters the horizon at the matter-radiation equality at scale factor $a_{eq} \sim 10^{-4}$, due to the fact that on small scales, the earlier a mode enters the horizon, the more suppression it has to experience.

1.5 Statistics of perturbations

Within the inflationary scenario, the perturbation field is inherently stochastic and non-deterministic. As the perturbation is random, it is impossible to make deterministic predictions for a specific realization. Instead, we can construct a statistical portrayal of the universe. When we refer to perturbations as random fields, we are suggesting that for any given position $\boldsymbol{x}$ at a particular time t, the perturbation (e.g. $\delta(\boldsymbol{x}, t)$) is a random variable.

We assume that our Universe is a chance occurrence from among all the conceivable universes that could have been a manifestation of the genuine underlying model. The ensemble comprises all possible realizations of this authentic underlying universe. In statistical inference, one may occasionally attempt to approximate the extent to which our individual realization of the universe differs from the genuine underlying version. A fundamental premise of standard cosmology is that the observable segment of the universe is a justifiable representation of the whole. This notion is closely linked to the Cosmological Principle, as it signifies that statistics such as correlation functions must be assessed as averages over the ensemble. However, we only possess a single universe, which is merely one realization from the ensemble. The fair sample hypothesis proposes that samples obtained from well-separated portions of the universe are self-governing realizations of the same physical phenomenon. Furthermore, in the observable segment of the universe, there exist sufficient independent samples to represent the statistical ensemble. This hypothesis is associated with the principle of ergodicity: averaging over numerous realizations is equivalent to averaging over a sufficiently large volume. The cosmological field that we are interested in, within a specific volume, is considered a realization of the statistical process. For the hypothesis of ergodicity, averaging over multiple realizations is comparable to averaging over a large volume.

Gaussian random fields play a critical role in cosmology for various reasons. Inflationary theory suggests that the primordial fluctuations that led to the current-day cosmological structures follow a Gaussian distribution, which is also corroborated by recent data. Additionally, the central limit theorem establishes that Gaussianity arises from the superimposition of numerous random processes, even without invoking inflation. It is noteworthy that a significant feature of Gaussian random fields is that the Fourier transform of a Gaussian field remains Gaussian. The phases of the Fourier modes are stochastic, while the real and imaginary components of the coefficients conform to a Gaussian distribution and are mutually uncorrelated. The expression for the probability distribution of a zero-mean Gaussian primordial perturbation ζ is as follows

$$P(\zeta) = \frac{1}{\sqrt{2\pi}\sigma} e^{-\frac{\zeta^2}{2\sigma^2}} , \tag{1.5.1}$$

where $\sigma^2 = \langle \zeta^2(\boldsymbol{x}, \eta) \rangle$ is the variance, defined as the two-point correlation function, when the two points coincide. A crucial statistical measure of the primordial fluctuations is the dimension-less power-spectrum

$\Delta^2_\zeta(k)$, the Fourier transform of the two-point correlation function

$$\langle\zeta(\boldsymbol{k},\eta)\zeta(\boldsymbol{k'},\eta)\rangle = (2\pi)^3\delta^3(\boldsymbol{k}+\boldsymbol{k'})\frac{2\pi^2}{k^3}\Delta^2_\zeta(k)\,, \tag{1.5.2}$$

where for isotropy, $\Delta^2_\zeta(k)$ depends only on the modulus of the wave-number. Here, $\langle ...\rangle$ defines the ensemble average of the fluctuations. The scalar spectral index n_s (or tilt) characterizes the scale-dependence of the power-spectrum

$$n_s - 1 \equiv \frac{d\ln\Delta^2_\zeta}{d\ln k}\,, \tag{1.5.3}$$

where scale-invariance corresponds to $n_s = 1$. We may also define the running of the spectral index by

$$\alpha_s \equiv \frac{dn_s}{d\ln k}\,, \tag{1.5.4}$$

with which the power-spectrum is

$$\Delta^2_\zeta(k) = A_\zeta(k_*)\left(\frac{k}{k_*}\right)^{n_s(k_*)-1+\frac{1}{2}\alpha_s(k_*)\ln\frac{k}{k_*}}\,. \tag{1.5.5}$$

Likewise, the same can be done for the tensor perturbations

$$\Delta^2_T(k) = A_T(k_*)\left(\frac{k}{k_*}\right)^{n_T(k_*)+\frac{1}{2}\alpha_T(k_*)\ln\frac{k}{k_*}}\,, \tag{1.5.6}$$

where k_* is some pivot scale, $A_{\zeta,\mathrm{T}}(k_*)$ are scalar and tensor amplitudes, and n_T the tensor spectral index, it being zero signifies a scale-invariant tensor. The tensor perturbation amplitude is typically characterized by the tensor-to-scalar ratio

$$r(k_*) = \frac{\Delta^2_T(k_*)}{\Delta^2_\zeta(k_*)}\,. \tag{1.5.7}$$

For the simplest single-field slow-roll inflation, $r = -8n_T$ is satisfied. At present we have only an upper bound on r, $r < 0.032$, through the joint observation of Planck, BICEP2/Keck, and WMAP [39]. Recent studies incorporating data from LIGO-Virgo-KAGRA in addition to those obtained from CMB scales have resulted in a more stringent constraint, $r < 0.028$ [40]. The upcoming ground-based CMB experiment CMB-S4 aims to enhance this constraint further to $r < 0.001$ at a 95% Confidence Level (CL) [41]. Prior to CMB-S4, LiteBIRD [42] and Simons Observatory [43] plan to establish upper limits of $r < 0.002$ and $r < 0.01$ respectively.

If a field is Gaussian, then all the statistical information can be inferred from its power-spectrum. However, primordial non-Gaussianity is manifested in higher-order correlation functions of the field. In the context of single-field slow-roll inflation, non-Gaussianity is anticipated to be small. Nonetheless, non-Gaussianity may be significant in multi-field models or in single-field models that involve non-trivial kinetic terms and/or the violation of the slow-roll conditions (see [44] for a review). Similar to the power-spectrum, the Fourier transform of the three-point correlation function is known as the bispectrum.

$$\langle\zeta(\boldsymbol{k}_1,\eta)\zeta(\boldsymbol{k}_2,\eta)\zeta(\boldsymbol{k}_3,\eta)\rangle = (2\pi)^3\delta^3(\boldsymbol{k}_1+\boldsymbol{k}_2+\boldsymbol{k}_3)\mathcal{B}_\zeta\left(k_1,k_2,k_3\right)\,. \tag{1.5.8}$$

The presence of the delta function in the bispectrum, which enforces momentum conservation, arises from the translation invariance of the background. The bispectrum, denoted by $\mathcal{B}_\zeta$, is symmetric in its arguments, and for scale-invariant fluctuations, it behaves as a homogeneous function of degree -6. A common phenomenological method to parameterize non-Gaussianity is by introducing a non-linear correction to a Gaussian perturbation $\zeta_G(\boldsymbol{x})$

$$\zeta(\boldsymbol{x}) = \zeta_G(\boldsymbol{x}) + \frac{3}{5} f_{\rm NL} \left[\zeta_G(\boldsymbol{x})^2 - \langle \zeta_G(\boldsymbol{x})^2 \rangle \right] . \tag{1.5.9}$$

This definition is local in real space and therefore called local non-Gaussianity. For arbitrary shape functions, the magnitude of non-Gaussianity is measured by defining the generalized $f_{\rm NL}$ parameter

$$f_{\rm NL} \equiv \frac{5}{18} \frac{\mathcal{B}_\zeta\left(k,k,k\right)}{P_\zeta(k)^2} , \tag{1.5.10}$$

where $P_\zeta(k) = (2\pi^2/k^3)\Delta^2_\zeta(k)$ is the corresponding dimensional power-spectrum. Here, the amplitude of non-Gaussianity is normalized to the equilateral configuration.

Chapter 2

Gravitational Waves

2.1 Detection of gravitational waves

The detection of gravitational waves marked a significant milestone in the study of our universe. The confirmation of the existence of these waves has opened up a plethora of opportunities for both observational and theoretical research. After a century since the groundbreaking predictions of Einstein and Schwarzschild, it was finally possible to report the first direct observation of gravitational waves and the merging of a binary black hole system into a single black hole [6]. The discovery of this event, referred to as GW150914, confirmed the predictions of general relativity regarding the non-linear dynamics of highly disturbed black holes. Eight years after this discovery, Pulsar Timing Array (PTA) collaborations, namely NANOGrav, EPTA/InPTA, PPTA, and CPTA, have recently provided compelling evidence [23–26] of an isotropic stochastic gravitational wave background. This remarkable achievement represents yet another momentous stride towards unraveling the mysteries of the Universe.

Present GWs detectors include ground-based facilities such as LIGO, Virgo, KAGRA [46–48]. These ground-based detectors have already achieved significant breakthroughs in the field of gravitational wave astronomy. Additionally, the Einstein Telescope (ET) [49], and Cosmic Explorer (CE) [50] are planned third-generation ground-based detectors that aim to significantly enhance sensitivity and detection capabilities. Space-based detectors like LISA (Laser Interferometer Space Antenna) [51] are anticipated to be launched in the near future, providing complementary observations in a different frequency range. Furthermore, Pulsar Timing Arrays (PTAs), including NANOGrav, EPTA/InPTA, PPTA, and CPTA, are also contributing to our understanding of GWs by utilizing millisecond pulsars as natural cosmic clocks.

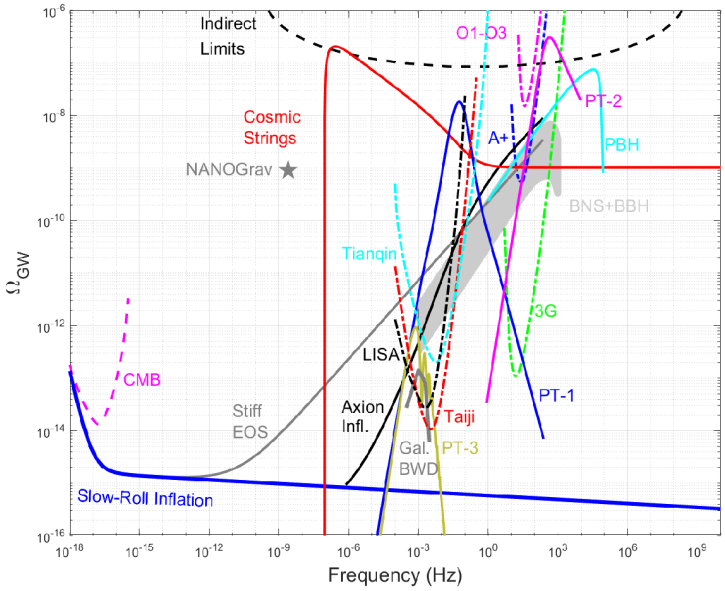

Figure 2.1: Landscape of gravitational wave cosmology [45].

2.2 Resolved sources and a background of gravitational waves

Binary systems containing compact objects are the primary targets for observation by most gravitational wave detectors [7]. These systems undergo millions of years of evolution before finally merging in a violent event that emits extremely luminous gravitational radiation. Neutron stars and black holes are the most compact objects in the universe, with orbital velocities that can approach the speed of light. As a result, the most luminous sources are also the most compact and strongly gravitating systems. As the binary system loses angular momentum and energy to gravitational radiation, its frequency increases. During the final stages of the system's evolution, the component stars are no longer able to maintain stable orbits. When the orbital frequency exceeds a certain value, the stars plunge toward each other, and the GWs luminosity reaches its peak.

Stellar-mass compact object binaries can contain two neutron stars (NS), a neutron star and a black hole (BH), or two black holes. Advanced LIGO and Virgo are well positioned to observe all of these systems. When galaxies merge, the two supermassive black holes (SMBHs) from their centers eventually form a bound pair and become a binary. This evolving MBH pair radiates gravitational waves at a range of low frequencies, typically around $\sim 1\,nHz - 1\,mHz$. As the binary evolves, the distance between the two SMBHs decreases, causing their gravitational wave emission to increase in frequency and intensity. At the higher end of this range, when the two SMBHs are closer to coalescing, their gravitational wave emission will make them a prime target for LISA mission [52]. LISA is a space-based gravitational wave observatory that is designed to detect SMBH binaries of 10 million solar masses $10^3 - 10^9\,M_\odot$ at frequencies ranging $0.1\,mHz - 10\,mHz$. If a population of BHs with masses $10^2 - 10^5\,M_\odot$ exists and they

grow by merging with smaller BHs, then the detection of these intermediate-mass black holes (IMBHs) and their binaries would be possible with the help of ET and the evolved Laser Interferometer Space Antenna (eLISA) [49, 53].

Isolated neutron stars with a time-varying quadrupole moment have the potential to emit gravitational waves, not just binary systems. The formation of a neutron star in a supernova, or a spinning neutron star that is not axisymmetric could also generate gravitational waves, which can be detected by ET and eLISA [7].

The LIGO-Virgo-KAGRA (LVK) collaboration conducted its third observing run, O3, which consisted of three phases: O3a lasting six months from April 2019, O3b lasting five months from November 2019, and O3GK lasting two weeks from April 2020. Throughout these phases, the data collected encompassed more than 80 compact object merger signals [54]. Following O3, LIGO commenced its O4 run on May 24, 2023, with Virgo and KAGRA set to join soon after. The upcoming O5 observing run is highly anticipated as the first extended run, spanning over two years, promising new and exciting discoveries in the field of GWs astronomy.

In addition to the well-known resolved astrophysical sources of GWs, there are two other important contributions to the overall GWs signal. The first one is the stochastic background of astrophysical GWs, which arises from the superposition of GWs from many unresolved sources in the Universe [8–10]. The second contribution is the background of cosmological GWs [55, 56], which is produced by early Universe phenomena such as cosmic inflation [1, 57, 58] or phase transitions [14, 59], topological defects [60, 61] etc. Both of these contributions are important to consider in order to fully understand the GWs signal detected by current and future observatories. The most effective approach to detect a stochastic background is to cross-correlate measurements from multiple detectors.

On July 29, 2023, the PTA collaboration made a significant announcement regarding the detection of a GWs background. However, the exact nature and source of this background still remain a mystery, inviting further investigation and exploration in the field of gravitational wave astronomy. This intriguing signal from PTA results has sparked various interpretations, the astrophysical candidate being the inspiral from the SMBHs [62], although there exists a mild tension between the theoretical predictions and the observational data [23, 24, 63]. There are cosmological interpretations as well, like phase transitions [64], and cosmic strings [65]. Among the various possibilities, one intriguing cosmological signal is the existence of Scalar-Induced Gravitational Waves (SIGWs), discussed in the next chapter. Further discussion regarding the SIGW interpretation of this PTA data will be discussed in Chapter 6.

In recent years, there has been a significant effort within the scientific community to properly characterize the astrophysical background of gravitational waves, using various methods such as anisotropy [66] and

polarization [67] analysis. For example, [66] developed Boltzmann equation for the perturbation in the distribution function of the gravitons, an approach similar to that employed in the case of CMB, and [67] showed that this background exhibits a non-negligible amount of circular polarization, induced by the anisotropic distribution of its sources. However, in this thesis, our focus will be on the cosmological background of gravitational waves, specifically those produced during the inflationary epoch of the early Universe.

2.3 Cosmological gravitational wave background

A cosmological stochastic GWs background is considered a significant indicator of inflation that could potentially be observed. GWs generated by inflation carry valuable information about the early Universe that cannot be obtained by any other means due to their weak interaction with all matter components. CMB radiation is an electromagnetic probe of the early Universe that has been instrumental in our understanding of cosmology until now. However, CMB only traces back to the last scattering surface at a redshift of 1100. In contrast, gravitational waves from inflation can provide a window into the Universe's early moments, reaching energy scales below the Planck scale that are inaccessible by any other means. Nevertheless, this same lack of interaction also makes the detection of these GWs extremely challenging.

For GWs on an isotropic, uniform, and flat spacetime, the metric is

$$ds^2 = a^2(\eta)\left[-d\eta^2 + (\delta_{ij} + \chi_{ij})dx^i dx^j\right] . \tag{2.3.1}$$

Their evolution is governed solely by the trace-less spatial component of the Einstein equation. In the presence of perfect fluids, this component is not directly influenced by the energy content of the Universe, except for its background dynamics

$$\chi_{ij}{}'' + 2\mathcal{H}\chi_{ij}{}' - \nabla^2\chi_{ij} = 0\,. \tag{2.3.2}$$

In Fourier space, they can be decomposed as

$$\chi_{ij}(\boldsymbol{x},\eta) = \frac{1}{(2\pi)^3}\int d^3k\, e^{i\boldsymbol{k}.\boldsymbol{x}}\,\chi_\sigma(\boldsymbol{k},\eta)\,\epsilon^\sigma_{ij}(\hat{\boldsymbol{k}})\,, \tag{2.3.3}$$

where the general solution can be written in terms of the corresponding zero-mean stochastic variable $A_\sigma(\boldsymbol{k})$ and the transfer function $\mathcal{T}\,(k,\eta)$, which describes the sub-horizon evolution of GWs modes after they entered the horizon

$$\chi_\sigma(\boldsymbol{k},\eta) = A_\sigma(\boldsymbol{k})\mathcal{T}\,(k,\eta)\,. \tag{2.3.4}$$

In Eq. (2.3.3), $\sigma = +,\times$ represents the polarisation index, and $\epsilon^{(\sigma)}_{ik}(\hat{\boldsymbol{k}})$, satisfying the relation $\epsilon^{(\sigma)}_{ik}(\hat{\boldsymbol{k}})\epsilon^{(\sigma')ik}(\hat{\boldsymbol{k}}) = 2\delta_{\sigma\sigma'}$, are the transverse and trace-less polarisation tensors. The transfer function

is normalized as $\mathcal{T}(0,\eta) = 1$. The time evolution of the GWs in given by the transfer function [68]

$$\mathcal{T}(k,\eta) = \begin{cases} j_0(k\eta) & \text{for } \eta < \eta_{\rm eq},\ k > k_{\rm eq}\,, \\ \frac{\eta_{\rm eq}}{\eta}\left[A_{\rm GW}(k) j_1(k\eta) + B_{\rm GW}(k) y_1(k\eta)\right] & \text{for } \eta_\Lambda \gg \eta > \eta_{\rm eq},\ k > k_{\rm eq}\,, \\ \frac{3j_1(k\eta)}{k\eta} & \text{for any } \eta \ll \eta_\Lambda,\ k < k_{\rm eq}\,. \end{cases} \tag{2.3.5}$$

The parameters $\eta_{\rm eq}$ and $k_{\rm eq}$ refer to the conformal time and wave-number, respectively, of the modes that enter the horizon at the time of matter-radiation equality. The coefficients $A_{\rm GW}(k)$ and $B_{\rm GW}(k)$ can be determined by equating the expressions of GWs from radiation and matter domination and their first derivatives at the matter-radiation equality. These coefficients have been obtained through a complete derivation presented in [68]. We define η_Λ as the conformal time in which density parameter of the matter is equal to that of the cosmological constant/Dark Energy.

A plethora of experiments worldwide are poised to measure GWs across an unprecedentedly wide range of frequencies. These experiments span a staggering 21 orders of magnitude in frequency, ranging from the cosmic microwave background (CMB) to ground-based GWs interferometers. Complementary but indirect bounds from big bang nucleosynthesis (BBN), CMB temperature and polarization power-spectrum, lensing, and baryon acoustic oscillations (BAO) measurements extend this frequency range even further, to a total of 29 orders of magnitude [69].

Currently, CMB is the most commonly used tool for probing the primordial GWs background. It forms when the photons decouple from ordinary matter. After this moment, photons propagate essentially unimpeded until they reach us, providing a snapshot of the Universe at the time of recombination. The temperature and polarization fluctuations of the CMB carry a wealth of information about the initial conditions at the end of inflation, including the imprint of primordial GWs [38, 70]. A GWs background at the recombination epoch leads to temperature and polarization anisotropies in the CMB. The most important signature is a "curl-like" (B-mode) polarization pattern in CMB polarization, which can not be generated by scalar modes in the first order. While vector modes in principle are able to generate these B-modes, they essentially decay after inflation. Thus, detecting primordial B-modes in the polarization pattern of CMB would serve as compelling evidence for the existence of a primordial GWs background. Till now, there is no detection, and the upper bound on the tensor-to-scalar ratio is discussed in the previous chapter. Relaxing the single field slow-roll inflation consistency condition, on CMB scales it is strongly constrained by the latest Planck data, $r_{0.01} < 0.066$ (at 95% Confidence Level (C.L.), PLANCK TT,TE,EE+lowE+lensing+BK15+LIGO&Virgo2016), constraining $-0.76 < n_T < 0.52$ [71]. Besides the imprints in CMB, GWs affect the cosmic mass distribution too, which is described in the next section.

In Fig. 2.1, bounds from different experiments and theoretical predictions have been shown. Various experimental results have contributed to the current bounds on the primordial gravitational wave back-

ground. These include upper limits set by the O1-O3 LIGO-Virgo runs [72], indirect limits obtained from big bang nucleosynthesis and CMB measurements [69], as well as the NANOGrav pulsar timing measurement [15]. Additionally, projected sensitivities of the third generation (3G) terrestrial GWs detectors [73] and space-based detectors such as LISA [74], Taiji [75], and Tianqin [76] are included in the plot. Theoretical models that are shown in the plot include examples of slow-roll inflation, first-order phase transitions such as PT-1 [77], PT-2 [78], and PT-3 [79], axion inflation [80], the primordial black hole model [81], hypothetical stiff equation of state in the early universe [82], as well as foregrounds due to binary black hole/neutron stars [72] and galactic binary white dwarfs [74].

2.4 Signatures of primordial gravitational waves on large scale structures

Due to its weak interaction with matter, various indirect methods have been proposed to probe the presence of the primordial GWs background. These waves left several imprints on different physical observables throughout the history of the Universe. In addition to the imprints on the CMB mentioned in the previous section, GWs also affect the cosmic mass distribution. Both early and late-time effects can be identified, such as the impact on the two-point function of cosmic structures, or a shear in galaxy distribution. These effects can be probed through observations of the large-scale structure of the Universe, providing complementary constraints on the primordial GWs background.

2.4.1 Tensor fossils

The two-point correlation function, or the power-spectrum in Fourier space, has been the primary tool used in clustering studies. It is typically determined under the assumption of statistical isotropy. Long-wavelength GWs generated during inflation can introduce local departures from this statistical isotropy. In general, hypothetical fossil fields, which can also be scalar or vector, may have been active only during the early phases of the Universe, leaving their imprint on structures [83]. Tensor modes with wavelengths longer than the distance over which observations are done can result in a quadrupolar distortion of spacetime over the observed volume. This quadrupole may then either be imprinted on the primordial mass distribution or induce a quadrupole in the observed distribution through projection effects.

The impact of fossil GWs on the primordial scalar correlation function can be observed through a primordial scalar-scalar-tensor bispectrum, which represents the distortion caused by these GWs. For various inflationary models, such as single-field slow-roll inflation, there exists a consistency relation between the isotropic components of the power-spectrum of the scalar field $P_\Phi(k)$ and the tensor field

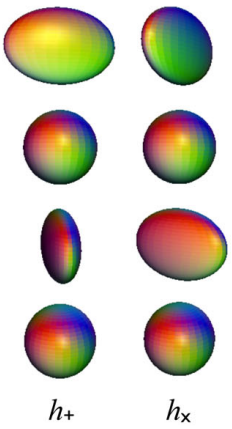

Figure 2.2: Distortions arise in the typically statistically isotropic two-point correlation function of scalar perturbations, when considering a single Fourier mode of GWs directed along the $\hat{\boldsymbol{z}}$ axis [87].

$P_h(k)$, and the bispectrum $\langle\Phi(\boldsymbol{k}_1)\Phi(\boldsymbol{k}_2)h_\lambda(\boldsymbol{K})\rangle$ in the squeezed limit $K \to 0$ [84–86]

$$\langle\Phi(\boldsymbol{k}_1)\Phi(\boldsymbol{k}_2)h_\lambda(\boldsymbol{K})\rangle \overset{K\to 0}{\longrightarrow} (2\pi)^3\delta(\boldsymbol{k}_1+\boldsymbol{k}_2+\boldsymbol{K})\frac{1}{2}\frac{d\ln P_\Phi}{d\ln k}\epsilon^\lambda_{ab}(\boldsymbol{K})\hat{k}_1^a\hat{k}_2^b P_\Phi(k)P_h(K)\,, \tag{2.4.1}$$

where $k = (k_2 - k_1)/2$. This bispectrum implies that in a given realization of the tensor field, the correlation between two scalar modes is [87, 88]

$$\begin{aligned}\langle\Phi(\boldsymbol{k}_1)\Phi(\boldsymbol{k}_2)\rangle_{h_\lambda(\boldsymbol{K})} = (2\pi)^3\,\delta(\boldsymbol{k}_1+\boldsymbol{k}_2+\boldsymbol{K})\,P_\Phi(k) + \int\frac{d^3\boldsymbol{K}}{(2\pi)^3}\sum_\lambda(2\pi)^3\delta(\boldsymbol{k}_1+\boldsymbol{k}_2+\boldsymbol{K})\\ \times\frac{1}{2}\frac{d\ln P_\Phi}{d\ln k}\,\epsilon^\lambda_{ab}(\boldsymbol{K})\,\hat{k}_1^a\,\hat{k}_2^b\,P_\Phi(k)\,h_\lambda(K)\,.\end{aligned} \tag{2.4.2}$$

This suggests that tensor modes with arbitrarily long wavelengths induce a large quadrupole in the scalar power-spectrum. When transformed to configuration space and examined in a local region associated with a Universe patch smaller than the tensor modes' wavelength, this quadrupolar modulation is discovered in the observed local power-spectrum for matter and galaxies.

2.4.2 Clustering of the galaxies

In the presence of GWs, the geodesics of photons emitted by LSS tracers, such as galaxies, are deflected. This results in the observed emission point being different from the true emission point, leading to the galaxy being charted at a different angular position and redshift than its actual location in the universe [89]. The effects of this are:

- **Volume distortion** As the observed coordinates are different than the true ones, this leads to a volume distortion. As a result, the observed co-moving number density of galaxies differs from the true co-moving number density.

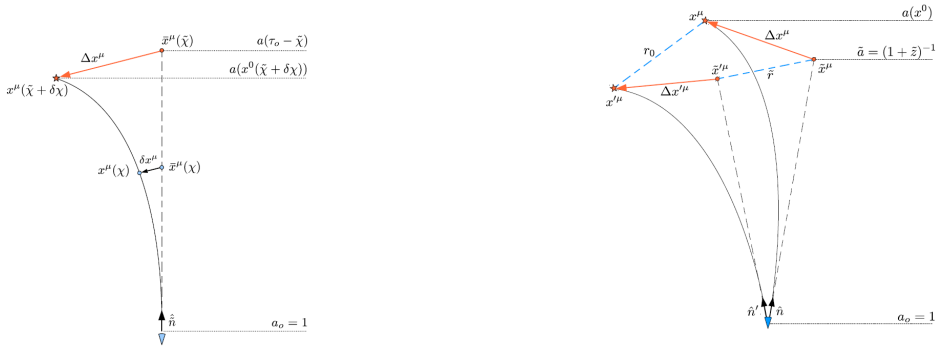

Figure 2.3: Left: Illustration of perturbed photon geodesics with an observer at the bottom. Solid line: actual photon geodesic to the source (star). Dashed line: apparent background photon geodesic to the inferred source position (circle) [89]. Right: Illustration of the apparent and actual standard ruler. $\tilde{r}$ is the apparent size of the ruler, while r_0 is the true ruler [90].

- **Redshift perturbation** When measuring clustering, which involves measuring the density contrast, we are essentially quantifying the excess number of galaxies compared to the cosmic mean at a certain redshift. However, due to the deflection of photons by GWs, the redshift of observed galaxies is shifted from their true redshift, leading to an additional clustering effect. This additional clustering effect is proportional to the evolution of the mean number density of galaxies with redshift.

  The observed comoving number density of galaxies, $a^3\tilde{n}_g$, is related to the true comoving number density $a^3 n_g$ through [89]

  $$a^3(\tilde{z})\tilde{n}_g = a^3(\overline{z}) n_g \left(1 + \frac{\partial \Delta x^i}{\partial \tilde{x}^i}\right) , \tag{2.4.3}$$

  where $\overline{z}$ is the source redshift in an unperturbed Universe, and is related to the measured redshift $\tilde{z}$ via

  $$1 + \tilde{z} = (1+\overline{z})(1+\delta z) , \tag{2.4.4}$$

  and $(1 + \partial \Delta x^i / \partial \tilde{x}^i)$ is the volume distortion due to GWs.

- **Magnification bias** In galaxy surveys, we typically set a threshold on the brightness of observed galaxies. However, due to the deflection of photons by GWs, the angular diameter distance to the source is changed, leading to an additional clustering effect. This additional clustering effect is proportional to the difference in the number of observed galaxies before and after accounting for the effects of GWs.

  The effect of magnification bias $\mathcal{M}_T$ on the observed galaxy density can be parametrized through a parameter $\mathcal{Q}$ [89]

  $$\tilde{\delta}_{gT} = \tilde{\delta}_{gT}(\text{no magn}) + \mathcal{Q}\mathcal{M}_\text{T} . \tag{2.4.5}$$

At linear order, the contributions of GWs to galaxy clustering are mainly due to projection effects resulting from the effects on the propagation of light. In contrast to gravitational lensing by scalar

perturbations, tensor perturbations mainly contribute at redshifts close to the source redshift. However, GWs decrease in amplitude after entering the horizon, whereas scalar perturbations increase. This leads to the suppression of the tensor contribution with respect to the scalar contributions.

Therefore, given that we are not currently able to directly distinguish between scalar and tensor contributions to the galaxy angular power-spectrum, detection possibility of significant contributions from GWs at the leading order effect on galaxy clustering is low [91].

2.4.3 Shape distortion of galaxies

When considering two geodesic lines instead of one, it becomes apparent that if we have a cosmic yardstick at high redshift, its length will be altered by GWs, as the two endpoints will have different observed coordinates than the true ones. This distortion can be parametrized as scalar, vector, and tensor components (this yardstick is on a spherical surface), with the spin-2 tensor component being the shear [90].

When measuring weak gravitational lensing, we need to choose a coordinate system in which galaxies appear round, such as Fermi normal coordinates (FNC). However, the transformation from the FLRW metric to FNC induces an additional shear term, which is called the metric shear. In addition to the usual line-of-sight integral that arises in weak lensing measurements, this metric shear term contributes to the galaxy shear. The contributions from both the weak lensing line-of-sight integral and the metric shear have opposite signs but similar magnitudes, leading to a cancellation effect that results in a small net shear [92]. This lensing shear can be written as [92]

$$
\begin{aligned}
{}_{\pm 2}\gamma(\hat{\boldsymbol{n}}) = -\frac{1}{2}h_{\pm o} - \frac{1}{2}h_{\pm} - \int_0^{\tilde{\chi}} d\chi \Big\{ \frac{\tilde{\chi}-\chi}{2}\frac{\chi}{\tilde{\chi}}(m_{\mp}^i m_{\mp}^j \partial_i \partial_j h_{kl})\hat{n}^k \hat{n}^l \\
+ \left(1 - 2\frac{\chi}{\tilde{\chi}}\right)\hat{n}^l m_{\mp}^k m_{\mp}^i \partial_i h_{kl} - \frac{1}{\tilde{\chi}}h_{\pm}\Big\},
\end{aligned}
\tag{2.4.6}
$$

where the first two terms make the metric shear, while the terms separately are GWs at observer and source points respectively. The rest is the lensing integral, χ is the distance along the line of sight, $\hat{n}^i$ is the unit vector along the same, and $m_{\pm}^i$ are the unit vectors of the circularly polarized basis.

When we transform to FNC, we observe an additional shear due to the effective potential in the g_{00} part of the metric perturbation, which is proportional to the time derivative of GWs

$$
g_{00}^F(\boldsymbol{x}_F, t_F) = -1 + (\dot{H} + H^2) r_F^2 - 2\Psi_F(\boldsymbol{x}_F, t_F)\,, \tag{2.4.7}
$$

$$
\Psi_F(\boldsymbol{x}_F, t_F) = -\frac{1}{4}\left[\ddot{h}_{ij}(\mathbf{0}, t_F) + 2H(t_F)\dot{h}_{ij}(\mathbf{0}, t_F)\right] x_F^i x_F^j\,, \tag{2.4.8}
$$

where $r_F^2 = \delta_{ij} x_F^i x_F^j$.

This creates a tidal field induced by GWs around the galaxies, causing the galaxies to align or anti-align

themselves along the field, resulting in intrinsic alignment. This intrinsic alignment is the source of the additional shear, and it dominates over the lensing signal [93]. Thus, the measurement of galaxy shear remains a rare opportunity in cosmology to search for the background of GWs.

Therefore, both galaxy shear and tensor fossils serve as excellent indirect probes of the primordial GWs background.

Chapter 3

Scalar Induced Gravitational Waves

3.1 An inevitable messenger

There exists an independent generation mechanism for GWs whether or not the primordial GWs are observable . The GWs are generated from curvature perturbations in the second order of perturbation theory, although the tensor and scalar modes are decoupled in the first order of perturbations as is well known. While it is true that the second-order scalar-induced GWs (SIGWs) is suppressed by the square of the curvature perturbations, it can still be sizable and even become larger than the primordial ones if the primordial curvature perturbations are enhanced at small scales compared to the CMB scale [94, 95] or if the density perturbations grow in a matter-dominated (MD) phase of the Universe [96–99]. The possibility of having GWs induced by density fluctuations was first noticed by K. Tomita [100, 101]. They were later rediscovered in [102] when studying second order cosmological perturbations in a dust dominated universe.

The enhancement of primordial curvature perturbations at small scales is realized in some models of inflation and motivates us to explore scenarios to produce primordial black holes (PBHs), which can explain dark matter and/or binary black hole merger event rates [103–108]. If scalar perturbations with an amplitude higher than a threshold value enter the horizon during RD, the entire Hubble patch can collapse and form a PBH. Induced gravitational waves are used as constraints on PBH scenarios, and conversely, PBH constraints can be recast as constraints on induced GWs [109]. Similarly, induced gravitational waves can put constraints on inflation models that lead to small-scale enhancement of perturbations [95, 110]. Through the study of induced GWs, we may acquire valuable insights into the last stage of inflation, around scales $k \sim 10^7 - 10^{18}\,\mathrm{Mpc}^{-1}$. Furthermore, even the lack of induced GWs could offer new limitations on the primordial spectrum in small scales, conceivably down to $P_{\mathcal{R}} \sim 10^{-4} - 10^{-5}$ [111].

Therefore, studies on induced GWs (in addition to primordial ones) are inspired and justified by their potential to further our understanding in the fields of cosmology, and have been the subject of much study in recent years [94, 97, 107, 112–118]. For an overall review, see [119].

3.2 Generation mechanism

In this thesis, to show the generation mechanism of the SIGW, we choose an approach, Arnowitt-Deser-Misner formalism (ADM formalism) [120], similar to the Poisson gauge, as this very same approach has been used by us in Chapter 6. Here the metric is

$$ds^2 = -N^2 dt^2 + \gamma_{ij} dx^i dx^j \,, \tag{3.2.1}$$

where $N = e^{\Phi}$ is the lapse function, and $\gamma_{ij} = a^2 e^{-2\Psi} h_{ij} = a^2 e^{-2\Psi} e^{\tilde{\gamma}_{ij}}$ is the metric for three dimensional hypersurface of constant t [1]. The scalar perturbation sector contains Φ and Ψ in linear order, and $\tilde{\gamma}_{ij}$ signifies the transverse tensor perturbations. The determinants of the full metric and the same for the three dimensional hypersurface is related by $\sqrt{-g} = N\sqrt{\gamma}$. The contravariant three-metric is given by

$$\gamma^{ij} = a^{-2} e^{2\Psi} h^{ij} = a^{-2} e^{2\Psi} e^{-\tilde{\gamma}^{ij}} \,. \tag{3.2.2}$$

Keeping the tensor terms up to the linear order, we have

$$\gamma_{ij} = a^2 e^{-2\Psi} (\delta_{ij} + \tilde{\gamma}_{ij}) \,, \tag{3.2.3}$$

$$\gamma^{ij} = a^{-2} e^{2\Psi} (\delta^{ij} - \tilde{\gamma}^{ij}) \,. \tag{3.2.4}$$

With these metric components, the extrinsic curvature reads [121]

$$K_{ij} = -\frac{1}{2N} \dot{\gamma}_{ij} \,. \tag{3.2.5}$$

To get an evolution equation of the tensor perturbations sourced by a mixing of first order scalar and tensor ones, we focus on the trace-less part of the ij-th Einstein equation. It can be written as below [121], defining the trace-less part of Eq. (3.2.5) as $\overline{K}_{ij} = K_{ij} - \frac{1}{3} K \gamma_{ij}$,

$$\frac{\partial \overline{K}^i_k}{\partial t} = -N^{|i}_{|k} + \frac{1}{3} N^{|l}_{|l} \, \delta^i_k + N \left(K \overline{K}^i_k + {}^{(3)}\overline{R}^i_k - 8\pi G \, \overline{S}^i_k \right) , \tag{3.2.6}$$

where ${}^{(3)}\overline{R}^i_k$ is the Ricci tensor associated with the three-metric γ_{ik}, and $\overline{S}^i_k$ is the space-space contribution of the matter energy-momentum tensor. Vertical bars denote three-space covariant derivatives with connection coefficients determined from γ_{ij}. Trace and trace-less parts of K_{ij} are

$$K = -\frac{1}{2N} \gamma^{ij} \dot{\gamma}_{ij} = -\frac{3}{N} (H - \dot{\Psi}) \,, \tag{3.2.7}$$

[1] In this chapter, we denote χ_{ij} by $\tilde{\gamma}_{ij}$. Note that we have written $\tilde{\gamma}_{ij}$ for the second order GWs, unlike our usual notation $\tilde{\gamma}_{ij}/2$.

$$\overline{K}^i_k = \gamma^{ij}\overline{K}_{jk} = -\frac{1}{2N}\,\dot{\tilde{\gamma}}^i_k\,. \tag{3.2.8}$$

Obtaining the rest of the terms from γ_{ij}, the trace-less ij-th equation (3.2.6) becomes (taking only scalar-scalar terms as the source)

$$\ddot{\tilde{\gamma}}^i_k + 3H\dot{\tilde{\gamma}}^i_k - \frac{\nabla^2\tilde{\gamma}^i_k}{a^2} = 2\frac{e^{2(\Phi+\Psi)}}{a^2}\left[\Phi_{,k}^{,i} + \Phi^{,i}\Phi_{,k} - \Psi^{,i}\Psi_{,k} - \Psi_{,k}^{,i} + \Phi^{,i}\Psi_{,k} + \Psi^{,i}\Phi_{,k}\right.$$
$$\left. -\frac{2}{3}\Phi^{,l}\Psi_{,l}\delta^i_k - \frac{1}{3}\Phi^{,l}\Phi_{,l}\delta^i_k + \frac{1}{3}\Psi^{,l}\Psi_{,l}\delta^i_k\right] + 16\pi G e^{2\Phi}\overline{S}^i_k\,, \tag{3.2.9}$$

where the last term is the contribution from the matter component of the Universe, $\overline{S}^i_k$. We consider no anisotropic stress, i.e. $\Phi = \Psi$. The stress-energy tensor in the radiation dominated Universe is

$$\overline{S}^i_k = \gamma^{ij}\overline{S}_{jk} = \gamma^{ij}(S_{jk} - \frac{1}{3}S\gamma_{jk}) = (\overline{\rho} + \overline{P})(v^{,i}v_{,k} - \frac{1}{3}v^2\delta^i_k)\,. \tag{3.2.10}$$

The evolution equation becomes

$$\ddot{\tilde{\gamma}}^i_k + 3H\dot{\tilde{\gamma}}^i_k + \frac{k^2}{a^2}\tilde{\gamma}^i_k = \frac{4}{a^2}\Phi^{,i}\Phi_{,k} + 16\pi G(\overline{\rho} + \overline{P})v^{,i}v_{,k}\,, \tag{3.2.11}$$

where

$$v^{,i} = -\frac{2}{8\pi G a^2(\overline{\rho} + \overline{P})}\,\partial^i(\Phi' + \mathcal{H}\Phi)\,. \tag{3.2.12}$$

Decomposing the perturbations into their Fourier modes, we have

$$\tilde{\gamma}^i_k(\boldsymbol{x}, t) = \frac{1}{(2\pi)^3}\int d^3k\, e^{i\boldsymbol{k}.\boldsymbol{x}}\tilde{\gamma}_{\boldsymbol{k}(\sigma)}(t)\epsilon^{(\sigma)i}_k(\hat{\boldsymbol{k}})\,,$$
$$\Phi(\boldsymbol{x}, t) = \frac{1}{(2\pi)^3}\int d^3k\, e^{i\boldsymbol{k}.\boldsymbol{x}}\Phi_{\boldsymbol{k}}(t)\,. \tag{3.2.13}$$

where $\sigma = +, \times$ represents the polarisation index, and $\epsilon^{(\sigma)}_{ik}(\hat{\boldsymbol{k}})$, satisfying the relation $\epsilon^{(\sigma)}_{ik}(\hat{\boldsymbol{k}})\epsilon^{(\sigma')ik}(\hat{\boldsymbol{k}}) = 2\delta_{\sigma\sigma'}$, are the transverse and trace-less polarisation tensors. We use conformal time to arrive at the final evolution equation

$$\tilde{\gamma}''_{\boldsymbol{k}} + 2\mathcal{H}\tilde{\gamma}'_{\boldsymbol{k}} + k^2\tilde{\gamma}_{\boldsymbol{k}} = 4\int\frac{d^3k_1}{(2\pi)^3}\Phi_{\boldsymbol{k}}(0)\Phi_{\boldsymbol{k}-\boldsymbol{k_1}}(0)\epsilon^k_i(\hat{\boldsymbol{k}})k^i_1 k_{1k}\left[T_\Phi(k_1\eta)T_\Phi(|\boldsymbol{k}-\boldsymbol{k_1}|\eta)\right.$$
$$\left. +\frac{1}{2}\left(\mathcal{H}T_\Phi(k_1\eta) + T'_\Phi(k_1\eta)\right)\left(\mathcal{H}T_\Phi(|\boldsymbol{k}-\boldsymbol{k_1}|\eta) + T'_\Phi(|\boldsymbol{k}-\boldsymbol{k_1}|\eta)\right)\right]\,, \tag{3.2.14}$$

where the terms having 0 in brackets signify their value at initial time, and T is the transfer function of the quantity in the subscript. Applying Green's method, the solution to Eq. (3.2.14) is

$$\tilde{\gamma}_{\boldsymbol{k}}(\eta) = \tilde{\gamma}_{\boldsymbol{k}}(0)\,j_0(k\eta) + \int_0^\eta d\tilde{\eta}\,S_{ss}(\boldsymbol{k}, \eta)\,G(\eta, \tilde{\eta})\,, \tag{3.2.15}$$

where $S_{ss}(\boldsymbol{k}, \eta)$ is the right hand side of Eq. (3.2.14), and $G(\eta, \tilde{\eta})$ is the Green's function of the same equation, given by

$$G(\eta, \tilde{\eta}) = \frac{y_1(\tilde{\eta})y_2(\eta) - y_2(\tilde{\eta})y_1(\eta)}{y_1(\tilde{\eta})y'_2(\tilde{\eta}) - y_2(\tilde{\eta})y'_1(\tilde{\eta})}\,, \tag{3.2.16}$$

y_1 and y_2 being the two solutions of the homogeneous part of Eq. (3.2.14). The first term of Eq. (6.1.11) is the usual first-order GWs, whereas the second one is the desired SIGW.

3.3 Power-spectrum and kernel function

The dimension-less power-spectrum $\Delta^2_{\tilde{\gamma}_1}(k)$ of $\tilde{\gamma}_1(\boldsymbol{k},\eta)$, i.e. the second term on the right hand side of Eq. (6.1.11), is defined by (for each polarisation λ of the induced wave)

$$\langle \tilde{\gamma}_1^{(\lambda)}(\boldsymbol{k},\eta)\tilde{\gamma}_1^{(\lambda')}(\boldsymbol{k}',\eta)\rangle = (2\pi)^3\delta_{\lambda\lambda'}\delta^3(\boldsymbol{k}+\boldsymbol{k}')\frac{2\pi^2}{k^3}\Delta^2_{\tilde{\gamma}_1}(k)\,, \tag{3.3.1}$$

which implies

$$\Delta^2_{\tilde{\gamma}_1}(k) = \frac{8k^3}{\pi}\int d^3k_1 \frac{\Delta^2_\Phi(k_1)\Delta^2_\Phi(|\boldsymbol{k}-\boldsymbol{k_1}|)}{k^3|\boldsymbol{k}-\boldsymbol{k_1}|^3}(\epsilon^{ik}(\hat{\boldsymbol{k}})k_{1\,i}k_{1\,k})^2\left(\int_0^\eta d\tilde{\eta}\, G(\eta,\tilde{\eta})\right.$$
$$\left.\times\left[T_\Phi(k_1\eta)T_\Phi(|\boldsymbol{k}-\boldsymbol{k_1}|\eta)+\frac{1}{2}\left(\mathcal{H}T_\Phi(k_1\eta)+T'_\Phi(k_1\eta)\right)\left(\mathcal{H}T_\Phi(|\boldsymbol{k}-\boldsymbol{k_1}|\eta)+T'_\Phi(|\boldsymbol{k}-\boldsymbol{k_1}|\eta)\right)\right]\right)^2, \tag{3.3.2}$$

where we have dropped the superscript λ, and used the definition of the two-point function of Φ and $\tilde{\gamma}^{(\sigma)}_{\boldsymbol{k}}$ (see (1.5.2)).

To solve such integrals, it is useful to work with the variables $v = k_1/k$, $u = |\boldsymbol{k}-\boldsymbol{k}_1|/k$, and use the dimensionless time variable $x = k\eta$. Summing over both polarisations, Eq. (3.3.2) reads

$$\Delta^2_{\tilde{\gamma}_1}(k) = 16k^2\int_0^\infty dv\int_{|v-1|}^{v+1} du\,\frac{v^2}{u^2}\left(1-\left(\frac{1+v^2-u^2}{2v}\right)^2\right)^2\Delta^2_\Phi(uk)\Delta^2_\Phi(vk)\left(\int_0^x d\tilde{x}\, G(x,\tilde{x})\right.$$
$$\left.\times\left[T_\Phi(v\tilde{x})T_\Phi(u\tilde{x})+\frac{1}{2}\left(\mathcal{H}T_\Phi(v\tilde{x})+k\dot{T}_\Phi(v\tilde{x})\right)\left(\mathcal{H}T_\Phi(u\tilde{x})+k\dot{T}_\Phi(u\tilde{x})\right)\right]\right)^2. \tag{3.3.3}$$

A dot here signifies a derivative w.r.t. x, and the Green's function is

$$G(x,\tilde{x}) = \frac{\pi}{2k}\,\tilde{x}\,\sqrt{\frac{\tilde{x}}{x}}\,\left(J_{1/2}(\tilde{x})Y_{1/2}(x)-J_{1/2}(x)Y_{1/2}(\tilde{x})\right). \tag{3.3.4}$$

We evaluate the kernel function first, taking the upper limit of integration as infinity

$$\begin{aligned} I &= \int_0^x d\tilde{x}\, G(x,\tilde{x})\left[T_\Phi(v\tilde{x})T_\Phi(u\tilde{x})+\frac{1}{2}\left(\mathcal{H}T_\Phi(v\tilde{x})+k\dot{T}_\Phi(v\tilde{x})\right)\left(\mathcal{H}T_\Phi(u\tilde{x})+k\dot{T}_\Phi(u\tilde{x})\right)\right], \\ &= \int_0^\infty d\tilde{x}\,\frac{3\pi^2}{8k\sqrt{uv}}\sqrt{\frac{3\tilde{x}}{x}}\,\left(J_{1/2}(\tilde{x})Y_{1/2}(x)-J_{1/2}(x)Y_{1/2}(\tilde{x})\right) \\ &\quad\times\left[J_{1/2}(v\tilde{x}/\sqrt{3})J_{1/2}(u\tilde{x}/\sqrt{3})+2J_{5/2}(v\tilde{x}/\sqrt{3})J_{5/2}(u\tilde{x}/\sqrt{3})\right], \end{aligned} \tag{3.3.5}$$

giving the oscillation average

$$\langle I^2\rangle = \frac{3^4}{2^5k^2}\left(\frac{1}{uvx}\right)^2\left\{\Theta\left(\frac{u+v}{\sqrt{3}}-1\right)\frac{9\pi^2}{4}s^4+\left(\frac{3s^2}{2}\ln\left|\frac{1+s}{1-s}\right|-3s\right)^2\right\}, \tag{3.3.6}$$

where $2uv/\sqrt{3}\cosh s = 1-v^2-u^2/3$. The power-spectrum, Eq. (3.3.3), becomes

$$\Delta^2_{\tilde{\gamma}_1}(k) = \frac{3^4}{2}\left(\frac{1}{x}\right)^2\int_0^\infty dv\int_{|v-1|}^{v+1} du\,\frac{1}{u^4}\left(1-\left(\frac{1+v^2-u^2}{2v}\right)^2\right)^2$$
$$\times\,\Delta^2_\Phi(uk)\Delta^2_\Phi(vk)\left\{\Theta\left(\frac{u+v}{\sqrt{3}}-1\right)\frac{9\pi^2}{4}s^4+\left(\frac{3s^2}{2}\ln\left|\frac{1+s}{1-s}\right|-3s\right)^2\right\}. \tag{3.3.7}$$

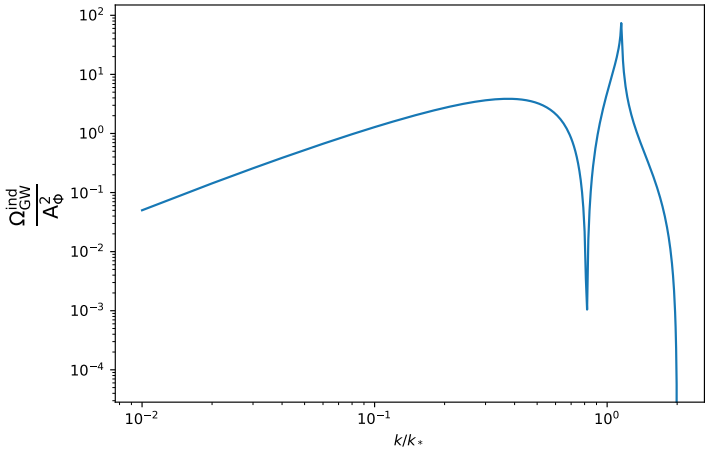

Figure 3.1: Gravitational wave density parameter induced by monochromatic scalars in the radiation era, having a peak at $k = k_*$.

3.3.1 Dirac delta primordial spectrum

Let us take a peaked (at $k = k_*$) source for the primordial scalar spectrum

$$\Delta^2_\Phi(k) = A_\Phi\, \delta\left(\ln \frac{k}{k_*}\right). \tag{3.3.8}$$

This type of peak can exist at scales that are lower than the ones observed by CMB, allowing them to evade detection. This scenario can be realized in certain multi-field inflation models [122–124]. In this monochromatic case, we have the following power-spectrum

$$\langle \Delta^2_{\tilde{\gamma}_1}(k)\rangle = 16 A^2_\Phi\, (k_*/k)^2 \left[1 - \frac{k^2}{4k_*^2}\right]^2 \langle I^2\rangle_{u=v=k_*/k}\, \Theta(2k_* - k)\,, \tag{3.3.9}$$

where

$$\begin{aligned}\langle I^2\rangle_{u=v=k_*/k} = \frac{3^6}{2^7 k^2}\frac{1}{x^2}\left(\frac{k}{k_*}\right)^4 \Bigg\{ &\frac{3^4\pi^2}{2^4}\left(1 - \frac{2k_*^2}{3k^2}\right)^4 \left(\frac{k}{k_*}\right)^8 \Theta\left(\frac{2}{\sqrt{3}} - \frac{k}{k_*}\right) \\ &+ \left[-\left(\frac{2}{3} - \frac{k^2}{k_*^2}\right) + \frac{3}{4}\left(1 - \frac{2k_*^2}{3k^2}\right)^2 \left(\frac{k}{k_*}\right)^4 \ln\left|1 - \frac{4k_*^2}{3k^2}\right|\right]^2 \Bigg\}.\end{aligned} \tag{3.3.10}$$

In this case, the spectrum is truncated at $k = 2k_*$ due to the presence of the Heaviside theta function. This is because in order to integrate the Dirac delta function, it is necessary to satisfy the condition $|k - k_*| < k_* < k + k_*$. There is also a logarithmic singularity at $k/k_* = 2/\sqrt{3}$, due to the resonant amplification. The source, being quadratic in scalars, has a frequency twice that of the gravitational potential: $2 \times k_*/\sqrt{3}$. The fraction of the GW energy density per logarithmic wavelength is [2]

$$\Omega^{\rm ind}_{\rm GW}(k,\eta) = \frac{1}{12}\left(\frac{k}{\mathcal{H}}\right)^2 \langle \Delta^2_{\tilde{\gamma}_1}(k)\rangle\,. \tag{3.3.11}$$

Fig. 3.1 shows $\Omega^{\rm ind}_{\rm GW}$ for Dirac delta scalar-induced GWs.

[2] $\mathcal{H} = 1/\eta$ in RD era.

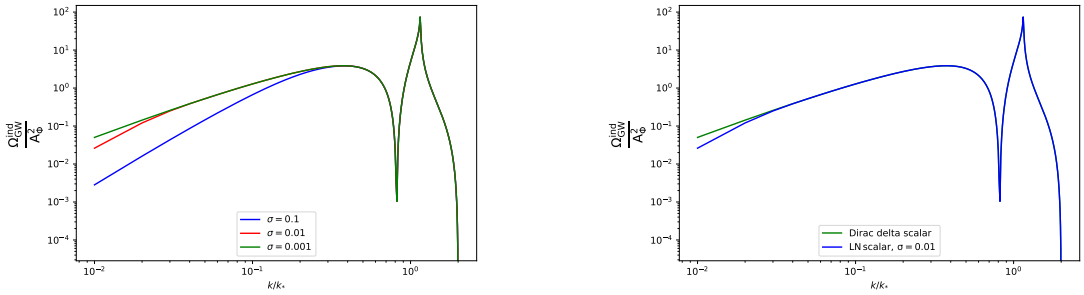

Figure 3.2: Left: Comparison of the gravitational wave density parameter induced by lognormal scalars with different widths. SIGW from $\sigma = 0.001$ case coincides with the same induced by a Dirac delta scalar with same peak location. Right: Same as left, with Dirac delta-peaked scalar and only one lognormally peaked scalar for comparison.

3.3.2 Log-normal primordial spectrum

A peaked primordial spectrum having a finite width can be realised in many theoretical models, e.g. models with potential having a near-inflection point [125], multi-field inflation [126, 127] etc.. This log-normally peaked primordial spectrum is [128, 129]

$$\Delta^2_\Phi(k) = \frac{A_\Phi}{\sqrt{2\pi}\sigma} \exp\left(-\frac{1}{2\sigma^2} \ln^2 \frac{k}{k_*}\right) , \tag{3.3.12}$$

where σ is the peak width, and the following normalisation condition is valid: $\int_0^\infty \Delta^2_\Phi(k)\, d\ln k = A_\Phi$. It coincides with the Dirac delta power-spectrum for $\sigma \to 0$. To compare the SIGW generated by this and the monochromatic cas, we take the narrow band approximation, where $\sigma \ll 1$. In [128], the authors gave an analytical approximation for this

$$\Omega^{\rm ind}_{\rm GW}(k,\eta) = \mathrm{erf}\left(\frac{1}{\sigma} \mathrm{arcsinh}\, \frac{k}{2k_*}\right) \Omega^{\rm ind}_{{\rm GW},\delta_{\rm D}}(k,\eta) , \tag{3.3.13}$$

$\Omega^{\rm ind}_{{\rm GW},\delta_{\rm D}}$ being the same induced by Dirac delta scalars. As we can see from the right panel of Fig. 3.2, the solutions deviate in the IR region. This break-point, where the deviation starts, is given by $k/k_* = 2\sigma \exp\left(-\sigma^2\right)$. Here the GWs spectrum from narrowly peaked lognormal scalars changes its infrared behavior from $\Omega^{\rm ind}_{\rm GW} \propto k^3$ to $\Omega^{\rm ind}_{\rm GW} \propto k^2$ [128]. In the right panel of Fig. 3.2, the break-point is $k/k_* = 0.02$. The input scalars having more or less width understandably give rise to spectra that deviate earlier or later. The ability to identify the origin of the curvature perturbation and measure the peak width makes this feature extremely interesting.

3.4 Gauge issue

Although it is well-known that GWs are invariant under gauge transformations at the linear order, this is not necessarily true for higher orders. The observation of gauge dependence was first made in [102].

A subsequent study by Hwang and Noh [130] utilized specific gauges, namely the co-moving, uniform curvature, and zero-shear and uniform expansion gauges, to investigate a dust-dominated Universe. They concluded that searching for the signatures of primordial GWs must take into account the detailed study of the induced tensor modes including their gauge dependence. This gauge-dependence is a result of the gauge-dependence inherent in the scalar perturbation variables. The equations governing the velocity field and gravitational potential are not the same across all gauges. These variations in the equations propagate to the amplitude of the induced GWs, leading to the gauge-dependence. Despite efforts [131–134], a definitive solution to the gauge problem has not been established. A gauge-invariant formulation is not applicable in this case, as there exist numerous gauge invariant variables, and it remains uncertain which one is detected by interferometers. In [117], the authors separated the induced tensor perturbations into two parts, one part of tensor perturbations is the freely propagating type that follows its equation of motion without any external source. These types of perturbations are commonly referred to as gravitational waves. Although they initially couple with scalar perturbations at their creation, they eventually decouple and propagate independently of scalar perturbations. Consequently, they are not affected by the choice of gauge, as they become independent of scalar perturbations after decoupling. The other part is the one that couples with scalar perturbations. This type includes freely propagating tensor perturbations until they decouple from scalar perturbations. However, as this type of tensor perturbation is influenced by scalar perturbations, its time dependence mirrors that of scalar perturbations. This type of tensor perturbation is susceptible to gauge dependence. They demonstrated that once the GWs decouple from the scalar sources, they become gauge-independent. By utilizing the synchronous and Poisson gauges, they were able to establish that the decay of the source term within the horizon resulted in the same GWs spectrum at observable time. It should be noted that this finding is not valid for the MD era, as the gravitational potential remains constant across all scales during this period.

Chapter 4

Signatures of Primordial Gravitational Waves on LSS

In Chapter 2, we discussed various methods for detecting GWs through their influence on the LSS. In this chapter, we explore a novel mechanism for detecting GWs, first proposed and analyzed in [100, 101, 135]. This mechanism involves tensor-induced scalar modes that are statistically independent of standard adiabatic density perturbations. As a result, the overall matter power-spectrum is simply the sum of the two components. We know that the linear perturbation theory is suitable for very large scales, particularly when considering only the power-spectrum. However, for higher-order correlators such as the bispectrum or trispectrum, or when describing LSS formation on mildly non-linear scales or in connection with galaxy bias schemes, higher-order perturbation theory [136, 137] or more sophisticated resummation techniques [138–140] are required.

In this context, one of the main focuses, recently revived, has been the scalar perturbations as seeds for second-order tensor perturbations, as they are dominant at linear order (see Chapter 3). However, in this work, we present the opposite case, searching for the signature of GWs on cosmic structures. By studying their effect on matter perturbations, we aim to provide a new way to constrain the tensor-to-scalar perturbation ratio on scales where current constraints are poor. We consider scales that entered the Hubble radius after matter-radiation equality, and we will present a more detailed analysis that includes smaller scales in the next chapter. This chapter is based on the paper [141].

4.1 Evolution equation of tensor-induced matter density perturbation in an MD regime

In our analysis, we consider a spatially flat Friedmann-Lematre-Robertson-Walker (FLRW) background metric perturbed up to second order, and choose the gauge as synchronous gauge, one of the most frequently used ones in cosmological perturbation theory [142–144]

$$ds^2 = a^2(\eta)[-d\eta^2 + \gamma_{ij}(\boldsymbol{x},\eta)dx^i dx^j]\,. \tag{4.1.1}$$

For our analysis, we restrict ourselves to a Universe composed of collision-less cold dark matter (CDM) and a cosmological constant, and choose observers co-moving with CDM. By choosing the synchronous and co-moving gauge (which, because of the absence of pressure gradients, can also be made time-orthogonal), we can ensure that the fluid four-velocity is orthogonal to the constant time spatial hypersurfaces with metric γ_{ij}. This means that the four-velocity in this gauge can be expressed as $u_\mu = [-a, 0, 0, 0]$. The conformal spatial metric γ_{ij} is given by

$$\begin{aligned}\gamma_{ij} &= \delta_{ij} + \gamma^{(1)}_{ij} + \frac{1}{2}\gamma^{(2)}_{ij}\,,\\ \gamma^{ij} &= \delta^{ij} - \gamma^{(1)ij} - \frac{1}{2}\gamma^{(2)ij} + \gamma^{(1)ik}\gamma^{(1)j}_{k}\,.\end{aligned} \tag{4.1.2}$$

We take only tensors in the first order perturbation

$$\gamma^{(1)}_{ij} = \chi_{ij}\,, \tag{4.1.3}$$

where

$$\chi^i_i = \partial^i\chi_{ij} = 0\,, \tag{4.1.4}$$

and only tensor-induced scalars in the second order one

$$\gamma^{(2)}_{ij} = -2\phi^{(2)}\delta_{ij} + +D_{ij}\chi^{(2)\parallel}\,. \tag{4.1.5}$$

The fluid deformation tensor is defined by subtracting the isotropic Hubble-flow from the covariant derivative of fluid four-velocity

$$\theta^\mu_\nu = a u^\mu_{;\nu} - \mathcal{H}\delta^\mu_\nu\,. \tag{4.1.6}$$

As u^μ is orthogonal to the spatial hypersurface, θ^μ_ν is purely spatial

$$\theta^i_j = -K^i_j\,, \tag{4.1.7}$$

where K^i_j is the extrinsic curvature of the hypersurface

$$K^i_j = -\frac{1}{2}\gamma^{ik}\gamma'_{kj}\,. \tag{4.1.8}$$

Now the continuity and Raychaudhuri equation read respectively

$$\delta' + (1+\delta)\theta = 0\,, \tag{4.1.9}$$

$$\theta' + \frac{2}{\eta}\theta + \theta^i_j\theta^j_i + \frac{6}{\eta^2}\delta = 0\,, \tag{4.1.10}$$

where θ is the peculiar volume expansion scalar and δ is the matter density contrast. The solution of the continuity equation is

$$\delta(\boldsymbol{x},\eta) = \frac{1+\delta_0(\boldsymbol{x})}{\sqrt{\gamma(\boldsymbol{x},\eta)/\gamma_0(\boldsymbol{x})}} - 1\,, \tag{4.1.11}$$

where $\gamma = \det\gamma_{ij}$. We write the density perturbation as $\delta = \delta^{(1)} + \delta^{(2)}/2$, and similarly for θ. We then get, from Eq. (4.1.11) (see Appendix A),

$$\delta^{(2)} = \frac{1}{2}\Big(\chi^{ij}\chi_{ij} - \chi_0^{ij}\chi_{0ij}\Big) + 3\phi^{(2)}\,. \tag{4.1.12}$$

Here the subscript '0' denotes the value of the variable at the initial time, i.e. the end of inflation. Initial values of the second order variables have been set to zero according to Appendix F.

Now, from Eqs. (4.1.9) and (4.1.10) at second order we get

$$\theta'^{(2)} + \mathcal{H}\theta^{(2)} + 2\theta^{(1)i}_j\theta^{(1)j}_i + 4\pi G a^2\overline{\rho}_m\delta^{(2)} = 0\,, \tag{4.1.13}$$

$$\delta'^{(2)} + 2\delta^{(1)}\theta^{(1)} + \theta^{(2)} = 0\,. \tag{4.1.14}$$

We combine these to get

$$\delta^{(2)''} + \mathcal{H}\delta^{(2)'} - 4\pi G a^2\overline{\rho}_m\delta^{(2)} = \frac{1}{2}\chi'^{ij}\chi'_{ij}\,. \tag{4.1.15}$$

The left-hand side of this equation is similar to the evolution equation for the linear density contrast, which is as expected. However, a source term appears on the right-hand side, which is quadratic in the tensor perturbation modes. Remembering that the GWs energy density is given by

$$\rho_{GW} = \frac{1}{32\pi G a^2}\langle\chi'^{ij}\chi'_{ij}\rangle\,, \tag{4.1.16}$$

it is clear that the quantity sourcing $\delta^{(2)}$ in Eq. (4.1.15) is nothing but the fluctuation of GWs radiation energy density. There are two important observations to make from Eq. (4.1.15). Firstly, since gravitational waves are frozen on scales larger than the horizon, their energy density vanishes in that region. Thus, they can only source second-order CDM perturbations on scales smaller than the horizon. Consequently, our effect does not produce CMB anisotropies on large scales, unlike the linear matter perturbations, which are present everywhere. Secondly, as the density contrast is sourced by the fluctuation of a radiation bath, it is effectively a linear perturbation, despite being derived in second order of perturbation theory. This belief is further validated by solving for it, as we will demonstrate below.

The homogeneous solution, i.e. the standard linear density contrast is

$$\delta^{(2)}_h = c_1\big(\boldsymbol{x}\big)D_+(\eta) + c_2\big(\boldsymbol{x}\big)D_-(\eta)\,. \tag{4.1.17}$$

We apply Green's method to get the sourced density contrast, and the result is

$$\delta^{(2)}_s = D_+(\eta)\int_0^\eta d\tilde{\eta}\frac{D_-(\tilde{\eta})}{W(\tilde{\eta})}\frac{1}{2}\chi'^{ij}\chi'_{ij} - D_-(\eta)\int_0^\eta d\tilde{\eta}\frac{D_+(\tilde{\eta})}{W(\tilde{\eta})}\frac{1}{2}\chi'^{ij}\chi'_{ij}\,, \tag{4.1.18}$$

where D_+, D_- are the linear growing and decaying homogeneous solutions, and $W(\eta) \equiv D_-(\eta)D'_+(\eta) - D_+(\eta)D'_-(\eta)$ is the Wronskian. We can see that the time-behaviour of $\delta^{(2)}$ is the same as $\delta^{(1)}$, confirming our intuition stated above.

4.2 Power-spectrum

Our objective is to investigate the impact of the tensor-induced perturbation on the present-day matter power-spectrum and to determine if this effect is significant and can be detected through its influence on LSS. In order to compute the power-spectrum, we move to Fourier space and write all quantities according to Eqs. (1.2.10), (2.3.3), and (2.3.4). The variable $A_\sigma(\boldsymbol{k})$ is characterized by the following auto-correlation function

$$\langle A_{\sigma_1}(\boldsymbol{k}_1) A_{\sigma_2}(\boldsymbol{k}_2)\rangle = (2\pi)^3 \delta^3(\boldsymbol{k}_1+\boldsymbol{k}_2)\delta_{\sigma_1\sigma_2}\frac{2\pi^2}{k_1^3}\Delta^2_\sigma(k_1)\,, \tag{4.2.1}$$

$\Delta^2_\sigma(k)$ being the power-spectrum for each polarisation. Just like Eq. (1.5.2), we can write the power-spectrum $\Delta^2_{\delta^{(2)}}(k)$ for $\delta^{(2)}$

$$\langle \delta^{(2)}(\boldsymbol{k},\eta)\,\delta^{(2)}(\boldsymbol{k}',\eta)\rangle = (2\pi)^3\delta^3(\boldsymbol{k}+\boldsymbol{k}')\frac{2\pi^2}{k^3}\Delta^2_{\delta^{(2)}}(k)\,. \tag{4.2.2}$$

From Eq. (4.1.18), we can get, using convolution,

$$\begin{aligned}\Delta^2_{\delta^{(2)}}(k) = \frac{k^3}{2\pi}\sum_{\sigma,\sigma'}\int d^3k_2 \frac{\Delta^2_{\sigma'}(k_2)\Delta^2_\sigma(|\boldsymbol{k}-\boldsymbol{k}_2|)}{k_2^3|\boldsymbol{k}-\boldsymbol{k}_2|^3} f(k,k_2,\theta) \\ \times\left[\frac{D_+(\eta)}{2}\int_0^\eta d\tilde\eta\,\frac{D_-(\tilde\eta)}{W(\tilde\eta)}\mathcal{T}'(k_2\tilde\eta)\mathcal{T}'(|\boldsymbol{k}-\boldsymbol{k}_2|\tilde\eta) - \frac{1}{2D_-(\eta)}\int_0^\eta d\tilde\eta\,\frac{D_+(\tilde\eta)}{W(\tilde\eta)}\,\mathcal{T}'(k_2\tilde\eta)\mathcal{T}'(|\boldsymbol{k}-\boldsymbol{k}_2|\tilde\eta)\right]^2 .\end{aligned} \tag{4.2.3}$$

In our analysis, we are interested in scalar modes that entered the horizon during the matter-dominated era. The time integral in the equation above can be split into two parts: one from the end of inflation to matter-radiation equality, and the other from equality to the observation time. For each of these intervals, the growing and decaying solutions for density perturbations and the transfer function for the source GWs should be chosen accordingly. In the first, radiation-dominated part, linear density perturbations involve two modes, $D_+ = \ln\eta$ and $D_- = \text{const.}$, whereas the GW transfer function behaves as $j_0(k\eta)$. While, in the matter era $D_+ = \eta^2$ and $D_- = \eta^{-3}$ and the GW transfer function is proportional to $j_1(k\eta)$. However, the contribution from the first part is negligible compared to the second one. Hence we put $D_+ = \eta^2$ and $D_- = \eta^{-3}$, and $W(\eta) = 5\eta^{-2}$ as the Wronskian. We will consider the effects of dark energy at a later stage. So the final expression for the tensor-sourced CDM density contrast in MD is

$$\delta^{(2)} = \frac{\eta^2}{10}\int_0^\eta d\tilde\eta\,\chi'^{ij}\chi'_{ij} - \frac{1}{10\eta^3}\int_0^\eta d\tilde\eta\,\chi'^{ij}\chi'_{ij}\,. \tag{4.2.4}$$

It can be verified that we will get the same expression from (4.1.12). Eq. (4.2.3) then becomes

$$\Delta^2_{\delta^{(2)}}(k) = \frac{k^3}{2\pi}\sum_{\sigma,\sigma'}\int d^3k_2 \frac{\Delta^2_{\sigma'}(k_2)\Delta^2_{\sigma}(|\boldsymbol{k}-\boldsymbol{k}_2|)}{k_2^3|\boldsymbol{k}-\boldsymbol{k}_2|^3} f(k,k_2,\theta) \times \left[\frac{\eta^2}{10}\int_0^\eta \frac{d\tilde{\eta}}{\tilde{\eta}}\Big(\frac{3j_1(k_2\tilde{\eta})}{k_2\tilde{\eta}}\Big)'\Big(\frac{3j_1(|\boldsymbol{k}-\boldsymbol{k}_2|\tilde{\eta})}{|\boldsymbol{k}-\boldsymbol{k}_2|\tilde{\eta}}\Big)' - \frac{1}{10\eta^3}\int_0^\eta d\tilde{\eta}\,\tilde{\eta}^4\Big(\frac{3j_1(k_2\tilde{\eta})}{k_2\tilde{\eta}}\Big)'\Big(\frac{3j_1(|\boldsymbol{k}-\boldsymbol{k}_2|\tilde{\eta})}{|\boldsymbol{k}-\boldsymbol{k}_2|\tilde{\eta}}\Big)'\right]^2, \tag{4.2.5}$$

where we have defined $f(k,k_2,\theta)$ to be the following contraction of the polarisation tensors

$$f(k,k_2,\theta) \equiv \sum_{\sigma,\sigma'}\epsilon^{\sigma'}_{ij}(\hat{\boldsymbol{k}}_2)\epsilon^{\sigma ij}(\widehat{\boldsymbol{k}-\boldsymbol{k}_2})\epsilon^{\sigma'}_{kl}(-\hat{\boldsymbol{k}}_2)\epsilon^{\sigma kl}(\widehat{-\boldsymbol{k}+\boldsymbol{k}_2}). \tag{4.2.6}$$

Here, the symbol θ represents the angle between the wave-vectors $\hat{\boldsymbol{k}}$ and $\hat{\boldsymbol{k}}_2$. In the convolution expression and in all the subsequent equations, $\boldsymbol{k}$ always refers to the induced scalar modes, while $\boldsymbol{k}_2$ and $(\boldsymbol{k}-\boldsymbol{k}_2)$ correspond to the source GW modes. We follow the usual convention of considering only the growing mode for simplicity.

The contribution from the GWs occurs after they have entered the horizon and started oscillating with an amplitude that decays as $\sim 1/a$. Since we are considering scalar modes that entered the horizon during matter domination, we can safely switch on the sourcing at $\eta = 0$, since at that early time these scalar modes are still super-horizon, and hence are un-triggered. Moreover, since GWs decay after entering the horizon, we can safely consider $\eta \to \infty$ as an upper bound of the time integral, instead of using the exact age of the Universe, since most of the contribution to the integral comes from the time around horizon-entry. the reasons explained above. This allows to solve the integral analytically, in terms of hyper-geometric functions.

Following the same procedure as shown in chapter 3, we introduce the variables $x = k_2/k$, $y = |\boldsymbol{k}-\boldsymbol{k}_2|/k$, and use the dimensionless time variable $\tau = k\tilde{\eta}$. Considering only the growing-mode term in the square brackets of Eq. (4.2.5), we get

$$\Delta^2_{\delta^{(2)}}(k) = \frac{81k^4\eta^4}{100}\int_0^\infty dx \int_{|x-1|}^{x+1} dy (xy)^{-2} f(x,y)\Delta^2_\sigma(xk)\Delta^2_\sigma(yk)\left[\int_0^\infty \frac{d\tau}{\tau^3} j_2(x\tau)j_2(y\tau)\right]^2, \tag{4.2.7}$$

where the function f in terms of x and y now reads

$$f(x,y) = \frac{1}{16x^4y^4}\Big[x^8 + (y^2-1)^4 + 4x^6(7y^2-1) + 4x^2(y^2-1)^2(7y^2-1) + x^4(6-60y^2+70y^4)\Big]. \tag{4.2.8}$$

The wave-vector integration domain, in terms of x and y, is now given by [145] $(x+y) \geq 1 \wedge (x+1) \geq y \wedge (y+1) \geq x$.

We would like to emphasize that while our density contrast modes strictly in the matter domination regime, we integrate over the entire frequency range of GWs modes in the calculation of Eq. (4.2.7). We use the relevant transfer functions as depicted in Eq. (4.2.5) despite them being valid only for tensor

modes that entered the horizon during matter domination. We have checked that tensor modes entering during radiation domination have an insignificant contribution, compared to the same entering in the matter domination.

4.3 Result for different GWs sources

The power-spectrum of the stochastic GWs background varies based on the mechanism responsible for its generation. Here, our main focus is on inflationary models, which exhibit either a monochromatic spectrum, a blue tensor spectrum, or a Gaussian bump. Additionally, we restrict our consideration to parity-invariant mechanisms for GWs production. This allows us to assume that both polarizations of GWs produce the same effect. We defer the analysis of parity-breaking early Universe models to future studies. We will now proceed to quantify the effect of different input GWs signals on the matter power-spectrum given by Eq. (4.2.7). The power-spectrum for each individual polarization mode is related to the GWs power-spectrum through the following relation: $\Delta^2_\sigma(k) = (1/2)\Delta^2_T(k)$.

On CMB scales, the amplitude of GWs is tightly constrained by the non-detection of B-mode polarization (as discussed in Chapter 1). However, these constraints are limited to a specific range of scales, and it is not possible to extract limits on other scales from these bounds. This leaves open the possibility of observing GWs at other scales using interferometer experiments, which could provide complementary information on the nature and amplitude of the GWs background. As we move away from the scales probed by the CMB, the constraints on the amplitude of the GWs background become less stringent. This means that we have more freedom to choose larger values for their amplitude. However, we should keep in mind that even if the current constraints on the GW background at these scales are weaker, future observations may provide stronger bounds. Below we discuss our results for some large-amplitude GWs models.

4.3.1 Power-law spectrum

As a first benchmark signal, we consider a power-law spectrum, which is typical of many single-field inflationary models [13]

$$\Delta^2_T(k_2) = A_T \left(\frac{k_2}{k_*}\right)^{n_T} . \tag{4.3.1}$$

On super-horizon scales, standard single-field, slow-roll inflationary models predict a power-spectrum that is nearly scale-invariant. This means that the amplitude of the scalar and tensor perturbations generated during inflation should be roughly constant across different scales. The tensor spectral index, denoted by n_T, is related to the slow-roll parameter ϵ and is predicted to be -2ϵ. As we want a

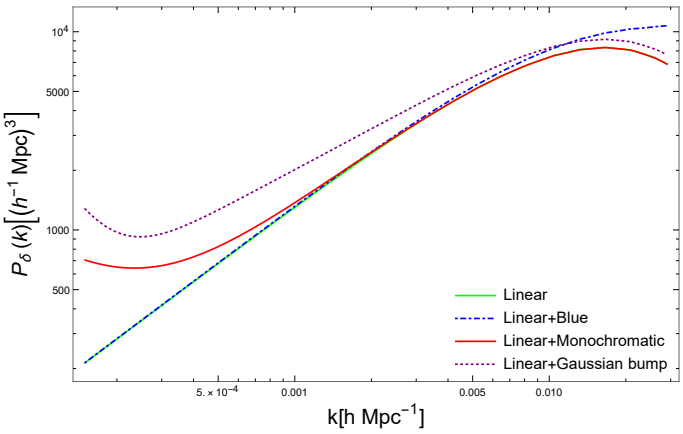

Figure 4.1: *Impact of different GWs power-spectrum on the matter power-spectrum: i) blue-tilted* $\left(A_T = 1.26\times10^{-10}, n_T = 0.32, k_* = k_{\rm CMB} = 0.01{\rm Mpc}^{-1}\right)$, *ii) monochromatic* $\left(A_T = 10^{-5}, k_* = 0.008{\rm Mpc}^{-1}\right)$, *iii) Gaussian bump* $\left(A_T = 10^{-5}, \sigma = 2, k_p = 0.04{\rm Mpc}^{-1}\right)$. *The value of h is fixed at* 0.68*[5].*

large amount of GWs for our purpose, we consider a blue spectrum, which rises on small scales, but is normalised to the Planck data. Relaxing the single-field slow-roll consistency condition $n_T = -r/8$, and adding LIGO-Virgo data to further constrain GWs, [71] obtained a limit of $r_{0.01} < 0.066$ (at 95% Confidence Level (C.L.), PLANCK TT,TE,EE+lowE+lensing+BK15+LIGO&Virgo2016), constraining $-0.76 < n_T < 0.52$. We consider the case of a blue-tilted tensor power-spectrum, choosing $n_T = 0.32$, which is still within the range of values allowed by present and future GW interferometers [71, 146], and fix the GW power-spectrum amplitude at $A_T = rA_s = 0.06\times2.1\times10^{-9} = 1.26\times10^{-10}$.

4.3.2 Monochromatic Spectrum

An illustrative example is a monochromatic tensor spectrum, which can be seen as an estimate of a spectrum with a distinct narrow peak. We previously observed this type of peak in the context of an SIGW background in Chapter 3. In light of this example, we aim to obtain an equation for the matter power-spectrum assuming a Dirac delta peak in the input GWs spectrum

$$\Delta_T^2(k_2) = A_T\,\delta\left(\ln\frac{k_2}{k_*}\right). \tag{4.3.2}$$

Typical models that predict such a spectrum are [147]. In this case, the form of the power-spectrum can be found analytically and it reads

$$\Delta^2_{\delta^{(2)}}(k) \quad = 4\times10^{-5}\left(k\,\eta_0\right)^4 A_T^2\left(\tfrac{8k_*^2}{k^2} + \tfrac{k^6}{16k_*^6} - \tfrac{k^4}{2k_*^4} + 3\tfrac{k^2}{k_*^2} - 8\right)\Theta(2k_* - k)\,, \tag{4.3.3}$$

where the condition $k < 2k_*$ comes from momentum conservation, similar to the SIGW case.

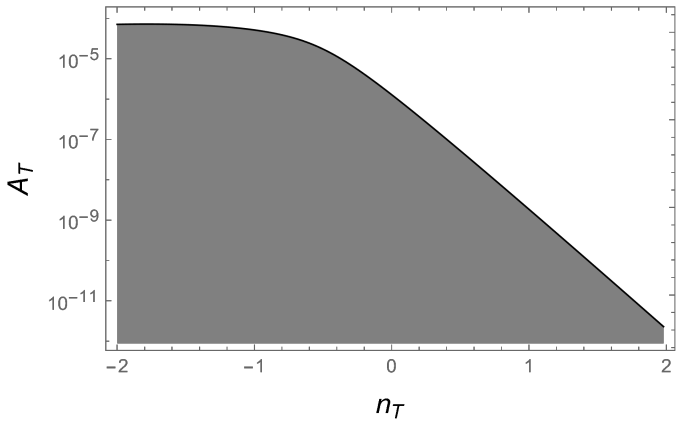

Figure 4.2: *The region of parameter space for n_T and A_T where the power-spectrum of the GW-sourced density perturbation mode with the wave-number $k = 0.006\,\mathrm{Mpc}^{-1}$ obeys a 4% error bound on the linear matter power-spectrum for a power-law GW source. The grey region shows the allowed range of the parameters assuming the mentioned error uncertainty.*

4.3.3 Gaussian-bump spectrum

A well-motivated early Universe scenario which predicts a large and characteristic amplitude for the GW spectrum consists in a GW signal endowed with a large Gaussian bump. An example where we see this kind of bump is an axion field coupled to SU(2) gauge fields as spectator fields besides the inflaton [148–150]. The GWs signal produced by the additional axion-gauge sector has several characteristic features, like non-Gaussianity, scale-dependence, and chirality (here we are going to restrict ourselves to non-chiral waves only). Such models result in GWs which are amplified at the same level as the scalar perturbation and so they are possible targets both for CMB B-mode observations [150] and interferometers [146, 151]. Therefore, for our purposes, one can study their signatures on the matter power-spectrum as another way to test or constrain such early Universe scenarios. The tensor power-spectrum is characterized by the following Gaussian bump

$$\Delta_T^2(k_2) = A_T e^{-\frac{1}{2\sigma^2}\ln^2\left(\frac{k_2}{k_p}\right)}\,. \tag{4.3.4}$$

Fig. 4.1 displays both the standard matter power-spectrum and the one that includes the effects computed in the present study. These scalar modes induced by tensor perturbations are statistically uncorrelated with the standard adiabatic density perturbations. Therefore, the total matter power-spectrum is simply the sum of the power-spectra from the two components. The plot shows the dimensional power-spectrum of matter, which is related to the dimensionless $\Delta^2_{\delta^{(2)}}(k)$ obtained from Eq. (4.2.7), through the relation $P_{\delta^{(2)}}(k) = (2\pi^2/k^3)\Delta^2_{\delta^{(2)}}(k)$. It is evident that different input power-spectrum give rise to contributions of different shapes, and they are relevant at different scales.

All of our previous analyses have assumed that the Universe was dominated by CDM after the matter-radiation equality epoch. However, if we choose a value of Ω_m different from 1, it results in a different

linear growth factor D_+ (as seen in Eqs. (4.1.17) and (4.1.18)), which in turn suppresses the matter growth. To account for this suppression, we can use a fitting formula for the growth suppression factor of linear density perturbations given in [152, 153]

$$\frac{\delta^{(2)}\left(z=0,\Omega_m\right)}{\delta^{(2)}\left(z=0,\Omega_m=1\right)} \simeq \frac{5}{2}\Omega_m\left[\Omega_m^{4/7}-1+\Omega_m+\left(1+\frac{\Omega_m}{2}\right)\left(1+\frac{1-\Omega_m}{70}\right)\right]^{-1}. \tag{4.3.5}$$

Using $\Omega_m = 0.32$ [5], we find our suppressed power-spectrum to be

$$\frac{P_{\delta^{(2)}}\left(z=0,\Omega_m=0.32\right)}{P_{\delta^{(2)}}\left(z=0,\Omega_m=1\right)} \simeq 0.59\,. \tag{4.3.6}$$

The effect of the dark energy component has already been incorporated into the results shown in Fig. 4.1. We obtain the parameter space shown in Fig. 4.2 by calculating Eq. (4.2.7) as a function of A_T and n_T for a power-law GW spectrum Eq. (4.3.1), and considering a 4% error bound with respect to the linear matter power-spectrum at $k = 0.006\text{Mpc}^{-1}$. The grey region in the figure indicates the range of n_T and A_T that is allowed within the mentioned error bound.

4.4 Summary

In this study, we have investigated the impact of "tensor-induced scalar modes" on the matter power-spectrum in the present-day Universe. Our analysis reveals that a significant GW power-spectrum can leave an imprint on the matter power-spectrum. One notable characteristic of our second-order matter perturbation is that it does not contribute to super-horizon scales, in contrast to linear matter perturbations, and thus, does not generate CMB temperature anisotropy on large scales, although it may have some effect on smaller scales (examined in Chapter 5). Moreover, on sub-horizon scales, our matter density contrast closely resembles the linear one and can be considered as a linear perturbation induced by gravitational radiation that vanishes outside the horizon. Additionally, we presented the parameter space for the tensor spectral index versus the GW amplitude, considering the uncertainties in the measurement of the matter power-spectrum. Our results indicate that this signature could provide a new and valuable way to detect and constrain GWs on a range of scales that are presently poorly understood and to improve the accuracy of matter power-spectrum estimation.

The correction to the density contrast sourced by GWs can be an indirect probe of GWs, and in the case of non-detection, it can help to constrain the amplitude of the same. Future LSS surveys such as Euclid [154], DESI [155], SPHEREx [156], SKA [157], Roman Space Telescope [158] and Vera Rubin Observatory (LSST)[159] are extremely good candidates for this purpose.

Chapter 5

Complete Analytical Study of Primordial Gravitational Waves-sourced Dark Matter and Radiation Density Perturbations

In the previous chapter, only the matter-dominated era was examined, which covered scales that entered the horizon after the matter-radiation equality. However, in order to fully understand and interpret the effect, it is necessary to expand the study to include smaller scales.

In this chapter, we investigate the same effect during the radiation-dominated era, taking into consideration the density perturbation modes that entered the horizon from the end of inflation up to the matter epoch. Finally, we present the expression for the tensor-induced CDM and radiation contrast modes that entered the Hubble radius during the matter era and their evolution during the late phase dominated by dark energy.

It should be noted that previous studies, such as [81] and [160], focused on second-order perturbations in synchronous gauge for scalar-tensor and tensor-tensor couplings during the radiation domination era. However, these studies made the assumption that radiation is the main component in both the background and perturbations throughout the entire radiation epoch. In contrast, our paper provides a comprehensive analysis of the second-order density contrast, which is sourced solely by linear GWs, while taking into account the entire radiation epoch up to matter-radiation equality. Additionally, we investigate the phenomenon during late times when the contribution of dark energy to the background energy density becomes significant. Our study is both complete and fully analytical, which paves the way for future numerical treatment of the problem. This chapter is based on the paper [161].

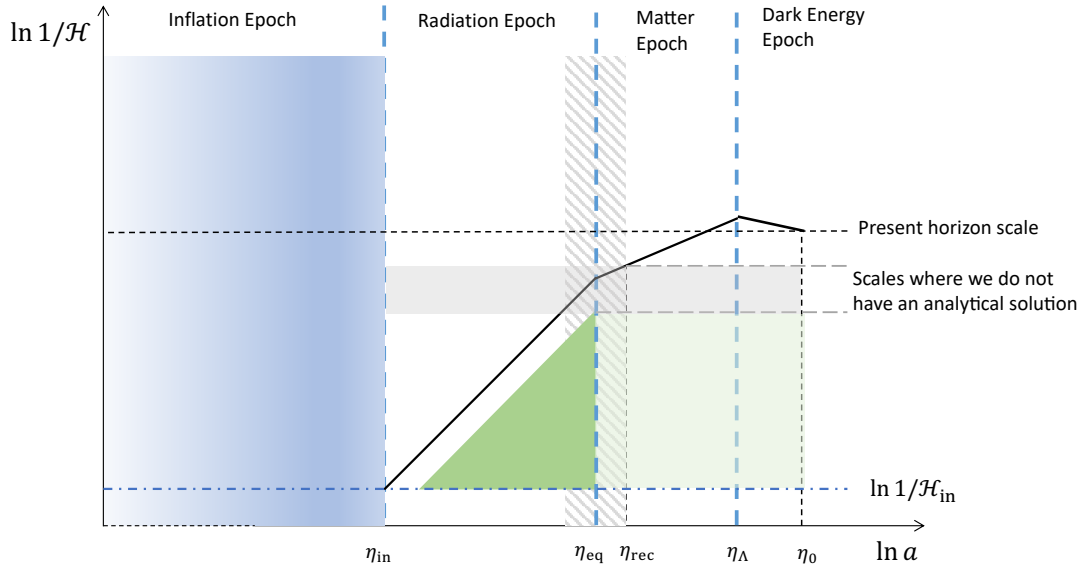

Figure 5.1: We show a plot of $\ln 1/\mathcal{H}$ versus $\ln a$ in the different epochs analyzed in this work, separated by a blue vertical dashed line. The solid black curve indicates the evolution of the modes that cross the horizon from the end of inflation until today, the black dashed line shows the extrapolation of the present horizon scale. The green region highlights sub-horizon scales during the radiation epoch in which Einsteins field equations are governed by the matter perturbations generated only by linear gravitational waves (discussed in Section 5.3). The area above the green region indicates all modes during the deep radiation epoch (for details see Section 5.2). The light-green area describes these sub-horizon scales, related to the green region described above, during matter and dark energy epochs (discussed in Section 5.5). The gray shaded area denotes those scales where we do not have an analytical solution. The dashed-dot blue line shows the horizon scale at the end of inflation.

5.1 Tensor-sourced scalar perturbations in a Universe with radiation and CDM

5.1.1 Perturbations in the metric and matter components

We begin by introducing the notation and conventions used for metric and matter perturbations. In the previous chapter, the focus was solely on a Universe dominated by CDM and a cosmological constant, where the absence of a pressure gradient in the matter sector allowed for the direct application of a synchronous, time-orthogonal, and co-moving (with CDM) gauge, as seen in [102]. However, in the presence of radiation, a more general approach may be required. Therefore, in this chapter, we begin with a co-moving and time-orthogonal gauge with CDM, setting δg_{0i} to zero and performing calculations in the rest frame of CDM. Nonetheless, as demonstrated later, our gauge becomes synchronous again in

our specific choice of perturbations that rely solely on the linear tensor contribution.

Phases of evolution				
Dominant component	Deep radiation epoch (Section 5.2)	Radiation epoch in sub-horizon scales (Section 5.3)	Intermediate regime (matter+radiation) for $1/\eta_{\rm rec} \lesssim k \lesssim 1/\eta_{\rm eq}$ (no analytical solutions)	After recombination (Section 5.5)
In background	radiation	radiation	radiation + CDM	CDM + DE
Dominant perturbation component	$\delta_{\rm r}^{(2)}$	$\delta_{\rm m}^{(2)}$	$\delta_{\rm m}^{(2)}$ & $\delta_{\rm r}^{(2)}$	$\delta_{\rm m}^{(2)}$

Table 5.1: The dominant component in different phases of evolution in the background and perturbation sector (see also Fig. 5.1).

In the time-orthogonal gauge, the perturbed flat FLRW metric is given by [31]

$$ds^2 = a^2(\eta)\left[-\big(1+2\psi\big)d\eta^2 + \gamma_{ij}\big(\boldsymbol{x},\eta\big)dx^i dx^j\right] . \tag{5.1.1}$$

The spatial metric γ_{ij} contains both second-order scalar and linear tensor modes, while again we ignore linear scalar and vector modes, which are statistically independent from tensor-sourced scalar modes and can be set to zero. At second order, there are scalar, vector, and tensor contributions, and their governing equations have source terms quadratic in the first-order perturbations with respect to scalars. These source terms mix linear scalars and tensors (i.e., "tensor fossils," tensor-induced vector and tensor modes [87, 102]), and scalar modes originating from linear tensors. Here, we focus on the contribution from scalar modes originating from linear tensors, which is our main interest and will be discussed in the following (see also [162, 163]). In the following, we show the decomposition of the metric components

$$\psi = \frac{\psi^{(2)}}{2}, \tag{5.1.2}$$

$$\gamma_{ij} = \delta_{ij} + \chi_{ij}^{(1)} - \phi^{(2)}\delta_{ij} + \frac{1}{2}D_{ij}\chi^{(2)||}, \tag{5.1.3}$$

$$\gamma^{ij} = \delta^{ij} - \chi^{ij(1)} + \phi^{(2)}\delta^{ij} - \frac{1}{2}D^{ij}\chi^{(2)||} + \chi^{ik(1)}\chi_k{}^{j(1)} . \tag{5.1.4}$$

The matter component of the Universe in this section is a combination of irrotational dust, with which the observer is co-moving, and radiation. It is important to note that perturbations in the energy-momentum tensor of the matter components are only sourced by the contribution related to primordial GWs. Both the irrotational dust and radiation are perfect fluids, as we assume that the coupling between baryons and radiation is neglected. We plan to investigate the significance of this coupling in future work. The energy-momentum tensor of the matter components can be expressed as: $T_{\mu\nu} = \big(\rho + p\big)u_\mu u_\nu + p g_{\mu\nu}$. Here $\rho_{\rm r}$, $\rho_{\rm m}$, and $p_{\rm r}$ are the energy density of radiation and matter respectively, and pressure of radiation (here we are assuming $p_{\rm m} = 0$), and ${u_{\rm r}}^\mu$ and ${u_{\rm m}}^\mu$ are their respective four-velocities, normalised as

$u_\mu u^\mu = -1$. Its components are, for matter

$$\begin{aligned} u_{\mathrm{m}0} &= -a\,(1+\psi)\ , \\ u_{\mathrm{m}}{}^{0} &= \frac{1}{a}\,(1-\psi)\ , \\ u_{\mathrm{m}}{}^{i} &= 0\,, \end{aligned} \tag{5.1.5}$$

and for radiation

$$\begin{aligned} u_{\mathrm{r}0} &= -a\,(1+\psi)\ , \\ u_{\mathrm{r}}{}^{0} &= \frac{1}{a}\,(1-\psi)\ , \\ u_{\mathrm{r}i} &= a\,v_{\mathrm{r}i} = a\,v_{\mathrm{r},i}\,, \\ u_{\mathrm{r}}{}^{i} &= \frac{1}{a}\,v_{\mathrm{r}}{}^{i} = \frac{1}{a}\,v_{\mathrm{r}}{}^{,i}\,. \end{aligned} \tag{5.1.6}$$

Here $_{,i} = \partial_i$ is used to indicate a derivative w.r.t. x^i, and v_{r} is the velocity potential of radiation.

5.1.2 Conservation equations

The energy-momentum tensors of the radiation and CDM components interact only gravitationally, thus satisfying the conservation laws $T^{\alpha\beta}{}_{;\beta} = 0$ separately. These conservation equations yield continuity and momentum conservation equations for $\alpha = 0$ and $\alpha = i$, respectively. The next two subsections will derive the contribution of tensor-scalar perturbations within the CDM and radiation components.

5.1.2.1 Conservation equation for matter

If we assume that the observer is co-moving with the CDM component, then the energy-momentum tensor of a pressure-free matter can be expressed as

$$\begin{aligned} T^{00}_{\mathrm{m}} &= \rho_{\mathrm{m}} u^0_{\mathrm{m}} u^0_{\mathrm{m}} = \frac{\overline{\rho}_{\mathrm{m}}\,(1+\delta_{\mathrm{m}})}{a^2}\,(1-2\psi)\ , \\ T^{ij}_{\mathrm{m}} &= T^{0i}_{\mathrm{m}} = 0\,, \end{aligned} \tag{5.1.7}$$

where $\delta_{\mathrm{m}} = (\rho_{\mathrm{m}} - \overline{\rho}_{\mathrm{m}})/\overline{\rho}_{\mathrm{m}}$ is the density contrast of CDM. At second order, the evolution equations for the density contrast are obtained from energy-momentum conservation

$$\delta^{(2)\prime}_{\mathrm{m}} - \gamma^{(1)ik}\gamma^{(1)\prime}_{ki} + \frac{1}{2}\delta^{ik}\gamma^{(2)\prime}_{ki} = 0\,. \tag{5.1.8}$$

Considering only tensor contribution at the first order, the evolution second-order density contrast reads

$$\delta^{(2)\prime}_{\mathrm{m}} = \frac{1}{2}\Big(\chi^{ij}\chi_{ij} + 6\phi^{(2)}\Big)^{\prime}\,, \tag{5.1.9}$$

and, consequently, we have

$$\delta^{(2)}_{\mathrm{m}} = \frac{1}{2}\Big(\chi^{ij}\chi_{ij} - \chi^{ij}_0\chi_{0ij}\Big) + 3\left(\phi^{(2)} - \phi^{(2)}_0\right) + \delta^{(2)}_{\mathrm{m}0}\,. \tag{5.1.10}$$

Following the analysis made in Appendix F we can set $\phi_0^{(2)}$ and $\delta_{\rm m0}^{(2)}$ equal to zero, and we can simply rewrite Eq. (5.1.10) in the following way

$$\delta_{\rm m}^{(2)} = \frac{1}{2}\Big(\chi^{ij}\chi_{ij} - \chi_0^{ij}\chi_{0ij}\Big) + 3\phi^{(2)}\,. \tag{5.1.11}$$

Note that this expression has exactly the same form as that obtained in Eq. (4.1.12), where the tensor-sourced matter perturbation in the co-moving (with CDM) and synchronous gauge, during the epoch of matter domination was studied (see also [102, 162]).

From the momentum conservation for matter

$$\partial^i\psi^{(2)} + 2\partial^i\psi^{(1)}\delta_{\rm m}^{(1)} - 4\psi^{(1)}\partial^i\psi^{(1)} = 0\,, \tag{5.1.12}$$

we can infer that $\psi^{(2)}$ is only influenced by the first-order scalar modes, which implies that ψ is negligible for our purposes. As a result, even though we started from the time-orthogonal gauge, we can directly express our equations in the synchronous gauge.

5.1.2.2 Conservation equation for radiation

According to the discussion in the last section, ψ can be ignored from hereon. The components of the energy-momentum tensor of radiation are

$$\begin{aligned} T_{\rm r}^{00} &= \frac{\overline{\rho}_{\rm r}(1+\delta_{\rm r})}{a^2}\,,\\ T_{\rm r}^{0i} &= \frac{4\overline{\rho}_{\rm r}}{3a^2}{v_{\rm r}}^{,i}\,,\\ T_{\rm r}^{ij} &= \frac{\overline{\rho}_{\rm r}(1+\delta_{\rm r})}{3a^2}\gamma^{ij}\,. \end{aligned} \tag{5.1.13}$$

From the continuity equation we have

$$\delta_{\rm r}^{(2)\prime} - \frac{4}{3}\chi^{(1)ij}\chi_{ij}^{(1)\prime} + \frac{4}{3}\nabla^2 v_{\rm r}^{(2)} - 4\phi^{(2)\prime} = 0\,. \tag{5.1.14}$$

Whereas the momentum conservation equation gives

$$4v_{\rm r}^{(2)\prime} + \delta_{\rm r}^{(2)} = 0\,. \tag{5.1.15}$$

5.1.3 Einstein equations

After the end of inflation, although radiation dominates the energy density of the background, it decays faster than CDM, leading to CDM becoming the main contributor to the energy density of the Universe at the matter-radiation equality. Thus, towards the end of radiation domination, the energy density of CDM ($\overline{\rho}_{\rm m}$) cannot be ignored anymore. During the end of the radiation era, similar to the linear case, the perturbative contribution of the CDM component may become greater than that of the radiation

component. In this study, we will also investigate this possibility and analyze the behavior of each component in detail during the radiation epoch and at the matter-radiation equality.

In this section, our main focus is on the evolution of the tensor-sourced CDM perturbation $\delta_{\rm m}^{(2)}$ in the presence of a perturbed radiation component, while considering adiabatic perturbations only. We use the metric (5.1.2) and stress-energy tensor decomposition (5.1.5). Keeping in mind the discussion in 5.1.2.1 that ψ effectively vanishes in our case, we can write the second-order Einstein equations. The 00-th, $0i$-th, and ij-th Einstein equations become

$$\nabla^2\phi^{(2)} + \frac{1}{2}\chi^{ij}\nabla^2\chi_{ij} - 3\mathcal{H}\phi^{(2)\prime} + \frac{1}{6}\nabla^2\nabla^2\chi^{||(2)} - \frac{1}{8}\chi^{ij\prime}\chi'_{ij} - \mathcal{H}\chi^{ij}\chi'_{ij} + \frac{3}{8}\chi^{kl,i}\chi_{kl,i} - \frac{1}{4}\chi^{ik,l}\chi_{li,k} = 4\pi G a^2(\overline{\rho}_{\rm m}\delta_{\rm m}^{(2)} + \overline{\rho}_{\rm r}\delta_{\rm r}^{(2)})\,, \tag{5.1.16}$$

$$\phi^{(2)\prime}{}_{,i} - \frac{1}{2}\chi^{jk}\chi'_{ki,j} + \frac{1}{4}D_{ij}\chi^{||(2),j\prime} + \frac{1}{2}\chi^{jk}\chi'_{jk,i} + \frac{1}{4}\chi^{jk\prime}\chi_{jk,i} = -\frac{16\pi G a^2}{3}\overline{\rho}_{\rm r}v^{(2)}_{{\rm r},i}\,, \tag{5.1.17}$$

$$\frac{1}{4}D_{ij}\chi^{||(2)\prime\prime} + \frac{\mathcal{H}}{2}D_{ij}\chi^{||(2)\prime} + \frac{1}{12}\nabla^2 D_{ij}\chi^{||(2)} - \frac{1}{18}\nabla^2\nabla^2\chi^{||(2)}\delta_{ij} + 2\mathcal{H}\phi^{(2)\prime}\delta_{ij} + \phi^{(2)\prime\prime}\delta_{ij} + \frac{1}{2}D_{ij}\phi^{(2)} - \frac{1}{3}\nabla^2\phi^{(2)}\delta_{ij} - \frac{1}{2}\chi^{kl}(\chi_{lj,ik} + \chi_{il,jk} - \chi_{ij,lk} - \chi_{kl,ij}) + \frac{1}{4}\chi^{kl}{}_{,j}\chi_{kl,i} - \frac{1}{2}\chi^{jk,l}\chi_{li,k} + \frac{1}{2}\chi^{jk,l}\chi_{ki,l} - \frac{3}{8}\chi^{kl,p}\chi_{kl,p}\delta_{ij} + \frac{1}{4}\chi^{kp,l}\chi_{lp,k}\delta_{ij} - \frac{1}{2}\chi_j^{k\prime}\chi_{ki}{}' + \frac{3}{8}\chi^{kl\prime}\chi_{kl}{}'\delta_{ij} = \frac{4\pi G\overline{\rho}_{\rm r}a^2}{3}\delta_{\rm r}^{(2)}\delta_{ij}\,. \tag{5.1.18}$$

In the Einstein equations, we have also used the evolution equation of the linear GWs

$$\chi_{ij}{}'' + 2\mathcal{H}\chi_{ij}{}' - \nabla^2\chi_{ij} = 0\,. \tag{5.1.19}$$

We are ignoring any effect related to the anisotropic stress tensor. Decomposing (5.1.18) into a trace equation and a trace-less one, the trace part becomes

$$\phi^{(2)\prime\prime} + 2\mathcal{H}\phi^{(2)\prime} - \frac{1}{3}\nabla^2\phi^{(2)} - \frac{1}{18}\nabla^2\nabla^2\chi^{||(2)} - \frac{1}{8}\chi^{kl,i}\chi_{kl,i} + \frac{1}{12}\chi^{ik,l}\chi_{li,k} + \frac{5}{24}\chi^{kl\prime}\chi_{kl}{}' + \frac{1}{6}\chi^{kl}\nabla^2\chi_{kl} = \frac{4\pi G\overline{\rho}_{\rm r}a^2}{3}\delta_{\rm r}^{(2)}\,. \tag{5.1.20}$$

The next sections are divided into two regimes: the deep radiation regime immediately after inflation, and the period leading up to matter-radiation equality. These two regimes have different dynamics depending on the dominant contributor to the background matter component as well as to the perturbation content. The sub-horizon evolution is the focus of our study since the GWs radiation that generates our second-order perturbations only exists in this regime, as stated in Chapter 4. Below, we will present a complete solution for the density contrast for modes that evolve (always in the sub-horizon regime) throughout radiation domination, including contributions from both phases. However, we would like to emphasize that for completeness, we have also conducted a comprehensive analysis of the deep radiation-dominated Universe for all scales in Appendix D.

5.2 Einstein equations in the deep radiation-dominated Universe

During the early stages of radiation domination, the energy density of the radiation component greatly exceeds that of the CDM component, which means that only the radiation component (sourced by tensors) contributes to the perturbations of the stress-energy tensor in the Einstein equations. These perturbations are sourced by tensors. As a result, the continuity equation Eq. (5.1.11) can be used to obtain the CDM perturbation from the potential, which is obtained as a solution to the Einstein equations.

In this phase of evolution, discarding the CDM perturbation, (5.1.16), (5.1.17), (5.1.18) become

$$\nabla^2\phi^{(2)} + \frac{1}{2}\chi^{ij}\nabla^2\chi_{ij} - 3\mathcal{H}\phi^{(2)\prime} + \frac{1}{6}\nabla^2\nabla^2\chi^{||(2)} - \frac{1}{8}\chi^{ij\prime}\chi_{ij}{}' - \mathcal{H}\chi^{ij}\chi_{ij}{}' + \frac{3}{8}\chi^{kl,i}\chi_{kl,i} - \frac{1}{4}\chi^{ik,l}\chi_{li,k} = \frac{3\mathcal{H}^2}{2}\delta_{\rm r}^{(2)}\,, \tag{5.2.1}$$

$$\phi^{(2)\prime}_{,i} - \frac{1}{2}\chi^{jk}\chi_{ki,j}{}' + \frac{1}{4}D_{ij}\chi^{||(2),j\prime} + \frac{1}{2}\chi^{jk}\chi_{jk,i}{}' + \frac{1}{4}\chi^{jk\prime}\chi_{jk,i} = -2\mathcal{H}^2 v^{(2)}_{{\rm r},i}\,, \tag{5.2.2}$$

$$\begin{aligned}&\frac{1}{4}D_{ij}\chi^{||(2)\prime\prime} + \frac{\mathcal{H}}{2}D_{ij}\chi^{||(2)\prime} + \frac{1}{12}\nabla^2 D_{ij}\chi^{||(2)} - \frac{1}{18}\nabla^2\nabla^2\chi^{||(2)}\delta_{ij}\\ &+ 2\mathcal{H}\phi^{(2)\prime}\delta_{ij} + \phi^{(2)\prime\prime}\delta_{ij} + \frac{1}{2}D_{ij}\phi^{(2)} - \frac{1}{3}\nabla^2\phi^{(2)}\delta_{ij} - \frac{1}{2}\chi^{kl}(\chi_{lj,ik} + \chi_{il,jk} - \chi_{ij,lk} - \chi_{kl,ij})\\ &+ \frac{1}{4}\chi^{kl}{}_{,j}\chi_{kl,i} - \frac{1}{2}\chi^{jk,l}\chi_{li,k} + \frac{1}{2}\chi^{jk,l}\chi_{ki,l} - \frac{3}{8}\chi^{kl,p}\chi_{kl,p}\delta_{ij} + \frac{1}{4}\chi^{kp,l}\chi_{lp,k}\delta_{ij}\\ &- \frac{1}{2}\chi^{k\prime}{}_{j}\chi_{ki}{}' + \frac{3}{8}\chi^{kl\prime}\chi_{kl}{}'\delta_{ij} = \frac{\mathcal{H}^2}{2}\delta_{\rm r}^{(2)}\delta_{ij}\,.\end{aligned} \tag{5.2.3}$$

Let us point out that $\delta_{\rm m}^{(2)} \ll \delta_{\rm r}^{(2)}$ is not assumed in this period; rather we take on that $\delta^{(2)}\rho_{\rm m}$ is negligible w.r.t. $\delta^{(2)}\rho_{\rm r}$. This assumption is only valid for the regime discussed in this section. The trace part becomes

$$\begin{aligned}&\phi^{(2)\prime\prime} + 2\mathcal{H}\phi^{(2)\prime} - \frac{1}{3}\nabla^2\phi^{(2)} - \frac{1}{18}\nabla^2\nabla^2\chi^{||(2)} - \frac{1}{8}\chi^{kl,i}\chi_{kl,i} + \frac{1}{12}\chi^{ik,l}\chi_{li,k} + \frac{5}{24}\chi^{kl\prime}\chi_{kl}{}'\\ &+ \frac{1}{6}\chi^{kl}\nabla^2\chi_{kl} = \frac{\mathcal{H}^2}{2}\delta_{\rm r}^{(2)}\,.\end{aligned} \tag{5.2.4}$$

Trace-less part of (5.2.3) gives

$$\begin{aligned}&D_{ij}\phi^{(2)} + \frac{1}{2}D_{ij}\chi^{||(2)\prime\prime} + \mathcal{H}D_{ij}\chi^{||(2)\prime} + \frac{1}{6}\nabla^2 D_{ij}\chi^{||(2)}\\ &- \chi^{kl}(\chi_{lj,ik} + \chi_{il,jk} - \chi_{ij,lk} - \chi_{kl,ij}) + \frac{1}{2}\chi^{kl}{}_{,j}\chi_{kl,i} - \chi^{jk,l}\chi_{li,k} + \chi^{jk,l}\chi_{ki,l}\\ &- \chi^{k\prime}_{j}\chi_{ki}{}' - \frac{1}{3}\chi^{kl}\nabla^2\chi_{kl}\delta_{ij} + \frac{1}{3}\chi^{kl\prime}\chi_{kl}{}'\delta_{ij} - \frac{1}{2}\chi^{kl,p}\chi_{kl,p}\delta_{ij} + \frac{1}{3}\chi^{kp,l}\chi_{lp,k}\delta_{ij} = 0.\end{aligned} \tag{5.2.5}$$

Replacing $\nabla^2\nabla^2\chi^{||(2)}$ from (5.2.4) in (5.2.1), and using (5.1.14) and (5.1.15), we get a third order differential equation of radiation velocity potential

$$v_{\rm r}^{(2)\prime\prime\prime} + \mathcal{H}v_{\rm r}^{(2)\prime\prime} - 4\mathcal{H}^2 v_{\rm r}^{(2)\prime} - \frac{1}{3}\nabla^2 v_{\rm r}^{(2)\prime} - \frac{\mathcal{H}}{3}\nabla^2 v_{\rm r}^{(2)} + \frac{1}{6}\chi^{kl\prime}\chi_{kl}{}' = 0\,. \tag{5.2.6}$$

In Fourier space[1] the same equation turns out

$$v_{\mathrm{r}\boldsymbol{k}}^{(2)\prime\prime\prime} + \mathcal{H} v_{\mathrm{r}\boldsymbol{k}}^{(2)\prime\prime} + \Big(\frac{k^2}{3} - 4\mathcal{H}^2\Big) v_{\mathrm{r}\boldsymbol{k}}^{(2)\prime} + \frac{\mathcal{H} k^2}{3} v_{\mathrm{r}\boldsymbol{k}}^{(2)} = S_{\boldsymbol{k}}. \tag{5.2.7}$$

where $S_{\boldsymbol{k}}$ is the Fourier transformation of the source term $-(1/6)\chi^{kl\prime}\chi_{kl}{}'$, i.e.

$$S_{\boldsymbol{k}}(\eta) = -\frac{1}{6}\sum_{\sigma,\sigma'}\int \frac{d^3q}{(2\pi)^3} A_{\sigma'}(\boldsymbol{q}) A_{\sigma}\left(\boldsymbol{k}-\boldsymbol{q}\right) \epsilon_{ij}^{\sigma'}(\hat{\boldsymbol{q}}) \epsilon^{\sigma ij} \left(\widehat{\boldsymbol{k}-\boldsymbol{q}}\right) \mathcal{T}'\left(q,\eta\right) \mathcal{T}'\left(|\boldsymbol{k}-\boldsymbol{q}|,\eta\right) \tag{5.2.8}$$

and the amplitude and transfer function of the tensor have been defined according to Chapter 2.3. Introducing a new definition

$$u_{\mathrm{r}\boldsymbol{k}}^{(2)} = v_{\mathrm{r}\boldsymbol{k}}^{(2)\prime} + \mathcal{H} v_{\mathrm{r}\boldsymbol{k}}^{(2)} = \frac{(a v_{\mathrm{r}\boldsymbol{k}}^{(2)})'}{a}\,,$$

we have[2]

$$u_{\mathrm{r}\boldsymbol{k}}^{(2)\prime\prime} + \Big(\frac{k^2}{3} - 2\mathcal{H}^2\Big) u_{\mathrm{r}\boldsymbol{k}}^{(2)} = S_{\boldsymbol{k}}\,, \tag{5.2.9}$$

which reduces (5.2.7) to a second-order equation. As we are interested in the regime $k\eta \gg 1$, this further simplifies to[3]

$$u_{\mathrm{r}\boldsymbol{k}}^{(2)\prime\prime} + \frac{k^2}{3} u_{\mathrm{r}\boldsymbol{k}}^{(2)} = S_{\boldsymbol{k}}\,. \tag{5.2.10}$$

The solution to this equation is

$$\begin{aligned} u_{\mathrm{r}\boldsymbol{k}}^{(2)}(\eta) = {} & A(\boldsymbol{k}) \cos\frac{k\eta}{\sqrt{3}} + B(\boldsymbol{k}) \sin\frac{k\eta}{\sqrt{3}} + \frac{\sqrt{3}}{k} \sin\frac{k\eta}{\sqrt{3}} \int_{\eta_{\mathrm{in}}}^{\eta} d\tilde{\eta}\, \cos\frac{k\tilde{\eta}}{\sqrt{3}}\, S_{\boldsymbol{k}}(\tilde{\eta}) \\ & - \frac{\sqrt{3}}{k} \cos\frac{k\eta}{\sqrt{3}} \int_{\eta_{\mathrm{in}}}^{\eta} d\tilde{\eta}\, \sin\frac{k\tilde{\eta}}{\sqrt{3}}\, S_{\boldsymbol{k}}(\tilde{\eta})\,, \end{aligned} \tag{5.2.11}$$

where $A(\boldsymbol{k})$ and $B(\boldsymbol{k})$ depend on the initial conditions at $\eta = \eta_{\mathrm{in}}$. Here η_{in} is indicating the end of inflation (i.e. the “last scattering" surface for gravitons).

Under the assumptions of initial adiabatic conditions and the synchronous co-moving gauge, and considering that all modes are outside the horizon at the initial time η_{in}, there is no initial source or contribution to the second-order perturbation of the GW density. Therefore, we can neglect the homogeneous solutions and derive the following results

$$v_{\mathrm{r}\boldsymbol{k}}^{(2)} = \frac{\sqrt{3}}{k^3\tau} \int_{\tau_{\mathrm{in}}}^{\tau} \tilde{\tau} d\tilde{\tau} \left[\int_{\tau_{\mathrm{in}}}^{\tilde{\tau}} d\tilde{\tilde{\tau}} \left(\sin\frac{\tilde{\tau}}{\sqrt{3}} \cos\frac{\tilde{\tilde{\tau}}}{\sqrt{3}} - \cos\frac{\tilde{\tau}}{\sqrt{3}} \sin\frac{\tilde{\tilde{\tau}}}{\sqrt{3}}\right) S_{\boldsymbol{k}}(\tilde{\tilde{\tau}}/k)\right]\,, \tag{5.2.12}$$

where we have defined $\tau = k\eta$. Here, we have ignored the integration constant as $v_{\mathrm{r}\boldsymbol{k}}^{(2)}(\eta_{\mathrm{in}}) = 0$, for the reason explained above. Finally, using the relation (5.1.15), the radiation density perturbation turns out

$$\delta_{\mathrm{r}}^{(2)}(\boldsymbol{k},\tau) = \frac{12}{k^2\tau^2} \int_{\tau_{\mathrm{in}}}^{\tau} d\tilde{\tau}\, \tilde{\tau} S_{\boldsymbol{k}}(\tilde{\tau}/k)$$

[1] Throughout this work, we use two notations for Fourier space representation of a generic variable $X(\boldsymbol{x})$: $X_{\boldsymbol{k}}$, or $X(\boldsymbol{k},\eta)$. Both are equivalent expressions.

[2] In principle, we can introduce another variable $\theta = \sqrt{3}/2a$, and solve the system according to the procedure demonstrated in [164]. In that case, we have $\left[\theta^2 (u_{\mathrm{r}\boldsymbol{k}}^{(2)}/\theta)'\right]' + c_{\mathrm{s}}^2 \theta k^2 u_{\mathrm{r}\boldsymbol{k}}^{(2)} = -\theta S_{\boldsymbol{k}}$.

[3] Without this approximation, the results for tensor-sourced scalar quantities like potential and density contrast derived in [81] can be accurately recovered with the help of the variable $u_{\mathrm{r}\boldsymbol{k}}^{(2)}$. See Appendix D for details.

$$- \frac{4\sqrt{3}}{k^2}\left[\left(1-\frac{3}{\tau^2}\right)\sin\frac{\tau}{\sqrt{3}}+\frac{\sqrt{3}}{\tau}\cos\frac{\tau}{\sqrt{3}}\right]\int_{\tau_{\rm in}}^{\tau} d\tilde{\tau}\,\cos\frac{\tilde{\tau}}{\sqrt{3}}\,S_{\boldsymbol{k}}(\tilde{\tau}/k)$$
$$+ \frac{4\sqrt{3}}{k^2}\left[\left(1-\frac{3}{\tau^2}\right)\cos\frac{\tau}{\sqrt{3}}-\frac{\sqrt{3}}{\tau}\sin\frac{\tau}{\sqrt{3}}\right]\int_{\tau_{\rm in}}^{\tau} d\tilde{\tau}\,\sin\frac{\tilde{\tau}}{\sqrt{3}}\,S_{\boldsymbol{k}}(\tilde{\tau}/k)\,. \tag{5.2.13}$$

On sub-Hubble scales, this expression can be further simplified. In fact, for $\tau(=k\eta)\gg 1$, we find

$$\delta_{\rm r}^{(2)}(\boldsymbol{k},\tau) = \frac{12}{k^2\tau^2}\int_{\tau_{\rm in}}^{\tau} d\tilde{\tau}\,\tilde{\tau}S_{\boldsymbol{k}}(\tilde{\tau}) - \frac{4\sqrt{3}}{k^2}\left[\sin\frac{\tau}{\sqrt{3}}+\frac{\sqrt{3}}{\tau}\cos\frac{\tau}{\sqrt{3}}\right]\int_{\tau_{\rm in}}^{\tau} d\tilde{\tau}\,\cos\frac{\tilde{\tau}}{\sqrt{3}}\,S_{\boldsymbol{k}}(\tilde{\tau})$$
$$+ \frac{4\sqrt{3}}{k^2}\left[\cos\frac{\tau}{\sqrt{3}}-\frac{\sqrt{3}}{\tau}\sin\frac{\tau}{\sqrt{3}}\right]\int_{\tau_{\rm in}}^{\tau} d\tilde{\tau}\,\sin\frac{\tilde{\tau}}{\sqrt{3}}\,S_{\boldsymbol{k}}(\tilde{\tau})\,. \tag{5.2.14}$$

Now, from (5.1.14), we get

$$\phi^{(2)}(\boldsymbol{k},\eta) = -v_{\rm r}^{(2)\prime}(\boldsymbol{k},\eta) - \frac{1}{6}\left[\mathcal{X}_{\boldsymbol{k}}(\eta)-\mathcal{X}_{\boldsymbol{k}}(\eta_{\rm in})\right] - \frac{k^2}{3}\int_{\eta_{\rm in}}^{\eta} d\tilde{\eta}\,v_{\rm r}\,, \tag{5.2.15}$$

where $\mathcal{X}_{\boldsymbol{k}}$ is the Fourier transform of $\chi^{kl}\chi_{kl}$, i.e.

$$\mathcal{X}_{\boldsymbol{k}}(\eta) = \sum_{\sigma,\sigma'}\int\frac{d^3q}{(2\pi)^3}A_{\sigma'}(\boldsymbol{q})A_{\sigma}\left(|\boldsymbol{k}-\boldsymbol{q}|\right)\epsilon_{ij}^{\sigma'}(\hat{\boldsymbol{q}})\epsilon^{\sigma ij}\left(\widehat{|\boldsymbol{k}-\boldsymbol{q}|}\right)\mathcal{T}\left(q,\eta\right)\mathcal{T}\left(|\boldsymbol{k}-\boldsymbol{q}|,\eta\right)\,. \tag{5.2.16}$$

Finally, using (5.1.11) and (5.2.15), we have the expression for $\delta_{\rm m}^{(2)}$. Precisely, using

$$\delta_{\rm m}^{(2)}(\boldsymbol{k},\eta) = -3v_{\rm r}^{(2)\prime} - k^2\int_{\eta_{\rm in}}^{\eta} d\tilde{\eta}\,v_{\rm r}\,, \tag{5.2.17}$$

we obtain

$$\delta_{\rm m}^{(2)}(\boldsymbol{k},\tau) = \frac{1}{k^2}\left(\frac{9}{\tau^2}-3\ln\tau\right)\int_{\tau_{\rm in}}^{\tau} d\tilde{\tau}\,\tilde{\tau}S_{\boldsymbol{k}}(\tilde{\tau}/k) - \frac{1}{k^2}\left[3\sqrt{3}\left(1-\frac{3}{\tau^2}+\ln\tau\right)\sin\frac{\tau}{\sqrt{3}}\right.$$
$$\left.+\left(\frac{9}{\tau^2}-3\ln\tau\right)\tau\cos\frac{\tau}{\sqrt{3}}\right]\int_{\tau_{\rm in}}^{\tau} d\tilde{\tau}\,\cos\frac{\tilde{\tau}}{\sqrt{3}}S_{\boldsymbol{k}}(\tilde{\tau}/k) - \frac{1}{k^2}\left[-3\sqrt{3}\left(1-\frac{3}{\tau^2}+\ln\tau\right)\right.$$
$$\left.\times\cos\frac{\tau}{\sqrt{3}}+\left(\frac{9}{\tau^2}-3\ln\tau\right)\tau\sin\frac{\tau}{\sqrt{3}}\right]\int_{\tau_{\rm in}}^{\tau} d\tilde{\tau}\,\sin\frac{\tilde{\tau}}{\sqrt{3}}S_{\boldsymbol{k}}(\tilde{\tau}/k)$$
$$+\frac{\sqrt{3}}{k^2}\int_{\tau_{\rm in}}^{\tau} d\tilde{\tau}\,\tilde{\tau}\ln\tilde{\tau}\left[\sin\frac{\tilde{\tau}}{\sqrt{3}}\int_{\tau_{\rm in}}^{\tilde{\tau}} d\tilde{\tilde{\tau}}\,\cos\frac{\tilde{\tilde{\tau}}}{\sqrt{3}}S_{\boldsymbol{k}}(\tilde{\tilde{\tau}}/k) - \cos\frac{\tilde{\tau}}{\sqrt{3}}\int_{\tau_{\rm in}}^{\tilde{\tau}} d\tilde{\tilde{\tau}}\,\sin\frac{\tilde{\tilde{\tau}}}{\sqrt{3}}S_{\boldsymbol{k}}(\tilde{\tilde{\tau}}/k)\right]\,. \tag{5.2.18}$$

Imposing again that $\tau = k\eta \gg 1$, it becomes

$$\delta_{\rm m}^{(2)}(\boldsymbol{k},\tau) = -\frac{3}{k^2}\ln\tau\int_{\tau_{\rm in}}^{\tau} d\tilde{\tau}\,\tilde{\tau}\,S_{\boldsymbol{k}}(\tilde{\tau}/k)$$
$$-\frac{1}{k^2}\left[3\sqrt{3}\left(1+\ln\tau\right)\sin\frac{\tau}{\sqrt{3}}-3\tau\ln\tau\cos\frac{\tau}{\sqrt{3}}\right]\int_{\tau_{\rm in}}^{\tau} d\tilde{\tau}\,\cos\frac{\tilde{\tau}}{\sqrt{3}}S_{\boldsymbol{k}}(\tilde{\tau}/k)$$
$$+\frac{1}{k^2}\left[3\sqrt{3}\left(1+\ln\tau\right)\cos\frac{\tau}{\sqrt{3}}+3\tau\ln\tau\sin\frac{\tau}{\sqrt{3}}\right]\int_{\tau_{\rm in}}^{\tau} d\tilde{\tau}\,\sin\frac{\tilde{\tau}}{\sqrt{3}}S_{\boldsymbol{k}}(\tilde{\tau}/k)$$
$$+\frac{\sqrt{3}}{k^2}\int_{\tau_{\rm in}}^{\tau} d\tilde{\tau}\,\tilde{\tau}\ln\tilde{\tau}\left[\sin\frac{\tilde{\tau}}{\sqrt{3}}\int_{\tau_{\rm in}}^{\tilde{\tau}} d\tilde{\tilde{\tau}}\,\cos\frac{\tilde{\tilde{\tau}}}{\sqrt{3}}S_{\boldsymbol{k}}(\tilde{\tilde{\tau}}/k) - \cos\frac{\tilde{\tau}}{\sqrt{3}}\int_{\tau_{\rm in}}^{\tilde{\tau}} d\tilde{\tilde{\tau}}\,\sin\frac{\tilde{\tilde{\tau}}}{\sqrt{3}}S_{\boldsymbol{k}}(\tilde{\tilde{\tau}}/k)\right]\,. \tag{5.2.19}$$

In addition, the potential can be obtained using (5.1.11). Then it reduces to

$$\begin{aligned}\phi^{(2)}(\boldsymbol{k},\tau) = &-\frac{1}{k^2}\ln\tau\int_{\tau_{\rm in}}^{\tau} d\tilde{\tau}\,\tilde{\tau}\,S_{\boldsymbol{k}}(\tilde{\tau}/k) - \frac{1}{6}\left(\mathcal{X}_{\boldsymbol{k}}(\eta) - \mathcal{X}_{\boldsymbol{k}}(\eta_{\rm in})\right)\\ &- \frac{1}{k^2}\left[\sqrt{3}\,(1+\ln\tau)\sin\frac{\tau}{\sqrt{3}} - \tau\ln\tau\cos\frac{\tau}{\sqrt{3}}\right]\int_{\tau_{\rm in}}^{\tau} d\tilde{\tau}\,\cos\frac{\tilde{\tau}}{\sqrt{3}}S_{\boldsymbol{k}}(\tilde{\tau}/k)\\ &+ \frac{1}{k^2}\left[\sqrt{3}\,(1+\ln\tau)\cos\frac{\tau}{\sqrt{3}} + \tau\ln\tau\sin\frac{\tau}{\sqrt{3}}\right]\int_{\tau_{\rm in}}^{\tau} d\tilde{\tau}\,\sin\frac{\tilde{\tau}}{\sqrt{3}}S_{\boldsymbol{k}}(\tilde{\tau}/k)\\ &+ \frac{1}{\sqrt{3}k^2}\int_{\tau_{\rm in}}^{\tau}\tilde{\tau}\ln\tilde{\tau}\left[\sin\frac{\tilde{\tau}}{\sqrt{3}}\int_{\tau_{\rm in}}^{\tilde{\tau}} d\tilde{\tilde{\tau}}\,\cos\frac{\tilde{\tilde{\tau}}}{\sqrt{3}}S_{\boldsymbol{k}}(\tilde{\tilde{\tau}}/k) - \cos\frac{\tilde{\tau}}{\sqrt{3}}\int_{\tau_{\rm in}}^{\tilde{\tau}} d\tilde{\tilde{\tau}}\,\sin\frac{\tilde{\tilde{\tau}}}{\sqrt{3}}S_{\boldsymbol{k}}(\tilde{\tilde{\tau}}/k)\right]d\tilde{\tau}\,.\end{aligned} \tag{5.2.20}$$

In this section we have discussed the epoch where the matter perturbation $\delta^{(2)}\rho_{\rm m}$ is negligible compared to its radiation counterpart, $\delta^{(2)}\rho_{\rm r}$. Looking at (5.2.14) and (5.2.19) one can realise that, as time progresses, the contribution of the CDM perturbation begins to become dominant with respect to that of the radiation. Comparing the absolute value of each additive term of in Eqs. (5.2.14) and (5.2.19), we note that, for example, terms proportional to

$$\int_{\tau_{\rm in}}^{\tau} d\tilde{\tau}\,\cos\frac{\tilde{\tau}}{\sqrt{3}}S_{\boldsymbol{k}}(\tilde{\tau}/k), \quad \int_{\tau_{\rm in}}^{\tau} d\tilde{\tau}\,\sin\frac{\tilde{\tau}}{\sqrt{3}}S_{\boldsymbol{k}}(\tilde{\tau}/k) \quad \text{or} \quad \int_{\tau_{\rm in}}^{\tau} d\tilde{\tau}\,\tilde{\tau}S_{\boldsymbol{k}}(\tilde{\tau}/k)$$

have an extra multiplicative factor which is proportional to τ, $\ln\tau$ and/or $\tau\ln\tau$ in $\delta_{\rm m}^{(2)}$, which are missing in $\delta_{\rm r}^{(2)}$. Then, $\delta_{\rm r}^{(2)}$ has extra terms which decays like

$$\sim\frac{1}{\tau}\cos\frac{\tilde{\tau}}{\sqrt{3}} \quad \text{or} \quad \sim\frac{1}{\tau}\sin\frac{\tilde{\tau}}{\sqrt{3}},$$

which are absent in $\delta_{\rm m}^{(2)}$. Finally, Eq. (5.2.19) includes other additional contributions (they are integrals that contain complicated sine or cosine functions that multiply the terms proportional to $\ln\tau$. Note that we are in the regime $\tau \gg 1$). These extra terms could also cause a faster growth of $\delta_{\rm m}^{(2)}$ w.r.t $\delta_{\rm r}^{(2)}$. In conclusion, these facts suggest the existence of a suitable time η and scale (through k) in which $\delta^{(2)}\rho_{\rm m}$ becomes of the same order as $\delta^{(2)}\rho_{\rm r}$.

Let us introduce a new variable

$$F(\boldsymbol{k},\eta) \equiv \frac{\delta^{(2)}\rho_{\rm m}(\boldsymbol{k},\eta)}{\delta^{(2)}\rho_{\rm r}(\boldsymbol{k},\eta)} = \frac{\bar{\rho}_{\rm m}(\eta)}{\bar{\rho}_{\rm r}(\eta)}\frac{\delta_{\rm m}^{(2)}(\boldsymbol{k},\eta)}{\delta_{\rm r}^{(2)}(\boldsymbol{k},\eta)}\,. \tag{5.2.21}$$

When the value of F approaches unity, indicating that $\delta^{(2)}\rho_{\rm m}$ and $\delta^{(2)}\rho_{\rm r}$ are of the same order, the contribution from matter perturbations starts to become dominant over that of radiation, even if the average density of matter $\bar{\rho}_{\rm m}$ is smaller than that of radiation $\bar{\rho}_{\rm r}$. This marks the onset of a new phase of dynamical evolution, where the time-time component of Einstein's field equations is primarily governed by the matter perturbations $\delta_{\rm m}^{(2)}$.

The next section will provide a detailed discussion on how to properly set the initial conditions for this new phase. It should be noted that the analysis in the subsequent sections requires matching the

solutions of the two phases at a specific conformal time $\eta = \eta_\alpha$, where $F(\boldsymbol{k}, \eta_\alpha) \equiv \alpha \simeq O(1)$ for a fixed value of $\boldsymbol{k}$ and for $\tau \gg 1$. The value of α is chosen to set the initial conditions for the solutions at $\eta \geq \eta_\alpha$. As discussed earlier, for $\eta > \eta_\alpha$, F has a value greater than α, based on the respective evolution of matter and radiation density perturbations. The appearance of this "new phase" during the radiation-dominated era at $k\eta \gg 1$ is a novel finding that has not been explored in previous studies of second order perturbations.

5.3 Sub-horizon evolution towards matter-radiation equality

In the previous section, we discussed how during the deep radiation epoch, the matter perturbation is determined by the potential sourced by primordial GWs, but does not affect the potential itself. However, as we approach the second phase of perturbation evolution, for modes that entered the Hubble radius during the radiation-dominated epoch, $\bar{\rho}_{\rm m}\delta^{(2)}{\rm m}$ grows sufficiently to surpass $\bar{\rho}{\rm r}\delta^{(2)}{\rm r}$ as the main contributor to Einstein's field equations, even though $\bar{\rho}{\rm m} \ll \bar{\rho}_{\rm r}$. In this section, we will derive the second-order differential equation governing the evolution of $\delta^{(2)}_{\rm m}$, which can be thought of as a new Meszaros equation due to the contribution of GWs.

As we approach the matter-radiation equality epoch, the contribution of $\bar{\rho}_{\rm m}$ can no longer be ignored, and it becomes convenient to use the variable $y = a/a_{\rm eq}$ as the evolution variable instead of η or a. Here, $a_{\rm eq} = a(\eta_{\rm eq})$ is the value of the scale factor when $\bar{\rho}_{\rm m}(a_{\rm eq}) = \bar{\rho}_{\rm r}(a_{\rm eq})$.

Trivially, this implies that

$$y = \frac{a}{a_{\rm eq}} = \frac{\bar{\rho}_{\rm m}}{\bar{\rho}_{\rm r}} \,.$$

Using y, the background dynamics can be described by the Friedmann equations in the following way

$$\mathcal{H}^2 = \mathcal{H}^2_{\rm eq}\frac{y+1}{2y^2} = k^2_{\rm eq}\frac{y+1}{2y^2} \qquad \text{and} \qquad \mathcal{H}' = -k^2_{\rm eq}\frac{2+y}{4y^2} \,, \tag{5.3.1}$$

where

$$k_{\rm eq} \equiv \mathcal{H}_{\rm eq} = a_{\rm eq}H_{\rm eq} \,, \qquad \mathcal{H}^2_{\rm eq} = \frac{8\pi G}{3}\bar{\rho}_{\rm eq}a^2_{\rm eq} \qquad \text{and} \qquad \bar{\rho}_{\rm eq} = 2\bar{\rho}_{\rm m}(a_{\rm eq}) \,.$$

In terms of y, Einstein equations (5.1.16), (5.1.17) and (5.1.18) become, respectively

$$\begin{aligned} &-3\mathcal{H}^2 y\frac{d\phi^{(2)}}{dy} + \nabla^2\phi^{(2)} + \frac{1}{6}\nabla^2\nabla^2\chi^{||(2)} - \frac{1}{8}\left(\mathcal{H}y\right)^2\frac{d\chi^{ij}}{dy}\frac{d\chi^{ij}}{dy} - \mathcal{H}^2 y\chi^{ij}\frac{d\chi^{ij}}{dy} + \frac{3}{8}\chi^{kl,i}\chi_{kl,i} \\ &-\frac{1}{4}\chi^{ik,l}\chi_{li,k} + \frac{1}{2}\chi^{ij}\nabla^2\chi_{ij} = \frac{3\mathcal{H}^2}{2(1+y)}\left(y\delta^{(2)}_{\rm m} + \delta^{(2)}_{\rm r}\right) \,, \end{aligned} \tag{5.3.2}$$

$$\frac{d\phi^{(2)}}{dy}_{,i} - \frac{1}{2}\chi^{jk}\frac{d\chi_{ki,j}}{dy} + \frac{1}{4}D_{ij}\frac{d\chi^{||(2),j}}{dy} + \frac{1}{2}\chi^{jk}\frac{d\chi_{jk,i}}{dy} + \frac{1}{4}\frac{d\chi^{jk}}{dy}\chi_{jk,i} = -\frac{2\mathcal{H}}{y(1+y)}v^{(2)}_{{\rm r},i} \,, \tag{5.3.3}$$

$$\mathcal{H}y\left[\mathcal{H}y\frac{d^2}{dy^2} + \left(\mathcal{H} + y\frac{d\mathcal{H}}{dy}\right)\frac{d}{dy}\right]\left(\frac{1}{4}D_{ij}\chi^{||(2)} + \phi^{(2)}\delta_{ij}\right) + \frac{\mathcal{H}^2 y}{2}D_{ij}\frac{d\chi^{||(2)}}{dy} + \frac{1}{12}\nabla^2 D_{ij}\chi^{||(2)}$$

$$
\begin{aligned}
&-\frac{1}{18}\nabla^2\nabla^2\chi^{||(2)}\delta_{ij}+2\mathcal{H}^2y\frac{d\phi^{(2)}}{dy}\delta_{ij}+\frac{1}{2}D_{ij}\phi^{(2)}-\frac{1}{3}\nabla^2\phi^{(2)}\delta_{ij}-\frac{1}{2}\chi^{kl}\left(\chi_{lj,ik}+\chi_{il,jk}\right.\\
&\left.-\chi_{ij,lk}-\chi_{kl,ij}\right)+\frac{1}{4}\chi^{kl}{}_{,j}\chi_{kl,i}-\frac{1}{2}\chi^{jk,l}\chi_{li,k}+\frac{1}{2}\chi^{jk,l}\chi_{ki,l}-\frac{3}{8}\chi^{kl,p}\chi_{kl,p}\delta_{ij}+\frac{1}{4}\chi^{kp,l}\chi_{lp,k}\delta_{ij}\\
&-\frac{\mathcal{H}^2y^2}{2}\frac{d\chi^k_j}{dy}\frac{d\chi_{ki}}{dy}+\frac{3\mathcal{H}^2y^2}{8}\frac{d\chi^{kl}}{dy}\frac{d\chi_{kl}}{dy}\delta_{ij}=\frac{\mathcal{H}^2}{2(1+y)}\delta^{(2)}_{\rm r}\delta_{ij}\,.
\end{aligned}
\tag{5.3.4}
$$

Its trace part is

$$
\begin{aligned}
&\mathcal{H}y\left[\mathcal{H}y\frac{d^2}{dy^2}+\left(\mathcal{H}+y\frac{d\mathcal{H}}{dy}\right)\frac{d}{dy}\right]\phi^{(2)}+2\mathcal{H}^2y\frac{d\phi^{(2)}}{dy}-\frac{1}{3}\nabla^2\phi^{(2)}-\frac{1}{18}\nabla^2\nabla^2\chi^{||(2)}\\
&-\frac{1}{8}\chi^{kl,i}\chi_{kl,i}+\frac{1}{12}\chi^{ik,l}\chi_{li,k}+\frac{5\mathcal{H}^2y^2}{24}\frac{d\chi^{kl}}{dy}\frac{d\chi_{kl}}{dy}+\frac{1}{6}\chi^{kl}\nabla^2\chi_{kl}=\frac{\mathcal{H}^2}{2(1+y)}\delta^{(2)}_{\rm r}\,.
\end{aligned}
\tag{5.3.5}
$$

Taking $\nabla^2\nabla^2\chi^{||(2)}$ from (5.3.2), and putting it in (5.3.5), we get

$$
\begin{aligned}
&\left[\mathcal{H}^2y^2\frac{d^2}{dy^2}+\left(2\mathcal{H}^2y+\mathcal{H}y^2\frac{d\mathcal{H}}{dy}\right)\frac{d}{dy}\right]\phi^{(2)}+\frac{\mathcal{H}^2y^2}{6}\frac{d\chi^{kl}}{dy}\frac{d\chi_{kl}}{dy}-\frac{1}{3}\mathcal{H}^2y\chi^{ij}\frac{d\chi^{ij}}{dy}+\frac{1}{3}\chi^{ij}\nabla^2\chi_{ij}\\
&=\frac{\mathcal{H}^2}{2(1+y)}\left(y\delta^{(2)}_{\rm m}+2\delta^{(2)}_{\rm r}\right)\,.
\end{aligned}
\tag{5.3.6}
$$

From Eq. (5.3.6), we can see that when $y\delta^{(2)}_{\rm m}\gg 2\delta^{(2)}_{\rm r}$, i.e., when $\bar\rho_{\rm m}\delta^{(2)}_{\rm m}=\delta\rho^{(2)}_{\rm m}\gg 2\bar\rho_{\rm r}\delta^{(2)}_{\rm r}=2\delta\rho^{(2)}_{\rm r}$, we can neglect $\delta^{(2)}_{\rm r}$. Now, according to the discussion at the end of the previous section, after the matter perturbation surpasses the radiation perturbation, i.e., when $F\simeq O(1)$, we can no longer neglect the contribution of the radiation perturbation. At the same time, we can actually discard $\delta^{(2)}_{\rm r}$ from the evolution equations when $F\simeq 2$, as shown in Eq. (5.3.6). Here, for simplicity and without loss of generality, we assume that F is positive. Therefore, at a fixed scale (e.g., at a given value of k), the beginning of this new phase is indicated by the range of values $1\lesssim F(\eta_\alpha,k)=\alpha\lesssim 2$. To set the initial condition at $\eta=\eta_\alpha$, we need to impose α between 1 and 2. However, we cannot determine the exact value of α with our current analytical approach. A numerical treatment would be necessary to obtain the exact value of α, which is beyond the scope of this work. Note that α should also depend on the cosmological parameters and the matter component of the Universe. In Fig. 5.1, the green and light-green regions, for $\eta\leq\eta_{\rm rec}$, highlight the modes and particular period that we analyze in this section, i.e., at each sub-horizon mode with $k\geq k_{\rm eq}$ and $\eta\geq\eta_\alpha$ up to recombination.

Now, using the definition of F, see Eq. (5.2.21), we are setting the initial conditions $y_\alpha=a(\eta_\alpha)/a_{\rm eq}$ which is defined, in implicit manner, from the following relation

$$
y_\alpha\delta^{(2)}_{\rm m}(y_\alpha)=\alpha\delta^{(2)}_{\rm r}(y_\alpha)\,.
\tag{5.3.7}
$$

By introducing y as a variable and using Eqs. (5.1.11) and (5.1.19), we can see that the evolution of the matter perturbation $\delta^{(2)}_{\rm m}$ during the second phase of radiation domination (i.e. for $y\geq y_\alpha$) is determined by the following second-order equation

$$
\frac{d^2\delta^{(2)}_{\rm m}}{dy^2}+\frac{2+3y}{2y(y+1)}\frac{d\delta^{(2)}_{\rm m}}{dy}-\frac{3}{2y(y+1)}\delta^{(2)}_{\rm m}=\frac{1}{2}\frac{d\chi^{ij}}{dy}\frac{d\chi_{ij}}{dy}\,.
\tag{5.3.8}
$$

This can be seen as a reformulation of the Meszaros equation [165], which describes the evolution of subhorizon matter perturbations. The left-hand side of the equation is exactly the same as the Meszaros equation, while the right-hand side contains a source term quadratic in tensors. It is worth noting that this is not surprising, since in this phase, $\delta_{\rm m}^{(2)}$ replaces $\delta_{\rm r}^{(2)}$ as the source of the Einstein equations, similar to the behavior observed in their linear counterparts. More information on the derivation can be found in references such as [38, 166]. Obviously, for the two solutions to the homogeneous equation, we find the same of Meszaros

- $D_1(y) = y + \frac{2}{3}$,
- $D_2(y) = D_1(y) \ln \frac{\sqrt{1+y}+1}{\sqrt{1+y}-1} - 2\sqrt{1+y}$.

It should be noted that these solutions are correct both during the epoch of radiation $y \ll 1$ (when $y \geq y_\alpha$) and of matter (for $y \gg 1$). Indeed, in matter era, they go as y and $y^{-3/2}$ respectively, whereas in radiation era (i.e., for $y_\alpha \lesssim y \ll 1$), they behave as a constant and $\ln y$. In conclusion, taking also into account the particular solution, the general solution of the matter perturbation $\delta_m^{(2)}$, on sub-horizon scales, takes the form

$$\delta_{\rm m}^{(2)}(\boldsymbol{x}, y) = P_1(\boldsymbol{x}) D_1(y) + P_2(\boldsymbol{x}) D_2(y) + \frac{1}{2} \int_{y_\alpha}^{y} d\tilde{y}\, G(y, \tilde{y}) \frac{d\chi^{ij}}{d\tilde{y}} \frac{d\chi_{ij}}{d\tilde{y}} \,, \tag{5.3.9}$$

where $G(y, \tilde{y})$ is the Green's function

$$\begin{aligned} G(y, \tilde{y}) = &- \frac{1}{4} \tilde{y} \sqrt{1+\tilde{y}} \left[6 \Big(\sqrt{1+\tilde{y}}(2+3y) - \sqrt{1+y}(2+3\tilde{y}) \Big) \right. \\ &\left. - (2+3\tilde{y})(2+3y) \ln \frac{(\sqrt{1+\tilde{y}}+1)(\sqrt{1+y}-1)}{(\sqrt{1+\tilde{y}}-1)(\sqrt{1+y}+1)} \right] \,, \end{aligned} \tag{5.3.10}$$

and $P_1(\boldsymbol{x})$, $P_2(\boldsymbol{x})$ are two time-independent functions. Let us rename the Fourier transformation of Eq. (5.3.9) as $\delta^{(2)}_{\rm m(Tmesz)}(\boldsymbol{k}, y)$, which can be written as

$$\delta^{(2)}_{\rm m(Tmesz)}(\boldsymbol{k}, y) = P_1(\boldsymbol{k}) D_1(y) + P_2(\boldsymbol{k}) D_2(y) + \frac{1}{2} \int_{y_\alpha}^{y} d\tilde{y}\, G(y, \tilde{y}) F_1(\boldsymbol{k}, \tilde{y}) \,, \tag{5.3.11}$$

where $F_1(\boldsymbol{k}, y)$ is the Fourier transform of $d\chi^{ij}/dy\, d\chi_{ij}/dy$, i.e.

$$\begin{aligned} F_1(\boldsymbol{k}, y) = &\sum_{\sigma,\sigma'} \int \frac{d^3q}{(2\pi)^3} A_{\sigma'}(\boldsymbol{q}) A_\sigma\left(\boldsymbol{k}-\boldsymbol{q}\right) \\ &\times \epsilon^{\sigma'}_{ij}(\hat{\boldsymbol{q}}) \epsilon^{\sigma ij}\left(\widehat{\boldsymbol{k}-\boldsymbol{q}}\right) \frac{d\mathcal{T}\left(q, y\right)}{dy} \frac{d\mathcal{T}\left(|\boldsymbol{k}-\boldsymbol{q}|, y\right)}{dy} \,. \end{aligned} \tag{5.3.12}$$

Note immediately that, using Eq. (5.3.1), we can easily relate the definition of F_1 with $S_{\boldsymbol{k}}$ in the following way

$$F_1(\boldsymbol{k}, y) = \frac{-12}{k_{\rm eq}^2 (y+1)} S_{\boldsymbol{k}} \,. \tag{5.3.13}$$

To obtain the full solution, which describes the evolution of $\delta_{\rm m}^{(2)}$ at all epochs, from the deep radiation to CDM era, at a given $k > k_{\rm eq}$, we need to know the value of P_1, P_2. As we are aware, the above solution, Eq. (5.3.11), is valid only for $y \geq y_\alpha$. At $y = y_\alpha$, we have

$$\delta^{(2)}_{\rm m(Tmesz)}(\boldsymbol{k}, y_\alpha) = P_1(\boldsymbol{k}) D_1(y_\alpha) + P_2(\boldsymbol{k}) D_2(y_\alpha)\,.$$

Consequently, we should analyse the matching conditions at $y = y_\alpha$. Then we need the solution of matter perturbation and its derivative obtained both during deep radiation epoch and in this second phase of radiation domination. The next section will be devoted to the study of the initial condition of Eq. (5.3.9).

Before concluding this section, in order to have a complete picture of the dynamics at these scales, it is also useful to get an expression for the radiation density contrast (for the complete derivation, see Appendix E)

$$\begin{aligned}
\delta^{(2)}_{\rm r(Tmesz)}(\boldsymbol{k}, y) =& A_{\rm r}(\boldsymbol{k}) \cos\left(2\sqrt{\frac{2}{3}}\frac{k}{k_{\rm eq}}\sqrt{1+y}\right) + B_{\rm r}(\boldsymbol{k}) \sin\left(2\sqrt{\frac{2}{3}}\frac{k}{k_{\rm eq}}\sqrt{1+y}\right) \\
&+ \frac{k_{\rm eq}}{4k}\sqrt{\frac{3}{2}}\int_{y_\alpha}^{y} \frac{d\tilde{y}}{\sqrt{1+y}}\, \mathcal{Q}_{\boldsymbol{k}}(\sqrt{1+\tilde{y}}) \left[\sin\left(2\sqrt{\frac{2}{3}}\frac{k}{k_{\rm eq}}\sqrt{1+y}\right)\cos\left(2\sqrt{\frac{2}{3}}\frac{k}{k_{\rm eq}}\sqrt{1+\tilde{y}}\right)\right. \\
&\left. - \cos\left(2\sqrt{\frac{2}{3}}\frac{k}{k_{\rm eq}}\sqrt{1+y}\right)\sin\left(2\sqrt{\frac{2}{3}}\frac{k}{k_{\rm eq}}\sqrt{1+\tilde{y}}\right)\right]\,, \qquad (5.3.14)
\end{aligned}$$

where

$$\begin{aligned}
\mathcal{Q}_{\boldsymbol{k}}(\sqrt{1+y}) =& \frac{4}{3}\left\{2P_1(\boldsymbol{k}) + \frac{1}{3y^2}\left[4(2-3y)\sqrt{1+y} + 6y^2 \ln\left(\frac{2+y+2\sqrt{1+y}}{y}\right)\right] P_2(\boldsymbol{k})\right\} \\
&- \frac{1}{2}\left\{\frac{1}{3y^2}\left[4(2-3y)\sqrt{1+y} + 6y^2 \ln\left(\frac{2+y+2\sqrt{1+y}}{y}\right)\right]\right. \\
&\times \int_{y_\alpha}^{y} d\tilde{y}\, \tilde{y}(2+3\tilde{y})\,\sqrt{1+\tilde{y}}\; F_1(\boldsymbol{k},\tilde{y}) + 2\int_{y_\alpha}^{y} d\tilde{y}\,\tilde{y}\sqrt{1+\tilde{y}}\left[6\sqrt{1+\tilde{y}}\right. \\
&\left.\left. + (2+3\tilde{y})\ln\left(\frac{2+\tilde{y}-2\sqrt{1+\tilde{y}}}{\tilde{y}}\right)\right] F_1(\boldsymbol{k},\tilde{y}) - \frac{16(1+y)}{3} F_1(\boldsymbol{k},\tilde{y})\right\}\,, \qquad (5.3.15)
\end{aligned}$$

where the naming of the variable in Eq. (5.3.14) is done in analogy its CDM counterpart. The coefficients $A_{\rm r}(\boldsymbol{k}), B_{\rm r}(\boldsymbol{k})$ can be obtained in a similar way as the coefficients $P_1(\boldsymbol{k})$ and $P_2(\boldsymbol{k})$ of $\delta_{\rm m}^{(2)}$ (see the complete expression in Appendix E). Finally, using (5.1.11) and (5.3.9) we can obtain the potential $\phi^{(2)}$. In fact we find

$$\begin{aligned}
\phi^{(2)}(\boldsymbol{x}, y) =& \frac{1}{3}\left[P_1(\boldsymbol{x})D_1(y) + P_2(\boldsymbol{x})D_2(y) + \frac{1}{2}\int_{y_\alpha}^{y} d\tilde{y}\, G(y,\tilde{y})\frac{d\chi^{ij}}{d\tilde{y}}\frac{d\chi_{ij}}{d\tilde{y}}\right] \\
&- \frac{1}{6}\left(\chi^{ij}\chi_{ij} - \chi_0^{ij}\chi_{0ij}\right)\,, \qquad (5.3.16)
\end{aligned}$$

in configuration space, where $G(y,\tilde{y})$ has already been defined in Eq. (5.3.10). Still note that here $\chi_0^{ij} = \chi^{ij}(\boldsymbol{x}, \eta_{\rm in})$. In Fourier space, $\phi^{(2)}$ becomes

$$\phi^{(2)}(\boldsymbol{k}, y) = \frac{1}{3}\left[P_1(\boldsymbol{k})D_1(y) + P_2(\boldsymbol{k})D_2(y) + \frac{1}{2}\int_{y_\alpha}^{y} d\tilde{y}\, G(y,\tilde{y})F_1(\boldsymbol{k},\tilde{y})\right]$$

$$-\frac{1}{6}\left(\mathcal{X}_{\boldsymbol{k}}(\eta)-\mathcal{X}_{\boldsymbol{k}}(\eta_{\rm in})\right)\,. \tag{5.3.17}$$

5.4 Determining the coefficients of the density contrast

The coefficients of the homogeneous parts of the solution $P_1(\boldsymbol{x})$ and $P_2(\boldsymbol{x})$ can be determined by matching the solutions obtained in section 5.2 and section 5.3. As discussed earlier, the perturbation and its derivatives must be continuous throughout the evolution, and hence they must be matched at a specific time η_α, which can be easily linked to the variable y_α that marks the beginning of the new phase. This matching conditions will be of the form

$$\delta^{(2)}_{\rm m(DRe)}(\boldsymbol{k},\tau_\alpha)=\delta^{(2)}_{\rm m(Tmesz)}(\boldsymbol{k},y_\alpha)\,, \tag{5.4.1}$$

$$\left(\frac{d}{dy}\delta^{(2)}_{\rm m(DRe)}(\boldsymbol{k},\tau)\right)\Bigg|_{\tau_\alpha}=\left(\frac{d}{dy}\delta^{(2)}_{\rm m(Tmesz)}(\boldsymbol{k},y)\right)\Bigg|_{y_\alpha}\,, \tag{5.4.2}$$

where $\tau_\alpha=k\eta_\alpha$. Here we have called with $\delta^{(2)}_{\rm m(DRe)}(\boldsymbol{k},\tau)$ the matter perturbation solution during the deep radiation era, while $\delta^{(2)}_{\rm m(Tmesz)}(\boldsymbol{k},y)$ is the solution obtained by the tensor-induced Meszaros equation.

Following [164], writing the scale factor as $a=a_{\rm eq}(\xi^2+2\xi)$, where $\xi=\eta/\eta_*$, with η_* being $\eta_{\rm eq}/(\sqrt{2}-1)$, in deep radiation era we have $\xi\ll1$ and we can write $a(\xi\ll1)=2a_{\rm eq}\xi$. Thus η can easily be related to y by the relation $\eta=\eta_* y/2$ and we find $\tau=k\eta_* y/2$. Then (5.2.19) can be expressed as

$$\begin{aligned}
\delta^{(2)}_{\rm m(DRe)}(\boldsymbol{k},y)=&-\frac{3\eta_*^2}{4}\ln\left(\frac{k\eta_* y}{2}\right)\int_{y_{\rm in}}^{y}d\tilde{y}\,\tilde{y}\,S_{\boldsymbol{k}}\left(\frac{\eta_*\tilde{y}}{2}\right)-\left\{\frac{3\sqrt{3}\eta_*}{2k}\left[1+\ln\left(\frac{k\eta_* y}{2}\right)\right]\sin\left(\frac{k\eta_* y}{2\sqrt{3}}\right)\right.\\
&\left.-\frac{3\eta_*^2 y}{4}\ln\left(\frac{k\eta_* y}{2}\right)\cos\left(\frac{k\eta_* y}{2\sqrt{3}}\right)\right\}\int_{y_{\rm in}}^{y}d\tilde{y}\,\cos\left(\frac{k\eta_*\tilde{y}}{2\sqrt{3}}\right)S_{\boldsymbol{k}}\left(\frac{\eta_*\tilde{y}}{2}\right)\\
&+\left\{\frac{3\sqrt{3}\eta_*}{2k}\left[1+\ln\left(\frac{k\eta_* y}{2}\right)\right]\cos\left(\frac{k\eta_* y}{2\sqrt{3}}\right)+\frac{3\eta_*^2 y}{4}\ln\left(\frac{k\eta_* y}{2}\right)\sin\left(\frac{k\eta_* y}{2\sqrt{3}}\right)\right\}\\
&\times\int_{y_{\rm in}}^{y}d\tilde{y}\,\sin\left(\frac{k\eta_*\tilde{y}}{2\sqrt{3}}\right)S_{\boldsymbol{k}}\left(\frac{\eta_*\tilde{y}}{2}\right)+\frac{\sqrt{3}\eta_*^3 k}{8}\int_{y_{\rm in}}^{y}d\tilde{y}\left\{\tilde{y}\ln\left(\frac{k\eta_* y}{2}\right)\right.\\
&\times\left[\sin\left(\frac{k\eta_*\tilde{y}}{2\sqrt{3}}\right)\int_{y_{\rm in}}^{\tilde{y}}d\tilde{\tilde{y}}\,\cos\left(\frac{k\eta_*\tilde{\tilde{y}}}{2\sqrt{3}}\right)S_{\boldsymbol{k}}\left(\frac{\eta_*\tilde{\tilde{y}}}{2}\right)\right.\\
&\left.\left.-\cos\left(\frac{k\eta_*\tilde{y}}{2\sqrt{3}}\right)\int_{y_{\rm in}}^{\tilde{y}}d\tilde{\tilde{y}}\,\sin\left(\frac{k\eta_*\tilde{\tilde{y}}}{2\sqrt{3}}\right)S_{\boldsymbol{k}}\left(\frac{\eta_*\tilde{\tilde{y}}}{2}\right)\right]\right\}\,.
\end{aligned} \tag{5.4.3}$$

Now we can finally match (5.4.3) with (5.3.9). The condition (5.4.1) can now be written as

$$\begin{aligned}
&-\frac{3\eta_*^2}{4}\ln\left(\frac{k\eta_* y}{2}\right)\int_{y_{\rm in}}^{y}d\tilde{y}\,\tilde{y}\,S_{\boldsymbol{k}}\left(\frac{\eta_*\tilde{y}}{2}\right)-\left\{\frac{3\sqrt{3}\eta_*}{2k}\left[1+\ln\left(\frac{k\eta_* y}{2}\right)\right]\sin\left(\frac{k\eta_* y}{2\sqrt{3}}\right)\right.\\
&\left.-\frac{3\eta_*^2 y}{4}\ln\left(\frac{k\eta_* y}{2}\right)\cos\left(\frac{k\eta_* y}{2\sqrt{3}}\right)\right\}\int_{y_{\rm in}}^{y}d\tilde{y}\,\cos\left(\frac{k\eta_*\tilde{y}}{2\sqrt{3}}\right)S_{\boldsymbol{k}}\left(\frac{\eta_*\tilde{y}}{2}\right)\\
&+\left\{\frac{3\sqrt{3}\eta_*}{2k}\left[1+\ln\left(\frac{k\eta_* y}{2}\right)\right]\cos\left(\frac{k\eta_* y}{2\sqrt{3}}\right)+\frac{3\eta_*^2 y}{4}\ln\left(\frac{k\eta_* y}{2}\right)\sin\left(\frac{k\eta_* y}{2\sqrt{3}}\right)\right\}
\end{aligned}$$

$$
\begin{aligned}
&\times \int_{y_{\rm in}}^{y} d\tilde{y}\, \sin\left(\frac{k\eta_* \tilde{y}}{2\sqrt{3}}\right) S_{\boldsymbol{k}}\left(\frac{\eta_* \tilde{y}}{2}\right) + \frac{\sqrt{3}\eta_*^3 k}{8} \int_{y_{\rm in}}^{y} d\tilde{y} \left\{ \tilde{y} \ln\left(\frac{k\eta_* y}{2}\right) \right. \\
&\times \left[\sin\left(\frac{k\eta_* \tilde{y}}{2\sqrt{3}}\right) \int_{y_{\rm in}}^{\tilde{y}} d\tilde{\tilde{y}}\, \cos\left(\frac{k\eta_* \tilde{\tilde{y}}}{2\sqrt{3}}\right) S_{\boldsymbol{k}}\left(\frac{\eta_* \tilde{\tilde{y}}}{2}\right) - \cos\left(\frac{k\eta_* \tilde{y}}{2\sqrt{3}}\right) \right. \\
&\left. \left. \times \int_{y_{\rm in}}^{\tilde{y}} d\tilde{\tilde{y}}\, \sin\left(\frac{k\eta_* \tilde{\tilde{y}}}{2\sqrt{3}}\right) S_{\boldsymbol{k}}\left(\frac{\eta_* \tilde{\tilde{y}}}{2}\right) \right] \right\} \\
&= P_1(\boldsymbol{k}) D_1(y_\alpha) + P_2(\boldsymbol{k}) D_2(y_\alpha)\,, \qquad (5.4.4)
\end{aligned}
$$

and (5.4.2) gives

$$
\begin{aligned}
&- \frac{3\eta_*}{2k y_\alpha} \int_{y_{\rm in}}^{y_\alpha} d\tilde{y}\, \tilde{y}\, S_{\boldsymbol{k}}\left(\frac{\eta_* \tilde{y}}{2}\right) \\
&- \left[\frac{3\sqrt{3}}{k^2 y_\alpha} \sin\frac{k\eta_* y_\alpha}{2\sqrt{3}} + \frac{3\eta_*^2}{4} \cos\frac{k\eta_* y_\alpha}{2\sqrt{3}} - \frac{3\eta_*}{2k} \cos\frac{k\eta_* y_\alpha}{2\sqrt{3}} \right] \int_{y_{\rm in}}^{y_\alpha} d\tilde{y}\, \cos\frac{k\eta_* \tilde{y}}{2\sqrt{3}}\, S_{\boldsymbol{k}}\left(\frac{\eta_* \tilde{y}}{2}\right) \\
&- \left[-\frac{3\sqrt{3}}{k^2 y_\alpha} \cos\frac{k\eta_* y_\alpha}{2\sqrt{3}} + \frac{3\eta_*^2}{4} \sin\frac{k\eta_* y_\alpha}{2\sqrt{3}} - \frac{3\eta_*}{2k} \sin\frac{k\eta_* y_\alpha}{2\sqrt{3}} \right] \int_{y_{\rm in}}^{y} d\tilde{y}\, \sin\frac{k\eta_* \tilde{y}}{2\sqrt{3}}\, S_{\boldsymbol{k}}\left(\frac{\eta_* \tilde{y}}{2}\right) \\
&= P_1(\boldsymbol{k}) + P_2(\boldsymbol{k}) \left(-\frac{2(1+3y_\alpha)}{3y_\alpha\sqrt{1+y_\alpha}} + \ln\frac{\sqrt{1+y_\alpha}+1}{\sqrt{1+y_\alpha}-1} \right). \qquad (5.4.5)
\end{aligned}
$$

Multiplying (5.4.5) by $D_1(y_\alpha)$ and subtracting it from (5.4.4), we have

$$
\begin{aligned}
P_2(\boldsymbol{k}) = {} & \frac{9y_\alpha\sqrt{1+y_\alpha}}{2(2+3y_\alpha)} \left[-\frac{3\eta_*^2}{4} \ln\frac{k\eta_* y_\alpha}{2} \int_{y_{\rm in}}^{y_\alpha} d\tilde{y}\, \tilde{y}\, S_{\boldsymbol{k}}\left(\frac{\eta_* \tilde{y}}{2}\right) - \left[\frac{3\sqrt{3}\eta_*}{2k} \right. \right. \\
&\left. \times \left(1 + \ln\frac{k\eta_* y_\alpha}{2}\right) \sin\frac{k\eta_* y_\alpha}{2\sqrt{3}} - \frac{3\eta_*^2 y_\alpha}{4} \ln\frac{k\eta_* y_\alpha}{2} \cos\frac{k\eta_* y_\alpha}{2\sqrt{3}} \right] \int_{y_{\rm in}}^{y_\alpha} d\tilde{y}\, \cos\frac{k\eta_* \tilde{y}}{2\sqrt{3}}\, S_{\boldsymbol{k}}\left(\frac{\eta_* \tilde{y}}{2}\right) \\
&- \left[-\frac{3\sqrt{3}\eta_*}{2k} \left(1 + \ln\frac{k\eta_* y_\alpha}{2}\right) \cos\frac{k\eta_* y_\alpha}{2\sqrt{3}} - \frac{3\eta_*^2 y_\alpha}{4} \ln\frac{k\eta_* y_\alpha}{2} \sin\frac{k\eta_* y_\alpha}{2\sqrt{3}} \right] \\
&\times \int_{y_{\rm in}}^{y_\alpha} d\tilde{y}\, \sin\frac{k\eta_* \tilde{y}}{2\sqrt{3}}\, S_{\boldsymbol{k}}\left(\frac{\eta_* \tilde{y}}{2}\right) + \frac{\sqrt{3}\eta_*^3 k}{8} \int_{y_{\rm in}}^{y_\alpha} d\tilde{y}\, \tilde{y} \ln\frac{k\eta_* y}{2} \\
&\times \left[\sin\frac{k\eta_* \tilde{y}}{2\sqrt{3}} \int_{y_{\rm in}}^{\tilde{y}} d\tilde{\tilde{y}}\, \cos\frac{k\eta_* \tilde{\tilde{y}}}{2\sqrt{3}}\, S_{\boldsymbol{k}}\left(\frac{\eta_* \tilde{\tilde{y}}}{2}\right) - \cos\frac{k\eta_* \tilde{y}}{2\sqrt{3}} \int_{y_{\rm in}}^{\tilde{y}} d\tilde{\tilde{y}}\, \sin\frac{k\eta_* \tilde{\tilde{y}}}{2\sqrt{3}}\, S_{\boldsymbol{k}}\left(\frac{\eta_* \tilde{\tilde{y}}}{2}\right) \right] \\
&+ \left(y_\alpha + \frac{2}{3}\right) \left(\frac{3\eta_*}{2k y} \int_{y_{\rm in}}^{y_\alpha} d\tilde{y}\, \tilde{y}\, S_{\boldsymbol{k}}\left(\frac{\eta_* \tilde{y}}{2}\right) \right. \\
&+ \left[\frac{3\sqrt{3}}{k^2 y_\alpha} \sin\frac{k\eta_* y_\alpha}{2\sqrt{3}} + \frac{3\eta_*^2}{4} \cos\frac{k\eta_* y_\alpha}{2\sqrt{3}} - \frac{3\eta_*}{2k} \cos\frac{k\eta_* y_\alpha}{2\sqrt{3}} \right] \int_{y_{\rm in}}^{y_\alpha} d\tilde{y}\, \cos\frac{k\eta_* \tilde{y}}{2\sqrt{3}} S_{\boldsymbol{k}}\left(\frac{\eta_* \tilde{y}}{2}\right) \\
&\left. \left. + \left[-\frac{3\sqrt{3}}{k^2 y_\alpha} \cos\frac{k\eta_* y_\alpha}{2\sqrt{3}} + \frac{3\eta_*^2}{4} \sin\frac{k\eta_* y_\alpha}{2\sqrt{3}} - \frac{3\eta_*}{2k} \sin\frac{k\eta_* y_\alpha}{2\sqrt{3}} \right] \int_{y_{\rm in}}^{y} d\tilde{y}\, \sin\frac{k\eta_* \tilde{y}}{2\sqrt{3}} S_{\boldsymbol{k}}\left(\frac{\eta_* \tilde{y}}{2}\right) \right) \right]. \qquad (5.4.6)
\end{aligned}
$$

Finally, substituting the above expression in (5.4.5), we get the expression for $P_1(\boldsymbol{k})$

$$
\begin{aligned}
P_1(\boldsymbol{k}) = {} & \left\{ 1 + 3y \left(1 - \frac{\sqrt{1+y}}{2} \ln\frac{\sqrt{1+y_\alpha}+1}{\sqrt{1+y_\alpha}-1} \right) \right\} \frac{3}{2+3y} \\
& \left[-\frac{3\eta_*^2}{4} \ln\frac{k\eta_* y_\alpha}{2} \int_{y_{\rm in}}^{y_\alpha} d\tilde{y}\, \tilde{y} S_{\boldsymbol{k}}\left(\frac{\eta_* \tilde{y}}{2}\right) - \left[\frac{3\sqrt{3}\eta_*}{2k} \left(1 + \ln\frac{k\eta_* y_\alpha}{2}\right) \sin\frac{k\eta_* y_\alpha}{2\sqrt{3}} \right. \right. \\
& \left. \left. - \frac{3\eta_*^2 y_\alpha}{4} \ln\frac{k\eta_* y_\alpha}{2} \cos\frac{k\eta_* y_\alpha}{2\sqrt{3}} \right] \int_{y_{\rm in}}^{y_\alpha} d\tilde{y}\, \cos\frac{k\eta_* \tilde{y}}{2\sqrt{3}} S_{\boldsymbol{k}}\left(\frac{\eta_* \tilde{y}}{2}\right) \right.
\end{aligned}
$$

$$
\begin{aligned}
&- \left[-\frac{3\sqrt{3}\eta_*}{2k}\left(1+\ln\frac{k\eta_* y_\alpha}{2}\right)\cos\frac{k\eta_* y_\alpha}{2\sqrt{3}} - \frac{3\eta_*^2 y_\alpha}{4}\ln\frac{k\eta_* y_\alpha}{2}\sin\frac{k\eta_* y_\alpha}{2\sqrt{3}}\right] \\
&\times \int_{y_{\rm in}}^{y_\alpha} d\tilde{y}\,\sin\frac{k\eta_*\tilde{y}}{2\sqrt{3}} S_{\boldsymbol{k}}\left(\frac{\eta_*\tilde{y}}{2}\right) + \frac{\sqrt{3}\eta_*^3 k}{8}\int_{y_{\rm in}}^{y_\alpha} d\tilde{y}\,\tilde{y}\ln\frac{k\eta_* y}{2} \\
&\times \left[\sin\frac{k\eta_*\tilde{y}}{2\sqrt{3}}\int_{y_{\rm in}}^{\tilde{y}} d\tilde{\tilde{y}}\,\cos\frac{k\eta_*\tilde{\tilde{y}}}{2\sqrt{3}} S_{\boldsymbol{k}}\left(\frac{\eta_*\tilde{\tilde{y}}}{2}\right) - \cos\frac{k\eta_*\tilde{y}}{2\sqrt{3}}\int_{y_{\rm in}}^{\tilde{y}} d\tilde{\tilde{y}}\,\sin\frac{k\eta_*\tilde{\tilde{y}}}{2\sqrt{3}} S_{\boldsymbol{k}}\left(\frac{\eta_*\tilde{\tilde{y}}}{2}\right)\right]\Bigg] \\
&+ 3y\left(1-\frac{\sqrt{1+y}}{2}\ln\frac{\sqrt{1+y_\alpha}+1}{\sqrt{1+y_\alpha}-1}\right)\left[\frac{3\eta_*}{2ky}\int_{y_{\rm in}}^{y_\alpha} d\tilde{y}\,\tilde{y} S_{\boldsymbol{k}}\left(\frac{\eta_*\tilde{y}}{2}\right)\right. \\
&+ \left[\frac{3\sqrt{3}}{k^2 y_\alpha}\sin\frac{k\eta_* y_\alpha}{2\sqrt{3}} + \frac{3\eta_*^2}{4}\cos\frac{k\eta_* y_\alpha}{2\sqrt{3}} - \frac{3\eta_*}{2k}\cos\frac{k\eta_* y_\alpha}{2\sqrt{3}}\right]\int_{y_{\rm in}}^{y_\alpha} d\tilde{y}\,\cos\frac{k\eta_*\tilde{y}}{2\sqrt{3}} S_{\boldsymbol{k}}\left(\frac{\eta_*\tilde{y}}{2}\right) \\
&+ \left.\left[-\frac{3\sqrt{3}}{k^2 y_\alpha}\cos\frac{k\eta_* y_\alpha}{2\sqrt{3}} + \frac{3\eta_*^2}{4}\sin\frac{k\eta_* y_\alpha}{2\sqrt{3}} - \frac{3\eta_*}{2k}\sin\frac{k\eta_* y_\alpha}{2\sqrt{3}}\right]\int_{y_{\rm in}}^{y} d\tilde{y}\,\sin\frac{k\eta_*\tilde{y}}{2\sqrt{3}} S_{\boldsymbol{k}}\left(\frac{\eta_*\tilde{y}}{2}\right)\right]. \qquad (5.4.7)
\end{aligned}
$$

The tensor-sourced $\delta_{\rm m}^{(2)}$ is given by (5.3.9), where the coefficients are shown in (5.4.6) and (5.4.7). In order to determine y_α, we should express $\delta_{\rm r}^{(2)}$, computed in (5.2.14) as well in terms of the variable y. Indeed, it becomes

$$
\begin{aligned}
\delta_{\rm r(DRe)}^{(2)}(\boldsymbol{k},y) = {}& \frac{12}{k^2 y^2}\int_{y_{\rm in}}^{y} d\tilde{y}\,\tilde{y}\,S_{\boldsymbol{k}}\left(\frac{\eta_*\tilde{y}}{2}\right) - \frac{2\sqrt{3}\eta_*}{k}\left[\sin\frac{k\eta_* y}{2\sqrt{3}} + \frac{2\sqrt{3}}{k\eta_* y}\cos\frac{k\eta_* y}{2\sqrt{3}}\right] \\
&\times \int_{y_{\rm in}}^{y} d\tilde{y}\,\cos\frac{k\eta_*\tilde{y}}{2\sqrt{3}}\,S_{\boldsymbol{k}}\left(\frac{\eta_*\tilde{y}}{2}\right) + \frac{2\sqrt{3}\eta_*}{k}\left[\cos\frac{k\eta_* y}{2\sqrt{3}} - \frac{2\sqrt{3}}{k\eta_* y}\sin\frac{k\eta_* y}{2\sqrt{3}}\right] \\
&\times \int_{y_{\rm in}}^{y} d\tilde{y}\,\sin\frac{k\eta_*\tilde{y}}{2\sqrt{3}}\,S_{\boldsymbol{k}}\left(\frac{\eta_*\tilde{y}}{2}\right). \qquad (5.4.8)
\end{aligned}
$$

(Here we have called with $\delta_{\rm r(DRe)}^{(2)}(\boldsymbol{k},y)$ the radiation perturbation solution during the deep radiation era.) Therefore, using the above relation Eq. (5.4.8), taking into account of Eq. (5.4.3) and the condition derived in Eq. (5.3.7), we can find an expression from which we can implicitly obtain the value of y_α

$$
\begin{aligned}
&\frac{\sqrt{3}\eta_* y_\alpha}{4}\ln\frac{k\eta_* y_\alpha}{2}\int_{y_{\rm in}}^{y_\alpha} d\tilde{y}\,\tilde{y}\,S_{\boldsymbol{k}}\left(\frac{\eta_*\tilde{y}}{2}\right) + \left[\frac{3y_\alpha}{2k}\left(1+\ln\frac{k\eta_* y_\alpha}{2}\right)\sin\frac{k\eta_* y_\alpha}{2\sqrt{3}}\right. \\
&\left. - \frac{\sqrt{3}\eta_* y_\alpha^2}{4}\ln\frac{k\eta_* y_\alpha}{2}\cos\frac{k\eta_* y_\alpha}{2\sqrt{3}}\right]\int_{y_{\rm in}}^{y_\alpha} d\tilde{y}\,\cos\frac{k\eta_*\tilde{y}}{2\sqrt{3}}\,S_{\boldsymbol{k}}\left(\frac{\eta_*\tilde{y}}{2}\right) \\
&+ \left[-\frac{3y_\alpha}{2k}\left(1+\ln\frac{k\eta_* y_\alpha}{2}\right)\cos\frac{k\eta_* y_\alpha}{2\sqrt{3}} - \frac{\sqrt{3}\eta_* y_\alpha^2}{4}\ln\frac{k\eta_* y_\alpha}{2}\sin\frac{k\eta_* y_\alpha}{2\sqrt{3}}\right] \\
&\times \int_{y_{\rm in}}^{y_\alpha} d\tilde{y}\,\sin\frac{k\eta_*\tilde{y}}{2\sqrt{3}}\,S_{\boldsymbol{k}}\left(\frac{\eta_*\tilde{y}}{2}\right) - \frac{\eta_*^2 k y_\alpha}{8}\int_{y_{\rm in}}^{y_\alpha} d\tilde{y}\,\tilde{y}\ln\frac{k\eta_* y}{2} \\
&\times \left[\sin\frac{k\eta_*\tilde{y}}{2\sqrt{3}}\int_{y_{\rm in}}^{\tilde{y}} d\tilde{\tilde{y}}\,\cos\frac{k\eta_*\tilde{\tilde{y}}}{2\sqrt{3}}\,S_{\boldsymbol{k}}\left(\frac{\eta_*\tilde{\tilde{y}}}{2}\right) - \cos\frac{k\eta_*\tilde{y}}{2\sqrt{3}}\int_{y_{\rm in}}^{\tilde{y}} d\tilde{\tilde{y}}\,\sin\frac{k\eta_*\tilde{\tilde{y}}}{2\sqrt{3}}\,S_{\boldsymbol{k}}\left(\frac{\eta_*\tilde{\tilde{y}}}{2}\right)\right] \\
&= -\frac{4\sqrt{3}\alpha}{\eta_* k^2 y_\alpha^2}\int_{y_{\rm in}}^{y_\alpha} d\tilde{y}\,\tilde{y}\,S_{\boldsymbol{k}}\left(\frac{\eta_*\tilde{y}}{2}\right) + \frac{2\alpha}{k}\left[\sin\frac{k\eta_* y_\alpha}{2\sqrt{3}} + \frac{2\sqrt{3}}{k\eta_* y_\alpha}\cos\frac{k\eta_* y_\alpha}{2\sqrt{3}}\right] \\
&\times \int_{y_{\rm in}}^{y_\alpha} d\tilde{y}\,\cos\frac{k\eta_*\tilde{y}}{2\sqrt{3}}\,S_{\boldsymbol{k}}\left(\frac{\eta_*\tilde{y}}{2}\right) - \frac{2\alpha}{k}\left[\cos\frac{k\eta_* y_\alpha}{2\sqrt{3}} - \frac{2\sqrt{3}}{k\eta_* y_\alpha}\sin\frac{k\eta_* y_\alpha}{2\sqrt{3}}\right] \\
&\times \int_{y_{\rm in}}^{y_\alpha} d\tilde{y}\,\sin\frac{k\eta_*\tilde{y}}{2\sqrt{3}}\,S_{\boldsymbol{k}}\left(\frac{\eta_*\tilde{y}}{2}\right). \qquad (5.4.9)
\end{aligned}
$$

As discussed earlier, it is not possible to obtain a precise value of α using our analytical approach alone. Numerical analysis is required to obtain a more accurate value. Based on our analytical approach, we know that α should be between 1 and 2. The next section is devoted to the analytical analysis of the density perturbations produced by gravitational waves entering the Hubble radius during the era of matter and their evolution in the late phase dominated by dark energy.

5.5 Tensor-sourced CDM and radiation perturbation during matter and Dark Energy domination

Our approach in this section will extend the one in the previous chapter to all modes, taking into account both the dark matter and dark energy eras. We will also provide an analytical solution for the radiation perturbations in the same time period. However, our analysis will only be valid for $\eta \gg \eta_{\rm eq}$ and for all k until the present time η_0. To ensure that we are in the CDM epoch, we will consider only the Universe for $\eta \geq \eta_{\rm rec}$, where $\eta_{\rm rec}$ is the conformal time at recombination. At this point, radiation perturbations become negligible compared to those of matter, and the Universe is dominated by matter at both the background and perturbation levels. It is important to note that our analytical approach cannot describe modes that enter the horizon around matter-radiation equality and for $1/\eta_{\rm rec} \leq k \lesssim 1/\eta_{\rm eq}$. For these scales, a numerical approach is required. However, we will provide a possible analytic prescription at the end of this section that may help to solve this matching.

For the scalar modes entering in matter domination [167], as discussed before, we can adopt co-moving, synchronous, and time-orthogonal gauge. Then, for $\eta \geq \eta_{\rm rec} \gg \eta_{\rm eq}$, we can discard the radiation perturbation within the Einstein field Equations. In this case, choosing co-moving observers, the deformation tensor is purely spatial and coincides with the extrinsic curvature of constant-time spatial hyper-surfaces, i.e. $\theta^i_j = -K^i_j = \gamma^{ik}\gamma'_{kj}/2$. (Here the prime denotes the differentiation w.r.t. conformal time.) In this case, let us consider the continuity and Raychaudhury equation [102, 168, 169]

$$\theta^{(2)\prime} + \mathcal{H}\theta^{(2)} + 2\theta^{(1)i}_j\theta^{(1)j}_i + 4\pi G a^2 \bar{\rho}_{\rm m}\delta^{(2)}_{\rm m} = 0\,, \tag{5.5.1}$$

$$\delta^{(2)\prime}_{\rm m} + 2\delta^{(1)}_{\rm m}\theta^{(1)} + \theta^{(2)} = 0\,, \tag{5.5.2}$$

where θ is the trace of θ^i_j and represents the inhomogeneous part of the volume expansion. Taking into account that the additive term $2\delta^{(1)}_{\rm m}\theta^{(1)}$ can be discarded because it is independent of the tensor contribution, we can combine these equations to obtain the evolution equation of $\delta^{(2)}_{\rm m}$

$$\delta^{(2)\prime\prime}_{\rm m} + \mathcal{H}\delta^{(2)\prime}_{\rm m} - 4\pi G a^2\bar{\rho}_{\rm m}\delta^{(2)}_{\rm m} = \frac{1}{2}\chi^{ij\prime}\chi_{ij}{}'\,. \tag{5.5.3}$$

Now, let us consider the usual relation

$$a^2\bar{\rho}_{\rm m} = \frac{3}{8\pi G}\mathcal{H}^2\Omega_{\rm m} = \frac{3}{8\pi G}\frac{\mathcal{H}_0^2\Omega_{\rm m0}}{a}\,,$$

where the cosmological parameter is defined as $\Omega_{\rm m} = 8\pi G\bar{\rho}_{\rm m}a^2/3\mathcal{H}^2$ and $\Omega_{\rm m0} = 8\pi G\bar{\rho}_{\rm m0}/3\mathcal{H}_0^2 = \Omega_{\rm m}(\eta = \eta_0)$ (here we have normalised the scale factor today as $a_0 = a(\eta_0) = 1$), and the usual background equations (that we set for $\eta \geq \eta_{\rm rec}$)

$$\mathcal{H}^2 = \frac{{\mathcal{H}_0}^2\Omega_{\rm m0}}{a}\left(1 + R_0 a^3\right) \qquad \text{and} \qquad \mathcal{H}' = \mathcal{H}^2\left(1 - \frac{3}{2}\Omega_{\rm m}\right),$$

where $R_0 = \Omega_{\Lambda 0}/\Omega_{\rm m0} = (1 - \Omega_{\rm m0})/\Omega_{\rm m0}$. Then Eq. (5.5.3), in terms of the variable $\iota = R_0^{1/3}a$, becomes

$$\iota^2\left(1 + \iota^3\right)\frac{d^2\delta_{\rm m}^{(2)}}{d\iota^2} + \frac{3}{2}\iota\left(1 + 2\iota^3\right)\frac{d\delta_{\rm m}^{(2)}}{d\iota} - \frac{3}{2}\delta_{\rm m}^{(2)} = S_{\rm m}\,, \tag{5.5.4}$$

where we have defined the source term in the following way

$$S_{\rm m}(\iota) = \frac{\iota^2(1 + \iota^3)}{2}\frac{d\chi^{ij}}{d\iota}\frac{d\chi_{ij}}{d\iota},$$

and the following variable transformation rules have been used

$$\frac{d}{d\eta} = \mathcal{H}_0 R_0^{1/6}\sqrt{\Omega_{\rm m0}\iota(1 + \iota^3)}\frac{d}{d\iota}\,, \tag{5.5.5}$$

$$\frac{d^2}{d\eta^2} = \mathcal{H}_0^2 R_0^{1/3}\Omega_{\rm m0}\left(\frac{1 + 4\iota^3}{2}\frac{d}{d\iota} + \iota(1 + \iota^3)\frac{d^2}{d\iota^2}\right). \tag{5.5.6}$$

The meaning of ι can be easily related to the normalized scale factor at η_Λ which is the conformal time when $\Omega_{\rm m} = \Omega_\Lambda$, i.e. $\iota(\eta) = a(\eta)/a(\eta_\Lambda)$ [164]. The general solution in Fourier space is

$$\delta_{\rm m}^{(2)}(\boldsymbol{k}, \iota) = D_-(\iota)C_-(\boldsymbol{k}) + D_+(\iota)C_+(\boldsymbol{k}) + \int_{\iota_{\rm rec}}^{\iota} d\tilde{\iota}\, G_{\rm m}(\iota, \tilde{\iota})\, S_{\rm m}(\tilde{\iota}, \tilde{\eta}, \boldsymbol{k})\,, \tag{5.5.7}$$

where $\tilde{\eta} = \eta(\tilde{\iota})$, $\iota_{\rm rec} = \iota(\eta_{\rm rec})$ and the source term is the Fourier transform of $S_{\rm m}(\iota)$, i.e.

$$S_{\rm m}(\boldsymbol{k}, \tilde{\iota}, \tilde{\eta}) = \frac{\tilde{\iota}^2(1 + \tilde{\iota}^3)}{2}F_2(\boldsymbol{k}, \tilde{\iota})\,, \tag{5.5.8}$$

where the functional form of F_2 is defined as the Fourier transform of $d\chi^{ij}/d\iota\, d\chi_{ij}/d\iota$, i.e.

$$\begin{aligned} F_2(\boldsymbol{k}, \iota) = &\sum_{\sigma,\sigma'}\int\frac{d^3q}{(2\pi)^3}A_{\sigma'}(\boldsymbol{q})A_\sigma\left(\boldsymbol{k} - \boldsymbol{q}\right) \\ &\times \epsilon_{ij}^{\sigma'}(\hat{\boldsymbol{q}})\epsilon^{\sigma ij}\left(\widehat{\boldsymbol{k} - \boldsymbol{q}}\right)\frac{d\mathcal{T}\left(q, \iota\right)}{d\iota}\frac{d\mathcal{T}\left(|\boldsymbol{k} - \boldsymbol{q}|, \iota\right)}{d\iota}. \end{aligned} \tag{5.5.9}$$

Obviously, we connect F_2 with $S_{\boldsymbol{k}}$ (see Eq. (5.2.8))

$$F_2(\boldsymbol{k}, \iota) = -\frac{6}{\mathcal{H}_0^2 R_0^{1/3}\Omega_{\rm m0}\iota}\frac{S_{\boldsymbol{k}}}{(1 + \iota^3)} \tag{5.5.10}$$

and, therefore, we have

$$S_{\rm m}(\boldsymbol{k}, \tilde{\iota}, \tilde{\eta}) = -\frac{3}{\mathcal{H}_0^2 R_0^{1/3}\Omega_{\rm m0}}\iota S_{\boldsymbol{k}}\,. \tag{5.5.11}$$

Here, D_- and D_+ are [164]

$$D_-(\iota) = \sqrt{1 + \iota^{-3}}\,, \tag{5.5.12}$$

$$D_+(\iota) = D_-(\iota)\int_0^\iota d\tilde{\iota}\left(\frac{\tilde{\iota}}{1+\tilde{\iota}^3}\right)^{3/2}\,, \tag{5.5.13}$$

and, consequently, the Green's function is defined as

$$G_{\rm m}(\iota,\tilde{\iota}) = (1+\tilde{\iota}^3)\sqrt{1+\iota^{-3}}\left(\int_0^\iota d\tilde{\iota}\left(\frac{\tilde{\iota}}{1+\tilde{\iota}^3}\right)^{3/2} - \int_0^{\tilde{\iota}} d\tilde{\tilde{\iota}}\left(\frac{\tilde{\tilde{\iota}}}{1+\tilde{\tilde{\iota}}^3}\right)^{3/2}\right)\,. \tag{5.5.14}$$

Here, for D_+, we have followed the conventions used in [164]. Consequently the integrals in $G_{\rm m}$ start at $\iota = 0$.

Eq. (5.5.9) shows that the source term $F_2(\iota,\boldsymbol{k})$ (and, correspondingly, $S_{\boldsymbol{k}}(\iota,\eta)$), containing two $\mathcal{T}$'s, cannot be evaluated using the analytical expressions provided in Eq. (2.3.5) [68]. This is because these expressions do not take into account the contribution of the cosmological constant/Dark Energy, which becomes significant at late times, leading to an acceleration in the expansion of the Universe. Consequently, a new definition of $\mathcal{T}$ is required, which is not analytical, and accounts for this acceleration in order to accurately describe the behavior of χ_{ij} for modes k such that $1/\eta_0 \geq k \geq 1/\eta_\Lambda$.

Now, as also pointed out in [167], for $k \leq 1/\eta_{\rm rec} < k_{\rm eq}$, we are focusing on density contrast for waves entering the horizon during matter and dark energy domination. In this case we will not consider the homogeneous solutions. Instead for $k > k_{\rm eq}$ we need to keep all the terms in Eq. (5.5.7). For these modes we need a matching conditions at $\eta = \eta_{\rm rec}$ between the general solution Eq. (5.5.7) and the one that we obtain in Section 5.3, i.e. Eq. (5.3.9) (e.g., see the light-green area for $\eta \geq \eta_{\rm rec}$ in Fig. 5.1). Moreover, for this match, if $\eta \to \eta^+_{\rm rec}$, $\iota \ll 1$. In this limit, we can discard the inhomogeneous solution and Eq. (5.5.7) reads [164]

$$\delta^{(2)}_{\rm m}(\iota \to \iota^+_{\rm rec},\mathbf{k}) = \iota^{-3/2}\,C_-(\mathbf{k}) + \frac{2}{5}\iota\,C_+(\mathbf{k})\,. \tag{5.5.15}$$

Now, using the definition of $\iota = R_0^{1/3}a$ and $y = a/a_{\rm eq}$, Eq. (5.5.15) can be written in the following way

$$\delta^{(2)}_{\rm m}(y \to y^+_{\rm rec},\mathbf{k}) = \left(a^3_{\rm eq}R_0\right)^{-1/2} y^{-3/2}\,C_-(\mathbf{k}) + \frac{2}{5}a_{\rm eq}R_0^{1/3}y\,C_+(\mathbf{k})\,. \tag{5.5.16}$$

Now we can impose the following matching conditions

$$\delta^{(2)}_{\rm m(Tmesz)}(\boldsymbol{k},y \to y^-_{\rm rec})\Big|_{y_{\rm rec}} = \delta^{(2)}_{\rm m}(\boldsymbol{k},y \to y^+_{\rm rec})\Big|_{y_{\rm rec}}\,, \tag{5.5.17}$$

$$\left(\frac{d}{dy}\delta^{(2)}_{\rm m(Tmesz)}(\boldsymbol{k},y \to y^-_{\rm rec})\right)\Bigg|_{y_{\rm rec}} = \left(\frac{d}{dy}\delta^{(2)}_{\rm m}(\boldsymbol{k},y \to y^+_{\rm rec})\right)\Bigg|_{y_{\rm rec}}\,, \tag{5.5.18}$$

which allow to get C_- and C_+. Here $\delta^{(2)}_{\rm m(Tmesz)}(\boldsymbol{k},y \to y^-_{\rm rec})$ is exactly Eq. (5.3.11) at $y \to y^-_{\rm rec}$. The matching conditions Eqs. (5.5.17) and (5.5.18) give us

$$\begin{aligned} &P_1(\boldsymbol{k})D_1(y_{\rm rec}) + P_2(\boldsymbol{k})D_2(y_{\rm rec}) + \frac{1}{2}\int_{y_\alpha}^{y_{\rm rec}} d\tilde{y}\,G(y,\tilde{y})F_1(\tilde{y},\boldsymbol{k}) \\ &= \left(a^3_{\rm eq}R_0\right)^{-1/2} {y_{\rm rec}}^{-3/2}\,C_-(\mathbf{k}) + \frac{2}{5}a_{\rm eq}R_0^{1/3}y_{\rm rec}\,C_+(\mathbf{k})\,, \end{aligned} \tag{5.5.19}$$

and

$$P_1(\boldsymbol{k}) + P_2(\boldsymbol{k}) \left(-\frac{2(1+3y_{\rm rec})}{3y_{\rm rec}\sqrt{1+y_{\rm rec}}} + \ln \frac{\sqrt{1+y_{\rm rec}}+1}{\sqrt{1+y_{\rm rec}}-1} \right)$$
$$= -\frac{3}{2} \left(a_{\rm eq}^3 R_0\right)^{-1/2} {y_{\rm rec}}^{-5/2}\, C_-(\mathbf{k}) + \frac{2}{5} a_{\rm eq} R_0^{1/3}\, C_+(\mathbf{k}) \tag{5.5.20}$$

respectively. Multiplying Eq. (5.5.20) with $y_{\rm rec}$ and subtracting it from Eq. (5.5.19), we obtain

$$C_-(\mathbf{k}) = \frac{4}{15} \left(a_{\rm eq}^3 y_{\rm eq}^3 R_0\right)^{1/2} \left[P_1(\boldsymbol{k}) + P_2(\boldsymbol{k}) \left(-\frac{2}{\sqrt{1+y_{\rm rec}}} + \ln \frac{\sqrt{1+y_{\rm rec}}+1}{\sqrt{1+y_{\rm rec}}-1} \right) \right.$$
$$\left. + \frac{3}{4} \int_{y_\alpha}^{y_{\rm rec}} d\tilde{y}\, G(y,\tilde{y}) F_1(\tilde{y},\boldsymbol{k}) \right] . \tag{5.5.21}$$

Similarly, multiplying Eq. (5.5.19) with $3/(2y_{\rm rec})$ and adding it to Eq. (5.5.20), we have

$$C_+(\mathbf{k}) = \frac{1}{a_{\rm eq} R_0^{1/3}} \left[\left(\frac{5}{2} + \frac{1}{y_{\rm rec}} \right) \left(P_1(\boldsymbol{k}) + P_2(\boldsymbol{k}) \ln \frac{\sqrt{1+y_{\rm rec}}+1}{\sqrt{1+y_{\rm rec}}-1} \right) \right.$$
$$\left. - \frac{P_2(\boldsymbol{k})}{3} \frac{11+15y_{\rm rec}}{y_{\rm rec}\sqrt{1+y_{\rm rec}}} + \frac{3}{4y_{\rm rec}} \int_{y_\alpha}^{y_{\rm rec}} d\tilde{y}\, G(y,\tilde{y}) F_1(\tilde{y},\boldsymbol{k}) \right] , \tag{5.5.22}$$

where $P_1(\boldsymbol{k}), P_2(\boldsymbol{k})$ are given by Eq. (5.4.7) and Eq. (5.4.6) respectively. The form of $D_1(y), D_2(y)$ is shown in Section 5.3.

Let us now turn our attention to the radiation contribution arising from the primordial GWs that enter the horizon during late times. Although radiation is not dominant at both the background and perturbation levels for $\eta \gtrsim \eta_{\rm rec}$, and can be discarded in the perturbed Einstein field equations, it can still have an impact on the CMB. In order to obtain an expression for the radiation density perturbation, we can make use of equations (5.1.11), (5.1.14), and (5.1.15), which remain valid in this regime.

Now, inserting (5.1.11) into (5.1.14), we have

$$\delta_{\rm r}^{(2)\prime} + \frac{4}{3} \nabla^2 v_{\rm r}^{(2)} = \frac{4}{3} \delta_{\rm m}^{(2)\prime} . \tag{5.5.23}$$

Differentiating the above equation w.r.t. time, and using (5.1.15), we obtain

$$\delta_{{\rm r}\boldsymbol{k}}^{(2)\prime\prime} + \frac{k^2}{3} \delta_{{\rm r}\boldsymbol{k}}^{(2)} = \frac{4}{3} \delta_{{\rm m}\boldsymbol{k}}^{(2)\prime\prime} , \tag{5.5.24}$$

which gives us an expression for $\delta_{\rm r}^{(2)}$

$$\delta_{{\rm r}\boldsymbol{k}}^{(2)}(\eta) = A_{\rm rMD}(\boldsymbol{k}) \cos\frac{k\eta}{\sqrt{3}} + B_{\rm rMD}(\boldsymbol{k}) \sin\frac{k\eta}{\sqrt{3}}$$
$$+ \frac{\sqrt{3}}{k} \int_{\eta_{\rm rec}}^{\eta} d\tilde{\eta} \left(\sin\frac{k\eta}{\sqrt{3}} \cos\frac{k\tilde{\eta}}{\sqrt{3}} - \cos\frac{k\eta}{\sqrt{3}} \sin\frac{k\tilde{\eta}}{\sqrt{3}} \right) S_{\boldsymbol{k}\rm MD}(\tilde{\eta}) , \tag{5.5.25}$$

where the source term $S_{\boldsymbol{k}\rm MD}$ can be obtained by differentiating Eq. (5.5.7) twice. Note that here $\eta = \eta(\iota)$, the exact functional form can be obtained by solving the Friedmann equations. Just as discussed in the case of $\delta_{\rm m}^{(2)}$, the solution can be divided for two separate range of scales. Firstly, for $k \leq 1/\eta_{\rm rec} < k_{\rm eq}$, we can ignore the homogeneous solution, and $\delta_{{\rm r}\boldsymbol{k}}^{(2)}$ is

$$\delta_{{\rm r}\boldsymbol{k}}^{(2)}(\iota) = \frac{\sqrt{3}}{k} \int_{\iota_{\rm rec}}^{\iota} d\tilde{\iota} \left(\sin\frac{k\eta(\iota)}{\sqrt{3}} \cos\frac{k\tilde{\eta}(\tilde{\iota})}{\sqrt{3}} - \cos\frac{k\eta(\iota)}{\sqrt{3}} \sin\frac{k\tilde{\eta}(\tilde{\iota})}{\sqrt{3}} \right) S_{\boldsymbol{k}\rm MD}(\tilde{\iota}) . \tag{5.5.26}$$

$S_{\boldsymbol{k}\mathrm{MD}}$ can be written in terms of ι, using rule (5.5.5), as

$$\begin{aligned}
S_{\boldsymbol{k}\mathrm{MD}} &= \frac{4}{3}\delta^{(2)\prime\prime}_{\mathrm{mk}} \\
&= \frac{4}{3}\mathcal{H}_0^2 R_0^{1/3}\Omega_{\mathrm{m}0}\left(\frac{1+4\iota^3}{2}\frac{d}{d\iota}+\iota(1+\iota^3)\frac{d^2}{d\iota^2}\right)\delta^{(2)}_{\mathrm{mk}} \\
&= \frac{4}{3}\mathcal{H}_0^2 R_0^{1/3}\Omega_{\mathrm{m}0}\left[3\iota^{-5/2}\sqrt{1+\iota^3}\int_{\iota_{\mathrm{rec}}}^{\iota}(1+\tilde{\iota}^3)S_{\mathrm{m}}(\tilde{\iota},\mathbf{k})\right. \\
&\times\left.\left[\int_0^{\iota}d\tilde{\iota}\left(\frac{\tilde{\iota}}{1+\tilde{\iota}^3}\right)^{3/2}-\int_0^{\tilde{\iota}}d\tilde{\tilde{\iota}}\left(\frac{\tilde{\tilde{\iota}}}{1+\tilde{\tilde{\iota}}^3}\right)^{3/2}-\frac{\iota^{5/2}}{3\sqrt{1+\iota^3}}\right]+\iota(1+\iota^3)S_{\mathrm{m}}(\iota,\mathbf{k})\right], \qquad (5.5.27)
\end{aligned}$$

where Eq. (5.5.7) has been used, without the homogeneous part. In the second range of scales ($k > k_{\mathrm{eq}}$) instead, the whole Eq. (5.5.7) should be used to get $S_{\boldsymbol{k}\mathrm{MD}}$

$$\begin{aligned}
S_{\boldsymbol{k}\mathrm{MD}}(\iota) &= 4\mathcal{H}_0^2 R_0^{1/3}\Omega_{\mathrm{m}0}\left[\iota^{-5/2}\sqrt{1+\iota^3}\left(\int_{\iota_{\mathrm{rec}}}^{\iota}(1+\tilde{\iota}^3)S_{\mathrm{m}}(\tilde{\iota},\mathbf{k})\right.\right. \\
&\times\left.\left[\int_0^{\iota}d\tilde{\iota}\left(\frac{\tilde{\iota}}{1+\tilde{\iota}^3}\right)^{3/2}-\int_0^{\tilde{\iota}}d\tilde{\tilde{\iota}}\left(\frac{\tilde{\tilde{\iota}}}{1+\tilde{\tilde{\iota}}^3}\right)^{3/2}-\frac{\iota^{5/2}}{3\sqrt{1+\iota^3}}\right]\right. \\
&+\left.\left.\left[C_-(\boldsymbol{k})+C_+(\boldsymbol{k})\int_0^{\iota}d\tilde{\iota}\left(\frac{\tilde{\iota}}{1+\tilde{\iota}^3}\right)^{3/2}\right]\right)+\frac{\iota(1+\iota^3)S_{\mathrm{m}}(\iota,\mathbf{k})}{3}-\frac{C_+(\boldsymbol{k})}{3(1+\iota^3)}(1+3\iota^3)\right]. \qquad (5.5.28)
\end{aligned}$$

For the initial conditions $A_{\mathrm{rMD}}(\boldsymbol{k}), B_{\mathrm{rMD}}(\boldsymbol{k})$, we have to connect Eq. (5.5.25) with eq (5.3.14) at $\eta = \eta_{\mathrm{rec}}$. For $\eta \to \eta_{\mathrm{rec}}^-$, remembering the argument before Eq. (5.4.3), we can write $y = \xi^2 = (\eta/\eta_\star)^2$, as $\xi \gg 1$. So Eq. (5.3.14) reads

$$\begin{aligned}
\delta^{(2)}_{\mathrm{r(Tmesz)}}(\boldsymbol{k},\eta) &= A_{\mathrm{r}}(\boldsymbol{k})\cos\left(2\sqrt{\frac{2}{3}}\frac{k}{k_{\mathrm{eq}}}\sqrt{1+\left(\frac{\eta}{\eta_\star}\right)^2}\right)+B_{\mathrm{r}}(\boldsymbol{k})\sin\left(2\sqrt{\frac{2}{3}}\frac{k}{k_{\mathrm{eq}}}\sqrt{1+\left(\frac{\eta}{\eta_\star}\right)^2}\right) \\
&+\frac{k_{\mathrm{eq}}}{k\eta_*^2}\sqrt{\frac{3}{2}}\int_{\eta_\alpha}^{\eta}d\tilde{\eta}\,\tilde{\eta}\mathcal{Q}_{\boldsymbol{k}}(\tilde{\eta})\left[\sin\left(2\sqrt{\frac{2}{3}}\frac{k}{k_{\mathrm{eq}}}\sqrt{1+(\frac{\eta}{\eta_\star})^2}\right)\cos\left(2\sqrt{\frac{2}{3}}\frac{k}{k_{\mathrm{eq}}}\sqrt{1+\left(\frac{\tilde{\eta}}{\eta_\star}\right)^2}\right)\right. \\
&-\left.\cos\left(2\sqrt{\frac{2}{3}}\frac{k}{k_{\mathrm{eq}}}\sqrt{1+\left(\frac{\eta}{\eta_\star}\right)^2}\right)\sin\left(2\sqrt{\frac{2}{3}}\frac{k}{k_{\mathrm{eq}}}\sqrt{1+\left(\frac{\tilde{\eta}}{\eta_\star}\right)^2}\right)\right]. \qquad (5.5.29)
\end{aligned}$$

Applying following matching conditions

$$\delta^{(2)}_{\mathrm{r(Tmesz)}}(\boldsymbol{k},\eta\to\eta_{\mathrm{rec}}^-)\big|_{\eta_{\mathrm{rec}}} = \delta^{(2)}_{\mathrm{r}}(\boldsymbol{k},\eta\to\eta_{\mathrm{rec}}^+)\big|_{\eta_{\mathrm{rec}}}, \qquad (5.5.30)$$

$$\left(\frac{d}{d\eta}\delta^{(2)}_{\mathrm{r(Tmesz)}}(\boldsymbol{k},\eta\to\eta_{\mathrm{rec}}^-)\right)\Big|_{\eta_{\mathrm{rec}}} = \left(\frac{d}{d\eta}\delta^{(2)}_{\mathrm{r}}(\boldsymbol{k},\eta\to\eta_{\mathrm{rec}}^+)\right)\Big|_{\eta_{\mathrm{rec}}}, \qquad (5.5.31)$$

where the rhs is the solution Eq. (5.5.25), we get, respectively,

$$\begin{aligned}
&A_{\mathrm{r}}(\boldsymbol{k})\cos\left(2\sqrt{\frac{2}{3}}\frac{k}{k_{\mathrm{eq}}}\sqrt{1+\left(\frac{\eta_{\mathrm{rec}}}{\eta_\star}\right)^2}\right)+B_{\mathrm{r}}(\boldsymbol{k})\sin\left(2\sqrt{\frac{2}{3}}\frac{k}{k_{\mathrm{eq}}}\sqrt{1+\left(\frac{\eta_{\mathrm{rec}}}{\eta_\star}\right)^2}\right) \\
&+\frac{k_{\mathrm{eq}}}{k\eta_*^2}\sqrt{\frac{3}{2}}\int_{\eta_\alpha}^{\eta_{\mathrm{rec}}}d\tilde{\eta}\,\tilde{\eta}\mathcal{Q}_{\boldsymbol{k}}(\tilde{\eta})\left[\sin\left(2\sqrt{\frac{2}{3}}\frac{k}{k_{\mathrm{eq}}}\sqrt{1+\left(\frac{\eta_{\mathrm{rec}}}{\eta_\star}\right)^2}\right)\cos\left(2\sqrt{\frac{2}{3}}\frac{k}{k_{\mathrm{eq}}}\sqrt{1+\left(\frac{\tilde{\eta}}{\eta_\star}\right)^2}\right)\right. \\
&-\left.\cos\left(2\sqrt{\frac{2}{3}}\frac{k}{k_{\mathrm{eq}}}\sqrt{1+\left(\frac{\eta_{\mathrm{rec}}}{\eta_\star}\right)^2}\right)\sin\left(2\sqrt{\frac{2}{3}}\frac{k}{k_{\mathrm{eq}}}\sqrt{1+\left(\frac{\tilde{\eta}}{\eta_\star}\right)^2}\right)\right]
\end{aligned}$$

$$= A_{\rm rMD}(\boldsymbol{k})\cos\frac{k\eta_{\rm rec}}{\sqrt{3}} + B_{\rm rMD}(\boldsymbol{k})\sin\frac{k\eta_{\rm rec}}{\sqrt{3}}\,, \tag{5.5.32}$$

and

$$\begin{aligned}
&\frac{2\sqrt{2}}{k_{\rm eq}}\frac{\eta_{\rm rec}}{\eta_*^2\sqrt{1+\left(\frac{\eta_{\rm rec}}{\eta_\star}\right)^2}}\left[-A_{\rm r}(\boldsymbol{k})\sin\left(2\sqrt{\frac{2}{3}}\frac{k}{k_{\rm eq}}\sqrt{1+\left(\frac{\eta_{\rm rec}}{\eta_\star}\right)^2}\right)\right.\\
&\left.+B_{\rm r}(\boldsymbol{k})\cos\left(2\sqrt{\frac{2}{3}}\frac{k}{k_{\rm eq}}\sqrt{1+\left(\frac{\eta_{\rm rec}}{\eta_\star}\right)^2}\right)\right] + \frac{2\sqrt{3}\eta_{\rm rec}}{k\eta_*^4\sqrt{1+\left(\frac{\eta_{\rm rec}}{\eta_\star}\right)^2}}\\
&\times\int_{\eta_\alpha}^{\eta_{\rm rec}} d\tilde{\eta}\,\tilde{\eta}\mathcal{Q}_{\boldsymbol{k}}(\tilde{\eta})\left[\cos\left(2\sqrt{\frac{2}{3}}\frac{k}{k_{\rm eq}}\sqrt{1+\left(\frac{\eta_{\rm rec}}{\eta_\star}\right)^2}\right)\cos\left(2\sqrt{\frac{2}{3}}\frac{k}{k_{\rm eq}}\sqrt{1+\left(\frac{\tilde{\eta}}{\eta_\star}\right)^2}\right)\right.\\
&\left.+\sin\left(2\sqrt{\frac{2}{3}}\frac{k}{k_{\rm eq}}\sqrt{1+\left(\frac{\eta_{\rm rec}}{\eta_\star}\right)^2}\right)\sin\left(2\sqrt{\frac{2}{3}}\frac{k}{k_{\rm eq}}\sqrt{1+\left(\frac{\tilde{\eta}}{\eta_\star}\right)^2}\right)\right]\\
&= -A_{\rm rMD}(\boldsymbol{k})\sin\frac{k\eta_{\rm rec}}{\sqrt{3}} + B_{\rm rMD}(\boldsymbol{k})\cos\frac{k\eta_{\rm rec}}{\sqrt{3}}\,.
\end{aligned} \tag{5.5.33}$$

Multiplying Eq. (5.5.32) with $\sin(k\eta_{\rm rec}/\sqrt{3})$, Eq. (5.5.33) with $\cos(k\eta_{\rm rec}/\sqrt{3})$, and adding them, we get

$$\begin{aligned}
B_{\rm rMD}(\boldsymbol{k}) = A_{\rm r}(\boldsymbol{k})&\left[\cos\left(2\sqrt{\frac{2}{3}}\frac{k}{k_{\rm eq}}\sqrt{1+\left(\frac{\eta_{\rm rec}}{\eta_\star}\right)^2}\right)\sin\frac{k\eta_{\rm rec}}{\sqrt{3}}\right.\\
&\left.-\frac{2\sqrt{2}}{k_{\rm eq}}\frac{\eta_{\rm rec}}{\eta_*^2\sqrt{1+\left(\frac{\eta_{\rm rec}}{\eta_\star}\right)^2}}\sin\left(2\sqrt{\frac{2}{3}}\frac{k}{k_{\rm eq}}\sqrt{1+\left(\frac{\eta_{\rm rec}}{\eta_\star}\right)^2}\right)\cos\frac{k\eta_{\rm rec}}{\sqrt{3}}\right]\\
&+B_{\rm r}(\boldsymbol{k})\left[\sin\left(2\sqrt{\frac{2}{3}}\frac{k}{k_{\rm eq}}\sqrt{1+\left(\frac{\eta_{\rm rec}}{\eta_\star}\right)^2}\right)\sin\frac{k\eta_{\rm rec}}{\sqrt{3}}\right.\\
&\left.+\frac{2\sqrt{2}}{k_{\rm eq}}\frac{\eta_{\rm rec}}{\eta_*^2\sqrt{1+\left(\frac{\eta_{\rm rec}}{\eta_\star}\right)^2}}\cos\left(2\sqrt{\frac{2}{3}}\frac{k}{k_{\rm eq}}\sqrt{1+\left(\frac{\eta_{\rm rec}}{\eta_\star}\right)^2}\right)\cos\frac{k\eta_{\rm rec}}{\sqrt{3}}\right]\\
&+\int_{\eta_\alpha}^{\eta_{\rm rec}} d\tilde{\eta}\,\tilde{\eta}\mathcal{Q}_{\boldsymbol{k}}(\tilde{\eta})\left\{\frac{k_{\rm eq}}{k\eta_*^2}\sqrt{\frac{3}{2}}\sin\frac{k\eta_{\rm rec}}{\sqrt{3}}\right.\\
&\times\left[\sin\left(2\sqrt{\frac{2}{3}}\frac{k}{k_{\rm eq}}\sqrt{1+\left(\frac{\eta_{\rm rec}}{\eta_\star}\right)^2}\right)\cos\left(2\sqrt{\frac{2}{3}}\frac{k}{k_{\rm eq}}\sqrt{1+\left(\frac{\tilde{\eta}}{\eta_\star}\right)^2}\right)\right.\\
&\left.-\cos\left(2\sqrt{\frac{2}{3}}\frac{k}{k_{\rm eq}}\sqrt{1+\left(\frac{\eta_{\rm rec}}{\eta_\star}\right)^2}\right)\sin\left(2\sqrt{\frac{2}{3}}\frac{k}{k_{\rm eq}}\sqrt{1+\left(\frac{\tilde{\eta}}{\eta_\star}\right)^2}\right)\right]\\
&+\frac{2\sqrt{3}\eta_{\rm rec}}{k\eta_*^4\sqrt{1+\left(\frac{\eta_{\rm rec}}{\eta_\star}\right)^2}}\cos\frac{k\eta_{\rm rec}}{\sqrt{3}}\left[\cos\left(2\sqrt{\frac{2}{3}}\frac{k}{k_{\rm eq}}\sqrt{1+\left(\frac{\eta_{\rm rec}}{\eta_\star}\right)^2}\right)\right.\\
&\left.\times\cos\left(2\sqrt{\frac{2}{3}}\frac{k}{k_{\rm eq}}\sqrt{1+\left(\frac{\tilde{\eta}}{\eta_\star}\right)^2}\right)+\sin\left(2\sqrt{\frac{2}{3}}\frac{k}{k_{\rm eq}}\sqrt{1+\left(\frac{\eta_{\rm rec}}{\eta_\star}\right)^2}\right)\right.
\end{aligned}$$

$$\times \sin\left(2\sqrt{\frac{2}{3}}\frac{k}{k_{\rm eq}}\sqrt{1+\left(\frac{\tilde{\eta}}{\eta_\star}\right)^2}\right)\Bigg]\Bigg\}. \tag{5.5.34}$$

Multiplying Eq. (5.5.32) with $\cos\left(k\eta_{\rm rec}/\sqrt{3}\right)$, Eq. (5.5.33) with $\sin\left(k\eta_{\rm rec}/\sqrt{3}\right)$, and subtracting the latter from the former, we get

$$\begin{aligned}
A_{\rm rMD}(\boldsymbol{k}) = A_{\rm r}(\boldsymbol{k})\Bigg[&\cos\left(2\sqrt{\frac{2}{3}}\frac{k}{k_{\rm eq}}\sqrt{1+\left(\frac{\eta_{\rm rec}}{\eta_\star}\right)^2}\right)\cos\frac{k\eta_{\rm rec}}{\sqrt{3}}\\
&+\frac{2\sqrt{2}}{k_{\rm eq}}\frac{\eta_{\rm rec}}{\eta_*^2\sqrt{1+\left(\frac{\eta_{\rm rec}}{\eta_\star}\right)^2}}\sin\left(2\sqrt{\frac{2}{3}}\frac{k}{k_{\rm eq}}\sqrt{1+\left(\frac{\eta_{\rm rec}}{\eta_\star}\right)^2}\right)\sin\frac{k\eta_{\rm rec}}{\sqrt{3}}\Bigg]\\
&+B_{\rm r}(\boldsymbol{k})\Bigg[\sin\left(2\sqrt{\frac{2}{3}}\frac{k}{k_{\rm eq}}\sqrt{1+\left(\frac{\eta_{\rm rec}}{\eta_\star}\right)^2}\right)\cos\frac{k\eta_{\rm rec}}{\sqrt{3}}\\
&-\frac{2\sqrt{2}}{k_{\rm eq}}\frac{\eta_{\rm rec}}{\eta_*^2\sqrt{1+\left(\frac{\eta_{\rm rec}}{\eta_\star}\right)^2}}\cos\left(2\sqrt{\frac{2}{3}}\frac{k}{k_{\rm eq}}\sqrt{1+\left(\frac{\eta_{\rm rec}}{\eta_\star}\right)^2}\right)\sin\frac{k\eta_{\rm rec}}{\sqrt{3}}\Bigg]\\
&+\int_{\eta_\alpha}^{\eta_{\rm rec}}d\tilde{\eta}\,\tilde{\eta}\mathcal{Q}_{\boldsymbol{k}}(\tilde{\eta})\Bigg\{\frac{k_{\rm eq}}{k\eta_*^2}\sqrt{\frac{3}{2}}\cos\frac{k\eta_{\rm rec}}{\sqrt{3}}\\
&\times\Bigg[\sin\left(2\sqrt{\frac{2}{3}}\frac{k}{k_{\rm eq}}\sqrt{1+\left(\frac{\eta_{\rm rec}}{\eta_\star}\right)^2}\right)\cos\left(2\sqrt{\frac{2}{3}}\frac{k}{k_{\rm eq}}\sqrt{1+\left(\frac{\tilde{\eta}}{\eta_\star}\right)^2}\right)\\
&-\cos\left(2\sqrt{\frac{2}{3}}\frac{k}{k_{\rm eq}}\sqrt{1+\left(\frac{\eta_{\rm rec}}{\eta_\star}\right)^2}\right)\sin\left(2\sqrt{\frac{2}{3}}\frac{k}{k_{\rm eq}}\sqrt{1+\left(\frac{\tilde{\eta}}{\eta_\star}\right)^2}\right)\Bigg]\\
&-\frac{2\sqrt{3}\eta_{\rm rec}}{k\eta_*^4\sqrt{1+\left(\frac{\eta_{\rm rec}}{\eta_\star}\right)^2}}\sin\frac{k\eta_{\rm rec}}{\sqrt{3}}\Bigg[\cos\left(2\sqrt{\frac{2}{3}}\frac{k}{k_{\rm eq}}\sqrt{1+\left(\frac{\eta_{\rm rec}}{\eta_\star}\right)^2}\right)\\
&\times\cos\left(2\sqrt{\frac{2}{3}}\frac{k}{k_{\rm eq}}\sqrt{1+\left(\frac{\tilde{\eta}}{\eta_\star}\right)^2}\right)+\sin\left(2\sqrt{\frac{2}{3}}\frac{k}{k_{\rm eq}}\sqrt{1+\left(\frac{\eta_{\rm rec}}{\eta_\star}\right)^2}\right)\\
&\times\sin\left(2\sqrt{\frac{2}{3}}\frac{k}{k_{\rm eq}}\sqrt{1+\left(\frac{\tilde{\eta}}{\eta_\star}\right)^2}\right)\Bigg]\Bigg\}.
\end{aligned} \tag{5.5.35}$$

As mentioned earlier, in the analytical analysis discussed in this work, the solutions for $1/\eta_{\rm rec} < k < k_{\rm eq}$ are missing (e.g., see the gray area Fig. 5.1). One possible way we can overcome this problem could be the following prescription. Let us define the general solutions, both for matter and radiation, in this way

$$\delta_A^{(2)}(\eta \geq \eta_{\rm rec}, \boldsymbol{k}) = \frac{\left[\delta_{A\boldsymbol{k}}^{(2)}(k < 1/\eta_{\rm rec}, \eta \geq \eta_{\rm rec}) + (k/k_{\rm eq})^{n_A}\,\delta_{A\boldsymbol{k}}^{(2)}(k > k_{\rm eq}, \eta \geq \eta_{\rm rec})\right]}{1+(k/k_{\rm eq})^{n_A}}\,, \tag{5.5.36}$$

with $A = \{{\rm m}, {\rm r}\}$ and $n_A > 0$ (e.g. $n_A \simeq 2$). Here, clearly, $k < 1/\eta_{\rm rec}$ indicates the solutions obtained above which do not contain the homogeneous solutions and for $k > k_{\rm eq}$ we are considering solutions in which the modes entered the horizon before equality. This guess has to be tested numerically.

5.6 Summary

This chapter explores the tensor-induced scalar modes produced by GWs from inflation introduced in the previous one, and examines this mechanism for matter and radiation density perturbations during all the epochs of the evolution. We first extend the treatment to smaller scales, which enter the horizon during a radiation-dominated period when two matter components contribute to the energy density of the Universe, and compute radiation-density perturbations produced by these tensor-induced scalar modes.

We start by showing that metric perturbations can be safely implemented in the synchronous gauge from the very beginning using a perturbative expansion up to the second order in which the source term consists only of linear tensor perturbations. Then, we shift our focus to the radiation period, which is split into two phases based on the relative importance of background and perturbed quantities of the components. The first phase, known as the epoch of deep radiation, begins after the end of inflation when radiation dominates both the background and perturbation sectors. During this period, we calculate the radiation and matter perturbation solutions sourced by primordial GWs. We observe that the matter perturbation grows faster than the radiation one, leading to a subsequent second phase in which the matter perturbation overcomes the radiation perturbation and becomes the main contributor to Einsteins field equations.

The study presents a full solution of tensor-induced density contrast in the radiation domination, which was not explored in previous papers [81, 160]. In the second phase, we derive a Meszaros' like equation with a source term quadratic in GWs, focusing on the subhorizon regime since the effect is non-existent on the superhorizon. To obtain initial conditions for the second phase, we match the solutions from the two phases at the junction, ignoring the initial conditions for the first phase since the effect is suppressed by the fact that all these modes enter within the horizon scale only during the radiation epoch. We derive the full solution of the tensor-sourced scalar modes entering the horizon starting from the end of inflation to matter epoch for modes $k > k_{\rm eq}$.

Finally, we extend the analysis of previous studies [167], computing the tensor contribution to matter and radiation perturbations at late times, i.e., from $\eta_{\rm eq} \ll \eta_{\rm rec} \leq \eta \leq \eta_0$, both for $k < 1/\eta_{\rm rec}$ and $k > k_{\rm eq}$, where η_0 is the conformal time today and $\eta_{\rm rec}$ is at the recombination epoch.

Chapter 6

Gravitational Waves Induced by Scalar-tensor Mixing

In the preceding two chapters, we were able to derive the matter density contrast from the fluctuation of the GWs radiation. In this chapter, we will discuss the second-order GWs. While the general expectation is that SIGWs dominate the secondary GWs signal, the product of scalar-tensor and tensor-tensor also source GWs at second order. It is thus important to systematically study the physics of these additional GWs signals and investigate their distinct signatures and any chance at detecting them. In this paper, we focus on GWs induced by interactions between scalar and tensor perturbations in the radiation-dominated Universe, by treating such scalar-tensor interactions as a source to GWs in the early Universe. A curious difference with the scalar-scalar induced GWs is that scalar-tensor induced GWs are purely a geometrical effect, namely that no matter fields appear directly as a source. In fact, the same scalar-tensor interactions are responsible for lensing of GWs. Thus, understanding these interactions in cosmology might be important for a general description of cosmic GWs propagating through an inhomogenous Friedmann-Lemaître-Robertson-Walker (FLRW) Universe.

Scalar-tensor induced GWs have been explored before in Refs. [170, 171]. In particular, Ref. [171] pointed out that, for Dirac delta primordial scalar and tensor spectra, scalar-tensor induced GWs may dominate the high-frequency regime of the total induced GWs. However, there is no general answer regarding the detectability of this signal compared to scalar-induced GWs. While GWs induced by scalar-tensor interactions are novel and intriguing in its own right, it is important to address this latter point. In our analysis, we assume that scalar perturbations are more pronounced on small scales than tensor perturbations, thus neglecting tensor-tensor interactions, which can be found in [170, 171]. Under the condition $A_T < A_S$, we investigate whether the scalar-tensor contribution to GWs can be distinguished from scalar-induced GWs. The content of this chapter is based on the paper [172].

6.1 Evolution equation of GWs induced by scalar-tensor interactions in an RD regime

We consider a flat FLRW space-time, which is described by the metric: $ds^2 = -dt^2 + a^2(t)d\boldsymbol{x}^2$, where t is the co-ordinate time, and $a(t)$, the scale factor. As before, $c = \hbar = 1$ is assumed. We choose RD era, as we intend to subsequently compare these GWs with the SIGWs, which are primarily discussed in the same era due to their connection to the PBHs. We begin by defining our metric convention in a perturbed FLRW Universe, containing scalar, vector, and tensor perturbations according to Chapter 3. In ADM formalism we have

$$ds^2 = -N^2dt^2 + \gamma_{ij}dx^idx^j\,, \tag{6.1.1}$$

where $N = e^{\Phi}$ is the lapse function, and $\gamma_{ij} = a^2e^{-2\Psi}h_{ij} = a^2e^{-2\Psi}e^{\tilde{\gamma}_{ij}}$ is the metric for three dimensional hypersurface of constant t. The scalar perturbation sector contains linear Φ and Ψ, and $\tilde{\gamma}_{ij}$ signifies the transverse vector and tensor perturbations.

Proceeding according to the same approach we took in Chapter 3, we arrive up to the trace-less part of the ij-th equation, i.e. Eq. (3.2.6). As we have all the components, we take only scalar-tensor(or vector) terms on the right hand side, and we have

$$\begin{aligned}\ddot{\tilde{\gamma}}^i_k - \dot{\Phi}e^{\Phi}\dot{\tilde{\gamma}}^i_k + 3(H-\dot{\Psi})\dot{\tilde{\gamma}}^i_k - \frac{e^{2(\Phi+\Psi)}}{a^2}\nabla^2\tilde{\gamma}^i_k = 2\frac{e^{2(\Phi+\Psi)}}{a^2}\Big[\Phi^{,i}_{,k} + \Phi^{,i}\Phi_{,k} - \Psi^{,i}\Psi_{,k} - \Psi^{,i}_{,k}\\ +\Phi^{,i}\Psi_{,k} + \Psi^{,i}\Phi_{,k} - \frac{2}{3}\Phi^{,l}\Psi_{,l}\delta^i_k - \frac{1}{3}\Phi^{,l}\Phi_{,l}\delta^i_k + \frac{1}{3}\Psi^{,l}\Psi_{,l}\delta^i_k\Big] + \mathcal{S}\,,\end{aligned} \tag{6.1.2}$$

where $\mathcal{S}$ contains scalar-tensor mixed terms like $\sim \Phi(\tilde{\gamma}_{ij})$, and contribution from the matter component of the Universe, $\overline{S}^i_k$

$$\begin{aligned}\mathcal{S} = 2\frac{e^{2(\Phi+\Psi)}}{a^2}\Big[&-\tilde{\gamma}^{ij}(\Phi-\Psi)_{,jk} + \frac{1}{3}\tilde{\gamma}^{lm}(\Phi-\Psi)_{,lm}\,\delta^i_k - \frac{1}{2}\tilde{\gamma}^{im}_{,k}(\Phi-\Psi)_{,m} + \frac{1}{2}\tilde{\gamma}^{i,m}_{k}(\Phi-\Psi)_{,m}\\ &-\frac{1}{2}\tilde{\gamma}^{m,i}_{k}(\Phi-\Psi)_{,m} + \frac{1}{3}\tilde{\gamma}^{lm}_{,l}(\Phi-\Psi)_{,m}\delta^i_k - \tilde{\gamma}^{ij}\Psi_{,k}\Phi_{,j} - \tilde{\gamma}^{ij}\Phi_{,k}\Psi_{,j} - \tilde{\gamma}^{ij}\Phi_{,k}\Phi_{,j}\\ &\frac{1}{3}\tilde{\gamma}^{lm}\Phi_{,l}(\Phi+2\Psi)_{,m}\delta^i_k + \tilde{\gamma}^{ij}\Psi_{,k}\Psi_{,j} - \frac{1}{3}\tilde{\gamma}^{lm}\Psi_{,l}\Psi_{,m}\delta^i_k - \frac{1}{2}\tilde{\gamma}^{m,i}_{k,m} - \frac{1}{2}\tilde{\gamma}^{im}_{,km} + \frac{1}{3}\tilde{\gamma}^{lm}_{,lm}\delta^i_k\Big]\\ &+ 16\pi G e^{2\Phi}\overline{S}^i_k\,.\end{aligned} \tag{6.1.3}$$

We now proceed to make a number of assumptions which will help us extract the induced gravitational waves only from the interaction of linear scalar and tensor modes.

- $\tilde{\gamma}^{im}_{,m} = 0$, i.e. we will ignore the linear vector perturbations.
- $\Phi = \Psi$, i.e. we will ignore the anisotropic stress.
- $\tilde{\gamma}^{im} \times O(\Phi^2(\Psi^2)) = 0$, i.e. higher order contributions will be ignored.

- $\overline{S}^i_k = 0$, i.e. matter contribution is ignored.

Hence, taking only scalar-tensor terms as the source, and linearizing the exponential term, the evolution equation for the induced waves Eq. (6.1.2) becomes

$$\ddot{\tilde{\gamma}}^i_k + 3H\dot{\tilde{\gamma}}^i_k - \frac{1}{a^2}\nabla^2\tilde{\gamma}^i_k = \frac{4\Phi}{a^2}\nabla^2\tilde{\gamma}^i_k + 4\dot{\Phi}\dot{\tilde{\gamma}}^i_k\,. \tag{6.1.4}$$

In Fourier space Eq. (6.1.4) becomes

$$\ddot{\tilde{\gamma}}_{\boldsymbol{k}} + 3H\dot{\tilde{\gamma}}_{\boldsymbol{k}} + \frac{k^2}{a^2}\tilde{\gamma}_{\boldsymbol{k}} = -\frac{2}{a^2}\int \frac{d^3k_1}{(2\pi)^3}\Phi_{\boldsymbol{k}-\boldsymbol{k}_1}k_1^2\tilde{\gamma}^i_k(\boldsymbol{k}_1,t)\epsilon^k_i(\hat{\boldsymbol{k}}) + 2\int \frac{d^3k_1}{(2\pi)^3}\dot{\Phi}_{\boldsymbol{k}-\boldsymbol{k}_1}\dot{\tilde{\gamma}}^i_k(\boldsymbol{k}_1,t)\epsilon^k_i(\hat{\boldsymbol{k}})\,. \tag{6.1.5}$$

for each polarization of the induced GWs, and $\tilde{\gamma}^i_k(\boldsymbol{k}_1,t) = \tilde{\gamma}_{\boldsymbol{k}_1(\sigma)}(t)\epsilon_k^{(\sigma)i}(\hat{\boldsymbol{k}}_1)$. Moving to conformal time η, we have

$$\tilde{\gamma}''_{\boldsymbol{k}} + 2\mathcal{H}\tilde{\gamma}'_{\boldsymbol{k}} + k^2\tilde{\gamma}_{\boldsymbol{k}} = -2\int \frac{d^3k_1}{(2\pi)^3}\epsilon^k_i(\hat{\boldsymbol{k}})\left[\Phi_{\boldsymbol{k}-\boldsymbol{k}_1}k_1^2\tilde{\gamma}^i_k(\boldsymbol{k}_1,\eta) - \Phi'_{\boldsymbol{k}-\boldsymbol{k}_1}\tilde{\gamma}^{i'}_k(\boldsymbol{k}_1,\eta)\right]\,. \tag{6.1.6}$$

In the last two terms, we will feed the solution for the zero-th order equation

$$\tilde{\gamma}''_{0\boldsymbol{k}} + 2\mathcal{H}\tilde{\gamma}'_{0\boldsymbol{k}} + k^2\tilde{\gamma}_{0\boldsymbol{k}} = 0\,, \tag{6.1.7}$$

which gives, in RD era

$$\tilde{\gamma}_{0\boldsymbol{k}}(\eta) = \tilde{\gamma}_{\boldsymbol{k}}(0)T_{\tilde{\gamma}}(k\eta) = \tilde{\gamma}_{\boldsymbol{k}}(0)\sqrt{\frac{\pi}{2k\eta}}J_{1/2}(k\eta)\,, \tag{6.1.8}$$

which decomposes $\tilde{\gamma}_{0\boldsymbol{k}}(\eta)$ into its primordial value and the transfer function. Likewise, $\Phi_{\boldsymbol{k}-\boldsymbol{k}_1}(\eta)$ can be decomposed as

$$\Phi_{\boldsymbol{k}-\boldsymbol{k}_1}(\eta) = \Phi_{\boldsymbol{k}-\boldsymbol{k}_1}(0)T_\Phi(|\boldsymbol{k}-\boldsymbol{k}_1|\eta) = \Phi_{\boldsymbol{p}}(0)\,2^{\frac{3}{2}}\,\Gamma(5/2)\left(\frac{p\eta}{\sqrt{3}}\right)^{-\frac{3}{2}}J_{3/2}\left(\frac{p\eta}{\sqrt{3}}\right), \tag{6.1.9}$$

where $\boldsymbol{k}-\boldsymbol{k}_1 = \boldsymbol{p}$. The evolution equation of induced GWs, Eq. (6.1.6), then becomes

$$\begin{aligned}\tilde{\gamma}''_{\boldsymbol{k}} + 2\mathcal{H}\tilde{\gamma}'_{\boldsymbol{k}} + k^2\tilde{\gamma}_{\boldsymbol{k}} = -2\int \frac{d^3k_1}{(2\pi)^3}\Phi_{\boldsymbol{k}-\boldsymbol{k}_1}(0)\tilde{\gamma}^{(\sigma)}_{\boldsymbol{k}_1}(0)\epsilon_k^{(\sigma)i}(\hat{\boldsymbol{k}}_1)\epsilon^k_i(\hat{\boldsymbol{k}})\\ \times\left[k_1^2T_{\tilde{\gamma}}(k_1\eta)T_\Phi(|\boldsymbol{k}-\boldsymbol{k}_1|\eta) - T'_{\tilde{\gamma}}(k_1\eta)T'_\Phi(|\boldsymbol{k}-\boldsymbol{k}_1|\eta)\right].\end{aligned} \tag{6.1.10}$$

Applying Green's method, the solution to Eq. (6.1.10) is

$$\tilde{\gamma}_{\boldsymbol{k}}(\eta) = \tilde{\gamma}_{\boldsymbol{k}}(0)j_0(k\eta) + \int_0^\eta d\tilde{\eta}\,S_{st}(\boldsymbol{k},\eta)\,G(\eta,\tilde{\eta}), \tag{6.1.11}$$

where $S_{st}(\boldsymbol{k},\eta)$ is the right hand side of Eq. (6.1.10), and $G(\eta,\tilde{\eta})$ is the Green's function of the same equation, given by Eq. (3.2.16). The second term refers to the modulated GWs.

6.2 Power-spectrum and kernel function

6.2.1 For non-chiral primordial gravitational waves

Keeping in mind Eq. (3.3.1) for the dimension-less power-spectrum of the correction $\tilde{\gamma}_1(k)$, we have

$$\Delta^2_{\tilde{\gamma}_1}(k) = \frac{k^3}{\pi}\int d^3k_1\,\frac{\Delta^2_\Phi(|\boldsymbol{k}-\boldsymbol{k}_1|)\Delta^{(\sigma)2}_{\tilde{\gamma}_0}(k_1)}{k_1^3|\boldsymbol{k}-\boldsymbol{k}_1|^3}\epsilon_k^{(\sigma)i}(\hat{\boldsymbol{k}}_1)\epsilon^{(\lambda)k}_i(\hat{\boldsymbol{k}})\epsilon^{(\sigma)m}_n(-\hat{\boldsymbol{k}}_1)\epsilon^{(\lambda)n}_m(-\hat{\boldsymbol{k}})$$

$$\times \left(\int_0^\eta d\tilde{\eta}\, G(\eta,\tilde{\eta}) \left[k_1^2 T_{\tilde{\gamma}}(k_1\tilde{\eta}) T_\Phi(|\boldsymbol{k}-\boldsymbol{k}_1|\tilde{\eta}) - T'_{\tilde{\gamma}}(k_1\tilde{\eta}) T'_\Phi(|\boldsymbol{k}-\boldsymbol{k}_1|\tilde{\eta}) \right] \right)^2 , \tag{6.2.1}$$

where we have dropped the superscript λ as there is no parity violation after inflation as per our assumption in this sub-section, and used the definition of the two-point function of Φ and $\tilde{\gamma}_{\boldsymbol{k}}^{(\sigma)}$

$$\langle \Phi_{\boldsymbol{k}-\boldsymbol{k}_1}(0) \Phi_{\boldsymbol{k}'-\boldsymbol{k}'_1}(0) \rangle = (2\pi)^3 \delta^3(\boldsymbol{k}-\boldsymbol{k}_1+\boldsymbol{k}'-\boldsymbol{k}'_1) \frac{2\pi^2}{|\boldsymbol{k}-\boldsymbol{k}_1|^3} \Delta^2_\Phi(|\boldsymbol{k}-\boldsymbol{k}_1|) , \tag{6.2.2}$$

$$\langle \tilde{\gamma}^{(\sigma)}_{\boldsymbol{k}_1}(0) \tilde{\gamma}^{(\sigma')}_{\boldsymbol{k}'_1}(0)) \rangle = (2\pi)^3 \delta^3(\boldsymbol{k}_1+\boldsymbol{k}'_1) \delta_{\sigma\sigma'} \frac{2\pi^2}{k_1^3} \Delta^{(\sigma)2}_{\tilde{\gamma}_0}(k) . \tag{6.2.3}$$

As usual, we work with the variables $v = k_1/k$, $u = |\boldsymbol{k}-\boldsymbol{k}_1|/k$, and use the dimensionless time variable $x = k\eta$. As we assume a non-chiral graviational wave at the earlier times, i.e. $\Delta^{(\sigma)2}_{\tilde{\gamma}_0}(k) = \Delta^2_{\tilde{\gamma}_0}(k)/2$, Eq. (6.2.1) reads

$$\Delta^2_{\tilde{\gamma}_1}(k) = \iint (uv)^{-2}\, du\, dv\, \Delta^2_\Phi(uk)\, \frac{\Delta^2_{\tilde{\gamma}_0}(vk)}{2} \left[\frac{(1+v^2-u^2)^2}{v^2} + \left(1 + \left(\frac{1+v^2-u^2}{2v} \right)^2 \right)^2 \right] \times \left(\int_0^x k\, d\tilde{x}\, G(x,\tilde{x}) \left[v^2 T_{\tilde{\gamma}}(v\tilde{x}) T_\Phi(u\tilde{x}) - \dot{T}_{\tilde{\gamma}}(v\tilde{x}) \dot{T}_\Phi(u\tilde{x}) \right] \right)^2 , \tag{6.2.4}$$

for each polarisation of $\tilde{\gamma}_1(k)$, dot here means derivative w.r.t. x. Accounting for both polarisations of $\tilde{\gamma}_1(k)$, we have

$$\Delta^2_{\tilde{\gamma}_1}(k) = \int_0^\infty dv \int_{|v-1|}^{v+1} du\, (uv)^{-2}\, \Delta^2_\Phi(uk)\, \Delta^2_{\tilde{\gamma}_0}(vk) \left[\frac{(1+v^2-u^2)^2}{v^2} + \left(1 + \left(\frac{1+v^2-u^2}{2v} \right)^2 \right)^2 \right] \times \left(\int_0^x k\, d\tilde{x}\, G(x,\tilde{x}) \left[v^2 T_{\tilde{\gamma}}(v\tilde{x}) T_\Phi(u\tilde{x}) - \dot{T}_{\tilde{\gamma}}(v\tilde{x}) \dot{T}_\Phi(u\tilde{x}) \right] \right)^2 , \tag{6.2.5}$$

where the Green's function becomes

$$G(x,\tilde{x}) = \frac{\pi}{2k}\, \tilde{x} \sqrt{\frac{\tilde{x}}{x}} \left(J_{1/2}(\tilde{x}) Y_{1/2}(x) - J_{1/2}(x) Y_{1/2}(\tilde{x}) \right) . \tag{6.2.6}$$

It is worth noting that in the subsequent analysis, we consider the upper limit of the time integral in Eq. (6.2.5) to be formally infinite. This is justified by the fact that the gravitational wave frequencies of interest enter the horizon well within the radiation-dominated epoch, satisfying the condition $k\eta_{\rm eq} \gg 1$, where $\eta_{\rm eq}$ represents the time of radiation-matter equality. As a result, the contribution from large values of the conformal time becomes negligible. Taking the upper limit to be ∞, the kernel in Eq. (6.2.5) turns out to be

$$\begin{aligned} \mathcal{I} &= \int_0^\infty k\, d\tilde{x}\, G(x,\tilde{x}) \left[v^2 T_{\tilde{\gamma}}(v\tilde{x}) T_\Phi(u\tilde{x}) - \dot{T}_{\tilde{\gamma}}(v\tilde{x}) \dot{T}_\Phi(u\tilde{x}) \right] , \\ &= \frac{\pi}{4} \frac{v}{u/\sqrt{3}} \frac{1}{x} \Bigg\{ - \cos x \left(1 - P_2^0(\cos m) \right) \Theta\left(v + \frac{u}{\sqrt{3}} - 1 \right) \Theta\left(1 - \left| v - \frac{u}{\sqrt{3}} \right| \right) \\ &- \frac{2}{\pi} \sin x \Bigg[(Q_0^0(\cosh n) - Q_2^0(\cosh n)) \Theta\left(1 - v - \frac{u}{\sqrt{3}} \right) \\ &- (Q_0^0(\cos m) - Q_2^0(\cos m)) \Theta\left(v + \frac{u}{\sqrt{3}} - 1 \right) \Theta\left(1 - \left| v - \frac{u}{\sqrt{3}} \right| \right) \Bigg] \Bigg\} , \end{aligned} \tag{6.2.7}$$

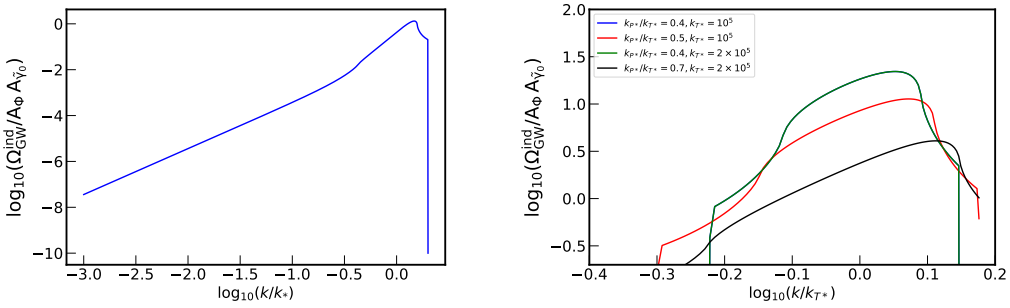

Figure 6.1: Left: Properly normalised density parameter for monochromatic scalar and non-chiral tensors, having same k_*. Right: Same as the left, with different peak locations. Blue and Green curves have coincided. The two dips in the right one comes from the first Heaviside theta: $0.3 < k_*/k_{T*} < 1.7$ for the bottom-most curve. As can be seen, different peaks contribution is for a small range due to two thetas.

where $2uv/\sqrt{3}\cos m = v^2 + u^2/3 - 1$ and $2uv/\sqrt{3}\cosh n = 1 - v^2 - u^2/3$, and P^l_m, Q^l_m are the associated Legendre polynomials of the first and second kind. It gives the oscillation average of the kernel squared $(\cos m = s = -\cosh n)$

$$\langle \mathcal{I}^2 \rangle = \frac{9}{2^7 x^2}\left(\frac{v}{u/\sqrt{3}}\right)^2 \left[\pi^2(1-s^2)^2\Theta\left(1-|s|\right) + \left(2s + (1-s^2)\log\left|\frac{1+s}{1-s}\right|\right)^2\right] . \tag{6.2.8}$$

The final expression for the oscillation averaged power-spectrum of the induced gravitational waves from the scalar-tensor interactions is

$$\langle \Delta^2_{\tilde\gamma_1}(k)\rangle = \int_0^\infty dv \int_{|v-1|}^{v+1} du\, (uv)^{-2}\, \Delta^2_\Phi(uk)\, \Delta^2_{\tilde\gamma_0}(vk) \left[\frac{(1+v^2-u^2)^2}{v^2} + \left(1 + \left(\frac{1+v^2-u^2}{2v}\right)^2\right)^2\right] \langle \mathcal{I}^2\rangle \,, \tag{6.2.9}$$

with $\langle \mathcal{I}^2\rangle$ given by Eq. (6.2.8). Let us examine the infrared ($k \to 0$) behavior of the kernel. In this limit, $u \sim v \sim 1/k \gg 1$. Hence, s takes the value

$$s = \frac{2}{\sqrt{3}} . \tag{6.2.10}$$

In contrast, SIGWs exhibit a different behavior, as s approaches 1 in this limit (see Chapter 3). In that scenario, a logarithmic divergence arises, which is not observed in scalar-tensor-induced GWs due to the fact that s never reaches the value of 1 in IR. This logarithmic running has been regarded as a distinctive characteristic of SIGWs, setting them apart from primordial GWs in the infrared (IR) region. Notably, our findings demonstrate that such a feature is absent in our case.

In the opposite limit ($k \to \infty$), i.e. the UV one, $v \to 1$ and $u \to 0$, which corresponds to the large wavelength limit for the scalars, we observe that the variable s approaches u. As a result, the kernel exhibits the behavior

$$\langle \mathcal{I}^2\rangle \sim \frac{1}{u^2} . \tag{6.2.11}$$

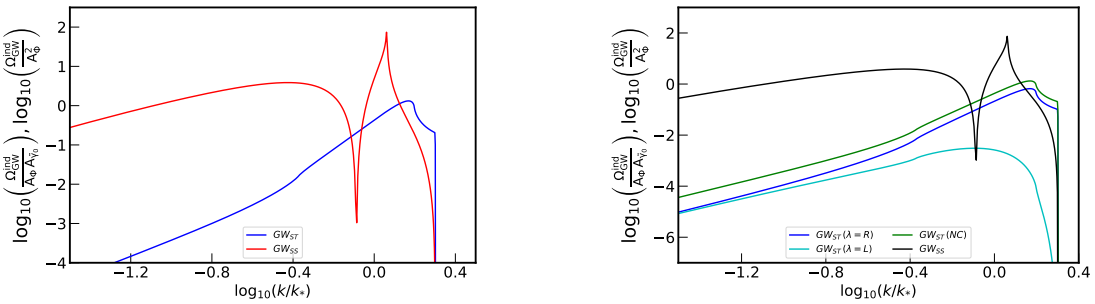

Figure 6.2: Left: Comparison of the gravitational wave density parameter (properly normalised) induced by monochromatic scalar and non-chiral tensors (blue), and monochromatic scalars only (red) having same peak location. Right: Same as the left panel, with the induced right- and left-handed chiral GWs added for comparison, when primordial GWs are right-handed. NC signifies non-chiral.

Consequently, the integral in Eq. (6.2.9) becomes proportional to $1/u^4$. On the other hand, if we take $v \to 1$ and $u \to 0$, then we have $s \to 1/v$, which does not lead to any divergence.

In Eq. (6.2.8), another notable feature occurs when $s = \pm 1$. In the case of SIGWs, this scenario can lead to a logarithmic resonance. However, in our case, the presence of the term $(1 - s^2)$ prevents such resonance from occurring. In fact, for $s = \pm 1$, or $v = \pm(1 - u/\sqrt{3})$, we have

$$\langle \mathcal{I}^2 \rangle = \frac{9}{2^5} \left(1 - \frac{1}{u/\sqrt{3}} \right)^2 . \tag{6.2.12}$$

This diverges in the $u \to 0$ limit.

Now, we proceed to demonstrate the effect using a specific choice of input scalar and tensor perturbations: peaked sources. We do so for simplicity and because enhancements of primordial scalar and tensor fluctuations during inflation often lead to peaked primordial spectra [80, 148, 151, 173]. We first consider monochromatic primordial spectra and later discuss the effects of a finite width. The fraction of the GWs energy density per logarithmic wavelength is given by Eq. (3.3.11). To evaluate the amplitude of the GWs spectral density today, we use [119]

$$\Omega_{\mathrm{GW},0}^{\mathrm{ind}} h^2 = 1.62 \times 10^{-5} \left(\frac{\Omega_{\mathrm{rad},0} h^2}{4.18 \times 10^{-5}} \right) \left(\frac{g_\rho(T_c)}{106.75} \right) \left(\frac{g_s(T_c)}{106.75} \right)^{-4/3} \Omega_{\mathrm{GW,c}}^{\mathrm{ind}} , \tag{6.2.13}$$

where $\Omega_{\mathrm{rad},0} h^2 = 4.18 \times 10^{-5}$ is the density fraction of radiation today [5], and $g_\rho(T_c)$ and $g_s(T_c)$ are the effective degrees of freedom in the energy density and entropy evaluated. The subscript 'c' denotes evaluation at a time where GWs are deep inside the horizon so that they behave as radiation.

6.2.1.1 Monochromatic primordial spectra

For both scalar and tensor primordial power-spectrum, we take a Dirac delta source located at $k_{P/T*}$

$$\Delta_\Phi^2(uk) = A_\Phi \, \delta \left(\ln \frac{uk}{k_{P*}} \right) , \tag{6.2.14}$$

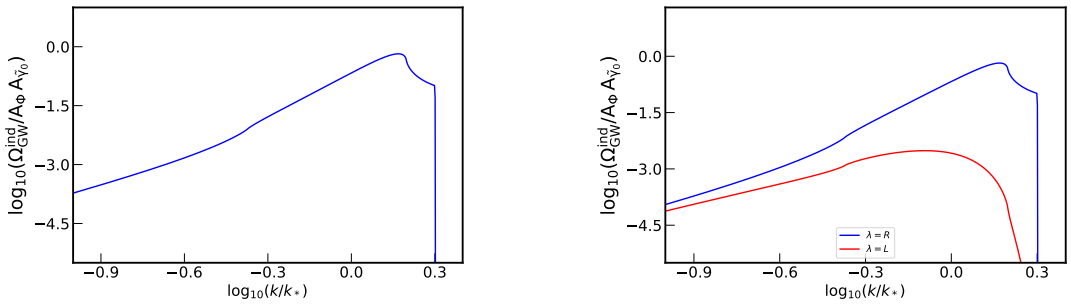

Figure 6.3: Left: Properly normalised total spectral density for induced GWs from monochromatic scalar and chiral GWs mixing. Right: Properly normalised density parameter of right- and left-handed induced GWs from right-handed primordial tensors. Both panels show cases with same peak location.

$$\Delta^2_{\tilde\gamma_0}(vk) = A_{\tilde\gamma_0}\,\delta\left(\ln\frac{vk}{k_{T*}}\right). \tag{6.2.15}$$

This kind of peaked scalar sources can be relevant for primordial black hole formation [174–176].

For same peak location ($k_{P*} = k_{T*} = k_*$), we have, from Eq. (6.2.9)

$$\langle\Delta^2_{\tilde\gamma_1}(k)\rangle = A_\Phi\, A_{\tilde\gamma_0}\left(\frac{k}{k_*}\right)^2\left[1+\frac{k^4}{16k_*^4}+\frac{3k^2}{2k_*^2}\right]\langle\mathcal{I}^2\rangle_{u=v=k_*/k}\,\Theta(2k_*-k)\,. \tag{6.2.16}$$

The left panel of Fig. 6.1 shows the GWs energy density for this case. The appearance of the Heaviside theta function is explained in Chapter 3.

For different peak locations,

$$\begin{aligned}\langle\Delta^2_{\tilde\gamma_1}(k)\rangle = A_\Phi\, A_{\tilde\gamma_0}\,\frac{k^2}{k_{P*}k_{T*}}&\left[\frac{(k^2+k_{T*}^2-k_{P*}^2)^2}{k^2k_{T*}^2}+\frac{(4k^2k_{T*}^2+(k^2+k_{T*}^2-k_{P*}^2)^2)^2}{16k^4k_{T*}^4}\right]\\ &\times\langle\mathcal{I}^2\rangle_{v=k_{T*}/k,u=k_{P*}/k}\,\Theta(k_{P*}-|k_{T*}-k|)\,\Theta(k_{T*}+k-k_{P*})\,.\end{aligned} \tag{6.2.17}$$

Naturally, the range of wave-number of the induced waves increases with a decreasing separation of the two different peaks, which can be seen from the two Heaviside thetas, and the right panel of Fig. 6.1.

The right panel of Fig. 6.1 and the left panel of Fig. 6.5 exhibit an enhancement in the induced GWs between the two dips that are determined by the first Heaviside theta function in Eq. (6.2.17), even though the scalar and tensor source peaks are located at different positions. This enhancement arises due to the infrared divergence described in the previous section. We have been able to obtain a solution in case of monochromatic primordial perturbations only because in this case the momenta acquire a single value. For other shapes of source primordial spectra, the integral should be regularised.

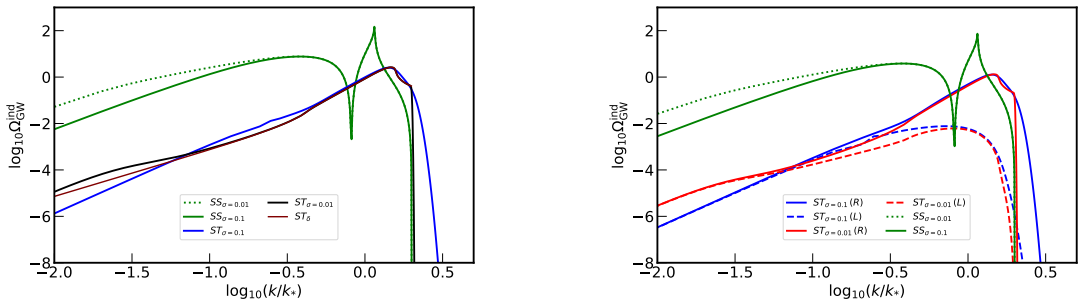

Figure 6.4: Left: Properly normalised total spectral density for induced GWs from log-normal scalar and non-chiral GWs mixing. SIGWs and Dirac delta-induced GWs are also presented for comparison. Right: The same for right- and left-handed induced GWs from right-handed primordial tensors. They are both normalised with $A_{\Phi/\tilde{\gamma}_0} = 1$.

6.2.1.2 Log-normal primordial spectra

Now, we consider a more realistic version of a Dirac delta peak, which is a peak with a finite width. This peak is located at the same position k_* for both scalar and tensor perturbations, a choice made for simplicity

$$\Delta^2_{\Phi/\tilde{\gamma}_0}(k) = \frac{A_{\Phi/\tilde{\gamma}_0}}{\sqrt{2\pi}\sigma} \exp\left(-\frac{1}{2\sigma^2}\ln^2\frac{k}{k_*}\right), \tag{6.2.18}$$

where we have also chosen the same width for both kind of perturbations, but extending to different widths is straightforward. Interestingly, we find that the amplitude of the scalar-tensor induced GWs spectrum is not very sensitive to the width of the primordial spectra. The spectral shape of course changes: it broadens for broader peaks. For the log-normal primordial spectra, we compute the scalar-tensor induced GWs numerically, and present our findings in Fig. 6.4. From the left panel, we can see that as one gets closer to the peak, all lines are similar to the Dirac delta case. Also, note that for a finite width primordial spectra, there is no sharp cut-offs in the scalar-tensor induced GWs, as expected.

In both panels of Fig. 6.2, it is evident that there exists only a limited range of scales (approximately $k/k_* \in [1.34, 2]$), where the scalar-induced GWs do not surpass the scalar-modulated ones. This trend is also seen in Fig. 6.4. Detecting the modulated waves amidst the dominance of the former requires an identifying characteristic that can distinguish our effect. As observed in this section, non-chiral primordial waves lack such a property. However, when scalar modulation affects chiral primordial GWs, a disparity in the energy density between left and right circularly polarized waves becomes apparent. This distinction offers a potential avenue for detecting and studying the modulated waves.

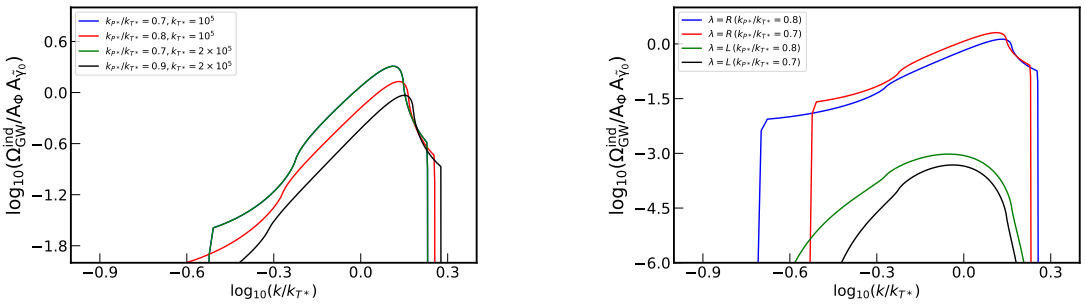

Figure 6.5: Left: Properly normalised total spectral density for induced GWs from monochromatic scalar and right-handed chiral GWs mixing. We can see that keeping the same wave-number ratio, changing the primordial GWs peak location does not affect the spectral density of the induced GWs. Right: Properly normalised density parameter of right- and left-handed induced GWs for right-handed primordial tensors, taking $k_{T*} = 10^5\,\mathrm{Mpc}^{-1}$. Both panels show cases with different peak locations of scalar and tensor perturbations.

6.2.2 For chiral primordial gravitational waves

To extend the assumptions beyond a non-chiral primordial GWs background, we can consider scenarios where the initial GWs are chiral. To accomplish this, we use left and right-handed polarisation tensors that are normalized by $\epsilon^{(\lambda)*}_{ij}(\hat{\boldsymbol{k}})\epsilon^{(\lambda')ij}(\hat{\boldsymbol{k}}) = 2\delta_{\lambda\lambda'}$, $(\lambda,\lambda' = \mathrm{R},\mathrm{L})$ instead of $\epsilon^{(\lambda)}_{ij}(\hat{\boldsymbol{k}})\epsilon^{(\lambda')ij}(\hat{\boldsymbol{k}}) = 2\delta_{\lambda\lambda'}$. Then, starting from Eq. (6.1.4), we have, for the power-spectrum of the induced waves,

$$\Delta^2_{\tilde\gamma_1}(k) = \frac{k^3}{\pi}\int d^3\boldsymbol{k}_1 \frac{\Delta^2_\Phi(|\boldsymbol{k}-\boldsymbol{k}_1|)\Delta^{(\sigma)2}_{\tilde\gamma_0}(k_1)}{k_1^3|\boldsymbol{k}-\boldsymbol{k}_1|^3}\epsilon^{(\sigma)i}_k(\hat{\boldsymbol{k}}_1)\epsilon^{(\lambda)*k}_i(\hat{\boldsymbol{k}})\epsilon^{(\sigma)m}_n(-\hat{\boldsymbol{k}}_1)\epsilon^{(\lambda)*n}_m(-\hat{\boldsymbol{k}}) \times\left(\int_0^\eta d\tilde\eta\, G(\eta,\tilde\eta)\left[k_1^2 T_{\tilde\gamma}(k_1\tilde\eta)T_\Phi(|\boldsymbol{k}-\boldsymbol{k}_1|\tilde\eta) - T'_{\tilde\gamma}(k_1\tilde\eta)T'_\Phi(|\boldsymbol{k}-\boldsymbol{k}_1|\tilde\eta)\right]\right)^2 . \tag{6.2.19}$$

Remembering the properties $\epsilon^{(\lambda)*}_{ij}(\hat{\boldsymbol{k}}) = \epsilon^{(\lambda)}_{ij}(-\hat{\boldsymbol{k}})$, and $\epsilon^{\lambda}_{ij}(-\hat{\boldsymbol{k}}) = \epsilon^{-\lambda}_{ij}(\hat{\boldsymbol{k}})$, we have the expression for both polarisations of the induced GWs, which are chiral, as

$$\begin{aligned}\Delta^2_{\tilde\gamma_1,\mathrm{R/L}}(k) &= \frac{k^3}{\pi}\int d^3\boldsymbol{k}_1 \frac{\Delta^2_\Phi(|\boldsymbol{k}-\boldsymbol{k}_1|)}{k_1^3|\boldsymbol{k}-\boldsymbol{k}_1|^3}\left[4\cos^8\theta/2\,\Delta^{(\sigma)2}_{\tilde\gamma_0,\mathrm{R/L}}(k_1) + 4\sin^8\theta/2\,\Delta^{(\sigma)2}_{\tilde\gamma_0,\mathrm{L/R}}(k_1)\right]\\ &\times\left(\int_0^\eta d\tilde\eta\, G(\eta,\tilde\eta)\left[k_1^2 T_{\tilde\gamma}(k_1\tilde\eta)T_\Phi(|\boldsymbol{k}-\boldsymbol{k}_1|\tilde\eta) - T'_{\tilde\gamma}(k_1\tilde\eta)T'_\Phi(|\boldsymbol{k}-\boldsymbol{k}_1|\tilde\eta)\right]\right)^2,\\ &= \frac{1}{32}\int_0^\infty dv\int_{|v-1|}^{v+1} du\,\frac{1}{v^6u^2}\,\Delta^2_\Phi(uk)\,\langle\mathcal{I}^2\rangle\\ &\times\left[\left((v+1)^2-u^2\right)^4\,\Delta^{(\sigma)2}_{\tilde\gamma_0,\mathrm{R/L}}(vk) + \left((v-1)^2-u^2\right)^4\,\Delta^{(\sigma)2}_{\tilde\gamma_0,\mathrm{L/R}}(vk)\right].\end{aligned} \tag{6.2.20}$$

It is worth mentioning that the presence of primordial parity violation can lead to induced GWs that exhibit a combination of left and right polarisations. The induced chiral GWs now have their spectral density defined as

$$\Omega^{\rm ind}_{\rm GW}(k,\eta) = \frac{1}{24}\left(\frac{k}{\mathcal{H}}\right)^2\sum_{\lambda=\mathrm{R,L}}\langle\Delta^2_{\tilde\gamma_1,\mathrm{R/L}}(k)\rangle\,. \tag{6.2.21}$$

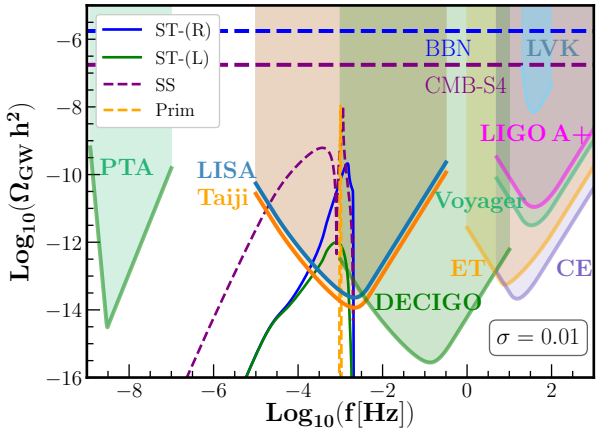

Figure 6.6: GWs spectra from primordial tensor modes (orange dashed), scalar-scalar induced GWs (purple dashed) and scalar-tensor left- (solid green) and right- (solid blue) handed induced GWs for log-normal spectra (Eq. (6.2.18)) with $A_{\tilde{\gamma}_{0,\mathrm{R}}} = 10^{-3}$ and $A_\Phi = 10^{-2}$, $f_* = 10^{-3}\,\mathrm{Hz}$. See how the scalar-tensor induced GWs extend primordial tensor parity violation to the high frequency part of the spectrum. Also note how the low frequency part of the spectrum quickly becomes non-chiral. We include the power-law integrated sensitivity curves [177] for PTA, LISA, Taiji [178, 179], DECIGO, Einstein Telescope (ET), Cosmic Explorer (CE), Voyager and LIGO A+ experiments. The sensitivity curves can be found in [180–183]. We also plot the upper bounds on the GW background from the LIGO/Virgo/KAGRA collaboration [72]. The horizontal thick long dashed lines qualitatively present the current constraint from BBN [184–186] (in blue) and future constraints from CMB-S4 experiments (in purple) [185, 187].

Hence, for primordial GWs, who have a delta-function peak in one of the polarisations at the same wave-number as the primordial scalars (Eq. (6.2.14)), the total spectral density of the induced GWs can be obtained from Eq. (6.2.21)

$$\Omega_{\mathrm{GW}}^{\mathrm{ind}}(k,\eta) = \frac{1}{768} A_\Phi\, A_{\tilde{\gamma}_{0(\mathrm{R/L})}} \left(\frac{k}{k_*}\right)^6 \left[2 + 32\left(\frac{k_*}{k}\right)^4 + 48\left(\frac{k_*}{k}\right)^2\right] \times \langle \mathcal{I}^2 \rangle_{u=v=k_*/k}\, \Theta(2k_* - k)\,. \tag{6.2.22}$$

The left panel of Fig. 6.3 displays the spectral density of induced gravitational waves resulting from the interaction between Dirac delta-peaked scalar and Dirac-delta-peaked chiral gravitational waves. In the right panel, and in the right panel of Fig. 6.4, it can be observed that when the primordial chiral gravitational waves induce gravitational waves of the same polarization, the peak of the spectrum, which is situated in the UV region, is more pronounced than that of the opposite polarization. In the IR region, however, we have an unpolarized induced wave. This could be attributed to the choice of peaked sources. Since the IR region is located far away from the peak of the GWs signal, there is effectively no detectable difference in the behaviour of the polarizations. Although only the case with the right-handed primordial gravitational waves are displayed, the same applies to the left-handed ones. The trend continues in the right panel of Fig. 6.5, which exhibits the same scenarios but with different peak locations of scalar and tensor perturbations.

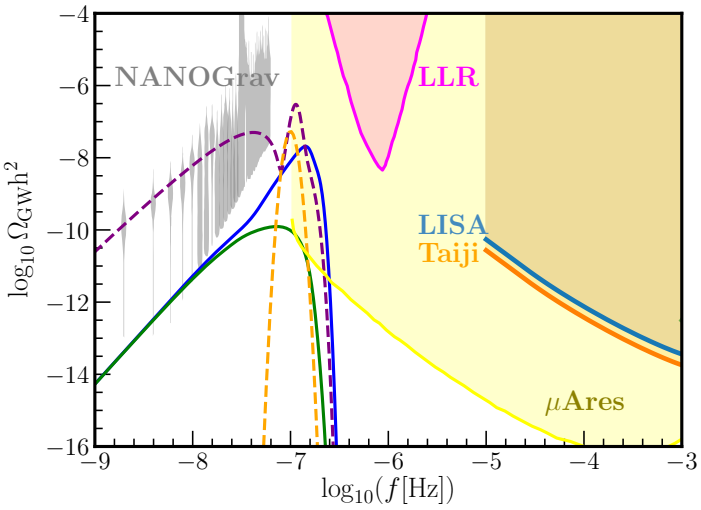

Figure 6.7: GWs spectrum from primordial tensor modes (orange dashed), scalar-scalar induced GWs (purple dashed) and scalar-tensor left (solid green) and right (solid blue) handed induced GWs for log-normal spectra (Eq. (6.2.18)) with $A_{\gamma_{0,R}} = 10^{-2}$ and $A_\Phi = 10^{-1}$, $f_* = 10^{-7}$ Hz. Gray violins indicate recent NANOGrav results [23]. We also include future sensitivity of μ-Ares [188] and Lunar Laser Ranging in magenta from Ref. [189]. See also [190] for other ideas to detect μHz GWs. Also included are the sensitivity curves of the LISA and Taiji detectors, to show that these detectors are unable to detect the peak of SIGWs, which could potentially explain the observations made by the NANOGrav collaboration.

6.3 Future prospects for scalar-tensor induced GWs

After demonstrating two examples of scalar-tensor-induced spectra, our attention now shifts to the detectability of these spectra. As stated earlier, we make the assumption that $A_{\tilde{\gamma}_0} < A_\Phi$, which enables us to neglect the tensor-tensor contribution and results in an effect that is subdominant compared to scalar-scalar induced GWs.

Fig. 6.6 provides a comprehensive comparison between the primordial GWs, the realistic log-normal case, and the sensitivities of various probes. It is evident from the plot that while scalar-tensor induced GWs can dominate over SIGWs in the high-frequency range, this dominance is limited to a small range of scales. On the other hand, the behaviour of the different-parity induced waves presents a distinguishing characteristic that sets them apart from SIGWs, particularly in the UV scales. This parity-violating behaviour of the scalar-tensor induced waves can be observed in Fig. 6.6, where it extends beyond the peak of the primordial tensor spectrum. We would like to clarify that the figure shown in Fig. 6.6 provides a quantitative description of the power-spectrum shape of the induced GWs, rather than the detectability of their chiral properties. It is important to note that planar detectors typically do not have the capability to directly detect the chirality of GWs, unless specific methods are employed, such as leveraging the motion of the solar system with respect to the cosmic reference frame (as discussed in [191], see also the refs. therein). However, studies have shown that by cross-correlating the output

of multiple detectors, such as LISA and Taiji, it is possible to detect and study the parity violation in the stochastic gravitational wave background [192, 193]. While we mention the potential of using this chirality to distinguish our induced GWs, the actual detectability of the same requires further detailed analysis beyond the scope of this work. In the low-frequency range, however, the induced waves consistently remain unpolarized, as depicted in the corresponding figures.

Upon examining Fig. 10 in [194] and Fig. 3 in [195], we observe a similar behaviour in the induced GWs in the UV region. It is noteworthy that these studies investigate GWs production mechanisms involving chiral dark photons, which are entirely distinct from our approach. Based on these observations, a hypothesis emerges, suggesting that there is a distinct polarization behaviour present in the UV region of induced GWs. It says that the polarized primordial component makes the peak of the induced GWs of the same polarization more enhanced compared to that of the oppositely polarized GWs, while the IR region remains unpolarized. However, the thorough investigation and verification of this hypothesis are left for future endeavours.

In Fig. 6.7, we present the recent results from the NANOGrav [23], which may have detected the stochastic gravitational wave background using pulsar timing arrays (PTAs). The SGWB observed by PTAs can be considered as the IR tail of the SIGWs [196]. We leave a detailed analysis of our scalar-tensor induced GWs signal with the new PTA data [23, 24] for future work. Here, we demonstrate an example where the peak of the SIGWs lies in the 0.1μHz range, which is currently beyond the sensitivity range of existing detectors. However, there has been proposals for a future detectors in this frequency range [188, 189]. If such a detector, preferably with better sensitivity and ability to detect chirality, is realized, it would be capable of detecting the peak, where it can be distinguishable from our signal based on the latter's chirality properties.

6.4 Summary

We conduct a comprehensive study on the non-linear interaction between first-order scalar perturbations and first-order tensor perturbations, focusing on the modulation of existing GWs. Unlike the direct generation of GWs from scratch by scalar perturbations, these interactions modify the pre-existing waves.

We enhance and provide further clarity to previous investigations on scalar-tensor induced gravitational waves (GWs) through the following advancements:

- We establish general formulas that incorporate the possibility of parity violation in primordial tensor modes. By considering the influence of parity violation on scalar-tensor induced GWs, we

see that while non-chiral waves are expected to surpass SIGWs only within a limited range of wave numbers, we can identify a distinguishing characteristic specific to chiral waves.

- We identify potential infra-red divergences in scalar-tensor induced GWs, which arise due to the inclusion of a constant scalar mode as a source for tensors. To address these divergences, we propose a rough regularization technique inspired by the concept of a locally inertial frame.
- We demonstrate that for peaked primordial spectra, the low-frequency tail of scalar-tensor induced GWs does not exhibit logarithmic running, in contrast to scalar-scalar induced GWs. Moreover, we observe the absence of resonant peaks in the scalar-tensor induced GWs.
- We presented our induced GWs energy density alongside the sensitivity curves of current and future detectors, demonstrating that this chirality property can serve as a distinguishing characteristic in the high-frequency region, relevant to multiple interferometers.

These improvements and clarifications contribute to a deeper understanding of scalar-tensor induced GWs and their distinct characteristics compared to scalar-scalar induced GWs.

Conclusion

In this thesis, we have conducted a comprehensive investigation into the impact of tensor-induced scalar modes on the matter power-spectrum in the present-day Universe. Our analysis has revealed that a significant gravitational wave (GWs) power-spectrum can leave an imprint on the matter power-spectrum. We have observed that the second-order matter perturbation, induced by these tensor modes, does not contribute to super-horizon scales, unlike linear matter perturbations. As a result, it does not generate large-scale temperature anisotropy in the cosmic microwave background (CMB), but it may have effects on smaller scales. Our findings indicate that this signature could serve as a valuable means to detect and constrain GWs on scales that are currently poorly understood, thereby improving the accuracy of matter power-spectrum estimation.

Furthermore, we have extended the analysis of tensor-induced scalar modes to various epochs of cosmic evolution. This includes the examination of their impact on matter and radiation density perturbations during different phases. We have derived full solutions for the tensor-induced density contrast in the radiation domination regime, providing a comprehensive understanding that was not explored in previous studies. Additionally, we have computed the tensor contribution to matter and radiation perturbations at late times, further expanding our knowledge in this area.

Lastly, we have conducted a detailed investigation into the non-linear interaction between first-order scalar perturbations and first-order tensor perturbations, focusing on the modulation of existing GWs. By expanding previous studies, we have established general formulae, accounted for parity violation in primordial tensor modes, addressed potential infra-red divergences, and examined the behavior of scalar-tensor induced GWs with peaked primordial spectra.

The findings presented here contribute to the ongoing research in cosmology and pave the way for further investigations into the rich and complex interplay between scalar and tensor perturbations in the Universe.

Outlook

The results presented in this thesis open up avenues for further exploration and investigation. It is important to note that certain assumptions and simplifications were made during the course of this research, and delving deeper into these aspects could enhance our understanding of the phenomena under study.

Regarding the correction to matter power-spectrum coming from the fluctuation in GWs energy density, it is of utmost importance to study the detectability of the effect by various probes stated in the summary. It is important to identify unique signatures that distinguish the effects being studied from other cosmological observables such as non-Gaussianity, projection effects, kinetic dipole, finger of the observer, and wide-angle effects (as discussed in references [89, 197–200]). This identification of unique signatures is vital for accurate signal identification and interpretation. For this purpose, we intend to further explore its high intrinsic non-Gaussianity. Due to its distribution following a χ^2-distribution, we can anticipate that the amplitude will be significant.

While extending our calculations to the smaller scales, the effects of baryons are ignored for simplicity, and we plan to explore this contribution in future studies. Another future research direction could be to calculate the power-spectrum, considering the matter contribution obtained in this paper, i.e., for $k > k_{\rm eq}$. We can also analyze and evaluate the corrections in the CMB anisotropies due to radiation perturbations induced by the energy density fluctuation of gravitational radiation, on small scales. Finally, we plan to compare this analytical work with a proper numerical analysis, particularly for $1/\eta_{\rm rec} \leq k \lesssim 1/\eta_{\rm eq}$, where a numerical approach is needed.

In the last chapter, we anticipated that the momentum integral in scalar-tensor induced GWs exhibits a divergence when the scalar mode momentum approaches zero. This divergence arises in the integrand as $1/u^4 \sim (k/q)^4$ for $q \ll k$, where k and q represent the external tensor and internal scalar mode momenta, respectively. The presence of a relatively flat scalar primordial spectrum further highlights this divergence. To mitigate the unphysical divergence arising from the long wavelength scalar modes, a common approach is to absorb them into the background. This technique, frequently employed in the

literature [201], allows for the separation of long and short modes of scalar perturbations

$$\Phi = \Phi_l + \Phi_s \,. \tag{6.4.1}$$

This leads to a redefinition of time and space coordinates

$$\begin{aligned} d\overline{\eta} &= e^{\Phi_l/2}\, d\eta \,, \\ d\overline{x} &= e^{-3\Phi_l/2}\, dx \,, \end{aligned} \tag{6.4.2}$$

resulting in the following metric

$$d\overline{s}^2 = a^2(\overline{\eta}) \left[-e^{2\Phi_s}\, d\overline{\eta}^2 + e^{-2\Phi_s} (\delta_{ij} + \tilde{\gamma}_{ij} d\overline{x}^i d\overline{x}^j \right] \,, \tag{6.4.3}$$

where the tensors and short-wavelength scalars lie on top of the new background. We leave this regularization for a future work which should provide a good estimate for the correct scalar-tensor induced GWs spectrum. Lastly, in light of recent PTA results, it is essential to analyze our findings in comparison to SIGWs. Additionally, further investigation of the hypothesis we proposed regarding the universal IR behavior of chirally induced GWs is warranted.

Appendices

Appendix A

Density perturbation up to third order in matter domination

From Eq. (4.1.11), we have the general solution of density perturbation. Putting $\gamma^{(2)}_{0ij} = \gamma^{(3)}_{0ij} = 0$, we can expand it upto third order in perturbations. The individual components are

$$\begin{aligned}
\gamma &= 1 + \gamma^{(1)i}_i + \frac{\gamma^{(2)i}_i}{2} - \frac{\gamma^{(1)ij}\gamma^{(1)}_{ij}}{2} + \frac{\gamma^{(1)i}_i\gamma^{(1)j}_j}{2} \\
&\quad + \frac{\gamma^{(3)i}_i}{6} - \frac{\gamma^{(1)ij}\gamma^{(2)}_{ij}}{2} + \frac{\gamma^{(1)i}_i\gamma^{(2)j}_j}{2} + \frac{\gamma^{(1)i}_i\gamma^{(1)j}_j\gamma^{(1)k}_k}{6} - \frac{\gamma^{(1)i}_i\gamma^{(1)mn}\gamma^{(1)}_{mn}}{2} \\
&\quad + \frac{\gamma^{(1)l}_i\gamma^{(1)n}_l\gamma^{(1)i}_n}{3}\,, \\
\gamma^{-1/2} &= 1 - \frac{\gamma^{(1)i}_i}{2} - \frac{\gamma^{(2)i}_i}{4} + \frac{\gamma^{(1)ij}\gamma^{(1)}_{ij}}{4} + \frac{\gamma^{(1)i}_i\gamma^{(1)j}_j}{8} \\
&\quad - \frac{\gamma^{(3)i}_i}{12} + \frac{\gamma^{(1)ij}\gamma^{(2)}_{ij}}{4} - \frac{\gamma^{(1)i}_i\gamma^{(2)j}_j}{4} - \frac{19}{48}\gamma^{(1)i}_i\gamma^{(1)j}_j\gamma^{(1)k}_k + \frac{\gamma^{(1)i}_i\gamma^{(1)mn}\gamma^{(1)}_{mn}}{4} \\
&\quad - \frac{\gamma^{(1)l}_i\gamma^{(1)n}_l\gamma^{(1)i}_n}{6}\,, \\
\gamma^{1/2} &= 1 + \frac{\gamma^{(1)i}_i}{2} + \frac{\gamma^{(2)i}_i}{4} - \frac{\gamma^{(1)ij}\gamma^{(1)}_{ij}}{4} + \frac{\gamma^{(1)i}_i\gamma^{(1)j}_j}{8} \\
&\quad + \frac{\gamma^{(3)i}_i}{12} - \frac{\gamma^{(1)ij}\gamma^{(2)}_{ij}}{4} + \frac{\gamma^{(1)i}_i\gamma^{(2)j}_j}{4} + \frac{11}{48}\gamma^{(1)i}_i\gamma^{(1)j}_j\gamma^{(1)k}_k - \frac{\gamma^{(1)i}_i\gamma^{(1)mn}\gamma^{(1)}_{mn}}{4} \\
&\quad + \frac{\gamma^{(1)l}_i\gamma^{(1)n}_l\gamma^{(1)i}_n}{6}\,.
\end{aligned} \tag{A.0.1}$$

From (4.1.11), we have

$$\begin{aligned}
\delta &= \delta_0 - \frac{1}{2}\gamma^{(1)i}_i + \frac{1}{2}\gamma^{(1)i}_{0i} - \frac{1}{4}\gamma^{(2)i}_i + \frac{1}{8}(\gamma^{(1)i}_i)^2 + \frac{1}{8}(\gamma^{(1)i}_{0i})^2 - \frac{1}{4}\gamma^{(1)i}_i\gamma^{(1)j}_{0j} \\
&\quad + \frac{1}{4}\gamma^{(1)ij}\gamma^{(1)}_{ij} - \frac{1}{4}\gamma^{(1)ij}_0\gamma^{(1)}_{0ij} - \frac{1}{2}\gamma^{(1)i}_i\delta_0 + \frac{1}{2}\gamma^{(1)i}_{0i}\delta_0 \\
&\quad - \frac{1}{8}\gamma^{(1)i}_{0i}\gamma^{(2)j}_j + \frac{11}{48}(\gamma^{(1)i}_{0i})^3 - \frac{19}{48}(\gamma^{(1)i}_i)^3 - \frac{\gamma^{(1)i}_{0i}\gamma^{(1)mn}_0\gamma^{(1)}_{0mn}}{4} + \frac{\gamma^{(1)i}_i\gamma^{(1)mn}\gamma^{(1)}_{mn}}{4} \\
&\quad + \frac{\gamma^{(1)l}_{0i}\gamma^{(1)n}_{0l}\gamma^{(1)i}_{0n}}{6} - \frac{\gamma^{(1)l}_i\gamma^{(1)n}_l\gamma^{(1)i}_n}{6} + \frac{\gamma^{(1)i}_i\gamma^{(1)mn}_0\gamma^{(1)}_{0mn}}{8} + \frac{\gamma^{(1)i}_{0i}\gamma^{(1)mn}\gamma^{(1)}_{mn}}{8}
\end{aligned}$$

$$
\begin{aligned}
&- \frac{1}{16}\gamma_i^{(1)i}(\gamma_{0j}^{(1)j})^2 + \frac{1}{16}\gamma_{0i}^{(1)i}(\gamma_j^{(1)j})^2 - \frac{\gamma_i^{(3)i}}{12} + \frac{\gamma^{(1)ij}\gamma_{ij}^{(2)}}{4} - \frac{\gamma_i^{(1)i}\gamma_j^{(2)j}}{4} \\
&- \frac{1}{4}\gamma_0^{(1)ij}\gamma_{0ij}^{(1)}\delta_0 + \frac{1}{4}\gamma^{(1)ij}\gamma_{ij}^{(1)}\delta_0 + \frac{1}{8}(\gamma_{0i}^{(1)i})^2\delta_0 + \frac{1}{8}(\gamma_i^{(1)i})^2\delta_0 \\
&- \frac{1}{4}\gamma_i^{(1)i}\gamma_{0j}^{(1)j}\delta_0 - \frac{1}{4}\gamma_i^{(2)i}\delta_0 \,. \qquad \text{(A.0.2)}
\end{aligned}
$$

Taking only linear tensors as the source, this gives Eq. (4.1.12) in the second order.

Appendix B

Contraction of polarisation tensors

To calculate Eq. (4.2.6), We set $\hat{\boldsymbol{k}}$ along $\hat{\boldsymbol{z}}$, and $\hat{\boldsymbol{k}}_{\boldsymbol{2}}$ at an angle θ to it.

$$\hat{\boldsymbol{k}}_{\boldsymbol{2}} = \sin\theta\cos\phi\hat{\boldsymbol{x}} + \sin\theta\sin\phi\hat{\boldsymbol{y}} + \cos\theta\hat{\boldsymbol{z}}\,, \tag{B.0.1}$$

$$\widehat{\boldsymbol{k}-\boldsymbol{k}_2} = \frac{-k_2\sin\theta(\cos\phi\hat{\boldsymbol{x}} + \sin\phi\hat{\boldsymbol{y}}) + (k - k_2\cos\theta)\hat{\boldsymbol{z}}}{\sqrt{k^2 + k_2^2 - 2kk_2\cos\theta}}\,. \tag{B.0.2}$$

The unit vectors orthogonal to $\hat{\boldsymbol{k}}_{\boldsymbol{2}}$ are:

$$\hat{m} = (\sin\phi, -\cos\phi, 0)\,, \tag{B.0.3}$$

$$\hat{n} = (\cos\theta\cos\phi, \cos\theta\sin\phi, -\sin\theta)\,. \tag{B.0.4}$$

The unit vectors orthogonal to $\widehat{\boldsymbol{k}-\boldsymbol{k}_2}$ are:

$$\hat{u} = (-\sin\phi, \cos\phi, 0)\,, \tag{B.0.5}$$

$$\hat{v} = \frac{-(k - k_2\cos\theta)\cos\phi, -(k - k_2\cos\theta)\sin\phi, -k_2\sin\theta}{\sqrt{k^2 + k_2^2 - 2kk_2\cos\theta}}\,. \tag{B.0.6}$$

Now, we use the following definitions of the polarisation tensors

$$\epsilon^{\times}_{ij}(\widehat{\boldsymbol{k}-\boldsymbol{k}_{\boldsymbol{2}}}) = \hat{u}_i\hat{v}_j + \hat{u}_j\hat{v}_i = -\epsilon^{\times}_{ij}(-\widehat{\boldsymbol{k}+\boldsymbol{k}_{\boldsymbol{2}}})\,, \tag{B.0.7}$$

$$\epsilon^{+}_{ij}(\widehat{\boldsymbol{k}-\boldsymbol{k}_{\boldsymbol{2}}}) = \hat{u}_i\hat{u}_j - \hat{v}_i\hat{v}_j = \epsilon^{+}_{ij}(-\widehat{\boldsymbol{k}+\boldsymbol{k}_{\boldsymbol{2}}})\,, \tag{B.0.8}$$

$$\epsilon^{\times}_{ij}(\hat{\boldsymbol{k}}_{\boldsymbol{2}}) = \hat{m}_i\hat{n}_j + \hat{m}_j\hat{n}_i = -\epsilon^{\times}_{ij}(-\hat{\boldsymbol{k}}_{\boldsymbol{2}})\,, \tag{B.0.9}$$

$$\epsilon^{+}_{ij}(\hat{\boldsymbol{k}}_{\boldsymbol{2}}) = \hat{m}_i\hat{m}_j - \hat{n}_i\hat{n}_j = \epsilon^{+}_{ij}(-\hat{\boldsymbol{k}}_{\boldsymbol{2}})\,, \tag{B.0.10}$$

and get the sum of the polarisation states as

$$\sum_{\sigma,\sigma'}\epsilon^{\sigma'}_{ij}(\hat{\boldsymbol{k}}_2)\epsilon^{\sigma ij}(\widehat{\boldsymbol{k}-\boldsymbol{k}_{\boldsymbol{2}}})\epsilon^{\sigma'}_{kl}(-\hat{\boldsymbol{k}}_{\boldsymbol{2}})\epsilon^{\sigma kl}(\widehat{-\boldsymbol{k}+\boldsymbol{k}_{\boldsymbol{2}}}) = \frac{1}{8\alpha^2}[35k^4 + 224k^2k_2^2 + 64k_2^4$$
$$- 32kk_2\cos\theta(7k^2 + 8k_2^2) + 4k^2\cos 2\theta(7k^2 + 40k_2^2) - 32k^3k_2\cos 3\theta + k^4\cos 4\theta]\,, \tag{B.0.11}$$

where $\alpha = k^2 + k_2^2 - 2kk_2\cos\theta$.

The same procedure can be pursued to get the contraction for scalar-scalar and scalar-tensor induced GWs.

Appendix C

Tensor induced vector and tensor modes

As mentioned in the main text, our analysis focuses on the scalar modes generated by linear tensors. However, for the sake of completeness, we also present a brief overview of the equations that involve the second-order vector and tensor modes sourced by the same mechanisms. These equations can be found in [81]. Appending second order vector and tensors to the metric Eq. (5.1.1), we have

$$\begin{aligned}\gamma_{ij} &= \delta_{ij} + \gamma_{ij}^{(1)} + \frac{\gamma_{ij}^{(2)}}{2}\,, \\ &= \delta_{ij} + \chi_{ij}^{(1)} - \phi^{(2)}\delta_{ij} + \frac{1}{2}\Big(D_{ij}\chi^{(2)||} + \partial_i\chi_j^{\perp(2)} + \partial_j\chi_i^{\perp(2)} + \chi_{ij}^{T(2)}\Big)\,,\end{aligned} \tag{C.0.1}$$

$$\gamma^{ij} = \delta^{ij} - \chi^{ij(1)} + \phi^{(2)}\delta^{ij} - \frac{1}{2}\Big(D^{ij}\chi^{(2)||} + \partial^i\chi^{\perp(2)j} + \partial^j\chi^{\perp(2)i} + \chi_{ij}^{T(2)}\Big) + \chi^{ik(1)}\chi_k{}^{j(1)}\,. \tag{C.0.2}$$

Second order vector and tensor perturbations satisfy $\partial^i\chi_i^{\perp(2)} = 0$, $\partial^i\chi_{ij}^{T(2)} = \chi_{ii}^{T(2)} = 0$. Due to the gauge chosen , the observers are co-moving with the CDM, $u_{\mathrm{m}\mu} = -a\delta_\mu^0$, and the components of the energy-momentum tensor for the matter does not contain any vector mode. Here only the radiation tensor has an additional term. Indeed, the four-vector of the radiation is defined as

$$u_{\mathrm{r}i} = a v_{\mathrm{r}i} = a\big(v_{\mathrm{r},i} + v_{\mathrm{r}i}^{\perp}\big)\,,$$

$$u_{\mathrm{r}}{}^i = \frac{1}{a} v_{\mathrm{r}}{}^i = \frac{1}{a}\big(v_{\mathrm{r}}{}^{,i} + v_{\mathrm{r}}^{\perp i}\big)\,.$$

Taking into account vector and tensor perturbations sourced by tensors, the conservation equations for matter remain the same. However, radiation now acquires a new component of the energy-momentum tensor given by $T_{\mathrm{r}}^{0i} = 4\overline{\rho}_{\mathrm{r}}/3a^2\big(v_{\mathrm{r}}{}^{,i} + v_{\mathrm{r}}^{\perp i}\big)$, which modifies the momentum conservation equation for radiation

$$4\big(v_{\mathrm{r},i}^{(2)\prime} + v_{\mathrm{r}i}^{\perp(2)\prime}\big) + \delta_{\mathrm{r},i}^{(2)} = 0\,. \tag{C.0.3}$$

We can immediately conclude that $v_{\mathrm{r}i}^{\perp(2)}$ is constant in time. The energy constraint remains the same as (5.2.1), but the momentum constraint has new components

$$\phi^{(2)\prime}{}_{,i}+\frac{1}{4}\big(D_{ij}\chi^{||(2),j\prime}+\nabla^2\chi_i^{\perp(2)\prime}\big)=-2\mathcal{H}^2\big(v_{\mathrm{r},i}^{(2)}+v_{\mathrm{r}i}^{\perp(2)}\big)+\frac{1}{2}\chi^{jk}\chi_{jk,i}{}'+\frac{1}{4}\chi^{jk\prime}\chi_{jk,i}-\frac{1}{2}\chi^{jk}\chi_{ki,j}{}', \quad \text{(C.0.4)}$$

and the $ij-$th equation reads

$$\begin{aligned}
&\frac{1}{4}\big(D_{ij}\chi^{||(2)\prime\prime}+\partial_i\chi_j^{\perp(2)\prime\prime}+\partial_j\chi_i^{\perp(2)\prime\prime}+\chi^{T(2)\prime\prime}{}_{ij}\big)+\frac{\mathcal{H}}{2}\big(D_{ij}\chi^{||(2)\prime}+\partial_i\chi_j^{\perp(2)\prime}+\partial_j\chi_i^{\perp(2)\prime}+\chi^{T(2)\prime}{}_{ij}\big)\\
&-\frac{1}{4}\nabla^2\chi_{ij}^{T(2)}+\frac{1}{12}\nabla^2D_{ij}\chi^{||(2)}-\frac{1}{18}\nabla^2\nabla^2\chi^{||(2)}\delta_{ij}+2\mathcal{H}\phi^{(2)\prime}\delta_{ij}+\phi^{(2)\prime\prime}\delta_{ij}+\frac{1}{2}D_{ij}\phi^{(2)}\\
&-\frac{1}{3}\nabla^2\phi^{(2)}\delta_{ij}-\frac{1}{2}\chi^{kl}(\chi_{lj,ik}+\chi_{il,jk}-\chi_{ij,lk}-\chi_{kl,ij})+\frac{1}{4}\chi^{kl}{}_{,j}\chi_{kl,i}-\frac{1}{2}\chi_j^{k,l}\chi_{li,k}+\frac{1}{2}\chi_j^{k,l}\chi_{ki,l}\\
&-\frac{3}{8}\chi^{kl,p}\chi_{kl,p}\delta_{ij}+\frac{1}{4}\chi^{kp,l}\chi_{lp,k}\delta_{ij}-\frac{1}{2}\chi^{k\prime}{}_j\chi_{ki}{}'+\frac{3}{8}\chi^{kl\prime}\chi_{kl}{}'\delta_{ij}=\frac{\mathcal{H}^2}{2}\delta_{\mathrm{r}}^{(2)}\delta_{ij}\,. \qquad \text{(C.0.5)}
\end{aligned}$$

Trace-less part of (C.0.5) now gives

$$\begin{aligned}
&D_{ij}\phi^{(2)}+\frac{1}{2}\big(D_{ij}\chi^{||(2)\prime\prime}+\partial_i\chi_j^{\perp(2)\prime\prime}+\partial_j\chi_i^{\perp(2)\prime\prime}+\chi^{T(2)\prime\prime}{}_{ij}\big)+\mathcal{H}\big(D_{ij}\chi^{||(2)\prime}+\partial_i\chi_j^{\perp(2)\prime}+\partial_j\chi_i^{\perp(2)\prime}\\
&+\chi^{T(2)\prime}{}_{ij}\big)-\frac{1}{2}\nabla^2\chi_{ij}^{T(2)}+\frac{1}{6}\nabla^2D_{ij}\chi^{||(2)}-\chi^{kl}(\chi_{lj,ik}+\chi_{il,jk}-\chi_{ij,lk}-\chi_{kl,ij})+\frac{1}{2}\chi^{kl}{}_{,j}\chi_{kl,i}\\
&-\chi_j^{k,l}\chi_{li,k}+\chi_j^{k,l}\chi_{ki,l}-\chi^{k\prime}{}_j\chi_{ki}-\frac{1}{3}\chi^{kl}\nabla^2\chi_{kl}\delta_{ij}+\frac{1}{3}\chi^{kl\prime}\chi_{kl}\delta_{ij}-\frac{1}{2}\chi^{kl,p}\chi_{kl,p}\delta_{ij}\\
&+\frac{1}{3}\chi^{kp,l}\chi_{lp,k}\delta_{ij}=0\,. \qquad \text{(C.0.6)}
\end{aligned}$$

The coupled system of tensor-sourced scalar, vector, and tensor perturbations can be found in (C.0.6). This equation is a generalization of Eq. (5.2.5). In order to obtain independent equations for vector and tensors, we can apply $3\nabla^{-2}\nabla^{-2}\partial_i\partial_j$ to (C.0.6) [81]. The result is the evolution equation for the scalar $\chi^{||(2)}$

$$\begin{aligned}
&\chi^{||(2)\prime\prime}+2\mathcal{H}\chi^{||(2)\prime}+\frac{1}{3}\nabla^2\chi^{||(2)}+2\phi^{(2)}=-\frac{3}{8}\chi^{kl}\chi_{kl}-\nabla^{-2}\left(\chi^{kl\prime}\chi_{kl}-\frac{1}{2}\chi^{kl,p}\chi_{kp,l}\right)\\
&+\frac{1}{4}\chi^{kl}\nabla^2\chi_{kl}+3\nabla^{-2}\nabla^{-2}\left(\chi^{kl,p\prime}\chi_{kp,l}{}'-\frac{1}{2}\chi^{kl}\nabla^2\nabla^2\chi_{kl}-\frac{1}{2}\chi^{kl,p}\nabla^2\chi_{kl,p}+\chi^{kl,p}\nabla^2\chi_{kp,l}\right)\,. \qquad \text{(C.0.7)}
\end{aligned}$$

Applying $\nabla^{-2}\Big\{\partial^i\left[(\text{C.0.6})-\frac{1}{2}D_{ij}(\text{C.0.7})\right]+(i\leftrightarrow j)\Big\}$, we obtain

$$\begin{aligned}
&\chi_i^{\perp(2)\prime\prime}+2\mathcal{H}\chi_i^{\perp(2)\prime}=2\nabla^{-2}\left[\left(\chi^{kl\prime}\chi_{ik,l}{}'-\frac{1}{2}\chi^{kl}\nabla^2\chi_{kl,i}+\chi^{kl}\nabla^2\chi_{ik,l}\right)\right.\\
&\left.+\partial_i\nabla^{-2}\left(\chi^{kl,j\prime}\chi_{jk,l}{}'-\frac{1}{2}\chi^{kl,j}\nabla^2\chi_{kl,j}-\frac{1}{2}\chi^{kl}\nabla^2\nabla^2\chi_{kl}+\chi^{kl,j}\nabla^2\chi_{jk,l}\right)\right]\\
&-4\partial_i\nabla^{-2}\nabla^{-2}\left(\chi^{kl,p\prime}\chi_{kp,l}{}'-\frac{1}{2}\chi^{kl}\nabla^2\nabla^2\chi_{kl}-\frac{1}{2}\chi^{kl,p}\nabla^2\chi_{kl,p}+\chi^{kl,p}\nabla^2\chi_{kp,l}\right) \qquad \text{(C.0.8)}
\end{aligned}$$

as the evolution equation of tensor-sourced vector perturbation. Furthermore, application of

$$\left[(\text{C.0.6})-\frac{1}{2}D_{ij}(\text{C.0.7})-(\text{C.0.8})\right]$$

gets us the evolution equation for tensor-sourced tensor modes

$$\chi^{T(2)\prime\prime}{}_{ij}+2\mathcal{H}\chi^{T(2)\prime}{}_{ij}-\nabla^2\chi^{T(2)}{}_{ij}=-\frac{5}{8}\chi^{kl}\chi_{kl,ij}-\frac{1}{4}\chi^{kl,p}\chi_{kp,l}\delta_{ij}-\frac{1}{8}\chi_{,i}^{kl}\chi_{kl,j}+\frac{3}{8}\chi^{kl,p}\chi_{kl,p}\delta_{ij}$$

$$
\begin{aligned}
&- \chi_j^{k,l}\chi_{ki,l} + \chi_j^{l,k}\chi_{ki,l} + \frac{1}{4}\chi^{kl}\nabla^2\chi_{kl}\delta_{ij} + \chi_i^{l\prime}\chi_{lj}{}' - \frac{1}{2}\chi^{kl\prime}\chi_{kl}{}'\delta_{ij} + \chi^{kl}\chi_{kj,il} + \chi^{kl}\chi_{ki,jl} \\
&- \chi^{kl}\chi_{ij,kl} + \frac{1}{2}\nabla^{-2}\left(\chi^{kl,p\prime}\chi_{kp,l}{}' + \chi^{kl,p}\nabla^2\chi_{kp,l} - \frac{1}{2}\chi^{kl}\nabla^2\nabla^2\chi_{kl} - \frac{1}{2}\chi^{kl,p}\nabla^2\chi_{kl,p}\right)\delta_{ij} \\
&+ \left[\partial_i\nabla^{-2}\left(\frac{1}{2}\chi^{kl}\nabla^2\chi_{kl,j} - \chi^{kl\prime}\chi_{jk,l}{}' - \chi^{kl}\nabla^2\chi_{jk,l}\right) + (i \leftrightarrow j)\right] \\
&+ \frac{1}{2}\partial_i\partial_j\nabla^{-2}\left(\chi^{kl\prime}\chi_{kl}{}' - \frac{1}{2}\chi^{kl,p}\chi_{kp,l} - \frac{1}{4}\chi^{kl}\nabla^2\chi_{kl}\right) \\
&+ \frac{1}{2}\partial_i\partial_j\nabla^{-2}\nabla^{-2}\left(\chi^{kl,p\prime}\chi_{kp,l}{}' + \chi^{kl,p}\nabla^2\chi_{kp,l} - \frac{1}{2}\chi^{kl}\nabla^2\nabla^2\chi_{kl} - \frac{1}{2}\chi^{kl,p}\nabla^2\chi_{kl,p}\right) . \qquad \text{(C.0.9)}
\end{aligned}
$$

These equations provide us with a comprehensive understanding of how vector and tensor perturbations evolve from the end of inflation until the present day. However, a detailed analysis of these equations and their solutions is beyond the scope of this work and will be presented in a future publication.

Appendix D

General solution during deep radiation dominance without subhorizon approximation

In the second part of Section 5.2, we restricted our attention to the regime where $k\eta \gg 1$, which corresponds to the modes being sub-Hubble during the first phase of the radiation era. However, it is also important to derive the general solution for any k. Let start again with Eq. (5.2.9)

$$u_{\mathrm{r}\boldsymbol{k}}^{''(2)} + \Big(\frac{k^2}{3} - 2\mathcal{H}^2\Big) u_{\mathrm{r}\boldsymbol{k}}^{(2)} = S_{\boldsymbol{k}}\,, \tag{D.0.1}$$

and using again the definition $\tau = k\eta$, this equation takes the form

$$\tau^2 \frac{d^2 u_{\mathrm{r}\boldsymbol{k}}^{(2)}}{d\tau^2} + \Big(\frac{\tau^2}{3} - 2\Big) u_{\mathrm{r}\boldsymbol{k}}^{(2)} = \tau^2 \frac{S_{\boldsymbol{k}}}{k^2}\,, \tag{D.0.2}$$

where $S_{\boldsymbol{k}}$ is given by Eq. (5.2.8). Now, we note that the solutions of the homogeneous part of this equation can easily be obtained if we consider the following second order differential equation

$$x^2 \frac{d^2 y}{dx^2}(x) + [a^2 x^2 - n(n+1)] y(x) = 0, \qquad \text{with} \qquad n = 0, 1, 2...\,,$$

or, equivalently,

$$y(x) x^{n+1} = \left(x^3 \frac{d}{dx}\right)^n \left(\frac{C_1 \cos ax + C_2 \sin ax}{x^{2n-1}}\right),$$

where C_1 and C_2 are two constants. Then if $y = u_{\mathrm{rk}}^{(2)}$, $x = \tau$, $a = 1/\sqrt{3}$ and $n = 1$, we get the homogeneous solutions

$$\frac{1}{\tau}\cos\frac{\tau}{\sqrt{3}} + \frac{1}{\sqrt{3}}\sin\frac{\tau}{\sqrt{3}} \qquad \text{and} \qquad \frac{1}{\tau}\sin\frac{\tau}{\sqrt{3}} - \frac{1}{\sqrt{3}}\cos\frac{\tau}{\sqrt{3}}\,.$$

Discarding the initial conditions according to the reasoning mentioned in the main text, we have

$$u_{\mathrm{r}\boldsymbol{k}}^{(2)}(\tau) = -\frac{\sqrt{3}}{k^2\tau}\int_{\tau_{\mathrm{in}}}^{\tau} d\tilde{\tau} S_{\boldsymbol{k}}(\tilde{\tau}) \left[\left(\sin\frac{\tilde{\tau}}{\sqrt{3}}\cos\frac{\tau}{\sqrt{3}} - \cos\frac{\tilde{\tau}}{\sqrt{3}}\sin\frac{\tau}{\sqrt{3}}\right)\left(\tau + \frac{3}{\tilde{\tau}}\right)\right.$$

$$+\sqrt{3}\left(\cos\frac{\tilde{\tau}}{\sqrt{3}}\cos\frac{\tau}{\sqrt{3}}+\sin\frac{\tilde{\tau}}{\sqrt{3}}\sin\frac{\tau}{\sqrt{3}}\right)\left(\frac{\tau}{\tilde{\tau}}-1\right)\Bigg]\,. \tag{D.0.3}$$

Then the perturbation $v^{(2)}_{\mathrm{r}\boldsymbol{k}}$ becomes

$$\begin{aligned}
v^{(2)}_{\mathrm{r}\boldsymbol{k}}(\tau) = {}& \frac{3}{k^3\tau}\int_{\tau_{\rm in}}^{\tau} d\tilde{\tau}\,\left(\tilde{\tau}+\frac{6}{\tilde{\tau}}\right)S_{\boldsymbol{k}}(\tilde{\tau}) \\
& -\left(\frac{2}{\tau}\cos\frac{\tau}{\sqrt{3}}+\frac{1}{\sqrt{3}}\sin\frac{\tau}{\sqrt{3}}\right)\int_{\tau_{\rm in}}^{\tau} d\tilde{\tau}\,\frac{9\cos\frac{\tilde{\tau}}{\sqrt{3}}+3\sqrt{3}\tilde{\tau}\sin\frac{\tilde{\tau}}{\sqrt{3}}}{k^3\tilde{\tau}}S_{\boldsymbol{k}}(\tilde{\tau}) \\
& -\left(\frac{2}{\tau}\sin\frac{\tau}{\sqrt{3}}-\frac{1}{\sqrt{3}}\cos\frac{\tau}{\sqrt{3}}\right)\int_{\tau_{\rm in}}^{\tau} d\tilde{\tau}\,\frac{9\sin\frac{\tilde{\tau}}{\sqrt{3}}-3\sqrt{3}\tilde{\tau}\cos\frac{\tilde{\tau}}{\sqrt{3}}}{k^3\tilde{\tau}}S_{\boldsymbol{k}}(\tilde{\tau})\,.
\end{aligned} \tag{D.0.4}$$

Therefore, using the relation (5.1.15), we obtain

$$\begin{aligned}
\delta^{(2)}_{\mathrm{r}}(\boldsymbol{k},\tau) = {}& \frac{12}{k^2\tau^2}\int_{\tau_{\rm in}}^{\tau} d\tilde{\tau}\,\left(\tilde{\tau}+\frac{6}{\tilde{\tau}}\right)S_{\boldsymbol{k}}(\tilde{\tau}) \\
& -4\left(\frac{2}{\tau^2}\cos\frac{\tau}{\sqrt{3}}+\frac{2}{\sqrt{3}\tau}\sin\frac{\tau}{\sqrt{3}}-\frac{1}{3}\cos\frac{\tau}{\sqrt{3}}\right)\int_{\tau_{\rm in}}^{\tau} d\tilde{\tau}\,\frac{9\cos\frac{\tilde{\tau}}{\sqrt{3}}+3\sqrt{3}\tilde{\tau}\sin\frac{\tilde{\tau}}{\sqrt{3}}}{k^2\tilde{\tau}}S_{\boldsymbol{k}}(\tilde{\tau}) \\
& -4\left(\frac{2}{\tau^2}\sin\frac{\tau}{\sqrt{3}}-\frac{2}{\sqrt{3}\tau}\cos\frac{\tau}{\sqrt{3}}-\frac{1}{3}\sin\frac{\tau}{\sqrt{3}}\right)\int_{\tau_{\rm in}}^{\tau} d\tilde{\tau}\,\frac{9\sin\frac{\tilde{\tau}}{\sqrt{3}}-3\sqrt{3}\tilde{\tau}\cos\frac{\tilde{\tau}}{\sqrt{3}}}{k^2\tilde{\tau}}S_{\boldsymbol{k}}(\tilde{\tau})\,.
\end{aligned} \tag{D.0.5}$$

For $\delta^{(2)}_{\mathrm{m}}(\boldsymbol{k},\tau)$, we use the relation (5.2.17). In (5.2.17), the first term ($v^{(2)\prime}_{\mathrm{r}\boldsymbol{k}}$) can be readily obtained from $\delta^{(2)}_{\mathrm{r}}(\boldsymbol{k},\tau)$ expression above (using relation (5.1.15)), and the integral in the second term is (in terms of τ)

$$\begin{aligned}
\int_{\tau_{\rm in}}^{\tau} d\tilde{\tau}\; v^{(2)}_{\mathrm{r}\boldsymbol{k}}(\tilde{\tau}) = {}& \frac{3}{k^3}\int_{\tau_{\rm in}}^{\tau} d\tilde{\tau}\,\ln\frac{\tau}{\tilde{\tau}}\left(\tilde{\tau}+\frac{6}{\tilde{\tau}}\right)S_{\boldsymbol{k}}(\tilde{\tau}) \\
& -\int_{\tau_{\rm in}}^{\tau} d\tilde{\tau}\frac{S_{\boldsymbol{k}}(\tilde{\tau})}{k^3\tilde{\tau}}\Bigg[9\left(\cos\frac{\tau}{\sqrt{3}}\cos\frac{\tilde{\tau}}{\sqrt{3}}+\sin\frac{\tau}{\sqrt{3}}\sin\frac{\tilde{\tau}}{\sqrt{3}}\right) \\
& +3\sqrt{3}\tilde{\tau}\left(\cos\frac{\tau}{\sqrt{3}}\sin\frac{\tilde{\tau}}{\sqrt{3}}-\sin\frac{\tau}{\sqrt{3}}\cos\frac{\tilde{\tau}}{\sqrt{3}}\right)\Bigg] \\
& -\int_{\tau_{\rm in}}^{\tau} d\tilde{\tau}\,\frac{9\cos\frac{\tilde{\tau}}{\sqrt{3}}+3\sqrt{3}\tilde{\tau}\sin\frac{\tilde{\tau}}{\sqrt{3}}}{k^3\tilde{\tau}}S_{\boldsymbol{k}}(\tilde{\tau})\times 2\int_{\tau_{\rm in}}^{\tau} d\tilde{\tau}\,\frac{\cos\frac{\tilde{\tau}}{\sqrt{3}}}{\tilde{\tau}} \\
& -\int_{\tau_{\rm in}}^{\tau} d\tilde{\tau}\,\frac{9\sin\frac{\tilde{\tau}}{\sqrt{3}}-3\sqrt{3}\tilde{\tau}\cos\frac{\tilde{\tau}}{\sqrt{3}}}{k^3\tilde{\tau}}S_{\boldsymbol{k}}(\tilde{\tau})\times 2\int_{\tau_{\rm in}}^{\tau} d\tilde{\tau}\,\frac{\sin\frac{\tilde{\tau}}{\sqrt{3}}}{\tilde{\tau}} \\
& +\int_{\tau_{\rm in}}^{\tau} d\tilde{\tau}\frac{S_{\boldsymbol{k}}(\tilde{\tau})}{k^3\tilde{\tau}}\Bigg[2\left(9\cos\frac{\tilde{\tau}}{\sqrt{3}}+3\sqrt{3}\tilde{\tau}\sin\frac{\tilde{\tau}}{\sqrt{3}}\right)\int_{\tau_{\rm in}}^{\tilde{\tau}}\frac{d\tilde{\tilde{\tau}}}{\tilde{\tilde{\tau}}}\cos\frac{\tilde{\tilde{\tau}}}{\sqrt{3}} \\
& +2\left(9\sin\frac{\tilde{\tau}}{\sqrt{3}}-3\sqrt{3}\tilde{\tau}\cos\frac{\tilde{\tau}}{\sqrt{3}}\right)\int_{\tau_{\rm in}}^{\tilde{\tau}}\frac{d\tilde{\tilde{\tau}}}{\tilde{\tilde{\tau}}}\sin\frac{\tilde{\tilde{\tau}}}{\sqrt{3}}-9\Bigg]\,,
\end{aligned} \tag{D.0.6}$$

where the expression of $v^{(2)}_{\mathrm{r}\boldsymbol{k}}$ from Eq. (D.0.4) has been used. Combining both the terms, we arrive at

$$\begin{aligned}
\delta^{(2)}_{\mathrm{m}}(\boldsymbol{k},\tau) = {}& \frac{3}{k^2}\int_{\tau_{\rm in}}^{\tau} d\tilde{\tau}\,\left[\left(\frac{3}{\tau^2}-\ln\frac{\tau}{\tilde{\tau}}\right)\left(\tilde{\tau}+\frac{6}{\tilde{\tau}}\right)+\frac{3}{\tilde{\tau}}\right]S_{\boldsymbol{k}}(\tilde{\tau}) \\
& -3\left(\frac{2}{\tau^2}\cos\frac{\tau}{\sqrt{3}}+\frac{2}{\sqrt{3}\tau}\sin\frac{\tau}{\sqrt{3}}\right)\int_{\tau_{\rm in}}^{\tau} d\tilde{\tau}\,\frac{9\cos\frac{\tilde{\tau}}{\sqrt{3}}+3\sqrt{3}\tilde{\tau}\sin\frac{\tilde{\tau}}{\sqrt{3}}}{k^2\tilde{\tau}}S_{\boldsymbol{k}}(\tilde{\tau}) \\
& -3\left(\frac{2}{\tau^2}\sin\frac{\tau}{\sqrt{3}}-\frac{2}{\sqrt{3}\tau}\cos\frac{\tau}{\sqrt{3}}\right)\int_{\tau_{\rm in}}^{\tau} d\tilde{\tau}\,\frac{9\sin\frac{\tilde{\tau}}{\sqrt{3}}-3\sqrt{3}\tilde{\tau}\cos\frac{\tilde{\tau}}{\sqrt{3}}}{k^2\tilde{\tau}}S_{\boldsymbol{k}}(\tilde{\tau})
\end{aligned}$$

$$+\,2\int_{\tau_{\rm in}}^{\tau} d\tilde{\tau}\,\frac{9\cos\frac{\tilde{\tau}}{\sqrt{3}}+3\sqrt{3}\tilde{\tau}\sin\frac{\tilde{\tau}}{\sqrt{3}}}{k^2\tilde{\tau}}S_{\boldsymbol{k}}(\tilde{\tau})\left[\int_{\tau_{\rm in}}^{\tau} d\tilde{\tau}\,\frac{\cos\frac{\tilde{\tau}}{\sqrt{3}}}{\tilde{\tau}}-\int_{\tau_{\rm in}}^{\tilde{\tau}} d\tilde{\tilde{\tau}}\,\frac{\cos\frac{\tilde{\tilde{\tau}}}{\sqrt{3}}}{\tilde{\tilde{\tau}}}\right]$$

$$+\,2\int_{\tau_{\rm in}}^{\tau} d\tilde{\tau}\,\frac{9\sin\frac{\tilde{\tau}}{\sqrt{3}}-3\sqrt{3}\tilde{\tau}\cos\frac{\tilde{\tau}}{\sqrt{3}}}{k^2\tilde{\tau}}S_{\boldsymbol{k}}(\tilde{\tau})\left[\int_{\tau_{\rm in}}^{\tau} d\tilde{\tau}\,\frac{\sin\frac{\tilde{\tau}}{\sqrt{3}}}{\tilde{\tau}}-\int_{\tau_{\rm in}}^{\tilde{\tau}} d\tilde{\tilde{\tau}}\,\frac{\sin\frac{\tilde{\tilde{\tau}}}{\sqrt{3}}}{\tilde{\tilde{\tau}}}\right], \qquad \text{(D.0.7)}$$

which is the expression for CDM density contrast in deep radiation domination, without subhorizon approximation. In [81], only radiation perturbation was studied. As a result, only (D.0.4) and (D.0.5) was derived there. Here we re-obtain them, along with the matter perturbation (D.0.7), which was missing in [81].

Appendix E

Calculation of δ_γ in the second phase

This section of the appendix is dedicated to calculating the radiation-density perturbations that arise from tensor-induced scalar modes during the second phase of the radiation epoch. As mentioned in the main text, during this phase, we have modes that are well within the Hubble radius ($k\eta \gg 1$) and have $y\delta_{\rm m}^{(2)} > 2\delta_{\rm r}^{(2)}$, where the matter perturbation is the main contributor to Einstein's field equations. In Section 5.3, we derived a new Meszaros equation that accounts for the contribution of gravitational waves to the dynamics of $\delta_{\rm m}^{(2)}$. Using (5.1.14) and (5.1.15), we can obtain a second-order differential equation for $\delta_{\rm r}^{(2)}$. Indeed, in Fourier space, we have

$$\delta_{{\rm r}\boldsymbol{k}}^{(2)\prime\prime} + \frac{k^2}{3}\delta_{{\rm r}\boldsymbol{k}}^{(2)} = \frac{4}{3}\delta_{{\rm m}\boldsymbol{k}}^{(2)\prime\prime}\,, \tag{E.0.1}$$

which, in terms of the variable y, turns out

$$\mathcal{H}y\left[\mathcal{H}y\frac{d^2}{dy^2} + \left(\mathcal{H} + y\frac{d\mathcal{H}}{dy}\right)\frac{d}{dy}\right]\delta_{{\rm r}\boldsymbol{k}}^{(2)} + \frac{k^2}{3}\delta_{{\rm r}\boldsymbol{k}}^{(2)} = \frac{4}{3}\mathcal{H}y\left[\mathcal{H}y\frac{d^2}{dy^2} + \left(\mathcal{H} + y\frac{d\mathcal{H}}{dy}\right)\frac{d}{dy}\right]\delta_{{\rm m}\boldsymbol{k}}^{(2)}\,. \tag{E.0.2}$$

We note immediately that the source term on the right-hand side depends on $\delta_{\rm m}^{(2)}$. Now, using

$$\frac{d\mathcal{H}}{dy} = \frac{1}{\mathcal{H}y}\mathcal{H}' = -\frac{\mathcal{H}}{2y}\frac{2+y}{1+y} \tag{E.0.3}$$

and the definition of $k_{\rm eq} \equiv \mathcal{H}_{\rm eq}$, Eq. (E.0.2) reads as follows

$$\frac{d^2\delta_{{\rm r}\boldsymbol{k}}^{(2)}}{dy^2} + \frac{1}{2(y+1)}\frac{d\delta_{{\rm r}\boldsymbol{k}}^{(2)}}{dy} + \frac{k^2}{k_{\rm eq}^2}\frac{2}{3(y+1)}\delta_{{\rm r}\boldsymbol{k}}^{(2)} = \frac{4}{3}\frac{d^2\delta_{{\rm m}\boldsymbol{k}}^{(2)}}{dy^2} + \frac{2}{3(y+1)}\frac{d\delta_{{\rm m}\boldsymbol{k}}^{(2)}}{dy}\,. \tag{E.0.4}$$

At this stage it is useful changing the variable $y \to w = \sqrt{1+y}$. In this case Eq. (E.0.4) becomes

$$\frac{d^2\delta_{{\rm r}\boldsymbol{k}}^{(2)}}{dw^2} + \frac{8}{3}\frac{k^2}{k_{\rm eq}^2}\delta_{{\rm r}\boldsymbol{k}}^{(2)} = \mathcal{Q}_{\boldsymbol{k}}(w)\,, \tag{E.0.5}$$

where

$$\mathcal{Q}_{\boldsymbol{k}}(w) = \frac{4}{3}\frac{d^2\delta_{{\rm m}\boldsymbol{k}}^{(2)}}{dw^2}\,.$$

Writing the solution of $\delta_{\rm m}^{(2)}$ from Eq. (5.3.9) w.r.t. the variable w, we have

$$\delta_{\rm m}^{(2)}(\boldsymbol{x}, w) = \left(w^2 - \frac{1}{3}\right)P_1(\boldsymbol{x}) + \left[\left(w^2 - \frac{1}{3}\right)\ln\frac{w+1}{w-1} - 2w\right]P_2(\boldsymbol{x})$$

$$+\frac{1}{4}\int_{w_\alpha}^{w}\frac{d\tilde{w}}{\tilde{w}}\,G\left(w^2-1,\tilde{w}^2-1\right)\frac{d\chi^{ij}}{d\tilde{w}}\frac{d\chi_{ij}}{d\tilde{w}}\,, \tag{E.0.6}$$

in configuration space, and

$$\begin{aligned}\delta_{\rm m}^{(2)}(\boldsymbol{k},w)=&\left(w^2-\frac{1}{3}\right)P_1(\boldsymbol{k})+\left[\left(w^2-\frac{1}{3}\right)\ln\frac{w+1}{w-1}-2w\right]P_2(\boldsymbol{k})\\&+\frac{1}{4}\int_{w_\alpha}^{w}\frac{d\tilde{w}}{\tilde{w}}\,G\left(w^2-1,\tilde{w}^2-1\right)F_3(\boldsymbol{k},\tilde{w})\,,\end{aligned} \tag{E.0.7}$$

in Fourier space. Here $F_3(\boldsymbol{k},w)$ is related to $F_1(\boldsymbol{k},y)$ via the following relation

$$F_3(\boldsymbol{k},w)=4(1+y)F_1(\boldsymbol{k},y) \tag{E.0.8}$$

and

$$\begin{aligned}G\left(w^2-1,\tilde{w}^2-1\right)=&-\frac{1}{4}\tilde{w}(\tilde{w}^2-1)\left[6\Big(\tilde{w}(3w^2-1)-w(3\tilde{w}^2-1)\Big)\right.\\&\left.-(3\tilde{w}^2-1)(3w^2-1)\ln\frac{(\tilde{w}+1)(w-1)}{(\tilde{w}-1)(w+1)}\right].\end{aligned} \tag{E.0.9}$$

Then, the source term of Eq. (E.0.5) can be written in the following way

$$\begin{aligned}\mathcal{Q}_{\boldsymbol{k}}(w)=&\frac{4}{3}\left[2P_1(\boldsymbol{k})+P_2(\boldsymbol{k})\left(\frac{4w(5-3w^2)}{3(w^2-1)^2}+2\ln\frac{w+1}{w-1}\right)\right]\\&-\frac{1}{2}\left[\left(\ln\frac{w+1}{w-1}+\frac{2w(5-3w^2)}{3(w^2-1)^2}\right)\int_{w_\alpha}^{w}d\tilde{w}\,(\tilde{w}^2-1)(3\tilde{w}^2-1)F_3(\boldsymbol{k},\tilde{w})\right.\\&\left.+\int_{w_\alpha}^{w}d\tilde{w}\,(\tilde{w}^2-1)\left(6\tilde{w}+(3\tilde{w}^2-1)\ln\frac{\tilde{w}-1}{\tilde{w}+1}\right)F_3(\boldsymbol{k},\tilde{w})-\frac{4}{3}F_3(\boldsymbol{k},w)\right],\end{aligned} \tag{E.0.10}$$

and the full solution of (E.0.5) reads

$$\delta_{\rm r}^{(2)}(\boldsymbol{k},w)=A_{\rm r}(\boldsymbol{k})\cos\left(2\sqrt{\frac{2}{3}}\frac{k}{k_{\rm eq}}w\right)+B_{\rm r}(\boldsymbol{k})\sin\left(2\sqrt{\frac{2}{3}}\frac{k}{k_{\rm eq}}w\right)+\int_{w_\alpha}^{w}d\tilde{w}\,G_{\rm r}(w,\tilde{w})\mathcal{Q}_{\boldsymbol{k}}(\tilde{w})\,, \tag{E.0.11}$$

where the Green's function of the above relation is defined as

$$\begin{aligned}G_{\rm r}(w,\tilde{w})=&\frac{k_{\rm eq}}{2k}\sqrt{\frac{3}{2}}\left[\sin\left(2\sqrt{\frac{2}{3}}\frac{k}{k_{\rm eq}}w\right)\cos\left(2\sqrt{\frac{2}{3}}\frac{k}{k_{\rm eq}}\tilde{w}\right)\right.\\&\left.-\cos\left(2\sqrt{\frac{2}{3}}\frac{k}{k_{\rm eq}}w\right)\sin\left(2\sqrt{\frac{2}{3}}\frac{k}{k_{\rm eq}}\tilde{w}\right)\right].\end{aligned} \tag{E.0.12}$$

Now, going back to the variable y, and naming the perturbation as $\delta^{(2)}_{\rm r(Tmesz)}(\boldsymbol{k},y)$, it becomes

$$\begin{aligned}\delta^{(2)}_{\rm r(Tmesz)}(\boldsymbol{k},y)=&A_{\rm r}(\boldsymbol{k})\cos\left(2\sqrt{\frac{2}{3}}\frac{k}{k_{\rm eq}}\sqrt{1+y}\right)+B_{\rm r}(\boldsymbol{k})\sin\left(2\sqrt{\frac{2}{3}}\frac{k}{k_{\rm eq}}\sqrt{1+y}\right)\\&+\int_{y_\alpha}^{y}\frac{d\tilde{y}}{2\sqrt{1+y}}\,G_r\left(\sqrt{1+y},\sqrt{1+\tilde{y}}\right)\,\mathcal{Q}_{\boldsymbol{k}}\left(\sqrt{1+\tilde{y}}\right)\,,\end{aligned} \tag{E.0.13}$$

where

$$\begin{aligned}G_{\rm r}\left(\sqrt{1+y},\sqrt{1+\tilde{y}}\right)=&\frac{k_{\rm eq}}{2k}\sqrt{\frac{3}{2}}\left[\sin\left(2\sqrt{\frac{2}{3}}\frac{k}{k_{\rm eq}}\sqrt{1+y}\right)\cos\left(2\sqrt{\frac{2}{3}}\frac{k}{k_{\rm eq}}\sqrt{1+\tilde{y}}\right)\right.\end{aligned}$$

$$- \cos\left(2\sqrt{\frac{2}{3}}\frac{k}{k_{\rm eq}}\sqrt{1+y}\right)\sin\left(2\sqrt{\frac{2}{3}}\frac{k}{k_{\rm eq}}\sqrt{1+\tilde{y}}\right)\Bigg]\,, \tag{E.0.14}$$

and

$$\begin{aligned}\mathcal{Q}_{\boldsymbol{k}}\left(\sqrt{1+y}\right) =& \frac{4}{3}\left[2P_1(\boldsymbol{k}) + P_2(\boldsymbol{k})\frac{4(2-3y)\sqrt{1+y}+6y^2\ln\frac{2+y+2\sqrt{1+y}}{y}}{3y^2}\right]\\ &-\frac{1}{2}\Bigg[\frac{4(2-3y)\sqrt{1+y}+6y^2\ln\frac{2+y+2\sqrt{1+y}}{y}}{3y^2}\int_{y_\alpha}^{y}\tilde{y}\sqrt{1+\tilde{y}}(2+3\tilde{y})\;F_1(\boldsymbol{k},\tilde{y})\\ &+2\int_{y_\alpha}^{y}\tilde{y}\sqrt{1+\tilde{y}}\;F_1(\boldsymbol{k},\tilde{y})\left(6\sqrt{1+\tilde{y}}+(2+3\tilde{y})\ln\frac{2+\tilde{y}-2\sqrt{1+\tilde{y}}}{\tilde{y}}\right)d\tilde{y}\\ &-\frac{16(1+y)}{3}F_1(\boldsymbol{k},y)\Bigg]\,,\end{aligned} \tag{E.0.15}$$

where we used Eq. (E.0.8). The coefficients $A_{\rm r}$ and $B_{\rm r}$ can be determined exactly the same way as the coefficients P_1 and P_2 of $\delta_{\rm m}^{(2)}$. Following the discussion related to $\delta_{\rm m}^{(2)}$, presented in Section 5.4, the perturbation $\delta_{\rm r}^{(2)}$ and its derivatives have to be continuous throughout evolution and, in particular, at $y = y_\alpha$. In other words, the following matching condition must be satisfied

$$\delta^{(2)}_{\rm r(DRe)}(\boldsymbol{k},\tau_\alpha) = \delta^{(2)}_{\rm r(Tmesz)}(\boldsymbol{k},y_\alpha), \tag{E.0.16}$$

$$\left(\frac{d}{dy}\delta^{(2)}_{\rm r(DRe)}(\boldsymbol{k},\tau)\right)\Bigg|_{\tau_\alpha} = \left(\frac{d}{dy}\delta^{(2)}_{\rm r(Tmesz)}(\boldsymbol{k},y)\right)\Bigg|_{y_\alpha}\,, \tag{E.0.17}$$

Also for radiation contribution, we have defined $\delta^{(2)}_{\rm r(DRe)}(\boldsymbol{k},\tau)$ as the radiation perturbation solution during the deep radiation era [i.e. Eq. (5.2.14) or, equivalently, (5.4.8)], while $\delta^{(2)}_{\rm r(Tmesz)}(\boldsymbol{k},y)$ is the solution obtained in Eq. (E.0.13). Using Eq. (5.4.8), the first condition, Eq. (E.0.16), gives us

$$\begin{aligned}&\frac{12}{k^2y_\alpha^2}\int_{y_{\rm in}}^{y_\alpha}d\tilde{y}\,\tilde{y}\,S_{\boldsymbol{k}}\left(\frac{\eta_*\tilde{y}}{2}\right) - \frac{2\sqrt{3}\eta_*}{k}\left[\sin\frac{k\eta_*y_\alpha}{2\sqrt{3}}+\frac{2\sqrt{3}}{k\eta_*y_\alpha}\cos\frac{k\eta_*y_\alpha}{2\sqrt{3}}\right]\\ &\times\int_{y_{\rm in}}^{y_\alpha}d\tilde{y}\,\cos\frac{k\eta_*\tilde{y}}{2\sqrt{3}}\,S_{\boldsymbol{k}}\left(\frac{\eta_*\tilde{y}}{2}\right) + \frac{2\sqrt{3}\eta_*}{k}\left[\cos\frac{k\eta_*y_\alpha}{2\sqrt{3}}-\frac{2\sqrt{3}}{k\eta_*y_\alpha}\sin\frac{k\eta_*y_\alpha}{2\sqrt{3}}\right]\\ &\times\int_{y_{\rm in}}^{y_\alpha}d\tilde{y}\,\sin\frac{k\eta_*\tilde{y}}{2\sqrt{3}}\,S_{\boldsymbol{k}}\left(\frac{\eta_*\tilde{y}}{2}\right) = A_{\rm r}(\boldsymbol{k})\cos\left(2\sqrt{\frac{2}{3}}\frac{k}{k_{\rm eq}}\sqrt{1+y_\alpha}\right)\\ &+B_{\rm r}(\boldsymbol{k})\sin\left(2\sqrt{\frac{2}{3}}\frac{k}{k_{\rm eq}}\sqrt{1+y_\alpha}\right),\end{aligned} \tag{E.0.18}$$

and the second condition, Eq. (E.0.17), becomes

$$\begin{aligned}&-\frac{24}{k^2y_\alpha^3}\int_{y_{\rm in}}^{y_\alpha}d\tilde{y}\,\tilde{y}\,S_{\boldsymbol{k}}\left(\frac{\eta_*\tilde{y}}{2}\right)\\ &-\left[\left(\eta_*^2-\frac{12}{k^2y_\alpha^2}\right)\cos\frac{k\eta_*y_\alpha}{2\sqrt{3}}-\frac{2\sqrt{3}\eta_*}{ky_\alpha}\sin\frac{k\eta_*y_\alpha}{2\sqrt{3}}\right]\int_{y_{\rm in}}^{y_\alpha}d\tilde{y}\,\cos\frac{k\eta_*\tilde{y}}{2\sqrt{3}}\,S_{\boldsymbol{k}}\left(\frac{\eta_*\tilde{y}}{2}\right)\\ &-\left[\left(\eta_*^2-\frac{12}{k^2y_\alpha^2}\right)\sin\frac{k\eta_*y_\alpha}{2\sqrt{3}}+\frac{2\sqrt{3}\eta_*}{ky_\alpha}\cos\frac{k\eta_*y_\alpha}{2\sqrt{3}}\right]\int_{y_{\rm in}}^{y_\alpha}d\tilde{y}\,\sin\frac{k\eta_*\tilde{y}}{2\sqrt{3}}\,S_{\boldsymbol{k}}\left(\frac{\eta_*\tilde{y}}{2}\right)\\ &=2\sqrt{\frac{2}{3}}\frac{k}{k_{\rm eq}}\left[-A_{\rm r}(\boldsymbol{k})\sin\left(2\sqrt{\frac{2}{3}}\frac{k}{k_{\rm eq}}\sqrt{1+y_\alpha}\right)+B_{\rm r}(\boldsymbol{k})\cos\left(2\sqrt{\frac{2}{3}}\frac{k}{k_{\rm eq}}\sqrt{1+y_\alpha}\right)\right].\end{aligned} \tag{E.0.19}$$

Multiplying Eq. (E.0.18) with

$$\sin\left(2\sqrt{\frac{2}{3}}\frac{k}{k_{\rm eq}}\sqrt{1+y_\alpha}\right),$$

Eq. (E.0.19) with

$$\left(2\sqrt{\frac{2}{3}}\frac{k}{k_{\rm eq}}\right)^{-1}\cos\left(2\sqrt{\frac{2}{3}}\frac{k}{k_{\rm eq}}\sqrt{1+y_\alpha}\right)$$

and adding them, we obtain

$$\begin{aligned}
B_r(\boldsymbol{k}) =& -\frac{6\sqrt{6}k_{\rm eq}}{k^3y_\alpha^3}\cos\left(2\sqrt{\frac{2}{3}}\frac{k}{k_{\rm eq}}\sqrt{1+y_\alpha}\right)\int_{y_{\rm in}}^{y_\alpha}d\tilde{y}\,\tilde{y}\,S_{\boldsymbol{k}}\left(\frac{\eta_*\tilde{y}}{2}\right)\\
&-\frac{\sqrt{3}}{2\sqrt{2}}\frac{k_{\rm eq}}{k}\cos\left(2\sqrt{\frac{2}{3}}\frac{k}{k_{\rm eq}}\sqrt{1+y_\alpha}\right)\Bigg\{\left[\left(\eta_*^2-\frac{12}{k^2y_\alpha^2}\right)\cos\frac{k\eta_*y_\alpha}{2\sqrt{3}}-\frac{2\sqrt{3}\eta_*}{ky_\alpha}\sin\frac{k\eta_*y_\alpha}{2\sqrt{3}}\right]\\
&\times\int_{y_{\rm in}}^{y_\alpha}d\tilde{y}\,\cos\frac{k\eta_*\tilde{y}}{2\sqrt{3}}\,S_{\boldsymbol{k}}\left(\frac{\eta_*\tilde{y}}{2}\right)+\left[\left(\eta_*^2-\frac{12}{k^2y_\alpha^2}\right)\sin\frac{k\eta_*y_\alpha}{2\sqrt{3}}+\frac{2\sqrt{3}\eta_*}{ky_\alpha}\cos\frac{k\eta_*y_\alpha}{2\sqrt{3}}\right]\\
&\times\int_{y_{\rm in}}^{y_\alpha}d\tilde{y}\,\sin\frac{k\eta_*\tilde{y}}{2\sqrt{3}}\,S_{\boldsymbol{k}}\left(\frac{\eta_*\tilde{y}}{2}\right)\Bigg\}+\frac{12}{k^2y_\alpha^2}\sin\left(2\sqrt{\frac{2}{3}}\frac{k}{k_{\rm eq}}\sqrt{1+y_\alpha}\right)\int_{y_{\rm in}}^{y_\alpha}d\tilde{y}\,\tilde{y}\,S_{\boldsymbol{k}}\left(\frac{\eta_*\tilde{y}}{2}\right)\\
&-\frac{2\sqrt{3}\eta_*}{k}\sin\left(2\sqrt{\frac{2}{3}}\frac{k}{k_{\rm eq}}\sqrt{1+y_\alpha}\right)\left[\sin\frac{k\eta_*y_\alpha}{2\sqrt{3}}+\frac{2\sqrt{3}}{k\eta_*y_\alpha}\cos\frac{k\eta_*y_\alpha}{2\sqrt{3}}\right]\\
&\times\int_{y_{\rm in}}^{y_\alpha}d\tilde{y}\,\cos\frac{k\eta_*\tilde{y}}{2\sqrt{3}}\,S_{\boldsymbol{k}}\left(\frac{\eta_*\tilde{y}}{2}\right)+\frac{2\sqrt{3}\eta_*}{k}\sin\left(2\sqrt{\frac{2}{3}}\frac{k}{k_{\rm eq}}\sqrt{1+y_\alpha}\right)\\
&\times\left[\cos\frac{k\eta_*y_\alpha}{2\sqrt{3}}-\frac{2\sqrt{3}}{k\eta_*y_\alpha}\sin\frac{k\eta_*y_\alpha}{2\sqrt{3}}\right]\int_{y_{\rm in}}^{y_\alpha}d\tilde{y}\,\sin\frac{k\eta_*\tilde{y}}{2\sqrt{3}}\,S_{\boldsymbol{k}}\left(\frac{\eta_*\tilde{y}}{2}\right)\\
=&\,\frac{6\sqrt{2}}{k^2y_\alpha^2}\left[\sqrt{2}\sin\left(2\sqrt{\frac{2}{3}}\frac{k}{k_{\rm eq}}\sqrt{1+y_\alpha}\right)-\frac{\sqrt{3}k_{\rm eq}}{ky_\alpha}\cos\left(2\sqrt{\frac{2}{3}}\frac{k}{k_{\rm eq}}\sqrt{1+y_\alpha}\right)\right]\\
&\times\int_{y_{\rm in}}^{y_\alpha}d\tilde{y}\,\tilde{y}\,S_{\boldsymbol{k}}\left(\frac{\eta_*\tilde{y}}{2}\right)-\frac{\sqrt{3}}{k}\Bigg\{\frac{k_{\rm eq}}{2\sqrt{2}}\cos\left(2\sqrt{\frac{2}{3}}\frac{k}{k_{\rm eq}}\sqrt{1+y_\alpha}\right)\\
&\times\left[\left(\eta_*^2-\frac{12}{k^2y_\alpha^2}\right)\cos\frac{k\eta_*y_\alpha}{2\sqrt{3}}-\frac{2\sqrt{3}\eta_*}{ky_\alpha}\sin\frac{k\eta_*y_\alpha}{2\sqrt{3}}\right]+2\eta_*\sin\left(2\sqrt{\frac{2}{3}}\frac{k}{k_{\rm eq}}\sqrt{1+y_\alpha}\right)\\
&\times\left[\sin\frac{k\eta_*y_\alpha}{2\sqrt{3}}+\frac{2\sqrt{3}}{k\eta_*y_\alpha}\cos\frac{k\eta_*y_\alpha}{2\sqrt{3}}\right]\Bigg\}\int_{y_{\rm in}}^{y_\alpha}d\tilde{y}\,\cos\frac{k\eta_*\tilde{y}}{2\sqrt{3}}\,S_{\boldsymbol{k}}\left(\frac{\eta_*\tilde{y}}{2}\right)\\
&-\frac{\sqrt{3}}{k}\Bigg\{\frac{k_{\rm eq}}{2\sqrt{2}}\cos\left(2\sqrt{\frac{2}{3}}\frac{k}{k_{\rm eq}}\sqrt{1+y_\alpha}\right)\left[\left(\eta_*^2-\frac{12}{k^2y_\alpha^2}\right)\sin\frac{k\eta_*y_\alpha}{2\sqrt{3}}+\frac{2\sqrt{3}\eta_*}{ky_\alpha}\cos\frac{k\eta_*y_\alpha}{2\sqrt{3}}\right]\\
&-2\eta_*\sin\left(2\sqrt{\frac{2}{3}}\frac{k}{k_{\rm eq}}\sqrt{1+y_\alpha}\right)\left[\cos\frac{k\eta_*y_\alpha}{2\sqrt{3}}-\frac{2\sqrt{3}}{k\eta_*y_\alpha}\sin\frac{k\eta_*y_\alpha}{2\sqrt{3}}\right]\Bigg\}\\
&\times\int_{y_{\rm in}}^{y_\alpha}d\tilde{y}\,\sin\frac{k\eta_*\tilde{y}}{2\sqrt{3}}\,S_{\boldsymbol{k}}\left(\frac{\eta_*\tilde{y}}{2}\right).
\end{aligned}\tag{E.0.20}$$

Similarly, multiplying Eq. (E.0.18) with

$$\cos\left(2\sqrt{\frac{2}{3}}\frac{k}{k_{\rm eq}}\sqrt{1+y_\alpha}\right),$$

Eq. (E.0.19) with

$$\left(2\sqrt{\frac{2}{3}}\frac{k}{k_{\rm eq}}\right)^{-1}\sin\left(2\sqrt{\frac{2}{3}}\frac{k}{k_{\rm eq}}\sqrt{1+y_\alpha}\right),$$

and subtracting the latter from the former, we obtain

$$
\begin{aligned}
A_{\rm r}(\boldsymbol{k}) =& \frac{6\sqrt{6}k_{\rm eq}}{k^3y_\alpha^3}\sin\left(2\sqrt{\frac{2}{3}}\frac{k}{k_{\rm eq}}\sqrt{1+y_\alpha}\right)\int_{y_{\rm in}}^{y_\alpha}d\tilde{y}\,\tilde{y}\,S_{\boldsymbol{k}}\left(\frac{\eta_*\tilde{y}}{2}\right)\\
&+\frac{\sqrt{3}}{2\sqrt{2}}\frac{k_{\rm eq}}{k}\sin\left(2\sqrt{\frac{2}{3}}\frac{k}{k_{\rm eq}}\sqrt{1+y_\alpha}\right)\Bigg\{\left[\left(\eta_*^2-\frac{12}{k^2y_\alpha^2}\right)\cos\frac{k\eta_*y_\alpha}{2\sqrt{3}}-\frac{2\sqrt{3}\eta_*}{ky_\alpha}\sin\frac{k\eta_*y_\alpha}{2\sqrt{3}}\right]\\
&\times\int_{y_{\rm in}}^{y_\alpha}d\tilde{y}\,\cos\frac{k\eta_*\tilde{y}}{2\sqrt{3}}\,S_{\boldsymbol{k}}\left(\frac{\eta_*\tilde{y}}{2}\right)+\left[\left(\eta_*^2-\frac{12}{k^2y_\alpha^2}\right)\sin\frac{k\eta_*y_\alpha}{2\sqrt{3}}+\frac{2\sqrt{3}\eta_*}{ky_\alpha}\cos\frac{k\eta_*y_\alpha}{2\sqrt{3}}\right]\\
&\times\int_{y_{\rm in}}^{y_\alpha}d\tilde{y}\,\sin\frac{k\eta_*\tilde{y}}{2\sqrt{3}}\,S_{\boldsymbol{k}}\left(\frac{\eta_*\tilde{y}}{2}\right)\Bigg\}+\frac{12}{k^2y_\alpha^2}\cos\left(2\sqrt{\frac{2}{3}}\frac{k}{k_{\rm eq}}\sqrt{1+y_\alpha}\right)\int_{y_{\rm in}}^{y_\alpha}d\tilde{y}\,\tilde{y}\,S_{\boldsymbol{k}}\left(\frac{\eta_*\tilde{y}}{2}\right)\\
&-\frac{2\sqrt{3}\eta_*}{k}\cos\left(2\sqrt{\frac{2}{3}}\frac{k}{k_{\rm eq}}\sqrt{1+y_\alpha}\right)\left[\sin\frac{k\eta_*y_\alpha}{2\sqrt{3}}+\frac{2\sqrt{3}}{k\eta_*y_\alpha}\cos\frac{k\eta_*y_\alpha}{2\sqrt{3}}\right]\\
&\times\int_{y_{\rm in}}^{y_\alpha}d\tilde{y}\,\cos\frac{k\eta_*\tilde{y}}{2\sqrt{3}}\,S_{\boldsymbol{k}}\left(\frac{\eta_*\tilde{y}}{2}\right)+\frac{2\sqrt{3}\eta_*}{k}\cos\left(2\sqrt{\frac{2}{3}}\frac{k}{k_{\rm eq}}\sqrt{1+y_\alpha}\right)\\
&\times\left[\cos\frac{k\eta_*y_\alpha}{2\sqrt{3}}-\frac{2\sqrt{3}}{k\eta_*y_\alpha}\sin\frac{k\eta_*y_\alpha}{2\sqrt{3}}\right]\int_{y_{\rm in}}^{y_\alpha}d\tilde{y}\,\sin\frac{k\eta_*\tilde{y}}{2\sqrt{3}}\,S_{\boldsymbol{k}}\left(\frac{\eta_*\tilde{y}}{2}\right)\\
=&\frac{6\sqrt{2}}{k^2y_\alpha^2}\left[\sqrt{2}\sin\left(2\sqrt{\frac{2}{3}}\frac{k}{k_{\rm eq}}\sqrt{1+y_\alpha}\right)+\frac{\sqrt{3}k_{\rm eq}}{ky_\alpha}\sin\left(2\sqrt{\frac{2}{3}}\frac{k}{k_{\rm eq}}\sqrt{1+y_\alpha}\right)\right]\\
&\times\int_{y_{\rm in}}^{y_\alpha}d\tilde{y}\,\tilde{y}\,S_{\boldsymbol{k}}\left(\frac{\eta_*\tilde{y}}{2}\right)+\frac{\sqrt{3}}{k}\Bigg\{\frac{k_{\rm eq}}{2\sqrt{2}}\sin\left(2\sqrt{\frac{2}{3}}\frac{k}{k_{\rm eq}}\sqrt{1+y_\alpha}\right)\\
&\times\left[\left(\eta_*^2-\frac{12}{k^2y_\alpha^2}\right)\cos\frac{k\eta_*y_\alpha}{2\sqrt{3}}-\frac{2\sqrt{3}\eta_*}{ky_\alpha}\sin\frac{k\eta_*y_\alpha}{2\sqrt{3}}\right]\\
&+2\eta_*\cos\left(2\sqrt{\frac{2}{3}}\frac{k}{k_{\rm eq}}\sqrt{1+y_\alpha}\right)\left[\sin\frac{k\eta_*y_\alpha}{2\sqrt{3}}+\frac{2\sqrt{3}}{k\eta_*y_\alpha}\cos\frac{k\eta_*y_\alpha}{2\sqrt{3}}\right]\Bigg\}\\
&\times\int_{y_{\rm in}}^{y_\alpha}d\tilde{y}\,\cos\frac{k\eta_*\tilde{y}}{2\sqrt{3}}\,S_{\boldsymbol{k}}\left(\frac{\eta_*\tilde{y}}{2}\right)+\frac{\sqrt{3}}{k}\Bigg\{\frac{k_{\rm eq}}{2\sqrt{2}}\cos\left(2\sqrt{\frac{2}{3}}\frac{k}{k_{\rm eq}}\sqrt{1+y_\alpha}\right)\\
&\times\left[\left(\eta_*^2-\frac{12}{k^2y_\alpha^2}\right)\sin\frac{k\eta_*y_\alpha}{2\sqrt{3}}+\frac{2\sqrt{3}\eta_*}{ky_\alpha}\cos\frac{k\eta_*y_\alpha}{2\sqrt{3}}\right]\\
&-2\eta_*\sin\left(2\sqrt{\frac{2}{3}}\frac{k}{k_{\rm eq}}\sqrt{1+y_\alpha}\right)\left[\cos\frac{k\eta_*y_\alpha}{2\sqrt{3}}-\frac{2\sqrt{3}}{k\eta_*y_\alpha}\sin\frac{k\eta_*y_\alpha}{2\sqrt{3}}\right]\Bigg\}\\
&\times\int_{y_{\rm in}}^{y_\alpha}d\tilde{y}\,\sin\frac{k\eta_*\tilde{y}}{2\sqrt{3}}\,S_{\boldsymbol{k}}\left(\frac{\eta_*\tilde{y}}{2}\right). \qquad \text{(E.0.21)}
\end{aligned}
$$

In this case we are able to obtain the solution of $\delta_{\rm r}^{(2)}$ from end of inflation to CDM epoch.

Appendix F

Setup of the initial conditions

This Appendix is devoted to addressing some issues relating to the initial conditions, i.e. at the end of Inflation, used in this work, adopted in Section 5.1. First of all, let us focus on Eqs. (5.1.16), (5.1.20) and (5.1.19). Substituting $\nabla^2(\phi^{(2)} + \nabla^2\chi^{||(2)}/6)$ from (5.1.16) in (5.1.20), we have

$$\phi^{(2)\prime\prime} + \mathcal{H}\phi^{(2)\prime} - \frac{1}{3}\mathcal{H}\chi^{kl}\chi_{kl}{}' + \frac{1}{3}\chi^{kl}\nabla^2\chi_{kl} + \frac{1}{6}\chi^{kl\prime}\chi_{kl}{}' = \frac{4\pi G a^2}{3}\left(2\delta_{\rm r}^{(2)}\overline{\rho}_{\rm r} + \delta_{\rm m}^{(2)}\overline{\rho}_{\rm m}\right) . \tag{F.0.1}$$

The fourth additive term may be rewritten by replacing $\nabla^2\chi_{kl}$ with $\chi_{ij}{}'' + 2\mathcal{H}\chi_{ij}{}'$, see Eq. (5.1.19), and the above equation can be written in the following way

$$\phi^{(2)\prime\prime} + \mathcal{H}\phi^{(2)\prime} + \frac{1}{3}\mathcal{H}\chi^{kl}\chi_{kl}{}' + \frac{1}{3}\chi^{kl}\chi_{kl}{}'' + \frac{1}{6}\chi^{kl\prime}\chi_{kl}{}' = \frac{4\pi G a^2}{3}\left(2\delta_{\rm r}^{(2)}\overline{\rho}_{\rm r} + \delta_{\rm m}^{(2)}\overline{\rho}_{\rm m}\right) . \tag{F.0.2}$$

In this work, we are setting the initial conditions at the end of inflation. Before discussing them, two important observations are in order.

- In several expressions considered in this work [see, e.g., the above Eq. (F.0.2)], in each source term defined in Fourier space, we have a loop integral which runs at all scales (or, equivalently, we are integrating over the whole frequency range of GW modes). However, at $\eta = \eta_{\rm in}$, all GW modes that we are interested in here are already outside the the horizon scale $1/\mathcal{H}(\eta_{\rm in})$. This means that, if $\boldsymbol{k}$ corresponds to the induced scalar modes and $\boldsymbol{q}$ is the loop momentum, the loop integral is truncated on horizon scales and, consequently, q and $|\boldsymbol{k} - \boldsymbol{q}|$ of tensor perturbations cannot be larger than $\mathcal{H}(\eta_{\rm in})$ (see also Fig. 5.1). In conclusion, at initial time GW modes will be frozen outside the horizon. This point is crucial for the below discuss.

- As we already pointed out in the main text, assuming initial adiabatic conditions and the synchronous co-moving gauge fixed here, the induced scalar modes will be zero because the contribution will come only after horizon entry, i.e. when GW tensor perturbations start oscillating [68]. This imply that, at $\eta_{\rm in}$ and $k < \mathcal{H}(\eta_{\rm in})$, $\delta_{\rm m}^{(2)}$, $\delta_{\rm r}^{(2)}$, $v_{\rm r}^{(2)}$ and $v_{\rm r}^{(2)\prime}$ can be set to zero.

As a result of these comments, at $\eta = \eta_{\rm in}$, ${\chi^{kl}}'_0$ and ${\chi^{kl}}''_0$ can set to zero in (F.0.2). (As we already pointed out in the main text, also here the subscript '0' denotes the initial conditions, i.e. the end of inflation when $\eta = \eta_{\rm in}$.) Then, (F.0.2) reads

$$\phi_0^{(2)''} + \mathcal{H}\phi_0^{(2)'} = 0\,. \tag{F.0.3}$$

In this case, Eq. (F.0.3) suggests choosing $\phi_0 =$ const. (in time). This conclusion can be further justified and confirmed if we also look at Eqs. (5.1.9) and (5.1.14) at $\eta = \eta_{\rm in}$. Now let us examine $\nabla^2(\phi^{(2)} + \nabla^2\chi^{||(2)}/6)$ in Fourier space, at the initial time. Following all the arguments made so far, from Eq. (5.1.17), we can get directly the relation

$$\phi^{(2)}_{\boldsymbol{k}0} - \frac{k^2}{6}\chi^{||(2)}_{\boldsymbol{k}0} = \mathcal{F}(\boldsymbol{k})\,, \tag{F.0.4}$$

where $\mathcal{F}(\boldsymbol{k})$, being a constant of time, can be derived explicitly in configuration space from Eq. (5.1.16). Defining $\mathcal{F}(\boldsymbol{x})$ as its Fourier inverse, from (5.1.16), we find

$$\mathcal{F}(\boldsymbol{x}) = \frac{\nabla^{-2}}{4}\left(\chi_0^{ik,l}\chi_{0li,k} - \frac{3}{2}\chi_0^{kl,i}\chi_{0kl,i}\right)\,. \tag{F.0.5}$$

Note that the above results have been obtained in whole generality. However there is a residual ambiguity which could be related to the gauge chosen here in this work. For instance, one could fix this ambiguity imposing that $\phi_0^{(2)} = 0$. Then

$$\chi_0^{||(2)} = \frac{3}{2}\nabla^{-4}\left(\chi_0^{ik,l}\chi_{0li,k} - \frac{3}{2}\chi_0^{kl,i}\chi_{0kl,i}\right)\,. \tag{F.0.6}$$

This concludes the discussion related to the issue of how to set the initial conditions of the work.

Appendix G

Evolution equation of scalar-tensor induced gravitational waves

We get the components of the trace-less ij-th equation Eq. (3.2.6) from γ_{ij},

$$N^{|i}_{|k} = \tilde{\gamma}^{ij}N_{|jk} = \frac{Ne^{2\Psi}}{a^2}\Big[\Phi^{,i}_{,k} + \Phi^{,i}\Phi_{,k} - \Phi_{,m}\Psi^{,m}\delta^i_k + \Phi^{,i}\Psi_{,k} + \Psi^{,i}\Phi_{,k} + \frac{1}{2}\Phi_{,m}\tilde{\gamma}^{i,m}_k - \frac{1}{2}\Phi_{,m}\tilde{\gamma}^{im}_{,k}$$
$$-\frac{1}{2}\Phi_{,m}\tilde{\gamma}^{m,i}_k + \tilde{\gamma}^{mt}\Phi_{,m}\Psi_{,t}\delta^i_k - \tilde{\gamma}^{ij}\Phi_{,jk} - \tilde{\gamma}^{ij}\Phi_{,j}\Phi_{,k} - \Psi_{,k}\Phi_{,j}\tilde{\gamma}^{ij} - \Phi_{,k}\Psi_{,j}\tilde{\gamma}^{ij}\Big]\,, \tag{G.0.1}$$

$$N^{|l}_{|l} = \frac{Ne^{2\Psi}}{a^2}\left[\nabla^2\Phi - \Psi^{,l}\Phi_{,l} + \Phi^{,l}\Phi_{,l} - \Phi_{,m}\tilde{\gamma}^{lm}_{,l} + \tilde{\gamma}^{mt}\Phi_{,m}\Psi_{,t} - \Phi_{,ml}\tilde{\gamma}^{lm} - \Phi_{,m}\Phi_{,l}\tilde{\gamma}^{lm}\right]\,, \tag{G.0.2}$$

$${}^{(3)}R_{jk} = \nabla^2\Psi(\delta_{jk} + \tilde{\gamma}_{jk}) - \frac{1}{2}\nabla^2\tilde{\gamma}_{jk} - \frac{1}{2}\tilde{\gamma}_{jk,m}\Psi^{,m} + \Psi_{,j}\Psi_{,k} + \Psi_{,jk} + \frac{1}{2}\tilde{\gamma}^m_{j,km} + \frac{1}{2}\tilde{\gamma}^m_{k,jm}$$
$$-\tilde{\gamma}^{mt}_{,m}\Psi_{,t}\delta_{jk} - \tilde{\gamma}^{mt}\Psi_{,tm}\delta_{jk} - \Psi^{,\lambda}\Psi_{,\lambda}\delta_{jk} - \Psi^{,\lambda}\Psi_{,\lambda}\tilde{\gamma}_{jk} - \frac{1}{2}\Psi_{,\lambda}\tilde{\gamma}^\lambda_{j,k} - \frac{1}{2}\Psi_{,\lambda}\tilde{\gamma}^\lambda_{k,j} + \Psi_{,\lambda}\Psi_{,t}\tilde{\gamma}^{\lambda t}\delta_{jk}\,, \tag{G.0.3}$$

$${}^{(3)}R^i_{\ k} = \gamma^{ij}\,{}^{(3)}R_{jk} = \frac{e^{2\Psi}}{a^2}\Big[\nabla^2\Psi\delta^i_k - \frac{1}{2}\nabla^2\tilde{\gamma}^i_k - \frac{1}{2}\tilde{\gamma}^i_{k,m}\Psi^{,m} + \Psi^{,i}\Psi_{,k} + \Psi^{,i}_{,k} + \frac{1}{2}\tilde{\gamma}^{mi}_{,km} + \frac{1}{2}\tilde{\gamma}^{m,i}_{k,m}$$
$$-\tilde{\gamma}^{mt}_{,m}\Psi_{,t}\delta^i_k - \tilde{\gamma}^{mt}\Psi_{,tm}\delta^i_k - \Psi^{,\lambda}\Psi_{,\lambda}\delta^i_k - \frac{1}{2}\Psi_{,\lambda}\tilde{\gamma}^{i\lambda}_{,k} - \frac{1}{2}\Psi_{,\lambda}\tilde{\gamma}^{\lambda,i}_k$$
$$+\tilde{\gamma}^{\lambda t}\Psi_{,t}\Psi_{,\lambda}\delta^i_k - \Psi_{,jk}\tilde{\gamma}^{ij} - \Psi_{,k}\Psi_{,j}\tilde{\gamma}^{ij}\Big]\,, \tag{G.0.4}$$

$${}^{(3)}R = {}^{(3)}R^i_{\ i} = \frac{e^{2\Psi}}{a^2}\left[4\nabla^2\Psi - 2\Psi^{,i}\Psi_{,i} + \tilde{\gamma}^{mi}_{,im} - 3\tilde{\gamma}^{mt}_{,m}\Psi_{,t} - 3\tilde{\gamma}^{mt}\Psi_{,tm} - \Psi_{,m}\tilde{\gamma}^{im}_{,i}\right.$$
$$\left.+3\tilde{\gamma}^{mt}\Psi_{,t}\Psi_{,m} - \Psi_{,ji}\tilde{\gamma}^{ij} - \Psi_{,i}\Psi_{,j}\tilde{\gamma}^{ij}\right]\,, \tag{G.0.5}$$

$${}^{(3)}\overline{R}^i_{\ k} = {}^{(3)}R^i_{\ k} - \frac{1}{3}\,{}^{(3)}R\,\delta^i_k = \frac{e^{2\Psi}}{a^2}\Big[-\frac{1}{3}\nabla^2\Psi\delta^i_k - \frac{1}{2}\nabla^2\tilde{\gamma}^i_k - \frac{1}{2}\Psi^{,m}\tilde{\gamma}^i_{k,m} + \Psi^{,i}\Psi_{,k} + \Psi^{,i}_{,k}$$
$$+\frac{1}{2}\tilde{\gamma}^{mi}_{,km} + \frac{1}{2}\tilde{\gamma}^{m,i}_{k,m} + \frac{1}{3}\tilde{\gamma}^{mt}\Psi_{,t}\Psi_{,m}\delta^i_k + \frac{1}{3}\tilde{\gamma}^{mt}\Psi_{,mt}\delta^i_k - \frac{1}{3}\Psi^{,m}\Psi_{,m}\delta^i_k - \frac{1}{2}\tilde{\gamma}^{im}_{,k}\Psi_{,m}$$
$$-\frac{1}{2}\tilde{\gamma}^{m,i}_k\Psi_{,m} - \tilde{\gamma}^{ij}\Psi_{,jk} - \tilde{\gamma}^{ij}\Psi_{,k}\Psi_{,j} - \frac{1}{3}\tilde{\gamma}^{mt}_{,mt}\delta^i_k + \frac{1}{3}\tilde{\gamma}^{mt}_{,t}\Psi_{,m}\delta^i_k - \frac{1}{3}\nabla^2(\Phi - \Psi)\delta^i_k\Big]\,. \tag{G.0.6}$$

Combining all these, we can arrive at Eq. (6.1.2).

Appendix H

Useful formulae for the calculation of the kernel function in the induced gravitational waves integral

We here write down some formulae used to calculate Eq. (6.2.7)

$$\mathcal{I} = \int_0^\infty k\, d\tilde{x}\, G(x,\tilde{x}) \left[v^2 T_{\tilde{\gamma}}(v\tilde{x}) T_\Phi(u\tilde{x}) - \dot{T}_{\tilde{\gamma}}(v\tilde{x}) \dot{T}_\Phi(u\tilde{x}) \right] . \tag{H.0.1}$$

With $G(x,\tilde{x})$ defined in Eq. (6.2.6), and using

$$\begin{aligned}
T_\Phi(x) &= 2^{3/2}\Gamma(5/2) \left(\frac{x}{\sqrt{3}}\right)^{-3/2} J_{3/2}\left(\frac{x}{\sqrt{3}}\right) , \\
\dot{T}_\Phi(ux) &= -\frac{3}{x} j_2(ux/\sqrt{3}) = -\frac{3^{5/4}}{x\sqrt{x}} \sqrt{\frac{\pi}{2u}} J_{5/2}(ux/\sqrt{3}) , \\
T_{\tilde{\gamma}}(x) &= \sqrt{\frac{\pi}{2x}} J_{1/2}(x) , \\
\dot{T}_{\tilde{\gamma}}(vx) &= -v j_1(vx) = -\sqrt{\frac{\pi v}{2x}} J_{3/2}(vx) ,
\end{aligned} \tag{H.0.2}$$

the kernel turns out to be

$$\begin{aligned}
\mathcal{I} = \int_0^\infty d\tilde{x} \left(\frac{\pi}{2}\right)^2 3^{5/4} \sqrt{\frac{v}{u}} \frac{1}{\sqrt{x\tilde{x}}} \left(J_{1/2}(\tilde{x}) Y_{1/2}(x) - J_{1/2}(x) Y_{1/2}(\tilde{x}) \right) \\
\times \left[\sqrt{3} \frac{v}{u} J_{1/2}(v\tilde{x}) J_{3/2}(u\tilde{x}/\sqrt{3}) - J_{3/2}(v\tilde{x}) J_{5/2}(u\tilde{x}/\sqrt{3}) \right] .
\end{aligned} \tag{H.0.3}$$

Using the recurrence relation $2n/z J_n(z) = J_{n-1}(z) + J_{n+1}(z)$, we have, putting $n = 3/2$,

$$\begin{aligned}
\mathcal{I} &= \int_0^\infty d\tilde{x} \left(\frac{\pi}{2}\right)^2 v \sqrt{\frac{v}{u/\sqrt{3}}} \sqrt{\frac{\tilde{x}}{x}} \left(J_{1/2}(\tilde{x}) Y_{1/2}(x) - J_{1/2}(x) Y_{1/2}(\tilde{x}) \right) \\
&\quad \times \left[J_{1/2}(v\tilde{x}) J_{1/2}(u\tilde{x}/\sqrt{3}) - J_{5/2}(v\tilde{x}) J_{5/2}(u\tilde{x}/\sqrt{3}) \right] , \\
&= \left(\frac{\pi}{2}\right)^2 v \sqrt{\frac{v}{u/\sqrt{3}}} \frac{1}{\sqrt{x}} \Bigg\{ Y_{1/2}(x) \int_0^\infty d\tilde{x} \sqrt{\tilde{x}} J_{1/2}(\tilde{x}) \left[J_{1/2}(v\tilde{x}) J_{1/2}(u\tilde{x}/\sqrt{3}) - J_{5/2}(v\tilde{x}) J_{5/2}(u\tilde{x}/\sqrt{3}) \right]
\end{aligned}$$

$$- J_{1/2}(x)\int_0^\infty d\tilde{x}\sqrt{\tilde{x}}Y_{1/2}(\tilde{x})\left[J_{1/2}(v\tilde{x})J_{1/2}(u\tilde{x}/\sqrt{3}) - J_{5/2}(v\tilde{x})J_{5/2}(u\tilde{x}/\sqrt{3})\right]\Bigg\}. \tag{H.0.4}$$

Using the formulae given in [202], we have

$$\int_0^\infty d\tilde{\tau}\sqrt{\tilde{x}}\,J_{1/2}(\tilde{x})J_{1/2}(v\tilde{x})J_{1/2}(u\tilde{x}/\sqrt{3}) = \begin{cases}\sqrt{\frac{\sqrt{3}}{2\pi vu}} & |v-\frac{u}{\sqrt{3}}|<1<v+\frac{u}{\sqrt{3}}\\ 0 & |v-\frac{u}{\sqrt{3}}|>1\\ & \text{or } v+\frac{u}{\sqrt{3}}<1\end{cases}$$

$$\int_0^\infty d\tilde{x}\sqrt{\tilde{x}}\,J_{1/2}(\tilde{x})J_{5/2}(v\tilde{x})J_{5/2}(u\tilde{x}/\sqrt{3}) = \begin{cases}\sqrt{\frac{\sqrt{3}}{2\pi vu}}\,P_2^0(\cos m)\\ \text{for } |v-\frac{u}{\sqrt{3}}|<1<v+\frac{u}{\sqrt{3}}\\ 0\\ \text{for } 1<|v-\frac{u}{\sqrt{3}}| \text{ or } 1>v+\frac{u}{\sqrt{3}}\end{cases}$$

$$\int_0^\infty d\tilde{x}\sqrt{\tilde{x}}\,Y_{1/2}(\tilde{x})J_{1/2}(v\tilde{x})J_{1/2}(u\tilde{x}/\sqrt{3}) = \begin{cases}-\frac{1}{\pi}\sqrt{\frac{2\sqrt{3}}{\pi vu}}\,Q_0^0(\cos m)\\ \text{for } |v-\frac{u}{\sqrt{3}}|<1<v+\frac{u}{\sqrt{3}}\\ \frac{1}{\pi}\sqrt{\frac{2\sqrt{3}}{\pi vu}}\,Q_0^0(\cosh n)\\ \text{for } 1>v+\frac{u}{\sqrt{3}}\end{cases}$$

$$\int_0^\infty d\tilde{x}\sqrt{\tilde{x}}\,Y_{1/2}(\tilde{x})J_{5/2}(v\tilde{x})J_{5/2}(u\tilde{x}/\sqrt{3}) = \begin{cases}-\frac{1}{\pi}\sqrt{\frac{2\sqrt{3}}{\pi vu}}\,Q_2^0(\cos m)\\ \text{for } |v-\frac{u}{\sqrt{3}}|<1<v+\frac{u}{\sqrt{3}}\\ \frac{1}{\pi}\sqrt{\frac{2\sqrt{3}}{\pi vu}}\,Q_2^0(\cosh n)\\ \text{for } 1>v+\frac{u}{\sqrt{3}}\end{cases} \tag{H.0.5}$$

where $2uv/\sqrt{3}\cos m = v^2+u^2/3-1$ and $2uv/\sqrt{3}\cosh n = 1-v^2-u^2/3$, and

$$P_2^0(\cos m) = \frac{3\cos^2 m-1}{2}\,, \tag{H.0.6}$$

$$Q_0^0(\cos m) = \frac{1}{2}\ln\frac{1+\cos m}{1-\cos m}\,, \tag{H.0.7}$$

$$Q_2^0(\cos m) = \frac{3\cos^2 m-1}{4}\ln\frac{1+\cos m}{1-\cos m} - \frac{3\cos m}{2}\,. \tag{H.0.8}$$

Applying all these, we have

$$\begin{aligned}\mathcal{I} = \frac{\pi}{4}\frac{v}{u/\sqrt{3}}\frac{1}{x}\Bigg\{ &-\cos x\left(1-P_2^0(\cos m)\right)\Theta\left(v+\frac{u}{\sqrt{3}}-1\right)\Theta\left(1-\left|v-\frac{u}{\sqrt{3}}\right|\right)\\ &-\frac{2}{\pi}\sin x\Bigg[(Q_0^0(\cosh n)-Q_2^0(\cosh n))\Theta\left(1-v-\frac{u}{\sqrt{3}}\right)\\ &-(Q_0^0(\cos m)-Q_2^0(\cos m))\Theta\left(v+\frac{u}{\sqrt{3}}-1\right)\Theta\left(1-\left|v-\frac{u}{\sqrt{3}}\right|\right)\Bigg]\Bigg\}.\end{aligned} \tag{H.0.9}$$

Remebering that $\langle\cos^2 x\rangle = \langle\sin^2 x\rangle = 1/2$, we have, for the oscillation average, Eq. (6.2.8). The same procedure can be applied to the scalar induced GWs.

Bibliography

[1] A. H. Guth, "The Inflationary Universe: A Possible Solution to the Horizon and Flatness Problems," *Phys. Rev. D*, vol. 23, L.-Z. Fang and R. Ruffini, Eds., pp. 347–356, 1981. DOI: 10.1103/PhysRevD.23.347.

[2] A. A. Starobinsky, "A New Type of Isotropic Cosmological Models Without Singularity," *Phys. Lett. B*, vol. 91, I. M. Khalatnikov and V. P. Mineev, Eds., pp. 99–102, 1980. DOI: 10.1016/0370-2693(80)90670-X.

[3] D. H. Lyth and A. Riotto, "Particle physics models of inflation and the cosmological density perturbation," *Phys. Rept.*, vol. 314, pp. 1–146, 1999. DOI: 10.1016/S0370-1573(98)00128-8. arXiv: hep-ph/9807278.

[4] N. Aghanim *et al.*, "Planck 2018 results. I. Overview and the cosmological legacy of Planck," *Astron. Astrophys.*, vol. 641, A1, 2020. DOI: 10.1051/0004-6361/201833880. arXiv: 1807.06205 [astro-ph.CO].

[5] N. Aghanim *et al.*, "Planck 2018 results. VI. Cosmological parameters," *Astron. Astrophys.*, vol. 641, A6, 2020, [Erratum: Astron.Astrophys. 652, C4 (2021)]. DOI: 10.1051/0004-6361/201833910. arXiv: 1807.06209 [astro-ph.CO].

[6] B. P. Abbott *et al.*, "Observation of Gravitational Waves from a Binary Black Hole Merger," *Phys. Rev. Lett.*, vol. 116, no. 6, p. 061 102, 2016. DOI: 10.1103/PhysRevLett.116.061102. arXiv: 1602.03837 [gr-qc].

[7] A. Buonanno and B. S. Sathyaprakash, "Sources of Gravitational Waves: Theory and Observations," in Oct. 2014. arXiv: 1410.7832 [gr-qc].

[8] V. Ferrari, S. Matarrese, and R. Schneider, "Stochastic background of gravitational waves generated by a cosmological population of young, rapidly rotating neutron stars," *Mon. Not. Roy. Astron. Soc.*, vol. 303, p. 258, 1999. DOI: 10.1046/j.1365-8711.1999.02207.x. arXiv: astro-ph/9806357.

[9] E. S. Phinney, "A Practical theorem on gravitational wave backgrounds," Jul. 2001. arXiv: astro-ph/0108028.

[10] T. Regimbau, "The astrophysical gravitational wave stochastic background," *Res. Astron. Astrophys.*, vol. 11, pp. 369–390, 2011. DOI: 10.1088/1674-4527/11/4/001. arXiv: 1101.2762 [astro-ph.CO].

[11] X.-J. Zhu, E. Howell, T. Regimbau, D. Blair, and Z.-H. Zhu, "Stochastic Gravitational Wave Background from Coalescing Binary Black Holes," *Astrophys. J.*, vol. 739, p. 86, 2011. DOI: 10.1088/0004-637X/739/2/86. arXiv: 1104.3565 [gr-qc].

[12] X.-J. Zhu, E. J. Howell, D. G. Blair, and Z.-H. Zhu, "On the gravitational wave background from compact binary coalescences in the band of ground-based interferometers," *Mon. Not. Roy. Astron. Soc.*, vol. 431, no. 1, pp. 882–899, 2013. DOI: 10.1093/mnras/stt207. arXiv: 1209.0595 [gr-qc].

[13] M. C. Guzzetti, N. Bartolo, M. Liguori, and S. Matarrese, "Gravitational waves from inflation," *Riv. Nuovo Cim.*, vol. 39, no. 9, pp. 399–495, 2016. DOI: 10.1393/ncr/i2016-10127-1. arXiv: 1605.01615 [astro-ph.CO].

[14] M. Kamionkowski, A. Kosowsky, and M. S. Turner, "Gravitational radiation from first-order phase transitions," *Physical Review D*, vol. 49, no. 6, pp. 2837–2851, Mar. 1994, ISSN: 0556-2821. DOI: 10.1103/physrevd.49.2837. [Online]. Available: http://dx.doi.org/10.1103/PhysRevD.49.2837.

[15] Z. Arzoumanian *et al.*, "The NANOGrav 12.5 yr Data Set: Search for an Isotropic Stochastic Gravitational-wave Background," *Astrophys. J. Lett.*, vol. 905, no. 2, p. L34, 2020. DOI: 10.3847/2041-8213/abd401. arXiv: 2009.04496 [astro-ph.HE].

[16] B. Goncharov *et al.*, "On the Evidence for a Common-spectrum Process in the Search for the Nanohertz Gravitational-wave Background with the Parkes Pulsar Timing Array," *Astrophys. J. Lett.*, vol. 917, no. 2, p. L19, 2021. DOI: 10.3847/2041-8213/ac17f4. arXiv: 2107.12112 [astro-ph.HE].

[17] S. Chen *et al.*, "Common-red-signal analysis with 24-yr high-precision timing of the European Pulsar Timing Array: inferences in the stochastic gravitational-wave background search," *Mon. Not. Roy. Astron. Soc.*, vol. 508, no. 4, pp. 4970–4993, 2021. DOI: 10.1093/mnras/stab2833. arXiv: 2110.13184 [astro-ph.HE].

[18] R. Flauger, N. Karnesis, G. Nardini, M. Pieroni, A. Ricciardone, and J. Torrado, "Improved reconstruction of a stochastic gravitational wave background with LISA," *JCAP*, vol. 01, p. 059, 2021. DOI: 10.1088/1475-7516/2021/01/059. arXiv: 2009.11845 [astro-ph.CO].

[19] M. Maggiore, "Gravitational wave experiments and early universe cosmology," *Phys. Rept.*, vol. 331, pp. 283–367, 2000. DOI: 10.1016/S0370-1573(99)00102-7. arXiv: gr-qc/9909001.

[20] S. Kawamura *et al.*, "Current status of space gravitational wave antenna DECIGO and B-DECIGO," *PTEP*, vol. 2021, no. 5, 05A105, 2021. DOI: 10.1093/ptep/ptab019. arXiv: 2006.13545 [gr-qc].

[21] N. Bartolo *et al.*, "Science with the space-based interferometer lisa. iv: Probing inflation with gravitational waves," *Journal of Cosmology and Astroparticle Physics*, vol. 2016, no. 12, pp. 026–026, Dec. 2016, ISSN: 1475-7516. DOI: 10.1088/1475-7516/2016/12/026. [Online]. Available: http://dx.doi.org/10.1088/1475-7516/2016/12/026.

[22] P. Auclair *et al.*, "Cosmology with the Laser Interferometer Space Antenna," Apr. 2022. arXiv: 2204.05434 [astro-ph.CO].

[23] A. Afzal *et al.*, "The NANOGrav 15 yr Data Set: Search for Signals from New Physics," *Astrophys. J. Lett.*, vol. 951, no. 1, p. L11, 2023. DOI: 10.3847/2041-8213/acdc91. arXiv: 2306.16219 [astro-ph.HE].

[24] J. Antoniadis *et al.*, "The second data release from the European Pulsar Timing Array: V. Implications for massive black holes, dark matter and the early Universe," Jun. 2023. arXiv: 2306.16227 [astro-ph.CO].

[25] H. Xu *et al.*, "Searching for the Nano-Hertz Stochastic Gravitational Wave Background with the Chinese Pulsar Timing Array Data Release I," *Res. Astron. Astrophys.*, vol. 23, no. 7, p. 075 024, 2023. DOI: 10.1088/1674-4527/acdfa5. arXiv: 2306.16216 [astro-ph.HE].

[26] D. J. Reardon *et al.*, "The Gravitational-wave Background Null Hypothesis: Characterizing Noise in Millisecond Pulsar Arrival Times with the Parkes Pulsar Timing Array," *Astrophys. J. Lett.*, vol. 951, no. 1, p. L7, 2023. DOI: 10.3847/2041-8213/acdd03. arXiv: 2306.16229 [astro-ph.HE].

[27] A. G. Riess *et al.*, "Observational evidence from supernovae for an accelerating universe and a cosmological constant," *Astron. J.*, vol. 116, pp. 1009–1038, 1998. DOI: 10.1086/300499. arXiv: astro-ph/9805201.

[28] J. M. Stewart and M. Walker, "Perturbations of spacetimes in general relativity," *Proc. Roy. Soc. Lond. A*, vol. 341, pp. 49–74, 1974. DOI: 10.1098/rspa.1974.0172.

[29] J. M. Bardeen, "Gauge Invariant Cosmological Perturbations," *Phys. Rev. D*, vol. 22, pp. 1882–1905, 1980. DOI: 10.1103/PhysRevD.22.1882.

[30] G. F. R. Ellis and M. Bruni, "Covariant and gauge-invariant approach to cosmological density fluctuations," *Phys. Rev. D*, vol. 40, pp. 1804–1818, 6 Sep. 1989. DOI: 10.1103/PhysRevD.40.1804. [Online]. Available: https://link.aps.org/doi/10.1103/PhysRevD.40.1804.

[31] H. Kodama and M. Sasaki, "Cosmological Perturbation Theory," *Prog. Theor. Phys. Suppl.*, vol. 78, pp. 1–166, 1984. DOI: 10.1143/PTPS.78.1.

[32] V. F. Mukhanov, H. A. Feldman, and R. H. Brandenberger, "Theory of cosmological perturbations. Part 1. Classical perturbations. Part 2. Quantum theory of perturbations. Part 3. Extensions," *Phys. Rept.*, vol. 215, pp. 203–333, 1992. DOI: 10.1016/0370-1573(92)90044-Z.

[33] S. Weinberg, *Gravitation and Cosmology: Principles and Applications of the General Theory of Relativity*. 1972.

[34] P. J. E. Peebles, *The large-scale structure of the universe*. 1980.

[35] R. Schaeffer, J. Silk, M. Spiro, and Zinn-Justin, Eds., *Proceedings, Les Houches Summer School on Cosmology and Large Scale Structure (Session 60): Les Houches, France, August 1-28, 1993*, Cosmology and large scale structure, North Holland: Elsevier, 1996.

[36] C.-P. Ma and E. Bertschinger, "Cosmological perturbation theory in the synchronous and conformal Newtonian gauges," *Astrophys. J.*, vol. 455, pp. 7–25, 1995. DOI: 10.1086/176550. arXiv: astro-ph/9506072.

[37] D. Blas, J. Lesgourgues, and T. Tram, "The cosmic linear anisotropy solving system (CLASS). part II: Approximation schemes," *Journal of Cosmology and Astroparticle Physics*, vol. 2011, no. 07, pp. 034–034, Jul. 2011. DOI: 10.1088/1475-7516/2011/07/034. [Online]. Available: https://doi.org/10.1088%2F1475-7516%2F2011%2F07%2F034.

[38] S. Dodelson, *Modern cosmology*. London, United Kingdom: Academic Press, 2021, ISBN: 978-0-12-815948-4.

[39] M. Tristram *et al.*, "Improved limits on the tensor-to-scalar ratio using BICEP and Planck data," *Phys. Rev. D*, vol. 105, no. 8, p. 083 524, 2022. DOI: 10.1103/PhysRevD.105.083524. arXiv: 2112.07961 [astro-ph.CO].

[40] G. Galloni, N. Bartolo, S. Matarrese, M. Migliaccio, A. Ricciardone, and N. Vittorio, "Updated constraints on amplitude and tilt of the tensor primordial spectrum," Jul. 2022. arXiv: 2208.00188 [astro-ph.CO].

[41] K. Abazajian *et al.*, "CMB-S4: Forecasting Constraints on Primordial Gravitational Waves," *Astrophys. J.*, vol. 926, no. 1, p. 54, 2022. DOI: 10.3847/1538-4357/ac1596. arXiv: 2008.12619 [astro-ph.CO].

[42] E. Allys *et al.*, "Probing Cosmic Inflation with the LiteBIRD Cosmic Microwave Background Polarization Survey," Feb. 2022. arXiv: 2202.02773 [astro-ph.IM].

[43] P. Ade *et al.*, "The Simons Observatory: Science goals and forecasts," *JCAP*, vol. 02, p. 056, 2019. DOI: 10.1088/1475-7516/2019/02/056. arXiv: 1808.07445 [astro-ph.CO].

[44] N. Bartolo, E. Komatsu, S. Matarrese, and A. Riotto, "Non-Gaussianity from inflation: Theory and observations," *Phys. Rept.*, vol. 402, pp. 103–266, 2004. DOI: 10.1016/j.physrep.2004.08.022. arXiv: astro-ph/0406398.

[45] R. Caldwell *et al.*, "Detection of early-universe gravitational-wave signatures and fundamental physics," *Gen. Rel. Grav.*, vol. 54, no. 12, p. 156, 2022. DOI: 10.1007/s10714-022-03027-x. arXiv: 2203.07972 [gr-qc].

[46] B. P. Abbott *et al.*, "GW170104: Observation of a 50-Solar-Mass Binary Black Hole Coalescence at Redshift 0.2," *Phys. Rev. Lett.*, vol. 118, no. 22, p. 221 101, 2017, [Erratum: Phys.Rev.Lett. 121, 129901 (2018)]. DOI: 10.1103/PhysRevLett.118.221101. arXiv: 1706.01812 [gr-qc].

[47] F. Acernese *et al.*, "Advanced Virgo: a second-generation interferometric gravitational wave detector," *Class. Quant. Grav.*, vol. 32, no. 2, p. 024 001, 2015. DOI: 10.1088/0264-9381/32/2/024001. arXiv: 1408.3978 [gr-qc].

[48] T. Akutsu *et al.*, "Overview of KAGRA: Detector design and construction history," *PTEP*, vol. 2021, no. 5, 05A101, 2021. DOI: 10.1093/ptep/ptaa125. arXiv: 2005.05574 [physics.ins-det].

[49] J. R. Gair, I. Mandel, M. C. Miller, and M. Volonteri, "Exploring intermediate and massive black-hole binaries with the Einstein Telescope," *Gen. Rel. Grav.*, vol. 43, pp. 485–518, 2011. DOI: 10.1007/s10714-010-1104-3. arXiv: 0907.5450 [astro-ph.CO].

[50] M. Evans *et al.*, "A Horizon Study for Cosmic Explorer: Science, Observatories, and Community," Sep. 2021. arXiv: 2109.09882 [astro-ph.IM].

[51] P. Amaro-Seoane *et al.*, "Laser interferometer space antenna," *arXiv preprint arXiv:1702.00786*, 2017.

[52] M. Mannerkoski, P. H. Johansson, A. Rantala, T. Naab, S. Liao, and A. Rawlings, "Signatures of the Many Supermassive Black Hole Mergers in a Cosmologically Forming Massive Early-type Galaxy," *Astrophys. J.*, vol. 929, no. 2, p. 167, 2022. DOI: 10.3847/1538-4357/ac5f0b. arXiv: 2112.03576 [astro-ph.GA].

[53] P. A. Seoane *et al.*, "The Gravitational Universe," May 2013. arXiv: 1305.5720 [astro-ph.CO].

[54] R. Abbott *et al.*, "Open data from the third observing run of LIGO, Virgo, KAGRA and GEO," Feb. 2023. arXiv: 2302.03676 [gr-qc].

[55] C. Caprini and D. G. Figueroa, "Cosmological Backgrounds of Gravitational Waves," *Class. Quant. Grav.*, vol. 35, no. 16, p. 163 001, 2018. DOI: 10.1088/1361-6382/aac608. arXiv: 1801.04268 [astro-ph.CO].

[56] N. Bartolo *et al.*, "Characterizing the cosmological gravitational wave background: Anisotropies and non-Gaussianity," *Phys. Rev. D*, vol. 102, no. 2, p. 023 527, 2020. DOI: 10.1103/PhysRevD.102.023527. arXiv: 1912.09433 [astro-ph.CO].

[57] A. D. Linde, "A New Inflationary Universe Scenario: A Possible Solution of the Horizon, Flatness, Homogeneity, Isotropy and Primordial Monopole Problems," *Phys. Lett. B*, vol. 108, L.-Z. Fang and R. Ruffini, Eds., pp. 389–393, 1982. DOI: 10.1016/0370-2693(82)91219-9.

[58] A. Achúcarro *et al.*, "Inflation: Theory and Observations," Mar. 2022. arXiv: 2203.08128 [astro-ph.CO].

[59] A. Kosowsky, M. S. Turner, and R. Watkins, "Gravitational radiation from colliding vacuum bubbles," *Phys. Rev. D*, vol. 45, pp. 4514–4535, 12 Jun. 1992. DOI: 10.1103/PhysRevD.45.4514. [Online]. Available: https://link.aps.org/doi/10.1103/PhysRevD.45.4514.

[60] T. Vachaspati and A. Vilenkin, "Gravitational radiation from cosmic strings," *Phys. Rev. D*, vol. 31, pp. 3052–3058, 12 Jun. 1985. DOI: 10.1103/PhysRevD.31.3052. [Online]. Available: https://link.aps.org/doi/10.1103/PhysRevD.31.3052.

[61] D. G. Figueroa, M. Hindmarsh, and J. Urrestilla, "Exact scale-invariant background of gravitational waves from cosmic defects," *Physical Review Letters*, vol. 110, no. 10, Mar. 2013, ISSN: 1079-7114. DOI: 10.1103/physrevlett.110.101302. [Online]. Available: http://dx.doi.org/10.1103/PhysRevLett.110.101302.

[62] G. Agazie *et al.*, "The NANOGrav 15-year Data Set: Constraints on Supermassive Black Hole Binaries from the Gravitational Wave Background," Jun. 2023. arXiv: 2306.16220 [astro-ph.HE].

[63] G. Agazie *et al.*, "The NANOGrav 15 yr Data Set: Evidence for a Gravitational-wave Background," *Astrophys. J. Lett.*, vol. 951, no. 1, p. L8, 2023. DOI: 10.3847/2041-8213/acdac6. arXiv: 2306.16213 [astro-ph.HE].

[64] A. Addazi, Y.-F. Cai, A. Marciano, and L. Visinelli, "Have pulsar timing array methods detected a cosmological phase transition?," Jun. 2023. arXiv: 2306.17205 [astro-ph.CO].

[65] N. Kitajima and K. Nakayama, "Nanohertz gravitational waves from cosmic strings and dark photon dark matter," Jun. 2023. arXiv: 2306.17390 [hep-ph].

[66] C. R. Contaldi, "Anisotropies of Gravitational Wave Backgrounds: A Line Of Sight Approach," *Phys. Lett. B*, vol. 771, pp. 9–12, 2017. DOI: 10.1016/j.physletb.2017.05.020. arXiv: 1609.08168 [astro-ph.CO].

[67] L. Valbusa Dall'Armi, A. Nishizawa, A. Ricciardone, and S. Matarrese, "Circular Polarization of the Astrophysical Gravitational Wave Background," Jan. 2023. arXiv: 2301.08205 [astro-ph.CO].

[68] Y. Watanabe and E. Komatsu, "Improved Calculation of the Primordial Gravitational Wave Spectrum in the Standard Model," *Phys. Rev. D*, vol. 73, p. 123 515, 2006. DOI: 10.1103/PhysRevD.73.123515. arXiv: astro-ph/0604176.

[69] P. D. Lasky *et al.*, "Gravitational-wave cosmology across 29 decades in frequency," *Physical Review X*, vol. 6, no. 1, Mar. 2016, ISSN: 2160-3308. DOI: 10.1103/physrevx.6.011035. [Online]. Available: http://dx.doi.org/10.1103/PhysRevX.6.011035.

[70] W. Hu and N. Sugiyama, "Smallscale cosmological perturbations: An analytic approach," *The Astrophysical Journal*, vol. 471, no. 2, pp. 542–570, Nov. 1996, ISSN: 1538-4357. DOI: 10.1086/177989. [Online]. Available: http://dx.doi.org/10.1086/177989.

[71] Y. Akrami *et al.*, "Planck 2018 results. X. Constraints on inflation," *Astron. Astrophys.*, vol. 641, A10, 2020. DOI: 10.1051/0004-6361/201833887. arXiv: 1807.06211 [astro-ph.CO].

[72] R. Abbott *et al.*, "Upper limits on the isotropic gravitational-wave background from Advanced LIGO and Advanced Virgos third observing run," *Phys. Rev. D*, vol. 104, no. 2, p. 022 004, 2021. DOI: 10.1103/PhysRevD.104.022004. arXiv: 2101.12130 [gr-qc].

[73] *ET Documentation System — apps.et-gw.eu*, https://apps.et-gw.eu/tds/?content=3&r=8709.

[74] P. Amaro-Seoane *et al.*, *Laser interferometer space antenna*, 2017. arXiv: 1702.00786 [astro-ph.IM].

[75] W.-R. Hu and Y.-L. Wu, "The Taiji Program in Space for gravitational wave physics and the nature of gravity," *Natl. Sci. Rev.*, vol. 4, no. 5, pp. 685–686, 2017. DOI: 10.1093/nsr/nwx116.

[76] J. Luo *et al.*, "TianQin: a space-borne gravitational wave detector," *Class. Quant. Grav.*, vol. 33, no. 3, p. 035 010, 2016. DOI: 10.1088/0264-9381/33/3/035010. arXiv: 1512.02076 [astro-ph.IM].

[77] J. Ellis, M. Lewicki, J. M. No, and V. Vaskonen, "Gravitational wave energy budget in strongly supercooled phase transitions," *JCAP*, vol. 06, p. 024, 2019. DOI: 10.1088/1475-7516/2019/06/024. arXiv: 1903.09642 [hep-ph].

[78] L. Delle Rose, G. Panico, M. Redi, and A. Tesi, "Gravitational Waves from Supercool Axions," *JHEP*, vol. 04, p. 025, 2020. DOI: 10.1007/JHEP04(2020)025. arXiv: 1912.06139 [hep-ph].

[79] H. An, K.-F. Lyu, L.-T. Wang, and S. Zhou, "Gravitational waves from an inflation triggered first-order phase transition," *JHEP*, vol. 06, p. 050, 2022. DOI: 10.1007/JHEP06(2022)050. arXiv: 2201.05171 [astro-ph.CO].

[80] B. Thorne, T. Fujita, M. Hazumi, N. Katayama, E. Komatsu, and M. Shiraishi, "Finding the chiral gravitational wave background of an axion- su(2) inflationary model using cmb observations and laser interferometers," *Physical Review D*, vol. 97, no. 4, Feb. 2018, ISSN: 2470-0029. DOI: 10.1103/physrevd.97.043506. [Online]. Available: http://dx.doi.org/10.1103/PhysRevD.97.043506.

[81] B. Wang and Y. Zhang, "Second-order cosmological perturbations IV. Produced by scalar-tensor and tensor-tensor couplings during the radiation dominated stage," *Phys. Rev. D*, vol. 99, no. 12, p. 123 008, 2019. DOI: 10.1103/PhysRevD.99.123008. arXiv: 1905.03272 [gr-qc].

[82] L. A. Boyle and A. Buonanno, "Relating gravitational wave constraints from primordial nucleosynthesis, pulsar timing, laser interferometers, and the CMB: Implications for the early Universe," *Phys. Rev. D*, vol. 78, p. 043 531, 2008. DOI: 10.1103/PhysRevD.78.043531. arXiv: 0708.2279 [astro-ph].

[83] K. W. Masui and U.-L. Pen, "Primordial gravity wave fossils and their use in testing inflation," *Phys. Rev. Lett.*, vol. 105, p. 161 302, 2010. DOI: 10.1103/PhysRevLett.105.161302. arXiv: 1006.4181 [astro-ph.CO].

[84] J. M. Maldacena, "Non-Gaussian features of primordial fluctuations in single field inflationary models," *JHEP*, vol. 05, p. 013, 2003. DOI: 10.1088/1126-6708/2003/05/013. arXiv: astro-ph/0210603.

[85] P. Creminelli and M. Zaldarriaga, "Single field consistency relation for the 3-point function," *JCAP*, vol. 10, p. 006, 2004. DOI: 10.1088/1475-7516/2004/10/006. arXiv: astro-ph/0407059.

[86] E. Dimastrogiovanni, M. Fasiello, D. Jeong, and M. Kamionkowski, "Inflationary tensor fossils in large-scale structure," *JCAP*, vol. 12, p. 050, 2014. DOI: 10.1088/1475-7516/2014/12/050. arXiv: 1407.8204 [astro-ph.CO].

[87] D. Jeong and M. Kamionkowski, "Clustering Fossils from the Early Universe," *Phys. Rev. Lett.*, vol. 108, p. 251 301, 2012. DOI: 10.1103/PhysRevLett.108.251301. arXiv: 1203.0302 [astro-ph.CO].

[88] L. Dai, D. Jeong, and M. Kamionkowski, "Anisotropic imprint of long-wavelength tensor perturbations on cosmic structure," *Phys. Rev. D*, vol. 88, no. 4, p. 043 507, 2013. DOI: 10.1103/PhysRevD.88.043507. arXiv: 1306.3985 [astro-ph.CO].

[89] D. Jeong, F. Schmidt, and C. M. Hirata, "Large-scale clustering of galaxies in general relativity," *Phys. Rev. D*, vol. 85, p. 023 504, 2012. DOI: 10.1103/PhysRevD.85.023504. arXiv: 1107.5427 [astro-ph.CO].

[90] F. Schmidt and D. Jeong, "Cosmic Rulers," *Phys. Rev. D*, vol. 86, p. 083 527, 2012. DOI: 10.1103/PhysRevD.86.083527. arXiv: 1204.3625 [astro-ph.CO].

[91] D. Jeong and F. Schmidt, "Large-Scale Structure with Gravitational Waves I: Galaxy Clustering," *Phys. Rev. D*, vol. 86, p. 083 512, 2012. DOI: 10.1103/PhysRevD.86.083512. arXiv: 1205.1512 [astro-ph.CO].

[92] F. Schmidt and D. Jeong, "Large-Scale Structure with Gravitational Waves II: Shear," *Phys. Rev. D*, vol. 86, p. 083 513, 2012. DOI: 10.1103/PhysRevD.86.083513. arXiv: 1205.1514 [astro-ph.CO].

[93] F. Schmidt, E. Pajer, and M. Zaldarriaga, "Large-Scale Structure and Gravitational Waves III: Tidal Effects," *Phys. Rev. D*, vol. 89, no. 8, p. 083 507, 2014. DOI: 10.1103/PhysRevD.89.083507. arXiv: 1312.5616 [astro-ph.CO].

[94] K. N. Ananda, C. Clarkson, and D. Wands, "Cosmological gravitational wave background from primordial density perturbations," *Physical Review D*, vol. 75, no. 12, Jun. 2007, ISSN: 1550-2368. DOI: 10.1103/physrevd.75.123518. [Online]. Available: http://dx.doi.org/10.1103/PhysRevD.75.123518.

[95] L. Alabidi, K. Kohri, M. Sasaki, and Y. Sendouda, "Observable Spectra of Induced Gravitational Waves from Inflation," *JCAP*, vol. 09, p. 017, 2012. DOI: 10.1088/1475-7516/2012/09/017. arXiv: 1203.4663 [astro-ph.CO].

[96] S. Mollerach, D. Harari, and S. Matarrese, "CMB polarization from secondary vector and tensor modes," *Phys. Rev. D*, vol. 69, p. 063 002, 2004. DOI: 10.1103/PhysRevD.69.063002. arXiv: astro-ph/0310711.

[97] D. Baumann, P. Steinhardt, K. Takahashi, and K. Ichiki, "Gravitational wave spectrum induced by primordial scalar perturbations," *Physical Review D*, vol. 76, no. 8, Oct. 2007, ISSN: 1550-2368. DOI: 10.1103/physrevd.76.084019. [Online]. Available: http://dx.doi.org/10.1103/PhysRevD.76.084019.

[98] H. Assadullahi and D. Wands, "Gravitational waves from an early matter era," *Phys. Rev. D*, vol. 79, p. 083 511, 2009. DOI: 10.1103/PhysRevD.79.083511. arXiv: 0901.0989 [astro-ph.CO].

[99] L. Alabidi, K. Kohri, M. Sasaki, and Y. Sendouda, "Observable induced gravitational waves from an early matter phase," *JCAP*, vol. 05, p. 033, 2013. DOI: 10.1088/1475-7516/2013/05/033. arXiv: 1303.4519 [astro-ph.CO].

[100] K. Tomita, "Non-Linear Theory of Gravitational Instability in the Expanding Universe," *Progress of Theoretical Physics*, vol. 37, no. 5, pp. 831–846, May 1967. DOI: 10.1143/PTP.37.831.

[101] K. Tomita, "Non-Linear Theory of Gravitational Instability in the Expanding Universe. III," *Progress of Theoretical Physics*, vol. 47, no. 2, pp. 416–443, Feb. 1972. DOI: 10.1143/PTP.47.416.

[102] S. Matarrese, S. Mollerach, and M. Bruni, "Relativistic second-order perturbations of the einsteinde sitter universe," *Physical Review D*, vol. 58, no. 4, Jul. 1998, ISSN: 1089-4918. DOI: 10.1103/physrevd.58.043504. [Online]. Available: http://dx.doi.org/10.1103/PhysRevD.58.043504.

[103] J. Garcia-Bellido, M. Peloso, and C. Unal, "Gravitational Wave signatures of inflationary models from Primordial Black Hole Dark Matter," *JCAP*, vol. 09, p. 013, 2017. DOI: 10.1088/1475-7516/2017/09/013. arXiv: 1707.02441 [astro-ph.CO].

[104] N. Bartolo, V. De Luca, G. Franciolini, A. Lewis, M. Peloso, and A. Riotto, "Primordial Black Hole Dark Matter: LISA Serendipity," *Phys. Rev. Lett.*, vol. 122, no. 21, p. 211 301, 2019. DOI: 10.1103/PhysRevLett.122.211301. arXiv: 1810.12218 [astro-ph.CO].

[105] N. Bartolo *et al.*, "Gravitational wave anisotropies from primordial black holes," *JCAP*, vol. 02, p. 028, 2020. DOI: 10.1088/1475-7516/2020/02/028. arXiv: 1909.12619 [astro-ph.CO].

[106] E. D. Kovetz, "Probing Primordial-Black-Hole Dark Matter with Gravitational Waves," *Phys. Rev. Lett.*, vol. 119, no. 13, p. 131 301, 2017. DOI: 10.1103/PhysRevLett.119.131301. arXiv: 1705.09182 [astro-ph.CO].

[107] K. Kohri and T. Terada, "Primordial Black Hole Dark Matter and LIGO/Virgo Merger Rate from Inflation with Running Spectral Indices: Formation in the Matter- and/or Radiation-Dominated Universe," *Class. Quant. Grav.*, vol. 35, no. 23, p. 235 017, 2018. DOI: 10.1088/1361-6382/aaea18. arXiv: 1802.06785 [astro-ph.CO].

[108] M. Sasaki, T. Suyama, T. Tanaka, and S. Yokoyama, "Primordial black holesperspectives in gravitational wave astronomy," *Class. Quant. Grav.*, vol. 35, no. 6, p. 063 001, 2018. DOI: 10.1088/1361-6382/aaa7b4. arXiv: 1801.05235 [astro-ph.CO].

[109] R. Saito and J. Yokoyama, "Gravitational-wave background as a probe of the primordial black-hole abundance," *Physical Review Letters*, vol. 102, no. 16, Apr. 2009, ISSN: 1079-7114. DOI: 10.1103/physrevlett.102.161101. [Online]. Available: http://dx.doi.org/10.1103/PhysRevLett.102.161101.

[110] N. Orlofsky, A. Pierce, and J. D. Wells, "Inflationary theory and pulsar timing investigations of primordial black holes and gravitational waves," *Phys. Rev. D*, vol. 95, no. 6, p. 063 518, 2017. DOI: 10.1103/PhysRevD.95.063518. arXiv: 1612.05279 [astro-ph.CO].

[111] A. D. Gow, C. T. Byrnes, P. S. Cole, and S. Young, "The power spectrum on small scales: Robust constraints and comparing PBH methodologies," *JCAP*, vol. 02, p. 002, 2021. DOI: 10.1088/1475-7516/2021/02/002. arXiv: 2008.03289 [astro-ph.CO].

[112] G. Domènech, S. Pi, and M. Sasaki, "Induced gravitational waves as a probe of thermal history of the universe," *JCAP*, vol. 08, p. 017, 2020. DOI: 10.1088/1475-7516/2020/08/017. arXiv: 2005.12314 [gr-qc].

[113] J. Espinosa, D. Racco, and A. Riotto, "A cosmological signature of the SM higgs instability: Gravitational waves," *Journal of Cosmology and Astroparticle Physics*, vol. 2018, no. 09, pp. 012–012, Sep. 2018. DOI: 10.1088/1475-7516/2018/09/012. [Online]. Available: https://doi.org/10.1088/1475-7516/2018/09/012.

[114] S. Matarrese and S. Mollerach, "The Stochastic gravitational wave background produced by non-linear cosmological perturbations," in *ERE - Spanish Relativity Conference*, Sep. 1996. arXiv: astro-ph/9705168.

[115] N. Bartolo, S. Matarrese, O. Pantano, and A. Riotto, "Second-order matter perturbations in a ΛCDM cosmology and non-gaussianity," *Classical and Quantum Gravity*, vol. 27, no. 12, p. 124 009, May 2010. DOI: 10.1088/0264-9381/27/12/124009. [Online]. Available: https://doi.org/10.1088/0264-9381/27/12/124009.

[116] K. Nakamura, "Consistensy of Equations in the Second-order Gauge-invariant Cosmological Perturbation Theory," *Prog. Theor. Phys.*, vol. 121, p. 1321, 2009. DOI: 10.1143/PTP.121.1321. arXiv: 0812.4865 [gr-qc].

[117] K. Inomata and T. Terada, "Gauge independence of induced gravitational waves," *Physical Review D*, vol. 101, no. 2, Jan. 2020, ISSN: 2470-0029. DOI: 10.1103/physrevd.101.023523. [Online]. Available: http://dx.doi.org/10.1103/PhysRevD.101.023523.

[118] C. Yuan, Z.-C. Chen, and Q.-G. Huang, "Scalar induced gravitational waves in different gauges," *Physical Review D*, vol. 101, no. 6, Mar. 2020, ISSN: 2470-0029. DOI: 10.1103/physrevd.101.063018. [Online]. Available: http://dx.doi.org/10.1103/PhysRevD.101.063018.

[119] G. Domènech, "Scalar Induced Gravitational Waves Review," *Universe*, vol. 7, no. 11, p. 398, 2021. DOI: 10.3390/universe7110398. arXiv: 2109.01398 [gr-qc].

[120] R. L. Arnowitt, S. Deser, and C. W. Misner, "The Dynamics of general relativity," *Gen. Rel. Grav.*, vol. 40, pp. 1997–2027, 2008. DOI: 10.1007/s10714-008-0661-1. arXiv: gr-qc/0405109.

[121] D. Salopek and J. Bond, "Nonlinear evolution of long wavelength metric fluctuations in inflationary models," *Phys. Rev. D*, vol. 42, pp. 3936–3962, 1990. DOI: 10.1103/PhysRevD.42.3936.

[122] Y.-F. Cai, C. Chen, X. Tong, D.-G. Wang, and S.-F. Yan, "When Primordial Black Holes from Sound Speed Resonance Meet a Stochastic Background of Gravitational Waves," *Phys. Rev. D*, vol. 100, no. 4, p. 043 518, 2019. DOI: 10.1103/PhysRevD.100.043518. arXiv: 1902.08187 [astro-ph.CO].

[123] P. H. Frampton, M. Kawasaki, F. Takahashi, and T. T. Yanagida, "Primordial Black Holes as All Dark Matter," *JCAP*, vol. 04, p. 023, 2010. DOI: 10.1088/1475-7516/2010/04/023. arXiv: 1001.2308 [hep-ph].

[124] C. Chen and Y.-F. Cai, "Primordial black holes from sound speed resonance in the inflaton-curvaton mixed scenario," *JCAP*, vol. 10, p. 068, 2019. DOI: 10.1088/1475-7516/2019/10/068. arXiv: 1908.03942 [astro-ph.CO].

[125] J. Yokoyama, "Chaotic new inflation and formation of primordial black holes," *Phys. Rev. D*, vol. 58, p. 083 510, 1998. DOI: 10.1103/PhysRevD.58.083510. arXiv: astro-ph/9802357.

[126] J. Lesgourgues, "Features in the primordial power spectrum of double D term inflation," *Nucl. Phys. B*, vol. 582, pp. 593–626, 2000. DOI: 10.1016/S0550-3213(00)00301-1. arXiv: hep-ph/9911447.

[127] E. Bugaev and P. Klimai, "Constraints on the induced gravitational wave background from primordial black holes," *Phys. Rev. D*, vol. 83, p. 083 521, 8 Apr. 2011. DOI: 10.1103/PhysRevD.83.083521. [Online]. Available: https://link.aps.org/doi/10.1103/PhysRevD.83.083521.

[128] S. Pi and M. Sasaki, "Gravitational Waves Induced by Scalar Perturbations with a Lognormal Peak," *JCAP*, vol. 09, p. 037, 2020. DOI: 10.1088/1475-7516/2020/09/037. arXiv: 2005.12306 [gr-qc].

[129] K. Inomata and T. Nakama, "Gravitational waves induced by scalar perturbations as probes of the small-scale primordial spectrum," *Phys. Rev. D*, vol. 99, no. 4, p. 043 511, 2019. DOI: 10.1103/PhysRevD.99.043511. arXiv: 1812.00674 [astro-ph.CO].

[130] J.-C. Hwang, D. Jeong, and H. Noh, "Gauge dependence of gravitational waves generated from scalar perturbations," *Astrophys. J.*, vol. 842, no. 1, p. 46, 2017. DOI: 10.3847/1538-4357/aa74be. arXiv: 1704.03500 [astro-ph.CO].

[131] V. De Luca, G. Franciolini, A. Kehagias, and A. Riotto, "On the Gauge Invariance of Cosmological Gravitational Waves," *JCAP*, vol. 03, p. 014, 2020. DOI: 10.1088/1475-7516/2020/03/014. arXiv: 1911.09689 [gr-qc].

[132] C. Yuan, Z.-C. Chen, and Q.-G. Huang, "Scalar induced gravitational waves in different gauges," *Phys. Rev. D*, vol. 101, no. 6, p. 063 018, 2020. DOI: 10.1103/PhysRevD.101.063018. arXiv: 1912.00885 [astro-ph.CO].

[133] Z. Chang, S. Wang, and Q.-H. Zhu, "Gauge Invariant Second Order Gravitational Waves," Sep. 2020. arXiv: 2009.11994 [gr-qc].

[134] G. Domènech and M. Sasaki, "Approximate gauge independence of the induced gravitational wave spectrum," *Phys. Rev. D*, vol. 103, no. 6, p. 063 531, 2021. DOI: 10.1103/PhysRevD.103.063531. arXiv: 2012.14016 [gr-qc].

[135] S. Matarrese, S. Mollerach, and M. Bruni, "Second order perturbations of the Einstein-de Sitter universe," *Phys. Rev. D*, vol. 58, p. 043 504, 1998. DOI: 10.1103/PhysRevD.58.043504. arXiv: astro-ph/9707278.

[136] S. Matarrese, O. Pantano, and D. Saez, "General-relativistic approach to the nonlinear evolution of collisionless matter," *Phys. Rev. D*, vol. 47, pp. 1311–1323, 4 Feb. 1993. DOI: 10.1103/PhysRevD.47.1311. [Online]. Available: https://link.aps.org/doi/10.1103/PhysRevD.47.1311.

[137] S. Matarrese, O. Pantano, and D. Saez, "General relativistic dynamics of irrotational dust: Cosmological implications," *Phys. Rev. Lett.*, vol. 72, pp. 320–323, 3 Jan. 1994. DOI: 10.1103/PhysRevLett.72.320. [Online]. Available: https://link.aps.org/doi/10.1103/PhysRevLett.72.320.

[138] S. Matarrese and M. Pietroni, "Resumming Cosmic Perturbations," *JCAP*, vol. 06, p. 026, 2007. DOI: 10.1088/1475-7516/2007/06/026. arXiv: astro-ph/0703563.

[139] T. Matsubara, "Resumming Cosmological Perturbations via the Lagrangian Picture: One-loop Results in Real Space and in Redshift Space," *Phys. Rev. D*, vol. 77, p. 063 530, 2008. DOI: 10.1103/PhysRevD.77.063530. arXiv: 0711.2521 [astro-ph].

[140] Z. Vlah, U. Seljak, M. Y. Chu, and Y. Feng, "Perturbation theory, effective field theory, and oscillations in the power spectrum," *JCAP*, vol. 03, p. 057, 2016. DOI: 10.1088/1475-7516/2016/03/057. arXiv: 1509.02120 [astro-ph.CO].

[141] P. Bari, A. Ricciardone, N. Bartolo, D. Bertacca, and S. Matarrese, "Signatures of Primordial Gravitational Waves on the Large-Scale Structure of the Universe," *Phys. Rev. Lett.*, vol. 129, no. 9, p. 091 301, 2022. DOI: 10.1103/PhysRevLett.129.091301. arXiv: 2111.06884 [astro-ph.CO].

[142] E. Lifshitz, "Republication of: On the gravitational stability of the expanding universe," *J. Phys. (USSR)*, vol. 10, no. 2, p. 116, 1946. DOI: 10.1007/s10714-016-2165-8.

[143] E. M. Lifshitz and I. M. Khalatnikov, "Investigations in relativistic cosmology," *Adv. Phys.*, vol. 12, pp. 185–249, 1963. DOI: 10.1080/00018736300101283.

[144] L. D. Landau and E. M. Lifshitz, *The classical theory of fields*, 4th ed. Oxford, England: Butterworth-Heinemann, Jan. 1987.

[145] J. R. Espinosa, D. Racco, and A. Riotto, "A Cosmological Signature of the SM Higgs Instability: Gravitational Waves," *JCAP*, vol. 09, p. 012, 2018. DOI: 10.1088/1475-7516/2018/09/012. arXiv: 1804.07732 [hep-ph].

[146] N. Bartolo *et al.*, "Science with the space-based interferometer LISA. IV: Probing inflation with gravitational waves," *JCAP*, vol. 12, p. 026, 2016. DOI: 10.1088/1475-7516/2016/12/026. arXiv: 1610.06481 [astro-ph.CO].

[147] Y.-F. Cai, C. Lin, B. Wang, and S.-F. Yan, "Sound speed resonance of the stochastic gravitational wave background," *Phys. Rev. Lett.*, vol. 126, no. 7, p. 071 303, 2021. DOI: 10.1103/PhysRevLett.126.071303. arXiv: 2009.09833 [gr-qc].

[148] R. Namba, M. Peloso, M. Shiraishi, L. Sorbo, and C. Unal, "Scale-dependent gravitational waves from a rolling axion," *JCAP*, vol. 01, p. 041, 2016. DOI: 10.1088/1475-7516/2016/01/041. arXiv: 1509.07521 [astro-ph.CO].

[149] E. Dimastrogiovanni, M. Fasiello, and T. Fujita, "Primordial Gravitational Waves from Axion-Gauge Fields Dynamics," *JCAP*, vol. 01, p. 019, 2017. DOI: 10.1088/1475-7516/2017/01/019. arXiv: 1608.04216 [astro-ph.CO].

[150] B. Thorne, T. Fujita, M. Hazumi, N. Katayama, E. Komatsu, and M. Shiraishi, "Finding the chiral gravitational wave background of an axion-SU(2) inflationary model using CMB observations and laser interferometers," *Phys. Rev. D*, vol. 97, no. 4, p. 043 506, 2018. DOI: 10.1103/PhysRevD.97.043506. arXiv: 1707.03240 [astro-ph.CO].

[151] J. Garcia-Bellido, M. Peloso, and C. Unal, "Gravitational waves at interferometer scales and primordial black holes in axion inflation," *JCAP*, vol. 12, p. 031, 2016. DOI: 10.1088/1475-7516/2016/12/031. arXiv: 1610.03763 [astro-ph.CO].

[152] J. A. Peacock, *Cosmological physics*. Cambridge University Press, 2010.

[153] S. M. Carroll, W. H. Press, and E. L. Turner, "The cosmological constant.," *Ann. Rev. Astron. Astrophys.*, vol. 30, pp. 499–542, Jan. 1992. DOI: 10.1146/annurev.aa.30.090192.002435.

[154] A. Blanchard *et al.*, "Euclid preparation: VII. Forecast validation for Euclid cosmological probes," *Astron. Astrophys.*, vol. 642, A191, 2020. DOI: 10.1051/0004-6361/202038071. arXiv: 1910.09273 [astro-ph.CO].

[155] A. Dey *et al.*, "Overview of the DESI Legacy Imaging Surveys," *Astron. J.*, vol. 157, no. 5, p. 168, 2019. DOI: 10.3847/1538-3881/ab089d. arXiv: 1804.08657 [astro-ph.IM].

[156] O. Doré *et al.*, "Science Impacts of the SPHEREx All-Sky Optical to Near-Infrared Spectral Survey: Report of a Community Workshop Examining Extragalactic, Galactic, Stellar and Planetary Science," Jun. 2016, arxiv:1606.07039.

[157] D. J. Bacon *et al.*, "Cosmology with Phase 1 of the Square Kilometre Array: Red Book 2018: Technical specifications and performance forecasts," *Publ. Astron. Soc. Austral.*, vol. 37, e007, 2020. DOI: 10.1017/pasa.2019.51. arXiv: 1811.02743 [astro-ph.CO].

[158] B. M. Rose *et al.*, "A Reference Survey for Supernova Cosmology with the Nancy Grace Roman Space Telescope," Nov. 2021, arxiv:2111.03081.

[159] Vera C. Rubin Observatory LSST Solar System Science Collaboration, R. L. Jones, *et al.*, "The Scientific Impact of the Vera C. Rubin Observatory's Legacy Survey of Space and Time (LSST) for Solar System Science," Sep. 2020, arxiv:2009.07653.

[160] C. Döring, S. C. Chuliá, M. Lindner, B. M. Schaefer, and M. Bartelmann, "Gravitational wave induced baryon acoustic oscillations," *SciPost Phys.*, vol. 12, p. 114, 2022. DOI: 10.21468/SciPostPhys.12.3.114. arXiv: 2107.10283 [gr-qc].

[161] P. Bari, D. Bertacca, N. Bartolo, A. Ricciardone, S. Giardiello, and S. Matarrese, "An analytical study of the primordial gravitational-wave-induced contribution to the large-scale structure of the Universe," *JCAP*, vol. 07, p. 034, 2023. DOI: 10.1088/1475-7516/2023/07/034. arXiv: 2209.05329 [astro-ph.CO].

[162] Y. Zhang, F. Qin, and B. Wang, "Second-order cosmological perturbations. II. Produced by scalar-tensor and tensor-tensor couplings," *Phys. Rev. D*, vol. 96, no. 10, p. 103 523, 2017. DOI: 10.1103/PhysRevD.96.103523. arXiv: 1710.06639 [gr-qc].

[163] P. Carrilho and K. A. Malik, "Vector and tensor contributions to the curvature perturbation at second order," *Journal of Cosmology and Astroparticle Physics*, vol. 2016, no. 02, pp. 021–021, Feb. 2016, ISSN: 1475-7516. DOI: 10.1088/1475-7516/2016/02/021. [Online]. Available: http://dx.doi.org/10.1088/1475-7516/2016/02/021.

[164] V. Mukhanov, *Physical foundations of cosmology*. Cambridge, UK New York: Cambridge University Press, 2005, ISBN: 978-0-511-13679-5.

[165] P. Meszaros, "The behaviour of point masses in an expanding cosmological substratum," *Astron. Astrophys.*, vol. 37, pp. 225–228, 1974.

[166] S. Weinberg, "Cosmological fluctuations of short wavelength," *Astrophys. J.*, vol. 581, pp. 810–816, 2002. DOI: 10.1086/344441. arXiv: astro-ph/0207375.

[167] P. Bari, A. Ricciardone, N. Bartolo, D. Bertacca, and S. Matarrese, "Signatures of primordial gravitational waves on the large-scale structure of the universe," *Phys. Rev. Lett.*, vol. 129, p. 091 301, 9 Aug. 2022. DOI: 10.1103/PhysRevLett.129.091301. [Online]. Available: https://link.aps.org/doi/10.1103/PhysRevLett.129.091301.

[168] J. Ehlers, "Contributions to the relativistic mechanics of continuous media," *Abh. Akad. Wiss. Lit. Mainz. Nat. Kl.*, vol. 11, pp. 793–837, 1961. DOI: 10.1007/BF00759031.

[169] G. F. R. Ellis, "Republication of: Relativistic cosmology," *General Relativity and Gravitation*, vol. 41, no. 3, pp. 581–660, Mar. 2009. DOI: 10.1007/s10714-009-0760-7.

[170] J.-O. Gong, *Analytic integral solutions for induced gravitational waves*, 2019. arXiv: 1909.12708 [gr-qc].

[171] Z. Chang, X. Zhang, and J.-Z. Zhou, "Gravitational waves from primordial scalar and tensor perturbations," *Phys. Rev. D*, vol. 107, no. 6, p. 063 510, 2023. DOI: 10.1103/PhysRevD.107.063510. arXiv: 2209.07693 [astro-ph.CO].

[172] P. Bari, N. Bartolo, G. Domènech, and S. Matarrese, "Gravitational waves induced by scalar-tensor mixing," Jul. 2023, (Submitted to Phys. Rev. D.) arXiv: 2307.05404 [astro-ph.CO].

[173] M. Shiraishi, C. Hikage, R. Namba, T. Namikawa, and M. Hazumi, "Testing statistics of the CMB B -mode polarization toward unambiguously establishing quantum fluctuation of the vacuum," *Phys. Rev. D*, vol. 94, no. 4, p. 043 506, 2016. DOI: 10.1103/PhysRevD.94.043506. arXiv: 1606.06082 [astro-ph.CO].

[174] R. Saito and J. Yokoyama, "Gravitational wave background as a probe of the primordial black hole abundance," *Phys. Rev. Lett.*, vol. 102, p. 161 101, 2009, [Erratum: Phys.Rev.Lett. 107, 069901 (2011)]. DOI: 10.1103/PhysRevLett.102.161101. arXiv: 0812.4339 [astro-ph].

[175] S. Wang, T. Terada, and K. Kohri, "Prospective constraints on the primordial black hole abundance from the stochastic gravitational-wave backgrounds produced by coalescing events and curvature perturbations," *Phys. Rev. D*, vol. 99, no. 10, p. 103 531, 2019, [Erratum: Phys.Rev.D 101, 069901 (2020)]. DOI: 10.1103/PhysRevD.99.103531. arXiv: 1903.05924 [astro-ph.CO].

[176] C. T. Byrnes, P. S. Cole, and S. P. Patil, "Steepest growth of the power spectrum and primordial black holes," *JCAP*, vol. 06, p. 028, 2019. DOI: 10.1088/1475-7516/2019/06/028. arXiv: 1811.11158 [astro-ph.CO].

[177] E. Thrane and J. D. Romano, "Sensitivity curves for searches for gravitational-wave backgrounds," *Phys. Rev. D*, vol. 88, no. 12, p. 124 032, 2013. DOI: 10.1103/PhysRevD.88.124032. arXiv: 1310.5300 [astro-ph.IM].

[178] S. Barke, Y. Wang, J. J. Esteban Delgado, M. Tröbs, G. Heinzel, and K. Danzmann, "Towards a gravitational wave observatory designer: sensitivity limits of spaceborne detectors," *Class. Quant. Grav.*, vol. 32, no. 9, p. 095 004, 2015. DOI: 10.1088/0264-9381/32/9/095004. arXiv: 1411.1260 [physics.ins-det].

[179] W.-H. Ruan, Z.-K. Guo, R.-G. Cai, and Y.-Z. Zhang, "Taiji program: Gravitational-wave sources," *Int. J. Mod. Phys. A*, vol. 35, no. 17, p. 2 050 075, 2020. DOI: 10.1142/S0217751X2050075X. arXiv: 1807.09495 [gr-qc].

[180] *Cosmic explorer sensitivity curve*, https://cosmicexplorer.org/sensitivity.html, [Online; accessed 05-May-2023].

[181] *The A+ design curve*, https://dcc.ligo.org/LIGO-T1800042/public, [Online; accessed 05-May-2023].

[182] *Ligo unofficial sensitivity curves*, https://dcc.ligo.org/LIGO-T1500293/public, [Online; accessed 05-May-2023].

[183] K. Schmitz, "New Sensitivity Curves for Gravitational-Wave Signals from Cosmological Phase Transitions," *JHEP*, vol. 01, p. 097, 2021. DOI: 10.1007/JHEP01(2021)097. arXiv: 2002.04615 [hep-ph].

[184] R. H. Cyburt, B. D. Fields, K. A. Olive, and E. Skillman, "New BBN limits on physics beyond the standard model from ^4He," *Astropart. Phys.*, vol. 23, pp. 313–323, 2005. DOI: 10.1016/j.astropartphys.2005.01.005. arXiv: astro-ph/0408033.

[185] A. Arbey, J. Auffinger, P. Sandick, B. Shams Es Haghi, and K. Sinha, "Precision calculation of dark radiation from spinning primordial black holes and early matter-dominated eras," *Phys. Rev. D*, vol. 103, no. 12, p. 123 549, 2021. DOI: 10.1103/PhysRevD.103.123549. arXiv: 2104.04051 [astro-ph.CO].

[186] E. Grohs and G. M. Fuller, "Big Bang Nucleosynthesis," in *Handbook of Nuclear Physics*, I. Tanihata, H. Toki, and T. Kajino, Eds. 2023, pp. 1–21. DOI: 10.1007/978-981-15-8818-1_127-1. arXiv: 2301.12299 [astro-ph.CO].

[187] K. N. Abazajian *et al.*, "CMB-S4 Science Book, First Edition," Oct. 2016. arXiv: 1610.02743 [astro-ph.CO].

[188] A. Sesana *et al.*, "Unveiling the gravitational universe at μ-Hz frequencies," *Exper. Astron.*, vol. 51, no. 3, pp. 1333–1383, 2021. DOI: 10.1007/s10686-021-09709-9. arXiv: 1908.11391 [astro-ph.IM].

[189] D. Blas and A. C. Jenkins, "Bridging the μHz Gap in the Gravitational-Wave Landscape with Binary Resonances," *Phys. Rev. Lett.*, vol. 128, no. 10, p. 101 103, 2022. DOI: 10.1103/PhysRevLett.128.101103. arXiv: 2107.04601 [astro-ph.CO].

[190] M. A. Fedderke, P. W. Graham, and S. Rajendran, "Asteroids for μHz gravitational-wave detection," *Phys. Rev. D*, vol. 105, no. 10, p. 103 018, 2022. DOI: 10.1103/PhysRevD.105.103018. arXiv: 2112.11431 [gr-qc].

[191] V. Domcke *et al.*, "Measuring the net circular polarization of the stochastic gravitational wave background with interferometers," *JCAP*, vol. 05, p. 028, 2020. DOI: 10.1088/1475-7516/2020/05/028. arXiv: 1910.08052 [astro-ph.CO].

[192] G. Orlando, M. Pieroni, and A. Ricciardone, "Measuring Parity Violation in the Stochastic Gravitational Wave Background with the LISA-Taiji network," *JCAP*, vol. 03, p. 069, 2021. DOI: 10.1088/1475-7516/2021/03/069. arXiv: 2011.07059 [astro-ph.CO].

[193] N. Seto, "Measuring Parity Asymmetry of Gravitational Wave Backgrounds with a Heliocentric Detector Network in the mHz Band," *Phys. Rev. Lett.*, vol. 125, p. 251 101, 2020. DOI: 10.1103/PhysRevLett.125.251101. arXiv: 2009.02928 [gr-qc].

[194] B. Salehian, M. A. Gorji, S. Mukohyama, and H. Firouzjahi, "Analytic study of dark photon and gravitational wave production from axion," *JHEP*, vol. 05, p. 043, 2021. DOI: 10.1007/JHEP05(2021)043. arXiv: 2007.08148 [hep-ph].

[195] C. S. Machado, W. Ratzinger, P. Schwaller, and B. A. Stefanek, "Audible Axions," *JHEP*, vol. 01, p. 053, 2019. DOI: 10.1007/JHEP01(2019)053. arXiv: 1811.01950 [hep-ph].

[196] K. Inomata, K. Kohri, and T. Terada, "The Detected Stochastic Gravitational Waves and Subsolar-Mass Primordial Black Holes," Jun. 2023. arXiv: 2306.17834 [astro-ph.CO].

[197] A. Raccanelli, D. Bertacca, D. Jeong, M. C. Neyrinck, and A. S. Szalay, "Doppler term in the galaxy two-point correlation function: wide-angle, velocity, Doppler lensing and cosmic acceleration effects," *Phys. Dark Univ.*, vol. 19, pp. 109–123, 2018. DOI: 10.1016/j.dark.2017.12.003. arXiv: 1602.03186 [astro-ph.CO].

[198] L. R. Abramo and D. Bertacca, "Disentangling the effects of Doppler velocity and primordial non-Gaussianity in galaxy power spectra," *Phys. Rev. D*, vol. 96, no. 12, p. 123 535, 2017. DOI: 10.1103/PhysRevD.96.123535. arXiv: 1706.01834 [astro-ph.CO].

[199] M. Y. Elkhashab, C. Porciani, and D. Bertacca, "The large-scale monopole of the power spectrum in a Euclid-like survey: wide-angle effects, lensing, and the finger of the observer," *Mon. Not. Roy. Astron. Soc.*, vol. 509, no. 2, pp. 1626–1645, 2021. DOI: 10.1093/mnras/stab3010. arXiv: 2108.13424 [astro-ph.CO].

[200] B. Bahr-Kalus, D. Bertacca, L. Verde, and A. Heavens, "The Kaiser-Rocket effect: three decades and counting," *JCAP*, vol. 11, p. 027, 2021. DOI: 10.1088/1475-7516/2021/11/027. arXiv: 2107.00351 [astro-ph.CO].

[201] N. Bartolo, S. Matarrese, and A. Riotto, "Non-Gaussianity in the Cosmic Microwave Background Anisotropies at Recombination in the Squeezed limit," *JCAP*, vol. 02, p. 017, 2012. DOI: 10.1088/1475-7516/2012/02/017. arXiv: 1109.2043 [astro-ph.CO].

[202] A. Gervois and H. Navelet, "Integrals of three Bessel functions and Legendre functions. I," *Journal of Mathematical Physics*, vol. 26, no. 4, pp. 633–644, Apr. 1985. DOI: 10.1063/1.526600.